Kinetic Modeling of Homo- and Co- Polymerization of Water-Soluble *N*-vinyl Monomers

Submitted by

Sandhya Santana Krishnan

A thesis submitted to the Department of Chemical Engineering in conformity with the requirements for the degree of Doctor of Philosophy

Queen's University

Kingston, Ontario, Canada

December, 2011

Abstract

Functional water-soluble polymers find applications in a variety of fields including waste-water treatment, pharmaceuticals, cosmetics, drug delivery, and hygiene. Despite the increased demand for these products, understanding of their synthesis by free-radical aqueous-phase polymerization has lagged behind that of polymers produced in organic solvents. In this doctoral work, the free-radical batch and semibatch aqueous-phase polymerization of *N*-vinylpyrrolidone (NVP), *N*-vinylformamide (NVF), *N*-vinylimidazole (NVI) and quaternized vinylimidazole (QVI), as well as NVP polymerized in *n*-butanol, has been studied. Kinetic models are developed to describe monomer conversion and polymer molecular weight (MW) behaviour of these systems. The expressions developed from independent pulsed-laser studies for propagation (k_p) and termination (k_t) rate coefficients, including their variation with monomer concentration and conversion, are shown to provide an excellent description of aqueous-phase NVP polymerization. Polymerization of NVP in butanol and of NVF in water are well-represented by the base NVP model, with differences in polymerization rate and polymer MWs simply accounted for by the differences in k_p for the systems, indicating that the k_t behaviour must be quite similar. The NVI/QVI study demonstrates the importance of a pH-dependent degradative addition reaction to monomer for NVI, with polymerization behaviour identical to that of QVI for pH 1, an effect captured in the model developed to describe the system.

The aqueous-phase copolymerization of NVP and NVF was also studied, and reactivity ratios were determined to be very close to unity. This information was combined with the k_p and k_t expressions used to describe NVP and NVF homopolymerizations, with no other additional parameters required to model the copolymerization rate, copolymer composition and copolymer

MW. This result demonstrates that the improved homopolymerization knowledge of these water-soluble monomers can be easily extended to understand their behaviour in copolymerization.

Statement of Co-Authorship

The majority of the work presented in this thesis was conducted by me under the supervision of Prof. Robin Hutchinson. Chapters 3 and 4 are updated versions of published manuscripts. The experiments at 70 °C in the Chapter 3 were conducted by a previous M.Sc student, Lina Tang. An undergraduate student, Alan J. Saunders conducted some of the experiments presented in Chapter 4, under my guidance. All the SEC analyses were conducted by Dr. Marek Stach in the Polymer Institute of the Slovak Academy of Sciences. All published and in-preparation manuscripts are therefore in collaboration with Dr. Marek Stach and Dr. Igor Lacik for the SEC analyses and the related technical discussions.

Acknowledgements

I would like to thank my supervisor, Prof. Robin. A. Hutchinson for all his support, guidance and encouragement over the course of my Ph.D. His knowledge and guidance have played a key role in helping me shape up this doctoral work as well as a career in research.

I would like to thank the research groups of Dr. Igor Lacik and Dr. Michael Buback for sharing all their valuable research data with me and for all the technical discussions. A special thanks to Dr. Marek Stach for analysing all the SEC samples, his SEC expertise has been of great help to this work.

I would also like to thank BASF, Ludwigshafen for their financial support and the technical discussions with the research group of Dr. Klaus-Dieter Hungenberg at BASF.

Finally, I would like to thank my family, especially my parents and grandfather, all my lab mates and friends, especially Karthik for all their support and encouragement throughout.

Table of Contents

List of Figures

List of Tables

List of Schemes

Abbreviations

AA	Acrylic Acid
AM	Acrylamide
DMF	Dimethyl Formamide
DMSO	Dimethyl Sulfoxide
FRP	Free Radical Polymerization
IR	Infrared
MAA	Methacrylic Acid
MALLS	Multi-Angle Laser Light Scattering
MW	Molecular weight
MWD	Molecular Weight Distribution
NEP	*N*-ethyl-2-pyrrolidone
NIR	Near Infrared
NMR	Nuclear Magnetic Resonance
NVF	*N*-vinylformamide
NVI	*N*-vinylimidazole
NVP	*N*-vinylpyrrolidone
PAA	Poly(acrylic acid)
PDI	Poly Dispersity Index
PISAS	Polymer Institute of the Slovak Academy of Sciences
PLP	Pulsed Laser Polymerization
PMAA	Poly(methacrylic acid)

PVF	Poly(vinylformamide)
PVP	Poly(vinylpyrrolidone)
QVI	Quaternized vinylimidazole
RI	Refractive Index
SEC	Size Exclusion Chromatography
SP	Single Pulse
V-50	2,2’-azobis (2-methylpropionamidine) dihydrochloride

Nomenclature

α	degree of ionization
η_γ	relative bulk viscosity
ρ_i	density of species i
c_i	concentration of species i
C_{RD}	reaction diffusion constant
D_n	dead chains of length n
$E_a(k_p)$	activation energy for propagation
A	Arrhenius pre-exponential factor
f	initiator efficiency
f_i	mole fraction of monomer i in monomer mixture
F_i	mole fraction of monomer i in the copolymer
I	initiator
M	monomer
$[M]_0$	initial monomer concentration
M_n	number average molecular weight
M_{mon}^0	initial monomer mass
$M_{mon}(t)$	Mass of monomer at time t
$M_{pol}(t)$	Mass of polymer at time t
M_w	weight average molecular weight
M_{total}	total mass of reaction mixture
P_n	polymer radicals of length n
r_i	reactivity ratio of monomer i

RD	reaction diffusion
SD	segmental diffusion
TD	translational diffusion
w_i	weight fraction of species i
w_i^0	initial weight fraction of species i
x_p	fractional conversion

Rate Coefficients

k_d	(s^{-1})	initiator decomposition rate
k_p	($L.mol^{-1}.s^{-1}$)	propagation rate coefficient
k_{pij}	($L.mol^{-1}.s^{-1}$)	addition of monomer j to radical i
k_p^{cop}	($L.mol^{-1}.s^{-1}$)	composition-averaged propagation rate coefficient
k_p^{max}	($L.mol^{-1}.s^{-1}$)	propagation rate coefficient at infinite dilution
k_t	($L.mol^{-1}.s^{-1}$)	termination rate coefficient
$<k_t>$	($L.mol^{-1}.s^{-1}$)	chain-length averaged termination rate coefficient
k_{tc}	($L.mol^{-1}.s^{-1}$)	termination rate coefficient for termination by combination
k_{td}	($L.mol^{-1}.s^{-1}$)	termination rate coefficient for termination by disproportionation
k_{TD}^0	($L.mol^{-1}.s^{-1}$)	rate coefficient of translational diffusion at zero conversion
k_{SD}	($L.mol^{-1}.s^{-1}$)	rate coefficient of segmental diffusion
k_{tr}^{mon}	($L.mol^{-1}.s^{-1}$)	transfer to monomer rate coefficient
k_{tr}^{pol}	($L.mol^{-1}.s^{-1}$)	transfer to polymer rate coefficient
k_{tr}^{sol}	($L.mol^{-1}.s^{-1}$)	transfer to solvent rate coefficient

List of Publications

Santanakrishnan, S., Hutchinson, R. A., Učňová, L., Stach, M., Lacík, I., Buback, M. Polymerization Kinetics of Water-Soluble *N*-Vinyl Monomers in Aqueous and Organic Solution, *Macromolecular Symposia*, **2011**, *302(1)*, 216-223.

Santanakrishnan, S., Tang, L., Hutchinson, R. A., Stach, M., Lacík, I., Schrooten, J., Hesse, P., Buback, M. Kinetics and Modeling of Batch and Semibatch Aqueous-Phase *N*-vinylpyrrolidone Free-Radical Polymerization, *Macromolecular Reaction Engineering*, **2010**, *4(8)*, 499-509.

Stach, M., Lacík, I., Kasák, P., Chorvát, D, Jr., Saunders, A, H., **Santanakrishnan, S.**, Hutchinson, R. A. Free-Radical Propagation Kinetics of *N*-Vinyl Formamide in Aqueous Solution Studied by PLP–SEC, *Macromolecular Chemistry and Physics*, **2010**, *211(5)*, 580-593.

Santanakrishnan, S., Hutchinson, R. A., Stach, M., Lacík, I. Aqueous-phase Copolymerization of *N*-vinylpyrrolidone and *N*-vinylformamide, in preparation.

Santanakrishnan, S., Hutchinson, R. A., Stach, M., Lacík, I. Kinetics and Modeling of Free Radical Aqueous-Phase Polymerization of *N*-vinylimidazole and Quaternized vinylimidazole, in preparation.

Chapter 1. Introduction

Free-radical polymerization (FRP) is an important industrial process used to convert vinyl monomers to polymer products used widely in a variety of fields. The advantages of FRP lies in its higher tolerance of impurities and undemanding reaction conditions compared to ionic or coordination polymerization, allowing for very high molecular weight polymer to be produced,[1] obviating the necessity for rigorous purification of monomers and solvents to remove any traces of impurities. In addition to the production of important commercial homopolymers such as poly(ethylene), poly(styrene), poly(vinyl chloride), etc.[2], this technique can also be used for the copolymerization of multiple monomers resulting in the formation of polymers with properties dependent on the proportion of the monomers.[2]

An important class of free-radical polymers are water-soluble polymers, usually produced via FRP of water-soluble monomers in aqueous solution. These polymers are used in a range of applications, such as pharmaceuticals, hygiene, waste water treatment etc. Industrially important classes of water soluble monomers include carboxylic acids (acrylic, methacrylic acids etc.) and *N*-vinylamides (acrylamide, *N*-vinylpyrrolidone etc.). As will be discussed in Chapter 2, the kinetics of free-radical polymerization of water soluble monomers deviates from expected behaviour due to the influence of monomer concentration on k_p. Although the earlier works by Gromov,[3-6] Senogles and Thomas,[7] and others have shown that solvent medium plays an important role in polymerization kinetics, behaviour and influence of the individual rate coefficients, k_p and k_t could not be ascertained. This made a comprehensive study on the kinetic modeling of the individual monomers, let alone their copolymerization, almost impossible.

Despite the poorly understood polymerization kinetics, functional water-soluble polymers have widespread applications in a variety of growing markets. Thus, companies such as BASF would like to better understand these systems in order to improve control over their existing polymerization processes and to develop new process and product alternatives. The advent and application of specialized kinetic techniques allow for the determination of the individual rate coefficients k_p and k_t, and provide the opportunity to improve understanding of these industrially important aqueous systems. This work, part of a collaborative effort with the research groups of Dr. Buback (University of Göttingen, Germany) and Dr. Lacik (Polymer Institute of the Slovak Academy of Sciences, Bratislava, Slovakia) in cooperation with BASF, describes a systematic experimental study combined with kinetic modeling of batch and semibatch polymerization of water soluble monomers in aqueous and organic solvents. The kinetic models built using Predici make use of newly determined k_p and k_t expressions obtained by specialized experiments from the groups of Dr. Buback and Dr. Lacik. The ability of expressions from independent pulsed-laser polymerization (PLP) studies to represent continuously initiated systems validates their functional form as well as demonstrates the generality of these expressions.

The research work conducted in this doctoral work has been presented in four main chapters as outlined below

- **Chapter 3 - Kinetics and Modeling of Batch and Semibatch Aqueous-Phase *N*-Vinyl Pyrrolidone Free Radical Polymerization.** This chapter, which also includes some experimental work from a previous MSc graduate student,[8] is an updated version of the paper published in Macromolecular Reaction Engineering, 2010, *4(8)*, 499-509. A complete model to represent the behaviour of this system is developed and validated using experiments that

focus on the influence of initial monomer and initiator concentrations on conversion and polymer molecular weight in order to gain a better understanding of the polymerization behaviour under industrially-relevant conditions.

- **Chapter 4 - Polymerization Kinetics of Water-Soluble *N*-Vinyl Monomers in Aqueous and Organic Solution.** This chapter, an updated version of the manuscript published in Macromolecular Symposia, 2011, *302*, 216-223, discusses the experimental study of NVP in organic (butanol) solvent and that of a similar water soluble monomer, *N*-vinyl formamide (NVF) in water. The kinetic model used to represent the behaviour NVP in water (Chapter 3) was extended to these systems by making according changes in the PLP-SEC derived propagation rate expressions. The success of this treatment demonstrates that a generalised understanding of water-soluble monomer can be obtained once their k_p behaviour has been understood.

- **Chapter 5 - Aqueous-Phase Free-Radical Polymerization of *N*-vinylimidazole (NVI) and Quaternized vinylimidazole (QVI). W**hile chapters 3 and 4 investigate the kinetic behaviour of systems with a priori k_p knowledge obtained through PLP-SEC studies, this chapter investigates the behaviour of industrially important monomers for which no PLP-SEC derived k_p expressions have been determined, *N*-vinylimidazole (NVI) and its quaternized form (3-methyl-1-vinylimidazolium methyl sulphate, QVI). Although these monomers have been used in a number of copolymerization studies in the literature, there is no complete study that has investigated both the rate and molecular weight behaviour of the homopolymers. A simple kinetic model is developed for the aqueous-phase polymerization

of NVI and QVI by comparing their batch polymerization behaviour to the well understood NVP and NVF systems.

- **Chapter 6- Aqueous-Phase Free Radical Copolymerization of *N*-vinyl pyrrolidone (NVP) and *N*-vinyl formamide (NVF).** As copolymerization aims at developing polymers with tailor made properties derived from the constituent monomers, controlling the composition is of utmost importance. An understanding of the variation in relative reactivity ratios and reaction rates thereby gives us the flexibility to control the copolymer properties (composition and MW) and rate by varying the relative fractions of the co-monomers and initiator in the feed. This chapter tests the application of the improved knowledge of the homopolymerization behaviour of NVP and NVF to their aqueous-phase copolymerization and the influence of initial monomer and NVP mole fraction (f_{NVP}) in the feed on both rate and polymer molecular weight. A terminal model of copolymerization, combined with the PLP-SEC derived k_p and k_t expressions used in the homopolymerization studies is shown to well represent the experimental data.

References

1) Moad, G.; Solomon, D. H., Ch 7 in *The Chemistry of Radical Polymerization*. Elsevier, Netherlands, **2006**.

2) Hutchinson, R. A., Ch 4 in *Handbook of Polymer Reaction Engineering. Ed.,Meyer, Th., Keurentjes.* Wiley-VCH, Weinheim, **2005**.

3) Barabanova, A. I.; Bune, E. V.; Gromov, V. F. *Vysokomol. Soedin., Ser. A Ser. B*. **2001**, *43*, 732-736.

4) Gromov, V. F.; Galperina, N. I.; Osmanov, T. O.; Khomikovskii, P. M.; Abkin, A. D. *Eur. Polym. J.* **1980,** *16,* 529-535.

5) Bune, Y. V.; Barabanova, A. I.; Bogachev, Y. S.; Gromov, V. F. *Eur. Polym. J.* **1997**, *33*, 1313-1323.

6) Gromov, V. F.; Bogachev, Y. S.; Bune, Y. V.; Zhuravleva, I. L.; Teleshov, E. N. *Eur. Polym. J.* **1991**, *27*, 505-508.

7) Senogles, E.; Thomas, R. *J. Polym. Sci.: Symp.* **1975**, *49*, 203-210.

8) Tang, L., *MSc. Thesis, Queen's University* **2007**.

Chapter 2. Background Information & Literature Review

2.1 Free-Radical Homopolymerization of water soluble monomers

Functional polymers such as poly(acrylamides), poly(*N*-vinyl amides), poly(acrylic acid) and their copolymers find widespread applications in pharmaceuticals,[1] waste water treatment,[2] consumer products, paper manufacturing and cosmetics.[3] These polymers are mostly produced by free-radical aqueous-phase polymerization. Basic free radical homopolymerization mechanisms such as initiation, propagation, termination and transfer are shown in Table 2.1. The growing polymer radicals and dead chains are denoted by *P* and *D* respectively, with subscript n denoting the number of monomer units in the chains. The initiator (*I*) decomposes into two radicals with a initiator efficiency, *f*, which usually ranges between 0.4 - 0.9.[4] Chain initiation and subsequent propagation occurs by the addition of a first monomer unit to the initiator radical followed by successive and rapid addition of monomer units to the growing chain. Termination by coupling of two radicals can result in the formation of either one dead chain (combination, k_{tc}) or two dead chains (disproportionation, k_{td}). Growing radicals can also abstract a H atom from monomer (*M*), solvent or chain transfer agent (*S*) resulting in the formation of a dead chain as well as a new radical that can participate in initiation of new chains.

The polymerization rate is controlled to a great extent by the propagation rate coefficient, k_p, as seen by examining the rate equation for an isothermal free-radical batch polymerization with negligible volume contraction

$$-\frac{d[\mathrm{M}]}{dt} = k_p[\mathrm{M}]\left(\frac{fk_d[\mathrm{I}]}{k_t}\right)^{0.5} \qquad (2.1)$$

assuming radical stationarity.

Substituting

$$[\mathrm{M}] = [\mathrm{M}]_0 \left(1 - x_\mathrm{p}\right) \tag{2.2}$$

where $[\mathrm{M}]_0$ is the initial monomer concentration and x_p is the fractional conversion of monomer at any instant, eq (2.1) becomes

$$\frac{dx_\mathrm{p}}{dt} = k_\mathrm{p}\left(\frac{fk_\mathrm{d}[\mathrm{I}]}{k_\mathrm{t}}\right)^{0.5}\left(1 - x_\mathrm{p}\right) \tag{2.3}$$

According to eqn. (2.3), conversion profiles should have the same initial slope for polymerizations carried out at identical [I], independent of $[\mathrm{M}]_0$, provided there is no variation in rate coefficients with initial conditions. This is the case for the polymerization of methyl methacrylate (MMA) and other common monomers in organic solvents.[5] However, in aqueous-phase polymerization of water soluble monomers, such as methacrylic acid (MAA) and *N*-vinyl pyrrolidone (NVP), the rate of monomer conversion is significantly influenced by the initial monomer concentration, with an increased slope seen for experiments run with lower $[\mathrm{M}]_0$, as will be discussed later.

Table 2.1. Basic mechanisms in free radical homopolymerization[4]

Initiator Decomposition	$I \xrightarrow{k_d} 2 f I^{\bullet}$
Chain Initiation	$I^{\bullet} + M \xrightarrow{k_i} P_1$
Chain Propagation	$P_n + M \xrightarrow{k_p} P_{n+1}$
Chain Termination	
By Combination	$P_n + P_m \xrightarrow{k_{tc}} D_{n+m}$
By Disproportionation	$P_n + P_m \xrightarrow{k_{td}} D_n + D_m$
Chain Transfer	
To Monomer	$P_n + M \xrightarrow{k_{tr}^{mon}} D_n + M^{\bullet}$
	$M^{\bullet} + M \xrightarrow{k_i^{mon}} P_1$
To Solvent	$P_n + S \xrightarrow{k_{tr}^{sol}} D_n + S^{\bullet}$
	$S^{\bullet} + M \xrightarrow{k_i^{sol}} P_1$

The understanding of these aqueous-phase processes has lagged behind that of free-radical polymerization in organic solvents due to the influence of water on the polymerization kinetics. Some of the earlier studies included those of Shoaf and Poehlein on the influence of degree of neutralisation on rate of polymerization of MAA,[6] while the study of Cutié et al. examined the polymerization behaviour of acrylic acid.[7] Gu et al. studied the polymerization of *N*-vinyl formamide in bulk and dilute systems.[8] Gromov and co-workers have extensively studied the

kinetics of polymerization and copolymerization of acrylamide and its derivatives in water-solvent mixtures[9-12] as well as the hydrophobic interactions arising in the aqueous solutions containing their polymers.[12] Acrylamide derivatives exhibit faster rates in aqueous phase compared to organic phase polymerization (DMSO and formamide) and also at higher water concentrations in mixed solvents.[10] Gromov explained his observation through monomer-solvent interactions, which disrupt monomer-monomer (dimer) interactions; the participation of the single molecules is favoured over dimers.[10] He also discussed the formation of active radicals, as in the case of acrylamide in water, where water donates a proton resulting in the localisation of the unpaired electrons on nitrogen to form active radicals with higher reactivity,[11] and the formation of donor-acceptor complexes between polymer radicals and solvents that have high donor capabilities such as DMSO, which reduces radical reactivity causing a subsequent decrease in polymerization rate.[10] However, these explanations could not be extended to behaviour in mixed solvents, as a small addition of organic solvent does not significantly influence the extent of dimerization or formation of active acrylamide radicals. Therefore, the behaviour in mixed solvents was explained by the polymer coil density which increases with increase in organic solvent concentration, impacting the accessibility of polymer radicals to monomers and resulting in a decrease in k_p.[10] In another study, Chapiro claimed that in addition to dimers, some monomers also existed as plurimolecular aggregates and that the ability of solvents to associate or dissociate these aggregates influenced both homopolymerization and copolymerization kinetics.[13] A study on NVP by Senogles and Thomas showed solvent polarity to have a significant influence on the polymerization of NVP and also observed NVP to exhibit faster rate in aqueous phase compared to bulk.[14] Rate increased with an increase in concentration of water up to about 25% by volume, followed by a decrease in rate with further increase in

water concentration. This behaviour was explained by the formation of reactive complexes between NVP and water, reaching a maximum at 75% by volume NVP, after which monomer dilution led to decreased rate.

The varied, and sometimes contradicting, explanations offered in the earlier studies about these kinetic peculiarities were predominantly due to the non-availability of independent values of rate coefficients. This situation is starting to change with the advent and application of reliable techniques such as PLP-SEC (Pulsed Laser Polymerization – Size Exclusion Chromatography) and SP-PLP (Single Pulse – Pulsed Laser Polymerization).[15] The PLP-SEC method allows for determination of k_p by laser initiated polymerization followed by SEC analysis of the resulting polymer and the SP-PLP technique allows for determination of k_p/k_t by tracking the subsequent conversion of monomer by near infrared spectroscopy after initiation by a single laser pulse.

MAA is similar to the industrially important acrylic acid with fewer complications (i.e. no backbiting), making it an ideal choice for kinetic studies. The first PLP study on MAA conducted by Beuermann and co-workers focused on the influence of the monomer-dimer equilibrium on k_p of MAA.[16] FTIR spectroscopy was used to determine the extent of dimerisation in different solvents and at varying monomer concentrations in methanol. The influence of monomer concentration in methanol was reported to be within experimental uncertainties and was neglected. Interestingly, the variation in k_p was minor compared to the differences in the monomer-dimer equilibrium observed in the different solvents studied. It was therefore concluded that the variation in overall rates in different solvents cannot be solely attributed to the extent of dimerisation. Kuchta et al. investigated the influence of temperature and monomer concentration on propagation kinetics of MAA in water, DMSO and methanol.[17]

The significantly lower activation energy in water and the higher frequency factor in DMSO were attributed to the extent of dimerization and monomer – solvent complex formation, respectively. As for the influence of monomer concentration, dilution of the reacting system with water, from bulk conditions (~12 mol/L) down to about 8 mol/L, resulted in negligible changes in k_p. Beyond this point there was a significant increase in k_p as monomer concentration was decreased. As the influence of monomer concentration was deemed negligible in a previous study in methanol,[16] this behaviour could not be explained by just the change in extent of dimerisation, making it clear that there were other considerations that required further investigation in this area.

Following this, Beuermenn et al. investigated the influence of both monomer concentration and the degree of ionization (α) on MAA propagation kinetics in aqueous solution over a wide range of temperature.[18-20] Both monomer concentration and degree of ionisation were observed to influence k_p, as shown in Figure 2.1. PLP experiments conducted in the temperature range of 20 to 80 °C showed k_p to decrease by almost one order of magnitude as the monomer concentration was changed from very dilute (1 wt% MAA) to bulk system.[19] This enormous change in k_p could not be explained by any of the existing explanations in terms of dimerisation, difference in bulk and local monomer concentrations or specific association of MAA to poly(MAA). Kinetic explanation based on the decrease in $E_a(k_p)$ with increase in MAA content was also ruled out, as the Arrhenius fit to the k_p data above 5 wt% MAA demonstrated $E_a(k_p)$ to be almost constant in this concentration range. This dependence, a behaviour uniquely observed in water soluble systems, has been attributed to the interaction between the transition structure (TS) for propagation and the surrounding environment which hinders the conformational mobility of the TS in the presence of increased monomer concentration, thereby affecting its free rotation.[19-21]

The resistance to free rotation decreases with reduced monomer concentration, thus causing an increase in k_p with increasing dilution (or increasing conversion in a batch reaction). A follow-up study[22] was conducted to investigate the influence of conversion on k_p by simulating high conversion levels by adding poly(MAA) in addition to low levels of conversion achieved via the PLP technique. The study also investigated the influence of replacing a portion of MAA with isobutyric acid (the saturated analogue of MAA) which was considered to be polymer of chain length unity, keeping the overall carboxylic acid group content at 20 wt% in both cases. Isobutyric acid was observed to have the same influence as MAA while the addition of poly(MAA) did not influence the k_p value, demonstrating that the polymer coils were incapable of penetrating the intra coil environment while the acids were capable of penetrating the environment thereby hindering the conformational mobility of the TS for propagation. This study made it clear that k_p will increase with conversion of monomer to polymer in a batch polymerization. Degree of ionization (α) had a similar influence on k_p as monomer concentration. The influence of α was more pronounced at low initial MAA concentration $\left(w_{MAA}^0\right)$ of about 5 wt% and became weaker at higher w_{MAA}^0. The same was also true of the influence of monomer concentration on k_p of partially and fully ionized MAA. The influence of MAA content was most pronounced at α=0 (non-ionized) and gradually decreased with increasing α with almost a slight increase in k_p at α=1 (fully ionized), as shown in Figure 2.1.[19] The influence of both monomer concentration and degree of ionization is explained in terms of decrease in $A(k_p)$ caused by a decrease in the conformational mobility of the TS from intermolecular interactions with the surrounding environment via hydrogen bonds or ionic interactions.[19]

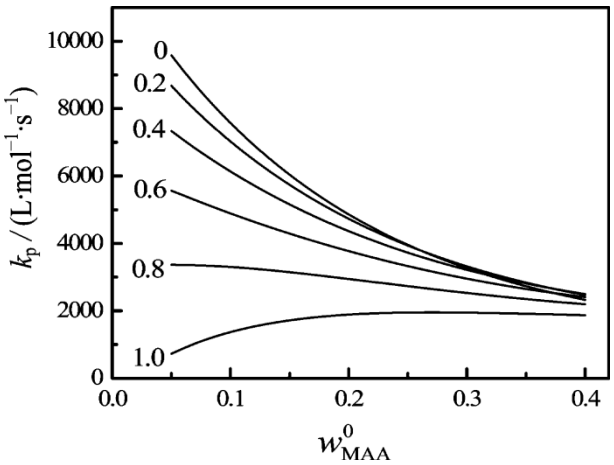

Figure 2.1. Variation of k_p of MAA in water at various degree of ionization (α) and initial weight fractions of MAA in water (w^0_{MAA}), at 50 °C.[19]

Other aqueous-phase PLP studies include those on non-ionized[23] and ionized[24] AA by Lacik et al. Similar to MAA, the k_p of non-ionized AA also showed a decreasing trend with increasing monomer concentration beyond 3 wt%. However, the k_p showed an increasing trend in the initial range of up to 3 wt% AA. This strange behaviour was explained by considering the two regions (c_{AA} < 3 wt% and c_{AA} > 3 wt%) individually. The region (c_{AA} < 3 wt%), where k_p was observed to decrease with decrease in AA concentration was explained by the specific association of AA to poly(acrylic acid) and macroradicals, which becomes negligible at concentrations beyond 5 wt%. The decrease in k_p with increasing AA concentration beyond 3 wt% was explained by the decrease in solvent quality with increasing AA concentration, enhancing the intra-segmental interactions between monomers and decreasing k_p. The influence of carboxylic acid groups on solvent quality was confirmed by replacing portions of AA with propionic acid and also by the addition of NaCl to aqueous solutions of AA. These studies showed that propionic acid influenced k_p to a similar extent as AA, and the salt had no influence on k_p. Ionization of AA caused its k_p to decrease by almost one order of magnitude as the degree of ionization (α) was increased from 0 to 1 with a steep increase with further addition of NaOH to fully ionized AA.[24]

A PLP-SEC study on NVP[21] showed the k_p of NVP to behave in a similar manner to MAA, with respect to concentration in water. Here again, the addition of N-ethyl-2-pyrrolidone (NEP) (saturated analogue of NVP) had a similar effect on k_p as did NVP, while replacing NVP by poly(NVP) enhanced the k_p values significantly confirming the increase in k_p with increasing monomer conversion (or increasing dilution), as shown in Figure 2.2. These results confirmed the observations made for methacrylic acid. Most recently a PLP-SEC study on the free-radical propagation kinetics of *N*-vinyl formamide (NVF) was conducted in aqueous-phase by Stach et al.[25] The study was conducted at varying initial monomer concentrations ranging from 3wt% to bulk over a temperature range of 5 - 60 °C. Similar to NVP and MAA, the k_p of NVF showed an increase with decreasing monomer concentration, which was again attributed to the hydrogen bonding between the transition structure for propagation and water which reduces the hindrance to internal mobility of the transition structure thereby reducing the activation energy barrier and thereby increasing k_p.[25] A comparison of the k_p behaviour for NVP, MAA and NVF is shown in Figure 2.3.[25] Although, the three monomers exhibit a decrease in k_p with increasing monomer concentration, the magnitude of variation of k_p with monomer concentration is different for the three monomers despite the similarity of their bulk k_p values. NVP, MAA and NVF exhibited a 20-fold, 8-fold and 6-fold increase, respectively, as the monomer concentration was change from bulk to very dilute monomer concentrations.[25] Also, the difference between the MAA and NVF k_p values were only significant in the lower monomer concentration range of up to 20 wt%, with the values becoming very similar at higher concentrations. These differences in the k_p of NVP in comparison to that of NVF and MAA were explained in terms of the structures of the monomers which in turn influences their ability to hydrogen bond among themselves and with water. NVP, being a cyclic amide, has the tendency to strongly hydrogen-bond with water, while, both MAA

and NVF have the tendency to hydrogen bond both among themselves as well as with water. As a result the intermolecular hydrogen bonding between the monomer units compete with the hydrogen bonding between the TS structure for propagation and water in the case of NVF and MAA, which leads to a decrease in the extent of interaction between the TS structure for propagation and water in these monomers. This explains the much higher magnitude of variation in NVP over NVF and MAA as well as the similarity in the k_p profiles of NVF and MAA.[25] These studies make it clear that the ability of water-soluble monomer to undergo dipole and hydrogen bonding interactions with themselves and the surrounding solvent environment has a significant influence on their propagation behaviour.

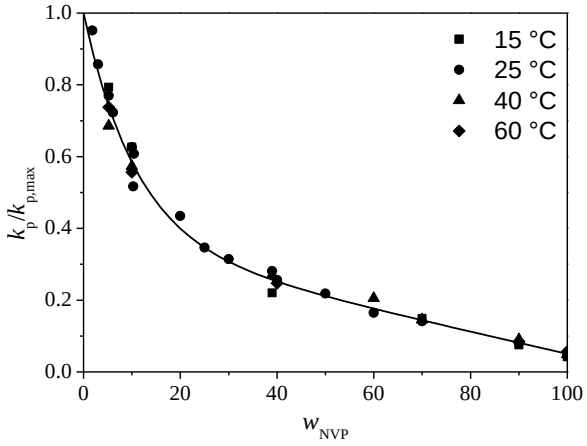

Figure 2.2. The influence of *N*-vinyl pyrrolidone concentration (w_{NVP}) in aqueous solution on its propagation rate coefficient (k_p) ratio to $k_{p,max}$, the k_p value estimated at infinite dilution for each temperature.[21]

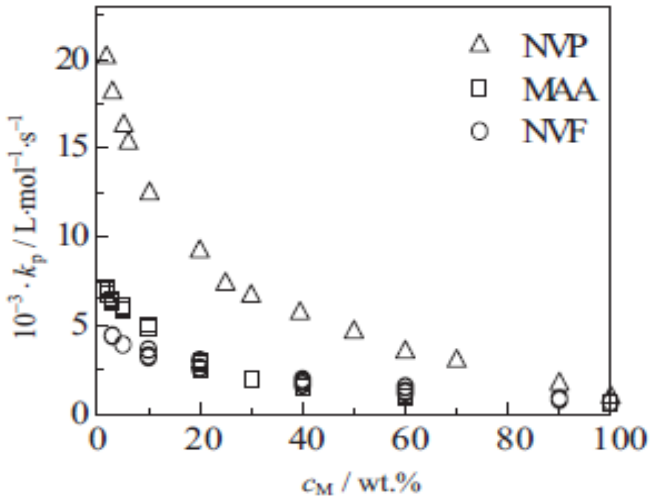

Figure 2.3. The influence of monomer concentration (c_M) in aqueous solution on its propagation rate coefficient (k_p), at 25 °C.[25]

Termination rate coefficient, k_t

In addition to these k_p studies, SP-PLP coupled with near-IR has been used to study the termination kinetics of non-ionized MAA in aqueous solution.[26] Once the non-idealities in k_p due to the presence of solvent effects were accounted for, the variation of k_t with conversion for MAA was similar to that found for methacrylates in organic solvents, with the k_t being controlled by segmental diffusion (SD) at low conversion levels of up to about 20%, followed by translational diffusion (TD) and reaction diffusion (RD) at high conversion levels, as shown in Figure 2.4.[26] Buback et al.[27] have modeled the kinetics of chemically initiated batch polymerization of non-ionized MAA at 50 °C in aqueous phase using a conversion dependent k_p and a functional form in terms of segmental, translational and reaction diffusion terms for k_t. More recently, Schrooten et al.[28] have applied the SP-PLP technique to the study of NVP termination kinetics in aqueous solution, over an initial NVP weight fraction range of 20 wt% to bulk at 40 °C and 2000 bar. The conversion dependence of the chain length averaged k_t at varying NVP weight fractions is shown in Figure 2.5.[28] The termination behaviour for NVP at

high monomer weight fractions was explained in terms of segmental diffusion control in the initial stages up to a conversion of ~12%, followed by translational diffusion resulting in a decrease in $<k_t>$ by almost an order of magnitude followed by reaction diffusion control at very high viscosities that were achieved only in systems of very high monomer concentrations. So, the k_t behaviour at the higher monomer concentrations was given by eqn. 2.4[28]

$$< k_t >= \frac{1}{\left[\frac{1}{k_{SD}} + \frac{\eta_r}{k_{TD}^0}\right]} + C_{RD}(1 - x_p)k_p \qquad (2.4)$$

where, k_{SD} is the rate coefficient of segmental diffusion, k_{TD}^0 is the rate coefficient of translational diffusion at zero conversion, η_γ is relative bulk viscosity, C_{RD} is the reaction diffusion constant and x_p is the monomer conversion. However, at lower monomer concentrations of up to 40 wt%, the termination rate coefficient for NVP was observed to be predominantly segmentally-controlled, as is demonstrated by the relatively flatter profiles at 20 and 40 wt% in Figure 2.5.[28] Similar to MAA, a clear dependence of the k_t on initial weight fraction of NVP was also observed.[28] So, at low monomer concentrations, the k_t for NVP was described by just segmental diffusion (SD), as a function of initial NVP weight fraction as shown in our publications on the kinetic modeling of NVP.[29]

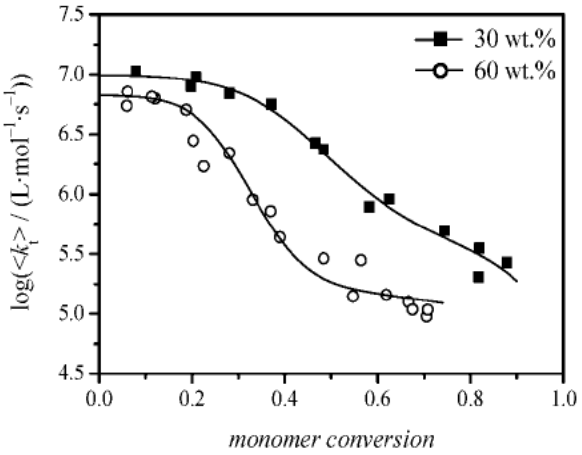

Figure 2.4. Conversion dependence of the chain-length averaged termination rate coefficient, <k_t> for MAA polymerization at 50 °C , 2000 bar, and initial monomer concentration of 30 and 60 wt% MAA.[26]

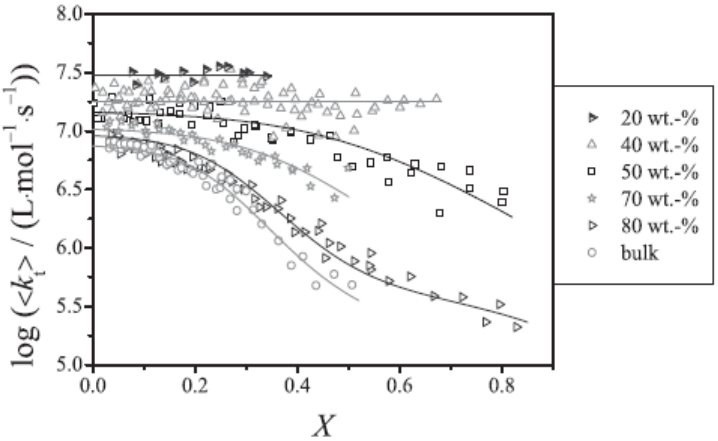

Figure 2.5. Conversion dependence of the chain-length averaged termination rate coefficient, <k_t> for NVP polymerization at 40 °C , 2000 bar, and initial monomer concentrations of 20 wt% to bulk, in aqueous solution.[28]

Other important water soluble *N*-vinyl monomers include *N*-vinylimidazole (NVI) and its quaternized form (QVI). *N*-vinylimidazole finds application as reactive diluent for UV coatings, UV inks, UV adhesives and general coatings. It is also used as a monomer for water soluble specialty polymers and copolymers.[30] However, there are very few studies that address the polymerization kinetics of NVI and almost none on its quaternized form. Some of the earlier studies on NVI include that by Bamford and Schofield[31] on the free-radical polymerization of *N*-vinylimidazole in ethanol, *N*-*N*-dimethylformamide (DMF), water and in bulk conditions. The rate in ethanol was observed to reach zero-order dependence in monomer at moderately high monomer concentrations. This unusual behaviour was explained by a degradative reaction between the propagating radicals and monomer, which occurs as a result of the addition of the propagating radical to the second position of the monomer resulting in the formation of a resonance stabilized radical, as shown in Scheme 2.1.

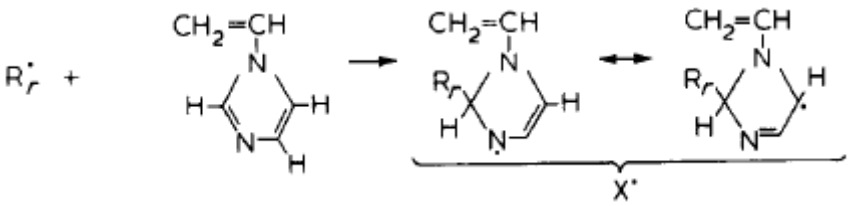

Scheme 2.1. Degradative addition of the propagation radical to the 2-position of NVI resulting in the formation of a resonance stabilized radical.[31]

This was verified by studying the polymerization of 2-methyl-1-vinylimidazole, wherein higher polymerization rates were observed due to the prevention of the degradative addition in this monomer as the 2-position of the monomer is blocked by a bulky methyl group. The polymerization of NVI in bulk was heterogeneous with a steady increase in rate, which was attributed to the radical occlusion by the precipitated polymer, while the polymerization curves in DMF were similar to that in ethanol, except with higher rates. The polymerization in water

showed strong NVI water interactions, with a maximum in rate observed at a monomer concentration of 8.5 mol/L, where water and monomer were present in approximately equal concentrations. This complexation between NVI and water was also verified by a maximum in the viscosity of the NVI-water mixture at this monomer concentration. A significant pH influence was also observed in water, with rates assuming a plateau profile in the pH region of ~8-6, followed by an increase up to a pH of 3.5, below which the pH assumes plateau profile. This study by Bamford was the first to give a reasonable explanation for unusual kinetic behaviour of NVI. Following this, there were a few other studies on NVI that supported Bamford's proposition of degradative addition mechanism. This includes the study on the photo-initiated polymerization of NVI by Joshi et al.,[32] where a 1-order dependence of rate on monomer at low monomer concentrations was followed by a plateau or even a decrease at higher monomer concentration of ~1-4 mol/L. They attributed this behaviour to be a consequence of the degradative chain addition proposed by Bamford. Soon after, Dambatta et al.[33] studied the free radical polymerization of NVI in ethanol, methanol and DMF using benzoyl peroxide and azoisobutyronitrile initiators; they found NVI to exhibit a rate dependence of 1 and 0 orders with respect to monomer at low and high monomer concentrations, respectively. Here again, the behaviour was attributed to Bamford's degradative addition mechanism. For quite some time, Bamford's mechanism of degradative addition was the only explanation in literature for the unusual kinetic behaviour of NVI. This changed when Chapiro[34] studied the polymerization of NVI in water, methanol, benzene, carbon tetrachloride (CCl_4) and bulk and observed all the systems studied to exhibit auto-acceleration behaviour, which was attributed to the molecular association between NVI and the solvents in case of the homogeneous systems. The molecular associations with water and methanol were verified by viscosity and refractive index

measurements. A plot of the rate with monomer concentration showed linear relationship at low monomer concentrations and a drop to zero or negative (in water and CCl_4) at higher monomer concentrations. Although this zero-order monomer dependence at high monomer concentrations was in agreement with Bamford's[31] findings, Chapiro disagreed with the occurrence of degradative addition to the monomer claiming degradative addition would result in the accumulation of unreactive radicals eventually decreasing the reaction rate, instead of the observed auto-acceleration. He instead proposed that the participation of the internal double bonds would lead to NVI behaving like a bi-functional monomer to form cross-linked polymer in all the cases, even though cross-linked gel was observed only at high monomer concentrations and in non-solvents to polymer. All these results led Chapiro to propose transfer to polymer, wherein the propagating chains interact with the internal double bond of the accumulated polymer, as shown in Scheme 2.2. Although this proposition of chain transfer to polymer explains the gelling observed in some of the cases, it fails to explain the low reaction order with respect to monomer. A more recent study by Arosio et al.[35] on the precipitative copolymerization of NVP and NVI in butyl acetate accepted Chapiro's proposed mechanism of transfer to polymer. They used Chapiro's mechanism to explain the tailing in the high molecular weight region of the molecular weight distribution (MWD), which they think is an indication of the presence of a large number of high molecular weight chains, most likely the result of chain transfer to accumulated polymer. It may be that both of these explanations by Bamford[31] and Chapiro[34] play a role in the unusual kinetic behaviour, with both degradative addition to monomer as well as transfer to polymer being important mechanisms in the free radical polymerization of NVI.

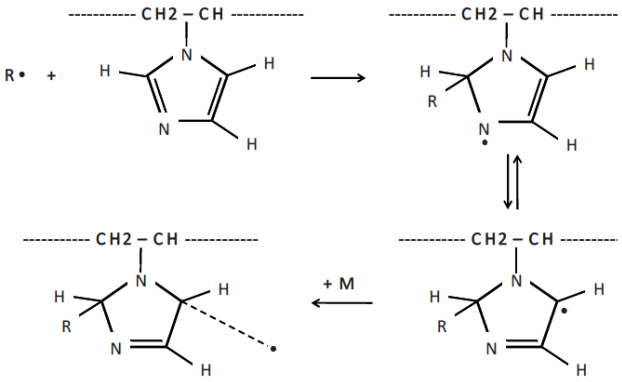

Scheme 2.2. Transfer to polymer in NVI polymerization, proposed by Chapiro.[35]

2.2 Free-Radical Copolymerization of water soluble monomers

The basic mechanisms in typical free radical copolymerization according to the terminal model are shown in Table 2.2. The subscripts i and j denote monomer type M_i and M_j, and the subscripts n and m denote the number of monomer units in the chains, with terminal monomer units on radical P_n indicated by superscript i or j.

Table 2.2. Basic mechanisms in free radical copolymerization according to the terminal model[4]

Initiator Decomposition	$I \xrightarrow{k_d} 2 f I^{\bullet}$
Chain Initiation	$I^{\bullet} + M_j \xrightarrow{ki_j} P_1^{\,j}$
Chain Propagation	$P_n^i + M_j \xrightarrow{kp_{ij}} P_{n+1}^j$
Chain Termination	
By Combination	$P_n^{\,i} + P_m^{\,j} \xrightarrow{ktc_{ij}} D_{n+m}$
By Disproportionation	$P_n^{\,i} + P_m^{\,j} \xrightarrow{ktd_{ij}} D_n + D_m$
Chain Transfer	
To Monomer	$P_n^{\,i} + M_j \xrightarrow{ktr_{ij}^{mon}} D_n + P_1^{\,j}$
To Solvent	$P_n^{\,i} + S \xrightarrow{ktr_i^{sol}} D_n + S^{\bullet}$
	$S^{\bullet} + M_j \xrightarrow{ki_j^{sol}} P_1^{\,j}$

Several models such as the terminal model, penultimate model and a few higher order models have been developed over the past years in order to explain the copolymerization behaviour of monomers. The applicability of a model to a system depends on the validity of the assumptions of the model for that particular system.[36] The terminal model, being the simplest model, has been widely used to describe the behaviour of a number of copolymerization systems. The copolymer composition based on the terminal model, is given by Mayo Lewis equation (eqn. 2.5)

$$F_{p1}^{inst} = \frac{r_1 f_1^2 + f_1 f_2}{r_1 f_1^2 + 2 f_1 f_2 + r_2 f_2^2} \tag{2.5}$$

where, f_1 and f_2 are the mole fractions of M_1 and M_2 in the monomer mixture. The reactivity ratios, r_1 and r_2, the ratio of the rate at which a monomer reacts with itself relative to the rate at which it reacts with the co-monomer, are given by

$$r_1 = \frac{kp_{11}}{kp_{12}} \text{ and } r_2 = \frac{kp_{22}}{kp_{21}} \tag{2.6}$$

where, kp_{ij} represents the addition of monomer j to radical i. The propagation rate coefficient for copolymerization, k_p^{cop} based on the terminal model, is given by

$$k_p^{cop} = \frac{r_1 f_1^2 + 2 f_1 f_2 + r_2 f_2^2}{(r_1 f_1 / kp_{11}) + (r_2 f_2 / kp_{22})} \tag{2.7}$$

However, several studies over the past years have questioned the applicability of the terminal model to a number of systems where the terminal model gives a good representation of the copolymer composition but fails to capture the propagation behaviour of the copolymerization system.[36] This led to the introduction of the implicit penultimate model wherein the composition behaviour is represented by the terminal model and the propagation is described by a non-terminal model equation. It has been argued that the implicit penultimate model is not correct theoretically, and that a full explicit model should be used.[36] Nonetheless, as most experimental copolymer composition data are well represented by the terminal model, the implicit penultimate model is used to provide a representation of copolymer composition and rate for a wide range of systems. In addition, most "conventional" monomers (not soluble in water) exhibit negligible change in copolymerization behaviour with solvent choice. The full penultimate model is more often used to describe the copolymerization of systems involving polar monomers such as acrylonitirile, maleic anhydride, vinyl chloride etc., where $r_{ABA} \neq r_{BBA}$ and/or $r_{BAB} \neq r_{AAB}$.[5]

Although, the terminal model fails to describe the behaviour of some systems, it is to be noted that the model is simple and suitable for cases where both co-monomers have very similar reactivity ratios.[36]

Copolymerization of water soluble monomers has gained very little attention compared to the specialized techniques that have been employed to study their homopolymerization kinetics. Some of the earlier studies that have explored solvent effects on copolymerization include that of Navolokina et al.[37] on the copolymerization of methacrylic acid (MAA) and methyl methacrylate (MMA) in different solvents such as dioxane-water mixture, dimethyl sulfoxide (DMSO), acetic acid and toluene. The reactivity ratios of MAA (r_1) and MMA (r_2) were estimated to be r_1=0.46±0.07 and r_2=0.77±0.2 in dioxane-water, r_1=0.23±0.03 and r_2=0.78±0.14 in DMSO, r_1=0.78±0.05 and r_2=0.08±0.06 in acetic acid and r_1=0.6±0.02 and r_2=0.13±0.05 in toluene. The variation of the instantaneous copolymer composition with conversion in the different solvents at varying initial molar ratios of MAA and MMA in the monomer mixture is shown in Figure 2.6.[37] The authors attempted to explain the changes in reactivity ratios in terms of the specific associations of MAA with the different solvents, but, the paper lacks clarity and fails to successfully explain the contradicting results.

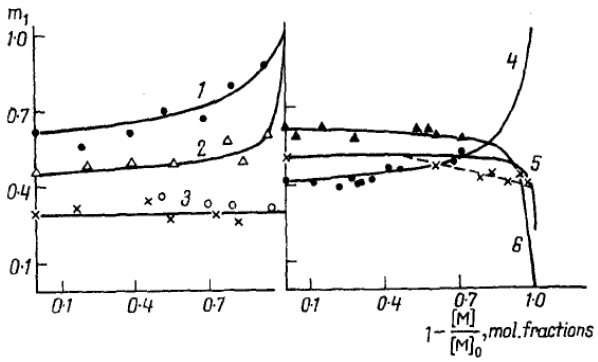

Figure 2.6. Instantaneous composition for the MAA-MMA copolymer as a function of conversion in the different solvents at varying MAA:MMA molar ratios of (1) 70:30 in dioxane-water (2) 50:50 in dioxane-water (3) 30:70 in dioxane-water (4) 50:50 in DMSO (5) 50:50 in acetic acid (6) 57:43 in toluene. The symbols and lines represent experimental and predicted profiles using the reactivity ratios respectively. The broken line indicates the deviation of experimental data from curve 5 obtained by calculation on the assumption that r_1 and r_2 are unchanged.[37]

Stahl[38] conducted a similar study on the copolymerization of MMA and AA in solvents with varying polarity and ability to form hydrogen bonds. Stahl has shown the incorporation of AA into the copolymer to be favored in non-polar, non-hydrogen bonding solvents like toluene and benzene, while a lower AA incorporation was found in solvents like isopentyl acetate and ethyl acetate which are non-polar but H–bonding solvents, with the lowest incorporation observed in t-butyl alcohol, a polar H-bonding solvent. However, as most cases studied by Stahl resulted in heterogeneous mixtures, the accuracy and applicability of these results is questionable. Endo et al.[39] have studied the copolymerization of NVP and MAA in methylene chloride and DMF mixtures and have shown both the rate and copolymer composition to be influenced by solvent polarity. However, a similar study by Chapiro et al. on the copolymerization of NVP with AA and MAA,[40] resulted in contradictory results, as the formation of strong intermolecular complexes between the carboxylic acids and NVP was shown to have a negligible influence on copolymer composition. This study also demonstrated negligible solvent effects and a higher reactivity of MAA with respect to NVP compared to AA. Cabaness et al.[41] have shown the

reactivity ratios of AA and acrylamide to decrease and increase, respectively, with increasing pH. Chapiro showed the incorporation of acrylamide to be lower in solvents that had a tendency to associate with the monomer in the copolymerization of acrylamide and acrylonitrile.[13] Chatterjee[42] established that in the copolymerization of acrylamide and NVP in glycerol-water mixtures, a higher concentration of glycerol favored incorporation of acrylamide. He also demonstrated that the increase in the reactivity of acrylamide was much higher than the decrease in the reactivity of NVP with increasing glycerol concentration, making it clear that the favorable incorporation of acrylamide was governed by other factors as well.

Interpretation of copolymerization systems cannot be made solely from the homopolymerization kinetics of the respective monomers as the composition of the resulting copolymer is governed by binary reactivity ratios. The reactivity ratios in turn can be influenced to a great extent by the reaction medium. The understanding of solvent effects on copolymerization kinetics therefore plays an important role in the kinetic understanding of the copolymerization behaviour of monomers. Some of the commonly known factors that influence the copolymerization behaviour of a system are discussed in the review by Barner-Kowollik et al.,[36] as summarized below:

Solvent polarity – This becomes important in cases when charge-transfer stabilisation of the transition structure is possible via polar interactions. In such cases, depending on the polarity of the reacting species, the extent to which the solvent polarity can affect the polar interactions and their subsequent effects on propagation can vary. The complexity of this effect is therefore to a great extent influenced by whether the solvent polarity remains constant or varies with the monomer mixture composition. In cases where the monomers have very similar dielectric constants such as in the bulk copolymerization of styrene and methyl methacrylate, the polarity of the reaction medium will be independent of the monomer mixture composition and as a result

the reactivity ratios tend to be the same irrespective of the monomer mixture composition. However, in cases such as the bulk copolymerization of styrene and acrylonitrile, which have very different dielectric constants the polarity of the reaction medium and as a result the reactivity ratios of the co-monomers tend to vary as a function of the monomer mixture composition.

Radical – Solvent complex **–** The solvent in some cases may interact with the radicals forming radical-solvent complexes, which are usually more stable than their free-radical counterparts. This is a reasonable assumption considering that it is most likely this stabilisation that drives the complexation in the first place. As a result, it is expected that these stabilized radicals in most cases do not participate in subsequent propagation or do so at a much lower rate. However, in cases where the complexing agent is one of the co-monomers, the complexed radical may propagate at a much faster rate if propagation via the complexed radical turns out to be the more energetically favoured option.

Monomer-solvent complex **–** The solvent can also interact with one of the monomers resulting in the formation of monomer-solvent complex which will in turn propagate at an altered rate in comparison to the monomer itself. The speed of propagation of this complex will again vary depending on whether or not the complexation provides an energetically-favoured pathway for propagation. Thus, the subsequent propagation of this complex will vary depending on whether the complexing agent is the added solvent or the co-monomer. In the event that the complexing agent is the added solvent, the complexed monomer may propagate at an altered rate or may not participate in subsequent propagation thereby affecting the free monomer concentration. Similarly, when the complexing agent is the co-monomer and the formed complex doesn't

participate in subsequent propagation, the overall free monomer concentration is affected. However, when the formed co-monomer complex can participate in subsequent propagation, there are two different possibilities. The complex can either propagate as a single entity in which case both monomers are incorporated into the copolymer or the complex can dissociate during the propagation step resulting in the incorporation of just one of the monomers. Either way, the propagation of a formed co-monomer complex is competitive to the propagation of the free monomer.

Bootstrap effect – Monomer partitioning resulting in differences between the bulk and local monomer concentrations is commonly referred to as bootstrap effect. A number of different factors can contribute to bootstrap effect. The formed radical-solvent or monomer-solvent complexes may not participate in subsequent propagation thereby affecting the monomer and radical concentrations resulting in bootstrap effect. Preferential sorption of one of the co-monomers to the growing or dead polymer in a bulk system may also result in bootstrap effect. This is mainly the case when one of the co-monomers is a poor solvent for the formed polymer. Additionally, bootstrap effect can also arise as a result of preferential solvation of the active chain end over the entire polymer chain by one of the co-monomers. In all the cases, the result is a difference between the bulk and localized monomer concentrations which in turn affects the propagation step accordingly.

Solvent effects generally tend to be more pronounced on hydrogen bonding monomers as is the case with most water soluble monomers.[5] It therefore becomes important to better understand these underlying solvent effects in order to understand the copolymerization kinetics of water soluble systems.

The relatively fewer number of studies, compared to homopolymerization and the difficulties associated with these water-soluble monomers have made it difficult for authors to come up with consistent explanations for the unusual copolymerization kinetics of water soluble monomers. Moreover, no one has looked simultaneously at composition and rate to examine these effects. It is therefore of interest to explore both the rate and composition behaviour of the copolymerization of water-soluble monomers especially in light of the improved understanding of the homopolymerization behaviour of these monomers.

2.3 Size Exclusion Chromatography

Size exclusion chromatography (SEC) is widely used for the analysis of polymer molecular weight. The principle of SEC is the separation of molecules based on differences in their molecular hydrodynamic volume by passing the sample dissolved in a suitable solvent through columns filled with porous packing material. Subsequently, an eluent (usually the solvent used to dissolve the sample) is passed through the columns and the molecules elute out in the descending order of their size.[43] Although SEC has been widely used for quite some time now, aqueous SEC of synthetic water-soluble polymers is a relatively less explored field. Only after the invention of high efficiency, high-speed silica and cross-linked synthetic hydrophilic gel packed columns by Toyo Soda Co. in 1980 was aqueous SEC of water-soluble synthetic polymers made a possibility.[44]

SEC calibration – As the data from SEC is relative to a standard and not absolute, the technique calls for calibration with polymer standards or the use of an online light scattering detector.[43] The SEC system can be calibrated by a few different methods. A relatively simple approach is the use of a series of narrow (PDI < 1.1) molecular mass distribution (MMD) calibrants and plotting

their elution volume or time against their molar masses. Alternately, a broad MMD calibrant can be used and this works best when the calibrant has been well characterized.[45] However, in either of these approaches, the limited availability of polymer types with narrow or broad MMD is a limiting factor. The alternate and most widely used approach is the universal calibration. Here, the objective is to relate the elution behaviour of polymers of differing composition to their hydrodynamic volume. This method assumes that the Mark Houwink parameters of the polymer and calibrant can be related by eqn. 2.8

$$\log[\eta]_p \bullet M_p = \log[\eta]_{pc} \bullet M_{pc} \tag{2.8}$$

However, the applicability of the universal calibration calls for a number of assumptions as well as appropriate testing on the Mark-Houwink parameters used.[43]

SEC detectors – SEC detectors can be classified into two main categories – concentration sensitive detectors and molar mass sensitive detectors.[46] The concentration sensitive detectors are further classified into detectors that are sensitive to the bulk property of the mobile-phase such as refractive index (RI), viscosity etc.[47] These are usually considered universal as all polymers change the refractive index and viscosity of the solvent they are dissolved in although these changes may be small. The other class of concentration sensitive detectors is those that are sensitive to solvent-specific property such as ultraviolet and infrared. Although these usually have much better sensitivity and better signal-to-noise ratio, these detectors can only be used with polymers that absorb radiation at wavelengths specific to the operable range of the detectors.[47] The molar mass sensitive detectors give the molar mass of each fraction of a polymer peak and as their response depends on both concentration and molar mass of the fraction, they have to be combined with a concentration sensitive detector.[46] Some of the commonly available molar mass sensitive detectors include light scattering, which give the absolute MMD directly

and differential viscometers, which give the intrinsic viscosity distribution from which the MMD can be determined using the universal calibration.[46] The remainder of this section will only focus on RI and light scattering detectors as this combination of detectors was used in the detection of molecular weight for this doctoral work.

Refractive-index (RI) detectors. These are one of the most commonly used SEC detectors. They work on the principle that the addition of a solute to a solvent will modify its refractive index. They constantly measure the difference in the refractive index of the pure mobile phase and that of the eluent leaving the column, relating this difference to the concentration of the solute (polymer).[47]

Light Scattering detectors.[46] These detectors measure the excess intensity of the scattered laser light passing through the measuring cell containing the sample, at one or multiple angles different from zero. This excess intensity at angle θ, $R(\theta)$ is related to the weight average molecular mass (M_w) of the polymer by eqn. 2.9

$$\frac{K^* c}{R(\theta)} = \frac{1}{M_w P(\theta)} + 2A_2 c \qquad (2.9)$$

where, A_2 is the second virial coefficient, c is the concentration of the polymer, $P(\theta)$ describes the scattered light's angular dependence and K^* is an optical constant which is a function of Avagadro's number, wavelength, refractive index of the solvent and the refractive index increment d*n*/dc. As a result, the MMD is quite sensitive to the RI increment d*n*/dc and it is therefore important to avoid any error in the measurement of these values. Additionally, the d*n*/dc value can vary with molar mass within the MMD in case of oligomers and copolymers,

where the composition varies within the MMD. In this case, a second concentration detector that detects the copolymer composition is required.[46]

Problems associated with the Aqueous SEC of water soluble polymers – Although the principle of SEC is the separation of samples at various elution times depending on their size or hydrodynamic volume, interactions between the samples and the mobile (eluent) or solid (packing) phase, which are especially predominant in aqueous SEC, can influence their time of elution.[48]

The determination of correct molecular weight data of ionic as well as non-ionic synthetic and biopolymers from aqueous SEC can be hindered by non-size exclusion effects such as ion exchange, ion exclusion, ion inclusion, intramolecular electrostatic interaction and adsorption, which can influence the elution time of the polymer.[49] Ion exchange, ion exclusion and ion inclusion effects arise as a result of intermolecular interactions between the polymer and the column packing. The residual anionic silanol or carboxyl groups on the surfaces of silica or polymer based packing material can act as cationic exchange sites with cationic polyelectrolytes (ion exchange), and repel anionic polyelectrolytes hindering them from entering the pores (ion exclusion). When a polyelectrolyte is passed through the column, in order to achieve electroneutrality between the pores and the interstitial volume, additional polymer may be forced into the packing resulting in ion inclusion. The fixed charges on the polyelectrolytes can lead to repulsion between the neighboring ionic sites causing the polymer chains to expand resulting in intramolecular electrostatic interactions. Ion exchange, hydrogen bonding and hydrophobic interaction can lead to the adsorption of the polymer to the packing.[49]

The rest of the discussion will be restricted to problems associated with non-ionic and cationic water-soluble polymers that comprise the polymers in this doctoral work.

Non-ionic polymers.[48] The use of pure distilled water as the eluent is usually suitable for some non-ionic polymers such as polyethylene glycol.[45] However, it may result in some minor peaks near the void volume or abnormalities in the chromatograms when used with samples with charged constituents which can react with the negative charges on the packing material. Salt solution in a concentration of just 0.1 M is usually sufficient to hinder adsorption and ion exclusion for most non-ionic polymers. However, in the case of certain non-ionic polymers such as poly(vinylpyrrolidone) (PVP) in salt solution, a slightly sharp leading edge may be observed indicating a slight adsorption, which is most likely due to the hydrophobic interactions between PVP and the packing material.[44] This is usually prevented by using a mixture of salt solution and organic solvent for non-ionic hydrophobic polymers. Due to the high molecular mass associated with some water-soluble polymers, viscous fingering which arises as a result of injection of high concentration samples is another common concern.[48]

Cationic polymers.[48] Cationic polymers exhibit a strong tendency to be adsorbed on the packing by ionic interactions. These interactions tend to be quite strong and require quite a high salt concentration of ~1 M in the case of hydrophilic cationic polymers. While, a salt concentration of 1 M or even an organic solvent such as acetonitrile in the concentration of 20% is ineffective in the case hydrophobic cationic polymers, calling for the addition of 0.5 M acetic acid and 0.3 M sodium sulphate.[48] However, polyamines cannot be analyzed using aqueous acetic acid and sodium sulphate mixture due to the insolubility of the high molecular mass samples in the presence of sodium sulphate. Alternately, other salts can be used with acetic acid solution. The

salt type is chosen carefully keeping in mind any possible interference of the salt peak with especially the low molecular mass components of the sample and the concentration is adjusted to completely hinder any adsorption.

In addition to these problems, the reproducibility of results as well as conflicting results from different laboratories is quite common considering that the SEC results are quite sensitive to changes in columns as well as calibration standards.[43] Although research workers have come up with solutions to overcome some of these commonly known problem, it is quite clear from the above discussion that the problems and solution can be specific for each polymer-packing-eluent system. As a result, each system should be considered individually.

References

1) Hassan, C. M.; Trakampan, P.; Peppas, N. A. Ch. 3 in *Water Soluble Polymers Solution Properties and Applications. Ed.,* Zahid, A. Springer – Verlag, USA, **1998**.

2) Chen, H. T. Ch. 16 in *Water Soluble Polymers Solution Properties and Applications. Ed.,* Zahid, A. Springer - Verlag, USA, **1998**.

3) Syed, A. N.; Habib, W. W.; Kuhajda, A. M. Ch. 18 in *Water Soluble Polymers Solution Properties and Applications. Ed.,* Zahid, A. Springer - Verlag, USA, **1998**

4) Hutchinson, R. A., Ch. 4 in *Handbook of Polymer Reaction Engineering. Ed.,Meyer, Th., Keurentjes.* Wiley-VCH, Weinheim, **2005**.

5) Moad, G.; Solomon, D. H., Ch. 7 in *The Chemistry of Radical Polymerization*. Elsevier, Netherlands, **2006**.

6) Shoaf, G. L.; Poehlein, G. W. *J. Appl. Polym. Sci.* **1991**, *42*, 1239-1257.

7) Cutie, S. S.; Smith, P. B.; Henton, D. E.; Staples, T. L.; Powell, C. J. *Polym. Sci., Part B: Polym. Phys*. **1997**, *35*, 2029-2047

8) Gu, L.; Zhu, S.; Hrymak, A. N.; Pelton, R. H. *Polymer* **2001**, *42*, 3077-3086.

9) Barabanova, A. I.; Bune, E. V.; Gromov, V. F. *Vysokomol. Soedin., Ser. A Ser. B*. **2001**, *43*, 732-736.

10) Gromov, V. F.; Galperina, N. I.; Osmanov, T. O.; Khomikovskii, P. M.; Abkin, A. D. *Eur. Polym. J.* **1980,** *16*, 529-535

11) Bune, Y. V.; Barabanova, A. I.; Bogachev, Y. S.; Gromov, V. F. *Eur. Polym. J.* **1997**, *33*, 1313-1323.

12) Gromov, V. F.; Bogachev, Y. S.; Bune, Y. V.; Zhuravleva, I. L.; Teleshov, E. N. *Eur. Polym. J.* **1991**, *27*, 505-508.

13) Chapiro, A. *Eur. Polym. J.* **1973,** *9*, 417-427.

14) Senogles, E.; Thomas, R. *J. Polym. Sci.: Symp.* **1975**, *49*, 203-210

15) Beuermann, S.; Buback, M. *Prog. Polym. Sci.* **2002**, *27*, 191-254

16) Beuermann, S.; Paquet, D. A., Jr.; McMinn, J. H.; Hutchinson, R. A. *Macromolecules* **1997**, *30*, 194-197.

17) Kuchta, F. D.; Van Herk, A. M.; German, A. L. *Macromolecules* **2000**, *33*, 3641-3649.

18) Beuermann, S.; Buback, M.; Hesse, P.; Kukuckova, S.; Lacik, I. *Macromol. Symp.* **2007**, *248*, 23-32.

19) Lacík, I.; Učňová, L.; Kukučková, S.; Buback, M.; Hesse, P.; Beuermann, S. *Macromolecules* **2009**, *42*, 7753-7761.

20) Beuermann, S.; Buback, M.; Hesse, P.; Lacik, I. *Macromolecules* **2006,** *39*, 184-193.

21) Stach, M.; Lacik, I.; Chorvat, D., Jr.; Buback, M.; Hesse, P.; Hutchinson, R. A.; Tang, L.*Macromolecules* **2008**, *41*, 5174-5185.

22) Beuermann, S.; Buback, M.; Hesse, P.; Kukuckova, S.; Lacik, I. *Macromol. Symp.* **2007,** *248*, 41-49.

23) Lacik, I.; Beuermann, S.; Buback, M. *Macromolecules* **2003**, *36*, 9355-9363.

24) Lacik, I.; Beuermann, S.; Buback, M. *Macromol. Chem. Phys*. **2004**, *205*, 1080-1087.

25) Stach, M.; Lacik, I.; Kasák, P.; Chorvát, D., Jr.; Saunders, A. J..; Santanakrishnan, S.; Hutchinson, R. A. *Macromol. Chem. Phys*. **2010**, *211*, 580-593.

26) S. Beuermann, M. Buback, P. Hesse, R. A. Hutchinson, S. Kukuckova, I. Lacík, *Macromolecules* **2008**, *41*, 3513.

27) Buback, M.; Hesse, P.; Hutchinson, R. A.; Kasak, P.; Lacik, I.; Stach, M.; Utz, I. *Ind.*

Eng. Chem. Res. **2008**, *47*, 8197-8204.

28) Schrooten, S.; Buback, M.; Hesse, P.; Hutchinson, R. A.; Lacik, I. *Macromol. Chem. Phys*. **2011**, *212*, 1400-1409.

29) Santanakrishnan, S.; Tang, L.; Hutchinson, R. A.; Stach, M.; Lacik, I.; Schrooten, S.; Hesse, P.; Buback, M. *Macromol. React. Eng*. **2010**, *4*, 499-509.

30) BASFdatasheet,http://www.basf.com/group/corporate/en/brand/1_VINYLIMIDAZOLE

31) Bamford, C. H.; Schofield, E. *Polymer*, **1981**, *22*, 1227-1235.

32) Joshi, M.; Rodriguez, F. *J. Polym. Sci.***1984**, *29*, 1354-1354.

33) Dambatta, B. B.; Ebdon, J. R. Eur. Polym. J. **1986**, *22*, 783-786.

34) Chapiro, A. *Radiat. Phys. Chem*. **1992**, *40*, 89-93.

35) Arosio, P.; Mosconi, M.; Storti, G.; Banaszak, B.; Hungenberg, K. D.; Morbidelli, M. *Macromol. React. Eng.*, **2011**, *5*, 501-517.

36) Barner-Kowollik, C.; Coote, M. L.; Davis, T. P.; Matyjaszewski, K; Vana, P. Ch. on Copolymerization in *Encyclopedia of Polymer Science and Technology*, *9*, John Wiley & Sons, **2004**.

37) Navolokina, R. A.; Zilberman, Ye. N.; Kirina, M. A. *Polym. Sci. U.S.S.R*, **1987**, *29*, 1243-1248.

38) Stahl, G. A. *J. Polym. Sci., Part A: Polym. Chem.* **1981**, *19*, 371-380.

39) Endo, T.; Numazava, R.; Okawara, *Makromol. Chem.* **1971**, *148*, 205-210.

40) Chapiro, A.; Trung, L. D. *Eur. Polym. J.* **1974**, *10*, 1103-1106.

41) Cabaness, W. R.; Lin, T. Y.; Párkányi, C. *J. Polym. Sci., Part A-1*. **1971**, *9*, 2155-2170.

42) Chatterjee, A. M.; Burns, C. M. *Can. J. Chem.* **1971**, *49*, 3249-3251.

43) Mori, S.; Barth, H. G. Ch. 2 in *Size Exclusion Chromatography*, Springer-Verlag, Germany, **1999**.

44) Dubin, P. L. Preface in *Aqueous Size Exclusion Chromatography*, Elsevier, Netherlands **1988**.

45) Holding, S. R., Ch. 7 in *Size Exclusion Chromatography*, Ed. Hunt, B. J.; Holding, S. R., Chapman and Hall, New York, **1989**.

46) Trathnigg, B. Ch. on Size Exclusion Chromatography of Polymers in *Encyclopedia of Analytical Chemistry*, Ed. Meyers, R. A., John Wiley & Sons, Chinchester, **2000**.

47) Hunt, B. J. Ch. 2 in *Size Exclusion Chromatography*, Chapman and Hall, New York **1989**.

48) Kato, Y., Ch. 7 in *Size Exclusion Chromatography*, Ed. Hunt, B. J.; Holding, S. R., Chapman and Hall, New York, **1989**.

49) Mori, S.; Barth, H. G. Ch. 11 in *Size Exclusion Chromatography*, Springer-Verlag, Germany, **1999**.

Chapter 3. Kinetics and Modeling of Batch and Semibatch Aqueous-Phase *N*-Vinylpyrrolidone Free Radical Polymerization

This chapter is an updated version of the paper published in Macromolecular Reaction Engineering, **2010**, *4(8)*, 499-509

3.1 Abstract

Aqueous-phase free-radical batch and semibatch polymerizations of *N*-vinyl pyrrolidone have been carried out at temperatures of 70 and 85 °C with varying initial monomer and initiator concentrations. The rate of conversion was observed to increase as the initial monomer concentration was lowered, a result explained by the dependence of the propagation rate coefficient, k_p, on monomer concentration. A kinetic model with termination and conversion-dependent k_p rate coefficients taken from independent studies provides a good representation of the conversion profiles. A reasonable representation of polymer molecular weight averages and the complete molecular weight distribution was obtained by assuming that the rate coefficient for transfer to monomer also varies as a function of monomer concentration and that a small amount of chain transfer to polymer occurs.

3.2 Introduction

Poly(*N*-vinylamides) are a class of water soluble polymers finding applications in science and medical practice.[1] This class comprises of a number of polymers with differing solution properties depending on their side group substituents, making it an interesting choice in chemical structure-aqueous solution physicochemical property studies.[1] Poly(vinylpyrrolidone) (PVP), developed in the 1930s by Reppe et al., possesses a unique combination chemical, physicochemical and biological properties. As a result, PVP exhibits film-forming and adhesive properties, complexing ability and relative inertness towards a number of salts and acids making

it the most commercially-important polymer in this class.[1] PVP and its copolymers find applications in a variety of fields such as medicine, pharmaceuticals, cosmetics, food, textiles etc.[1] These polymers are mostly produced by free-radical aqueous-phase polymerization. As discussed in Chapter 2, the kinetics of free-radical polymerization of water soluble monomers deviates from the expected behaviour due to the influence of monomer concentration on k_p. Although the earlier works by Gromov,[2-5] Senogles and Thomas,[6] and others have indicated that solvent medium plays an important role in polymerization kinetics, behaviour and influence of the individual rate coefficients, k_p and k_t could not be ascertained. This made a comprehensive study on the kinetic modeling of the individual monomers, let alone their copolymerization, almost impossible.

As discussed in Chapter 2, the advent and application of techniques such as PLP-SEC and SP-PLP-NIR which allow for the determination of the individual rate coefficients k_p and k_t has changed this situation considerably, providing the opportunity to develop a better understanding of these industrially important aqueous systems. A PLP-SEC study of methacrylic acid (MAA) by Kuchta et al.[7] showed that the propagation rate coefficient, k_p, for MAA is higher in water than in organic solvents and that k_p increases with decreasing MAA concentration in aqueous solution. Further PLP-SEC studies of MAA examined both the influence of monomer concentration and the degree of ionization (α) over a wide range of temperature,[8-11] demonstrating that the value of k_p decreases by an order of magnitude moving from dilute to bulk systems for non-ionized MAA, and as α is increased from 0 to 1 at low MAA concentrations. However, the influence of MAA concentration on k_p was found to become less significant with increasing degree of ionization. PLP-SEC studies on aqueous solutions containing MAA and poly(MAA) mixtures were performed to simulate conversion in a batch polymerization and

demonstrated that k_p also increases with an increase in conversion as the ratio of unreacted monomer to water decreases.[12]

Other PLP-SEC studies on non-ionized[13] and ionized[14] acrylic acid and acrylamide[15] have also found an increasing k_p value with decreasing monomer concentration in aqueous solution. More recently Stach and co-workers[16] have studied the propagation kinetics of NVP. As for the other monomers, an influence of monomer concentration on the propagation rate coefficient was observed. This dependence, a behaviour uniquely observed in water soluble systems, has been attributed to the interaction between the transition structure (TS) for propagation and the surrounding environment which hinders the conformation mobility of the TS in the presence of increased monomer concentration, thereby affecting its free rotation.[9,16] The resistance to free rotation decreases with reduced monomer concentration, thus causing an increase in k_p with increasing dilution (or increasing conversion in a batch reaction), as shown for NVP in Figure 3.1. The variation was captured as a function of temperature, initial weight fraction of NVP in water (w_{NVP}^0), temperature and fractional conversion of monomer to polymer (x_p) by the expressions:[16]

$$\frac{k_p}{k_{p,max}} = 0.36 + 0.64\exp\left(-\frac{9.2\cdot w_{NVP}^0\cdot\left(1-x_p\right)}{1-w_{NVP}^0\cdot x_p}\right) - \frac{0.31\cdot w_{NVP}^0\cdot\left(1-x_p\right)}{1-w_{NVP}^0\cdot x_p} \tag{3.1}$$

$$k_{p,max}\Big/\left(\mathrm{L\cdot mol^{-1}\cdot s^{-1}}\right) = 2.57\times10^7\exp\left(-\frac{2.12\times10^3}{\left(T/\mathrm{K}\right)}\right) \tag{3.2}$$

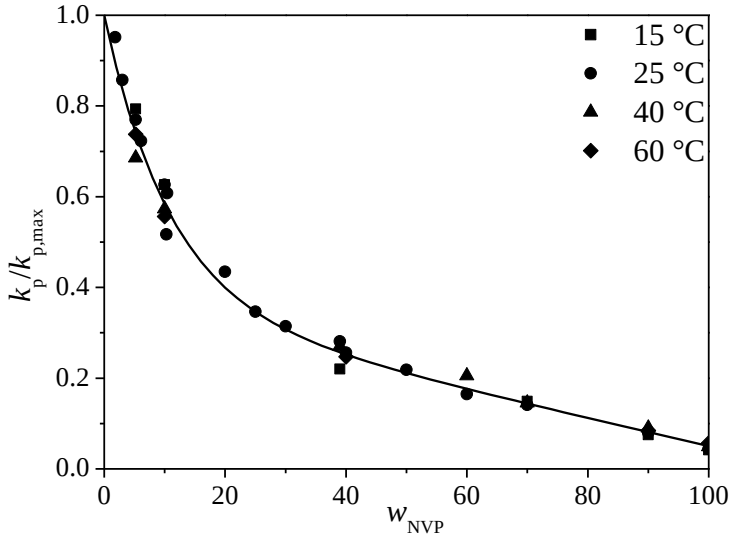

Figure 3.1. The influence of *N*-vinyl pyrrolidone concentration (w_{NVP}) in aqueous solution on its propagation rate coefficient (k_p) ratioed to $k_{p,max}$, the k_p value estimated at infinite dilution for each temperature.[16]

In addition to these k_p studies, SP-PLP coupled with near-IR has been used to study the termination kinetics of non-ionized MAA in aqueous solution.[17] Once the non-idealities in k_p due to the presence of solvent effects were accounted for, the variation of k_t with conversion for MAA was similar to that found for methacrylates in organic solvents. Most recently, Schrooten et al.[18] have applied the SP-PLP technique to the study of NVP termination kinetics in aqueous solution, with NVP initial fraction varied between 20 wt% and bulk at 40 °C and 2000 bar. The variation of k_t with conversion was found to be smaller than that of MAA, with systems containing 20 and 40 wt% NVP showing a negligible change in k_t over the conversion range studied (up to 60%). However, the k_t value in this predominantly segmentally-controlled regime was found to vary with the initial weight fraction of NVP,[18] a trend captured by the expression

$$k_t^0 \Big/ \left(\mathrm{L \cdot mol^{-1} \cdot s^{-1}}\right) = 4.87 \times 10^7 \exp\left(-w_{NVP}^0 / 0.29\right) + 5.47 \times 10^6 \qquad (3.3)$$

at 40 °C and 2000 bar, assuming the termination rate law $\frac{d[R^{\bullet}]}{dt} = -2k_t[R^{\bullet}]^2$. A multiplicative correction factor of 3.07 for polymerization at atmospheric pressure can be calculated using the measured activation volume of 14.6 $cm^3 \cdot mol^{-1}$.[18]

The k_p and k_t coefficients for MAA determined from these specialized techniques were shown to provide a good description of continuously-initiated aqueous-phase polymerization of MAA, including polymer molecular weight (MW) averages and molecular weight distribution (MWD).[19] Despite the large number of studies carried out on NVP, a complete model to represent the behaviour of this system has not been developed to date. The increasing interest expressed by companies like BASF to better understand the NVP system in order to gain better control over their existing polymerization processes and develop new process and product alternatives has motivated us to study and develop a similar kinetic model for polymerization rate and polymer MWs produced by continuously-initiated aqueous-phase free-radical polymerization of NVP. This study will focus on the influence of initial monomer and initiator concentrations on conversion and molecular weight behaviour of the system. It will be shown that the rate coefficients measured by PLP techniques provide a good representation of batch and semibatch experiments conducted over a range of initial monomer and initiator concentrations at two different temperatures. This will not only helps us gain a better understanding of the behaviour of this monomer in an industrially-similar set-up, but also help understand the role of solvent medium and initiator concentrations in controlling the rate and molecular weight properties of the final polymer.

3.3 Experimental

N-vinyl pyrrolidone (>99%, Aldrich, contains 100 ppm sodium hydroxide as inhibitor) and the thermal initiator 2,2'-azobis (2-methylpropionamidine) dihydrochloride (V-50, Fluka, $\geq$ 98%) were used as received. The initiator solution was prepared using deionized water, and the polymerizations were carried out isothermally using deionized water as solvent in a 1 L automated (MT Autochem) stirred reactor under nitrogen blanket. Conversion was tracked using online IR measurements and offline gravimetry analysis. For those runs for which IR measurement was not available, the gravimetry results were confirmed using NMR analysis. Semibatch reactions were carried out in the same reactor setup as the batch reactions, with an automated feed system used to control monomer addition to the reactor at a specified mass flow rate.

3.4 Characterization

ReactIR. A React-IR 4000 (MT Autochem) was used to track the extent of monomer conversion online by integrating the area under the peak representing the vinyl double bond, appearing at ~965 - 1000 cm^{-1}, and converting to monomer concentration using a calibration established via off-line studies. This online measurement yields an estimate of conversion every 2 min, which was checked using off-line gravimetry of selected samples dried in an air stream followed by hot air oven for 72 h to remove the residual monomer and water from the polymer sample.

NMR analysis. Proton NMR analysis was also performed on selected samples to measure conversion, using deuterated water as solvent. NMR spectra for the monomer and polymer are shown in Figures 3.3 (a) and (b) with peak assignments labelled according to Figure 3.2. The peaks 1, 2, 3 from hydrogen atoms attached to the carbon atoms in the ring appear between 2.1

and 3.5 ppm, while that for the hydrogen atoms attached to the double bond appear at 4.6 and ~6.9 ppm, respectively. Once polymerized, the peaks for the hydrogen atoms attached to C4 and C5 (along the polymer backbone) are found at 1.5 and 3.6 ppm respectively. The level of conversion is determined by comparing the area of the peak representing the double bond (monomer) to that of the peaks representing the hydrogen atoms attached to the carbon atoms in the ring. The accuracy of the technique was determined to be ±2%, by preparing samples of known levels of conversion by mixing quantities of monomer and polymer. The agreement between gravimetry and NMR results for 12.5 vol% NVP polymerized at 85 °C with initiator concentrations of 0.01 and 0.04 wt% is shown in Figure 3.4.

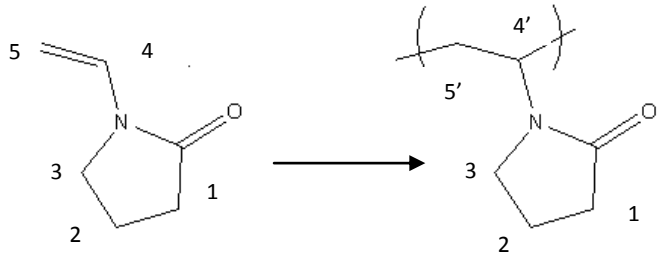

Figure 3.2. Conversion of *N*-vinyl pyrrolidone to poly(*N*-vinyl pyrrolidone)

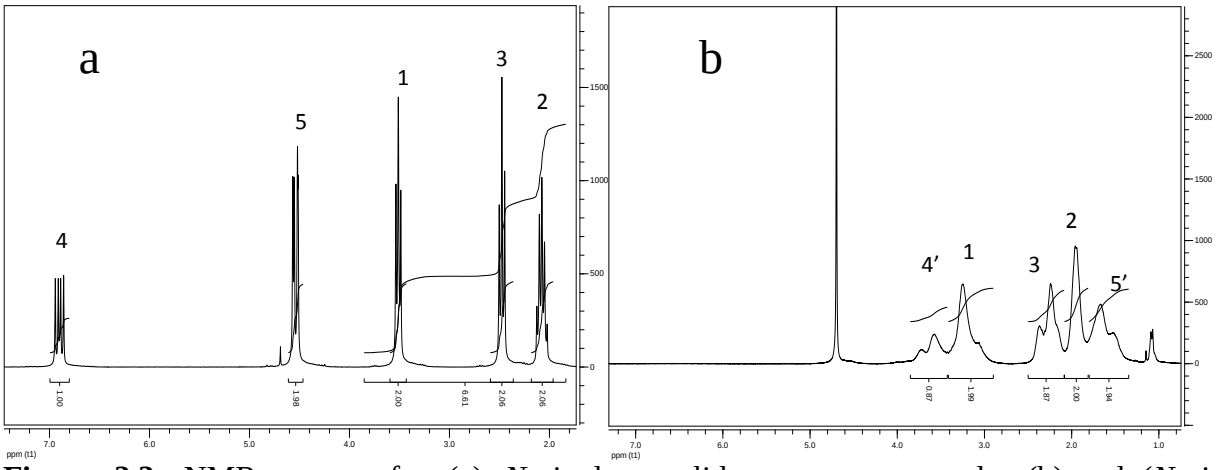

Figure 3.3. NMR spectra for (a) *N*-vinyl pyrrolidone monomer and (b) poly(*N*-vinyl pyrrolidone)

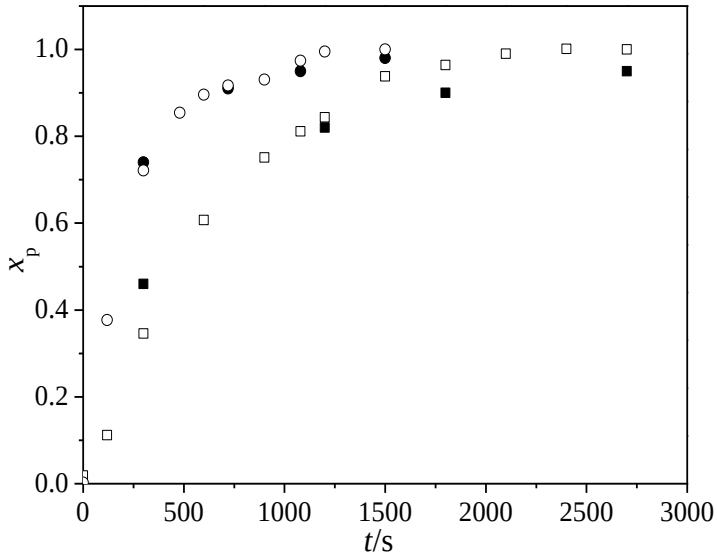

Figure 3.4. Comparison of conversion results obtained from NMR and gravimetry for the batch polymerization of NVP at 85 °C with initial NVP concentration of 12.5 vol% and initiator concentrations of 0.01 (□) and 0.04 (○) wt% V-50. The open and filled symbols represent the gravimetry and proton NMR results, respectively.

SEC analysis. The Molecular weight analysis was carried out by size-exclusion chromatography (SEC) at the Polymer Institute of the Slovak Academy of Sciences, Bratislava using a Polymer Standards Services (PSS, Mainz, Germany) column setup. Dimethyl acetamide (DMAc) containing 0.1% LiBr was used as the eluent. The PSS setup consists of an 8 x 50mm PSS GRAM 10µm guard column and three 8 x 300mm PSS GRAM 10µm columns with pore sizes 100, 1000 and 3000 Å placed in a column heater set to a temperature of 45 °C. The MW data was obtained using RI (with respect to PS calibration) and multi-angle light scattering (MALLS) detectors. A discrepancy was observed between the results from the RI and RI-MALLS detectors. Our co-workers in Bratislava who analyzed our SEC samples have noticed this disagreement between the PDI and M_w values from the two detectors for poly(AA) as well as poly(NVP) samples. This discrepancy is not very surprising considering that the precision of calibration decreases in the order of direct>universal>absolute>>effective. Unfortunately, the universal calibration is generally not applicable for aqueous SEC.[20] Likewise, there are problems

associated with the RI-MALLS as well. As the MW in RI-MALLS is determined by fitting the calibration curve at the peak of the MWD (highest concentration of macromolecules) and extrapolated over the entire MWD range, the M_W values from this system are most likely accurate, but, the fit over the lower range of the MWD becomes questionable and as a result, the PDI values may not be accurate. So, it was decided to use the PDI from RI and correct the RI MW averages (M_w and M_n) by the correction factor arrived at by a ratio of the $M_{w,\ MALLS}/M_{w,\ RI}$ in order to match the M_W values from RI-MALLS. The correction factor in this case was determined to be 1.17±0.09, which differs from the factor of 1.53 reported in ref. 16, a discrepancy that we are unable to explain. A comparison of the MALLS and corrected RI data at 6.25, 12.5 and 20 vol% NVP and 0.02 wt% V-50 at 85 °C is shown in Figures 3.5 (a), (b) and (c) respectively. It is to be noted that the MALLS MWDs at all the three monomer concentration is narrower than the RI data, which may be a result of the poor fitting of the calibration curve over the entire MWD range, as discussed above and the corrected RI data will therefore be used in the rest of the Chapter. A complete comparison of the MALLS and corrected RI MWDs for all the experiments is presented in Appendix A.1

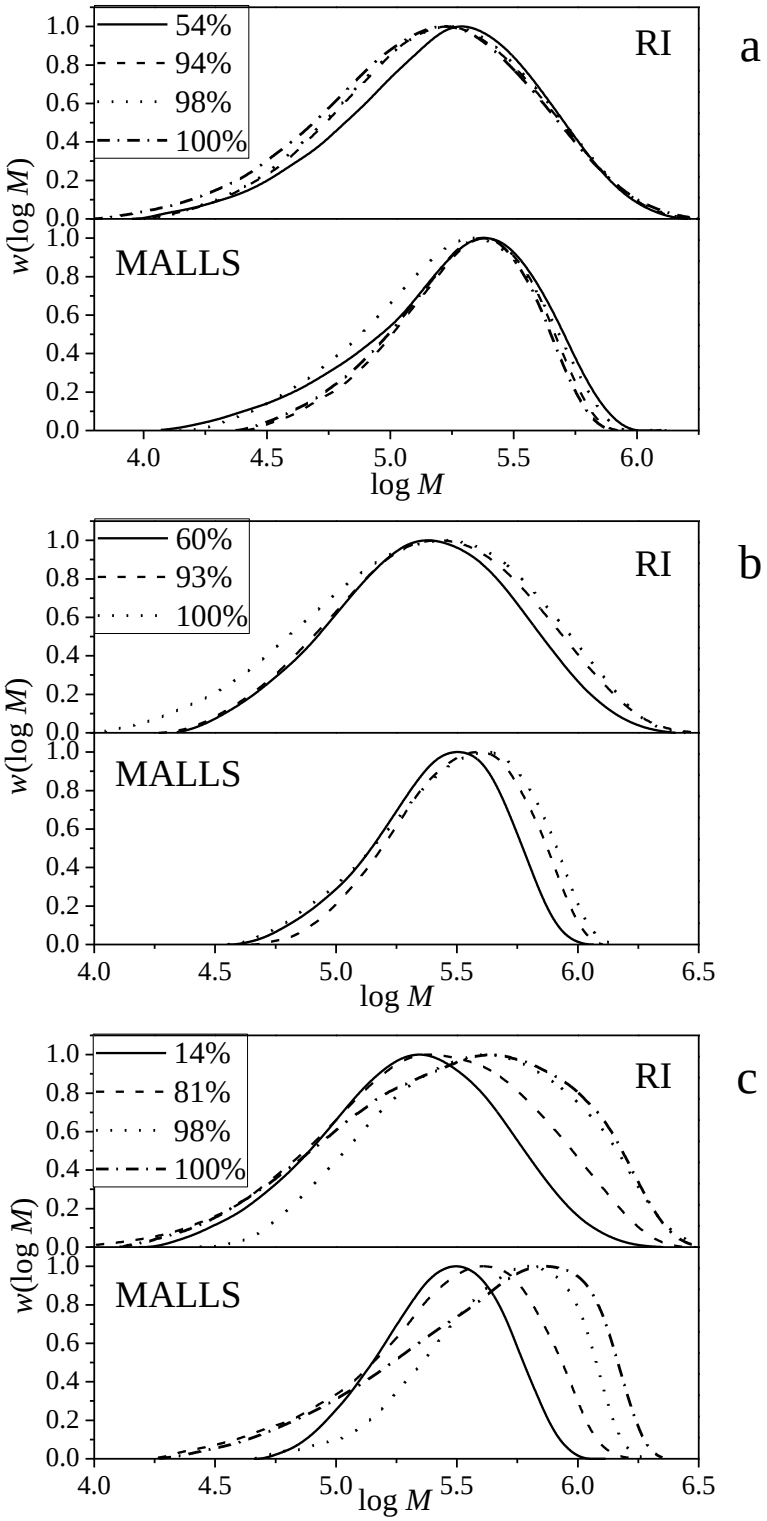

Figure 3.5. Comparison of MALLS and corrected RI data at (a) 6.25 (b) 12.5 and (c) 20 vol% NVP and 0.02 wt% V-50 at 85 °C.

3.5 Model Development

The kinetic model takes into consideration the basic free-radical polymerization mechanisms of initiation, propagation, transfer and termination shown in Table 3.1, with rate coefficients summarized in Table 3.2. V-50 initiator decomposes by a first order reaction with a half-life of 96 min at 70 °C and 16 min at 85 °C.[21] A typical azo initiator efficiency of 0.7 was assumed. The expression for k_p (eq 3.1 and 3.2) was developed from PLP studies of NVP kinetics in aqueous solution, and was implemented without modification. The k_t expression (eqn. 3.3), developed from SP-PLP measurements at 40 °C and 2000 bar, was able to provide a reasonable representation of NVP polymerizations at 70 and 85 °C after correcting for the known effect of pressure, suggesting that the activation energy for termination, like observed for many other systems, is small. Note that this representation is not valid for systems with higher NVP contents, for which a decrease in k_t due to translational diffusion limitations must be considered.[18]

Table 3.1. Mechanisms describing the free-radical polymerization of *N*-vinyl pyrrolidone

Initiator Decomposition	$I \xrightarrow{k_d} 2 f I^{\bullet}$
Chain Initiation	$I^{\bullet} + M \xrightarrow{k_p} P_1^{\bullet}$
Chain Propagation	$P_n^{\bullet} + M \xrightarrow{k_p} P_{n+1}^{\bullet}$
Chain Termination	
By Combination	$P_n^{\bullet} + P_m^{\bullet} \xrightarrow{k_{tc}} D_{n+m}$
By Disproportionation	$P_n^{\bullet} + P_m^{\bullet} \xrightarrow{k_{td}} D_n + D_m$
Chain Transfer	
To Monomer	$P_n^{\bullet} + M \xrightarrow{k_{tr}^{mon}} D_n + P_1^{\bullet}$
To Polymer	$P_n^{\bullet} + D_m \xrightarrow{m k_{tr}^{pol}} D_n + P_m^{\bullet}$
Inhibition	$I^{\bullet} + X \xrightarrow{k_{inhib}}$ dead products
	$P_n^{\bullet} + X \xrightarrow{k_{inhib}}$ dead products

Table 3.2. Values and expressions for the kinetic rate coefficients and physical parameters used in the model of aqueous-phase free-radical polymerization of *N*-vinyl pyrrolidone

Mechanism	Rate Expression	70 °C	85 °C	Ref
Initiator decomposition	$k_{\mathrm{d}}(s^{-1}) = 9.17\times10^{14}\exp\left(\frac{-1.49\times10^{4}}{(T/\mathrm{K})}\right)$	$1.22\text{x}10^{-4}$	$7.52\text{x}10^{-4}$	21
Propagation	$\frac{k_{\mathrm{p}}}{k_{\mathrm{p,max}}} = 0.36 + 0.64\exp\left(-\frac{9.2\cdot w^{0}_{\mathrm{NVP}}\cdot(1-x_{\mathrm{p}})}{1-w^{0}_{\mathrm{NVP}}\cdot x_{\mathrm{p}}}\right) - \frac{0.31\cdot w^{0}_{\mathrm{NVP}}\cdot(1-x_{\mathrm{p}})}{1-w^{0}_{\mathrm{NVP}}\cdot x_{\mathrm{p}}}$			16
	$k_{\mathrm{p,max}}\Big/\left(\mathrm{L}\cdot\mathrm{mol}^{-1}\cdot\mathrm{s}^{-1}\right) = 2.57\times10^{7}\exp\left(-\frac{2.12\times10^{3}}{(T/\mathrm{K})}\right)$	$5.38\text{x}10^{4}$	$6.97\text{x}10^{4}$	16
Termination	$k_{\mathrm{t}}\Big/\left(\mathrm{L}\cdot\mathrm{mol}^{-1}\cdot\mathrm{s}^{-1}\right) = 1.5\times10^{8}\exp\left(-w^{0}_{\mathrm{NVP}}/0.29\right) + 1.68\times10^{7}$ at P = 1 bar			18
Transfer to monomer	$\frac{k_{\mathrm{tr}}^{\mathrm{mon}}}{k_{\mathrm{p}}}$	$4.8\text{x}10^{-4}$	$6\text{x}10^{-4}$	This work
Transfer to polymer	$\frac{k_{\mathrm{tr}}^{\mathrm{poly}}}{k_{p}}$	$*6\text{x}10^{-5}$	$*6\text{x}10^{-5}$	This work
Density of NVP	$\rho_{\mathrm{NVP}}\Big/\left(\mathrm{g}\cdot\mathrm{mL}^{-1}\right) = 1.0592 - 7.7772\cdot10^{-4}(T/^{\circ}\mathrm{C}) - 4.6649\cdot10^{-7}(T/^{\circ}\mathrm{C})^{2}$	1.002	0.989	16
Density of Water	$\rho_{\mathrm{H2O}}\Big/\left(\mathrm{g}\cdot\mathrm{mL}^{-1}\right) = 0.9999 + 2.3109\cdot10^{-5}(T/^{\circ}\mathrm{C}) - 5.44807\cdot10^{-6}(T/^{\circ}\mathrm{C})^{2}$	0.972	0.959	16

* May be higher at higher NVP concentrations. See text.

Transfer also plays an important role in controlling the molecular weight of the polymer. In addition to transfer to monomer, the experimental MW data presented later indicates that some transfer to polymer occurs in the system. Table 3.2 summarizes the estimates for these rate coefficients, discussed along with the inhibition reaction in further detail in the following section. The set of mechanisms was implemented in the Predici© program, which combines the kinetics with specified component inlet and outlet flows to form detailed species balances for the reactor system, thereby allowing simulation of the complete polymer MWD as well as MW averages.[22]

3.6 Results and Discussion

The rate equation for an isothermal free-radical batch polymerization with negligible volume contraction is given by

$$-\frac{d[\mathrm{M}]}{dt} = k_\mathrm{p}[\mathrm{M}]\left(\frac{fk_\mathrm{d}[\mathrm{I}]}{k_\mathrm{t}}\right)^{0.5} \tag{3.4}$$

Substituting

$$[\mathrm{M}] = [\mathrm{M}]_0\left(1-x_\mathrm{p}\right) \tag{3.5}$$

where $[\mathrm{M}]_0$ is the initial monomer concentration and x_p is the fractional conversion of monomer at any instant, eq (3.4) becomes

$$\frac{dx_\mathrm{p}}{dt} = k_\mathrm{p}\left(\frac{fk_\mathrm{d}[\mathrm{I}]}{k_\mathrm{t}}\right)^{0.5}\left(1-x_\mathrm{p}\right) \tag{3.6}$$

According to eq (3.6), conversion profiles should have the same initial slope for polymerizations carried out at identical [I], independent of $[\mathrm{M}]_0$, provided there is no variation in rate coefficients with initial conditions. For MAA, the rate of monomer conversion was significantly influenced by the initial monomer concentration, with an increased slope seen for experiments run with

lower $[M]_0$. This influence was well explained by the variation in k_p with monomer concentration.[19] For NVP the situation is more complex, as it has been found that both k_p[16] and k_t[18] increase as monomer concentration decreases. Thus, the net effect on rate of conversion is expected to be smaller.

In order to test the predictive capabilities of the model, batch experiments were run at two different temperatures of 70 and 85 °C. The batch data at 70 °C was collected by a previous graduate student, Lina Tang.[23] Reproducibility of results was checked by repeating the experiment at 20 vol% NVP and 0.02 wt% V-50 at 85 °C and excellent agreement between the conversion profiles was observed as shown in Figure 3.6, except for one outlier at ~2100 s. Conversion profiles measured over a range of initial monomer and initiator concentrations are shown in Figures 3.7 (70 °C) and 3.8 (85 °C). At 85 °C (Figure 3.8(a)), the initial rate is slightly higher with 6.25 vol% NVP compared to higher monomer levels, but the difference is not large. At 70 °C (Figure 3.7(a)), the increase in conversion rate with decreasing NVP content is more evident, although complicated by an observable inhibition period most likely explained by the low rate of initiation at the lower temperature coupled with the effect of residual oxygen in the system. In the model, this is accounted for by introducing inhibition reactions, as shown in Table 3.1. The corresponding rate coefficient is set to $1x10^9$ $L \cdot mol^{-1} \cdot s^{-1}$, with the amount of inhibitor set for each simulation to match the delay in initial polymerization observed experimentally. Despite these difficulties, it is clear from Figures 3.7 and 3.8 that the k_p and k_t expressions determined from independent pulsed laser investigations provide a good representation of the experimental conversion profiles over a range of initial monomer concentrations, initiator concentrations and temperatures.

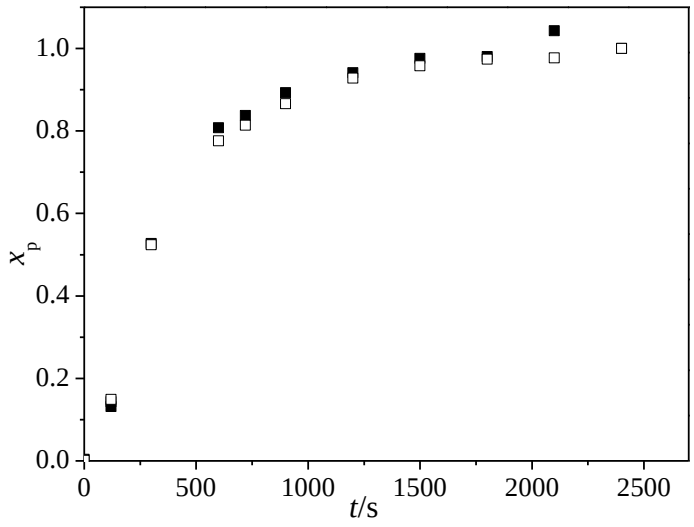

Figure 3.6. Reproducibility of conversion data measured by gravimetry for batch polymerization of *N*-vinyl pyrrolidone with 20 vol% NVP and 0.02 wt% V-50 in aqueous solution at 85 °C. The open symbols represent the repeat experiment.

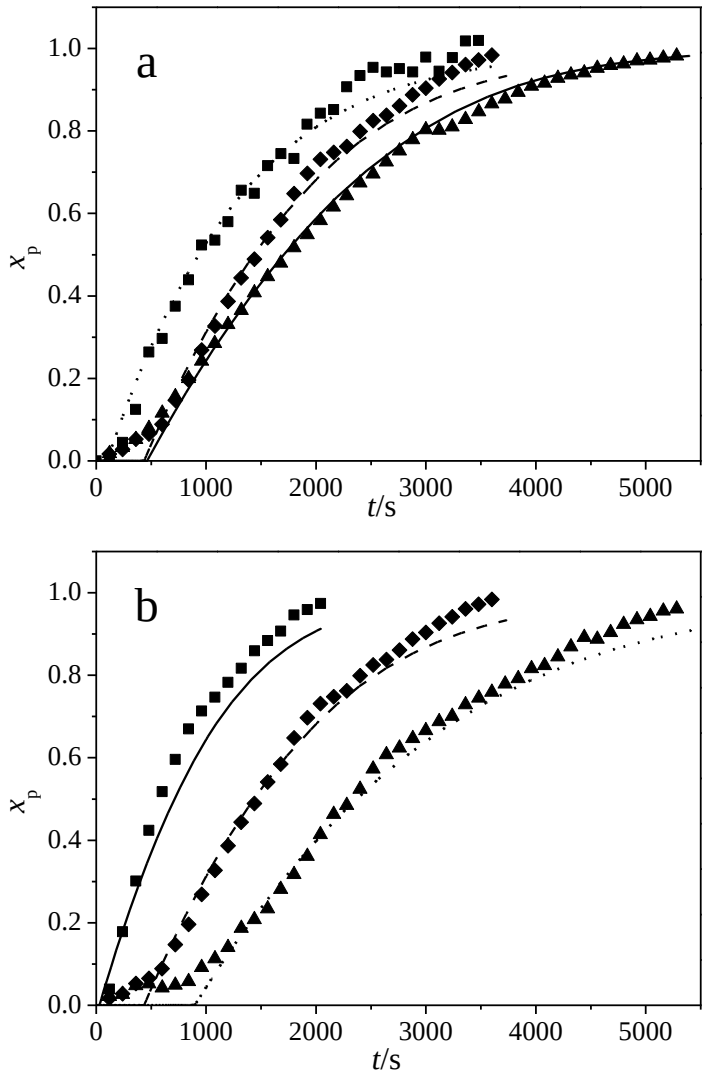

Figure 3.7. Conversion profiles for batch polymerizations of NVP, measured using online ReactIR, at 70 °C. (a) Influence of NVP concentrations of 6.25 (■, ·····), 12.5 (◆, − − −) and 25 (▲, ——) vol% at an initiator concentration of 0.02 wt% V-50. (b) Influence of initiator concentrations of 0.01 (▲, ·····), 0.02 (◆, − − −) and 0.04 (■, ——) wt% V-50 with initial NVP level of 12.5 vol%. The lines represent the simulations and symbols represent the experimental results.

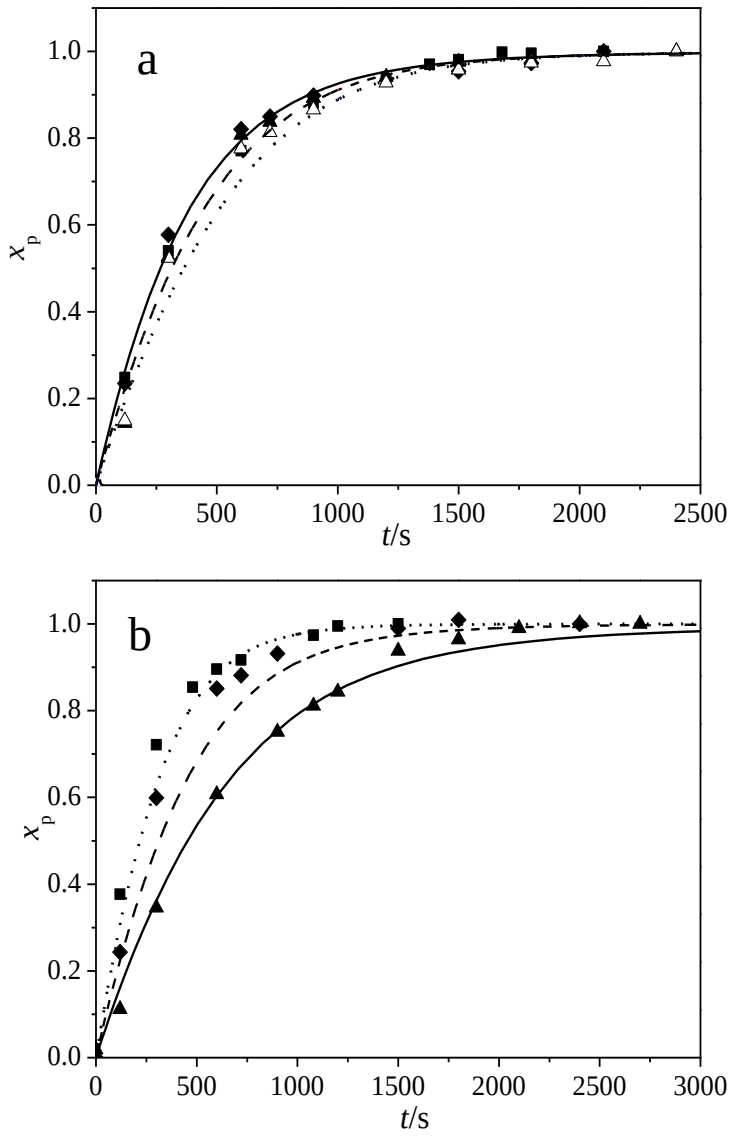

Figure 3.8. Conversion profiles for batch polymerizations of NVP, measured by gravimetry, at 85 °C. (a) Influence of NVP concentrations of 6.25 (■, ——), 12.5 (◆, − − −) and 20 (▲, ·····) vol% at an initiator concentration of 0.02 wt% V-50. (b) Influence of initiator concentrations of 0.01 (▲, ——), 0.02 (◆, − − −) and 0.04 (■, ·····) wt% V-50 with initial NVP level of 12.5 vol%. The lines represent the simulations and the filled and open symbols represent the experimental and repeat results respectively.

3.7 Molecular Weight Modeling

With a reasonable representation of reaction rate obtained, attention is now turned to the molecular weights of the polymer. The first simulations were carried out without considering any chain transfer mechanisms, such that polymer molecular weight is controlled entirely by relative rates of chain growth and termination. It can be seen from Figure 3.9 that the shapes of the MWD curves obtained experimentally and those predicted by the model are similar, but there is an offset, with the model over predicting values by a factor of 1.7 to 2.2. Therefore, it is clear that some chain transfer processes are occurring in the system, and transfer to monomer was added to the model. As done in the previous study[19] of MAA polymerization, the ratio k_{tr}^{mon}/k_p was fixed to a constant value such that k_{tr}^{mon} varies with monomer concentration in the same fashion as k_p. As shown in Figure 3.10, a value of k_{tr}^{mon}/k_p of 1.8×10^{-4} allowed the model to match the final number-average (M_n) and weight-average (M_w) molecular weight values measured at 70 °C for the system at full conversion, but not the significant increase in M_w that occurred over the course of reaction. A decrease in k_t at intermediate and high conversions due to translational diffusion limitations would lead to an increased M_w. However, the decrease in k_t required would be quite substantial, and would accelerate the rate of monomer conversion, which is currently well-described by the model. Furthermore, as previously discussed, the SP-PLP study found that k_t remained constant over the entire conversion range studied, up to 60%.[18] Thus, it can be concluded that additional mechanisms must be considered. This finding differs from our previous study of MAA batch polymerization,[19] for which consideration of chain transfer to monomer was sufficient to achieve a good representation of MW trends. For the NVP system, it was decided to increase the value of k_{tr}^{mon}/k_p to 4.8×10^{-4} (at 70 °C) in order to fit the MW averages obtained at low conversion (see Figure 3.10), and consider long-chain branching

as the mechanism responsible for the increasing MW with conversion. The inclusion of LCB in the mechanistic scheme is justified further in the subsequent paragraph.

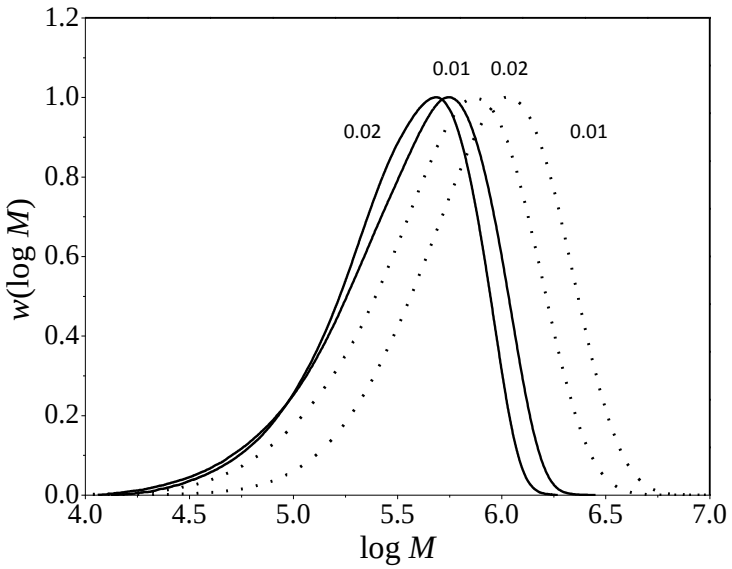

Figure 3.9. Polymer molecular weight distributions measured experimentally (solid lines) and simulated without consideration of chain-transfer events (dotted lines) for aqueous-phase polymerization conducted at 70 °C with initial levels of 6.25 vol% NVP and 0.01 and 0.02 wt% V-50 initiator. Distributions are for final polymer samples, obtained at >95% conversion.

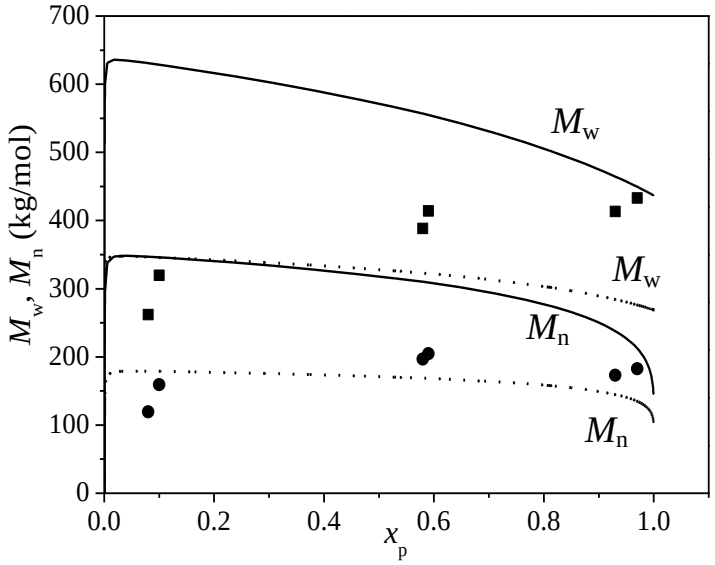

Figure 3.10. Molecular weight averages (M_w, M_n) versus monomer conversion for batch experiments conducted with 6.25 vol% NVP and 0.02 wt% V-50 at 70 °C. The lines represent the simulation and the squares and circles represent the experimental results for M_w and M_n, respectively. The simulation was carried out using $k_{tr}^{mon}/k_p = 1.8\times10^{-4}$ (solid lines) and $k_{tr}^{mon}/k_p = 4.8\times10^{-4}$ (dotted lines).

As the polymerization proceeds towards higher conversion levels, especially at higher initial monomer content, the values of the PDI and M_w show an increase while M_n remains fairly constant, suggesting that intermolecular chain transfer to polymer occurs in the system. (Intramolecular chain transfer to polymer, a mechanism common to acrylates but not believed to occur with NVP,[16] does not lead to an increase in M_w with conversion.) Moreover, PVP has been used as a stabilizer in several dispersion polymerization studies,[24, 25] where the polymer radical grafts onto the PVP stabilizer by the abstraction of the labile hydrogen in the polymer backbone. A scheme from a literature reference showing the H-abstraction from the PVP chain creating a radical site is shown in Scheme 3.1.[25] This serves as evidence for the possibility of H-abstraction from the PVP polymer backbone. Moreover, evidence for chain transfer to polymer in the free-radical polymerization of a similar water-soluble monomer, NVF[26] has been shown through 2-D NMR analysis by our co-workers. Therefore, to capture the upswing observed in evolution of the

molecular weight averages with conversion, transfer to polymer reaction was added to the mechanistic set in the model. Two possible cases were analyzed (a) assuming the rate coefficient for transfer to polymer, k_{tr}^{pol}, to be a constant value and (b) assuming that the ratio $\frac{k_{tr}^{pol}}{k_p}$ is constant such that transfer to polymer also varies with monomer concentration as k_p does (and as assumed for transfer to monomer). A comparison of the experimental and model predictions for batch polymerizations conducted at 85 °C with 12.5 and 20 vol% NVP is shown in Figure 3.11. (at 85 °C, a slightly higher value of $k_{tr}^{mon}/k_p = 6\times10^{-4}$ was used to match the MW averages at low conversions, compared to the value of 4.8×10^{-4} used at 70 °C.) As there is little difference in the MW profiles calculated according to case (a) (k_{tr}^{pol} constant at 4.5 L·mol^{-1}·s^{-1}) and case (b) (k_{tr}^{pol}/k_p constant at 9×10^{-5}), the rest of the simulation results presented are calculated assuming case (b). Discrimination between these two cases would be extremely difficult, if not impossible, from analysis of batch polymerization data; a computational study may provide some insight to the question.

Addition of a small amount of transfer to polymer causes the M_w profile to increase at higher conversion without affecting M_n predictions. The experimental data with 12.5 vol% NVP (Figure 3.11(a)) are better fit with a lower ratio of k_{tr}^{pol}/k_p of 6×10^{-5}, while those obtained with 20 vol% NVP (Figure 3.11(b)) require a ratio of 9×10^{-5} to match the upswing in M_w at conversions > 80%. However, the full MWDs calculated by the model do not match the shift in peak M_w observed experimentally with 20 vol% NVP (Figure 3.12(b)). This unexplained shift is not seen for experiments with lower NVP levels (Figure 3.12(a)). It is difficult to understand what

mechanism other than long chain branching may cause a shift in the MWD with conversion at higher NVP levels but not for the experiments with lower NVP content.

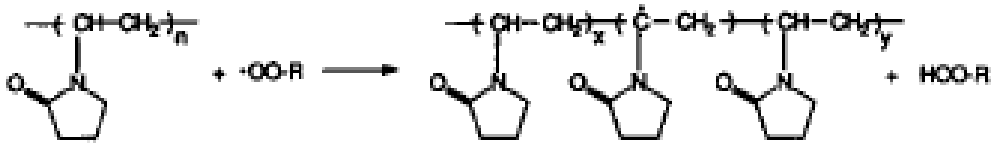

Scheme 3.1. H-abstraction from the PVP chain creating a radical site.[25]

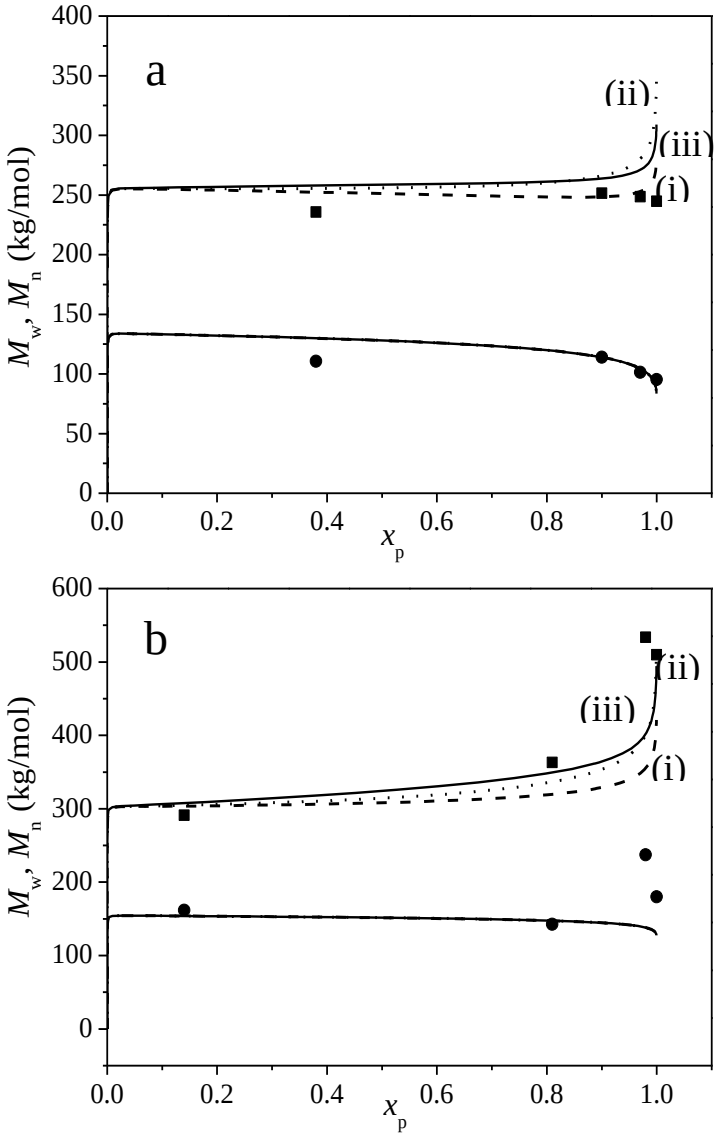

Figure 3.11. Polymer molecular-weight averages (M_w, M_n) plotted as a function of conversion for batch experiments conducted at 85 °C with (a) 12.5 vol% NVP and 0.04 wt% V-50 and (b) 20 vol% NVP and 0.02 wt% V-50. The lines represent the simulation results and the squares and circles represent the experimental results for M_w and M_n, respectively. The simulations were carried out using constant $k_{tr}^{mon}/k_p = 6\times10^{-4}$ and LCB values of (i) $k_{tr}^{pol}/k_p = 6\times10^{-5}$ (-----) (ii) $k_{tr}^{pol}/k_p = 9\times10^{-5}$ (·····) and (iii) k_{tr}^{pol} =4.5 L·mol^{-1}·s^{-1}(——).

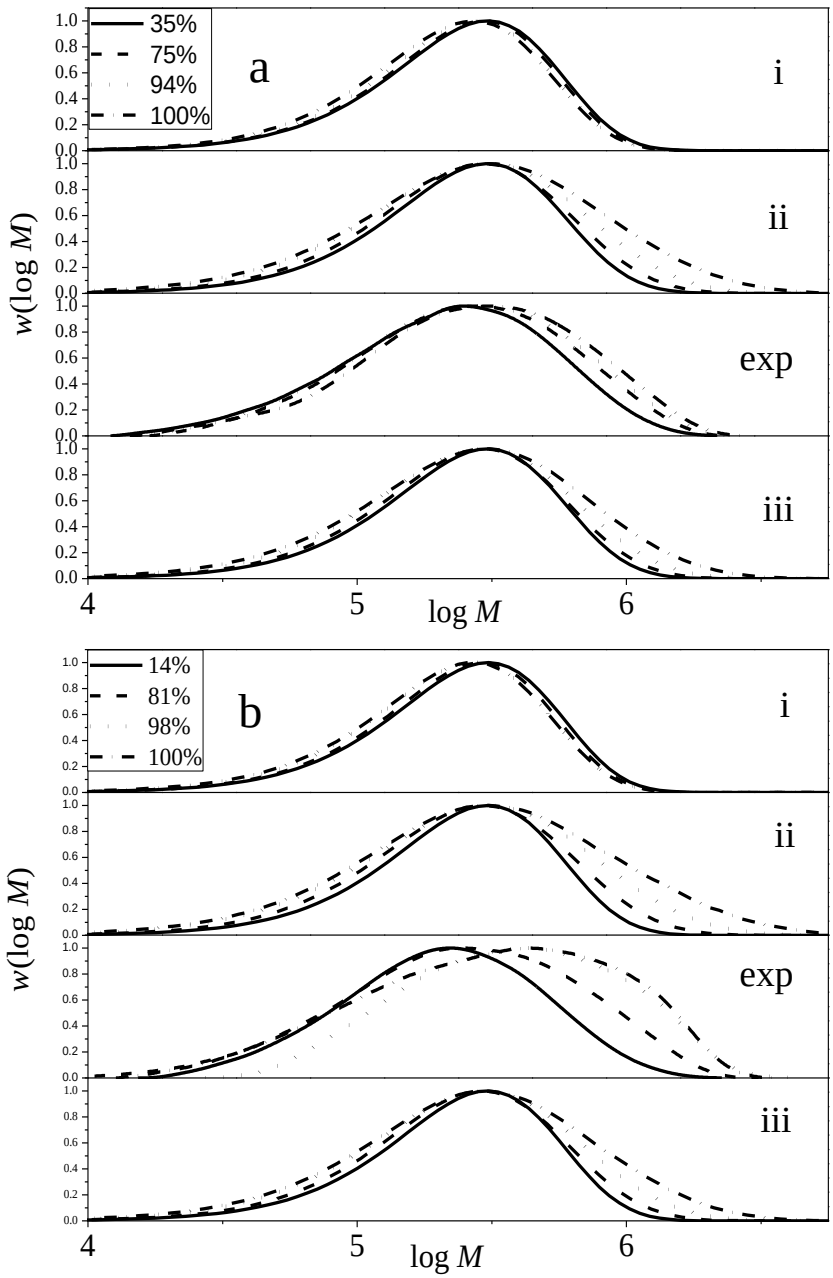

Figure 3.12. Comparison of simulations with varying levels of chain transfer to polymer – (i) $k_{tr}^{pol} = 0$, (ii) $k_{tr}^{pol}/k_p = 9\times10^{-5}$, (iii) $k_{tr}^{pol}/k_p = 6\times10^{-5}$ – with experimental molecular weight distributions obtained for (a) 12.5 vol% NVP and 0.01 wt% V-50 and (b) 20 vol% NVP and 0.02 wt% V-50 at 85 °C, and polymer conversions as indicated in the figure legends. $k_{tr}^{mon}/k_p = 6\times10^{-4}$ for all simulations.

Despite the difficulty in matching MW profiles with conversion for all cases, the changes in final polymer MW with initiator level, monomer level and temperature are represented reasonably

well assuming that a small amount of chain transfer to polymer occurs, using the coefficients in Table 3.2. A comparison of final (100% conversion) experimental and simulated MWD profiles at varying initial monomer and initiator concentrations at 85 °C are shown in the Figures 3.13 and 3.14 respectively. The MW averages for high-conversion batch polymerizations at varying initial conditions is shown in Table 3.3. As expected, the experimental data show a shift to higher MW with an increase in initial NVP concentration as well as with a decrease in initiator concentration and the overall trends are captured well by the model at both the temperatures studied. To fit the data, an increase in k_{tr}^{mon}/k_p ratios with temperature is required, as is common for free-radical polymerizations. However, a temperature-independent value of k_{tr}^{pol}/k_p was used; any temperature dependence of the chain transfer to polymer is small compared to experimental uncertainty.

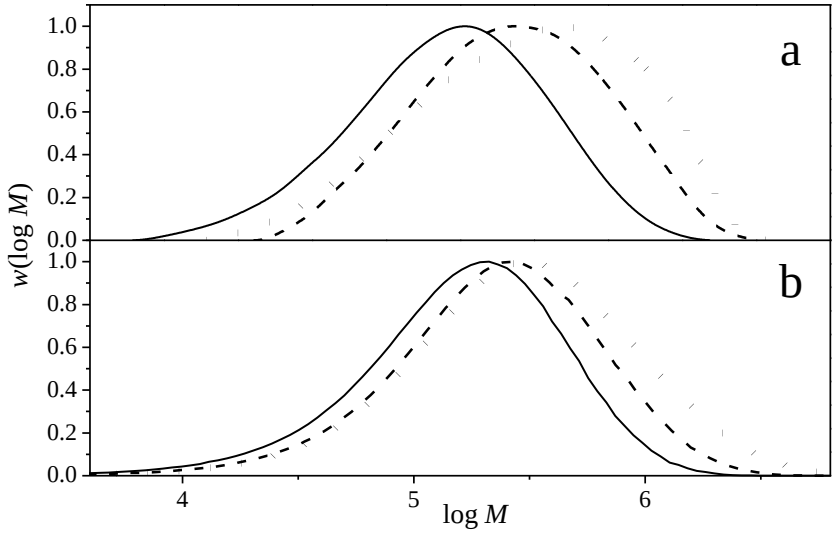

Figure 3.13. Comparison of (a) experimental and (b) model data for the influence of monomer concentrations of 6.25 (——), 12.5 (-----) and 20 (·····) vol% on polymer molecular weight distributions (MWDs).

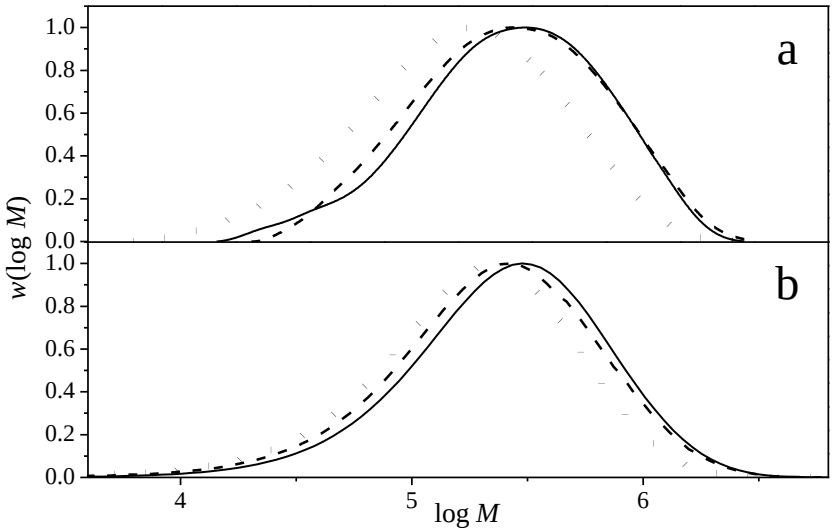

Figure 3.14. Comparison of (a) experimental and (b) model data for the imfluence of initiator concentrations of 0.01 (——), 0.02 (-----) and 0.04 (·····) wt% on polymer molecular weight distributions (MWDs).

Table 3.3. Comparison of simulated and experimental results for high-conversion batch polymerization of NVP with V-50 initiator. Model coefficients as shown in Table 3.2.

T (° C)	**initial conditions**		M_n **(kg·mol^{-1})**		M_w **(kg·mol^{-1})**	
	NVP (vol%)	**V-50 (wt%)**	**experiment**	**model**	**experiment**	**model**
85	12.5	0.01	170	135	393	393
		0.02	159	108	373	359
		0.04	95	84	245	281
85	6.25	0.02	91	76	216	246
	12.5		159	108	373	359
	20		180	128*	510	516*
70	6.25	0.02	183	103	433	416
	12.5		150	145	590	594
70	12.5	0.04	187	120	527	490
	25		269	159*	715	831*

* Calculated with $k_{tr}^{pol}/k_p = 9\times10^{-5}$

3.8 Semibatch Operation

Polymerizations are often conducted in industry using starved-feed semibatch operation instead of batch for heat removal and safety considerations. Thus, the instantaneous conversion of monomer-to-polymer remains high throughout the feeding period as the weight fraction of polymer in the system continuously increases. Monomer profiles are very different than in batch, providing an opportunity to test the suitability of the k_p (eq 3.1 and 3.2) and k_t (eq 3.3) expressions for NVP over different combinations of conversion and weight fraction polymer in solution than can be achieved in batch. The equations need to be modified slightly, as the definition of w_{mon}^0 (initial weight fraction of monomer) becomes meaningless in semibatch, as usually the reaction is started with no initial monomer charge. The modified expressions for weight fraction monomer on a polymer-free basis (w'_{mon}), weight fraction of total NVP (monomer+polymer) in solution, and fractional conversion (x_p) are shown in Table 3.4. The differences between the two modes (batch and semibatch) of operation are illustrated by the simulations shown in Figure 3.15, comparing monomer concentration (Figure 3.15(a)) and conversion profiles (Figure 3.15(b)) for NVP polymerized at 70 °C with 0.04 wt% V-50 based on total charge to the system. For the batch polymerization, the 20 vol% NVP charge is present at the beginning of the polymerization, while for the semibatch simulation, the monomer is fed at a constant rate over a period of 2 h; the kink in the conversion profile indicates the end of the dosing period in the semibatch. For the batch simulation, k_p increases from 21000 to a final value of 54000 $L \cdot mol^{-1} \cdot s^{-1}$ at 100% conversion, as calculated from eq 3.1 and 3.2. In semibatch, k_p is relatively constant, between 47000 and 54000 $L \cdot mol^{-1} \cdot s^{-1}$, due to the smaller change in free monomer concentration that occurs for this mode of operation.

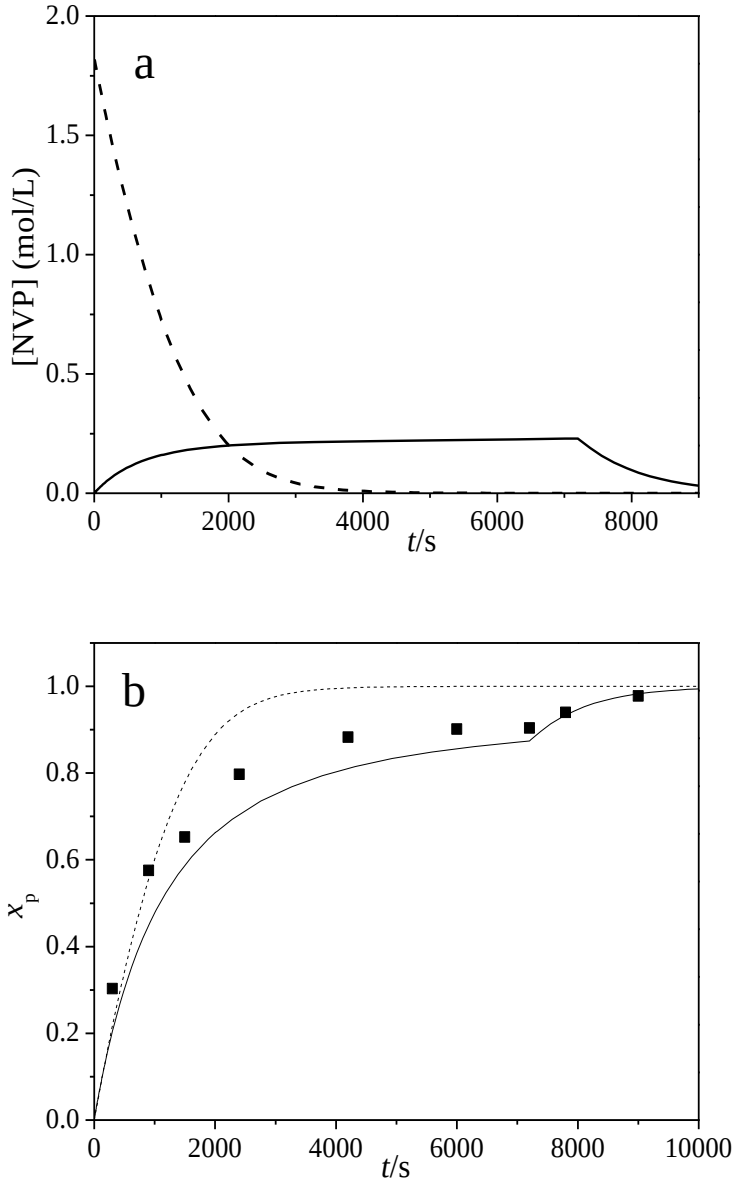

Figure 3.15. Comparison (by simulation) of the variation of (a) monomer concentration and (b) conversion profiles with time in batch (dashed line) and semibatch (solid line) operation of 20 vol% NVP and 0.04 wt% V-50 initiator at 70 °C, with monomer fed over a period of 2 h. Data points are experimental results from semibatch operation, measured by gravimetry.

Table 3.4. Comparison of expressions used in batch and semibatch systems. m_{total} indicates the total mass in the system

	Batch	Semibatch
Fractional conversion	$x_{\text{p}}(t) = \dfrac{m_{\text{pol}}(t)}{m^0_{\text{mon}}}$	$x_{\text{p}}(t) = \dfrac{m_{\text{pol}}(t)}{m_{\text{mon}}(t) + m_{\text{pol}}(t)}$
Weight fraction monomer (on polymer-free basis)	$w'_{\text{mon}}(t) = \dfrac{w^0_{\text{mon}}(1 - x_{\text{p}}(t))}{1 - w^0_{\text{mon}} x_{\text{p}}(t)}$	$w'_{\text{mon}}(t) = \dfrac{m_{\text{mon}}(t)}{\left(m_{\text{total}}(t) - m_{\text{pol}}(t)\right)}$
Weight fraction (monomer + polymer) in system	w^0_{mon}	$\dfrac{m_{\text{pol}} + m_{\text{mon}}}{m_{\text{total}}}$

Figure 3.15 also includes experimental conversion data for a semibatch NVP polymerization conducted with 0.04 wt% V-50 at 70 °C at a total amount of NVP of 20 vol%. It can be seen that the model captures the overall trend reasonably well. In order to test the predictive capabilities of the model, experiments were conducted at both 70 and 85 °C and at varying monomer feed times. The reproducibility of results was verified by repeating the experiment at 20 vol% NVP fed over a period of 30 minutes at 85 °C thrice. A comparison of the three sets of experimental data, along with the model predictions is shown in Figure 3.16. It is seen that there is a good agreement between two sets of experimental data with the third set giving slightly higher conversion values which matches the model data best. However, as the NMR data from one of the experiments also agrees best with the experiments giving lower (than model) conversion values, it is most likely that the model is over-predicting by a small factor. In order to check for possible discrepancies in the model, the experiment at 20 vol% NVP and 0.04 wt% V-50 concentration at 70 °C was conducted at a shorter dosing period of 30 minutes. A comparison of the experimental and model conversion data at the two different feed times is shown in Figure 3.17. At the relatively lower feeding period of 30 minutes, the monomer concentration in the system will increase at a much faster rate (compared to a dosing period of 120 minutes), reaching

its maximum at the end of the dosing period beyond which it proceeds like a batch experiment. Thus, the k_p change in the system with be more pronounced than with the longer dosing period. This behaviour seems to be captured well by the model at the shorter dosing period of 30 minutes with it slightly under-predicting the conversion values at the 120 minute dosing period. As the model over (Figure 3.16) and under (Figure 3.17) predicts in the different experiments, it becomes difficult to relate these discrepancies to any specific mechanism in the model. It may most likely just be due to differences in the dosing pattern of the labmax reactor (where the monomer is dosed in shots with periodic intervals in between) and Predici© (which assumes a continuous feed over the entire dosing period). However, the ability of the model to fit to these overall trends reasonably well is another strong indication that the k_p and k_t expressions developed from PLP studies capture the true kinetic behaviour of the system over a broad range of experimental conditions. As was observed for batch experiments run at higher NVP levels, the best fit for the MW averages was obtained by using the higher ratio of 9×10^{-5} for k_{tr}^{pol}/k_p (Figure 3.18), with the model providing a reasonable representation of the large increase in MW averages found experimentally at 85 °C.

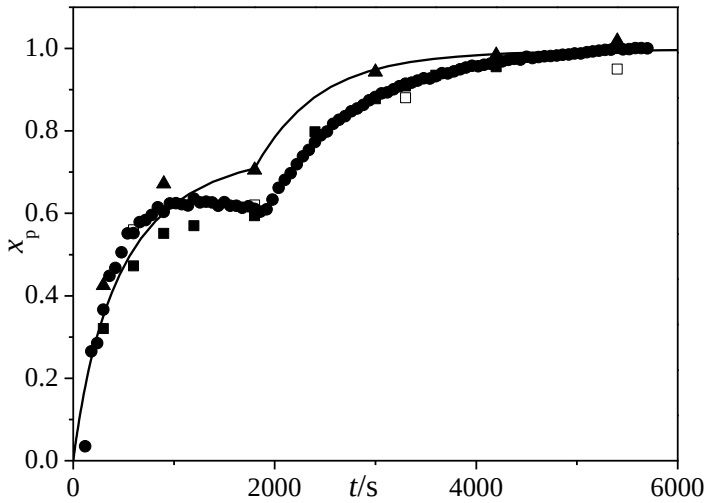

Figure 3.16. Reproducibility of conversion data for semibatch polymerization of 20 vol% NVP fed over a period of 30 minutes and 0.02 wt% V-50 in aqueous solution at 85 °C. The symbols and line represent the experimental and model results respectively. The circles represent data measured by IR, the squares and triangles represent data measured by gravimetry and the open symbols represent data measured by NMR.

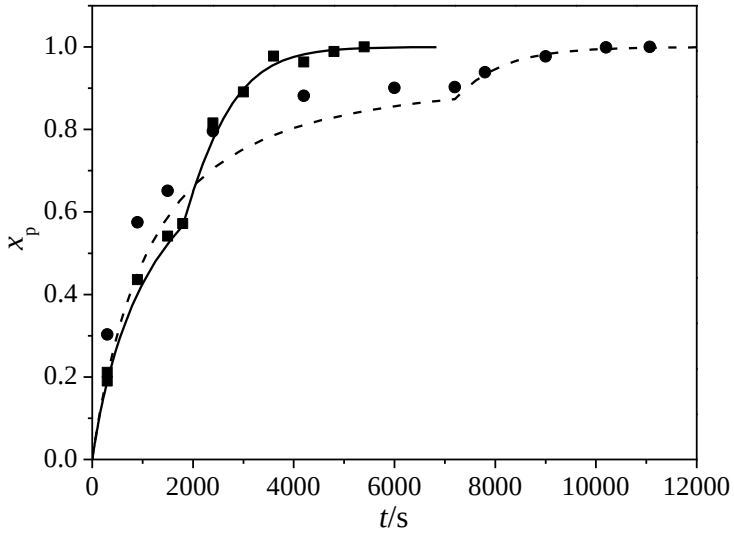

Figure 3.17. Comparison of experimental and model results for the influence of monomer feed times of 30 (■, ——) and 120 (●, -----) minutes on the semibatch conversion data, measured by gravimetry, at 20 vol% NVP and 0.04 wt% V-50 at 70 °C.

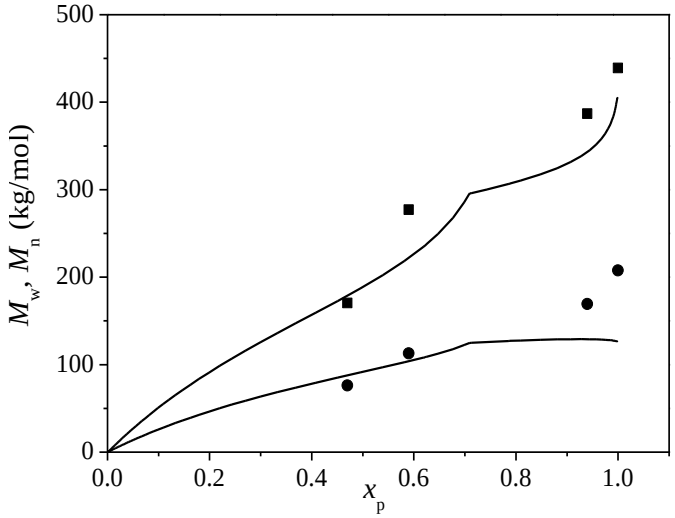

Figure 3.18. Polymer molecular-weight averages (M_w, M_n) plotted as a function of conversion for semibatch polymerization of 20 vol% NVP at 85 °C and 0.02 wt% V-50 initiator, with monomer fed over a period of 30 minutes. The lines represent the simulation predictions, and squares and circles are the experimental results for M_w and M_n, respectively. The simulations were carried out using $k_{tr}^{pol}/k_p = 9\times10^{-5}$ and $k_{tr}^{mon}/k_p = 6\times10^{-4}$.

3.9 Conclusions

The batch and semibatch free-radical polymerization of *N*-vinyl pyrrolidone in aqueous solution has been investigated at 70 and 85 °C over a range of monomer and initiator concentrations. The conversion profiles over all conditions and modes of operation are well represented by a model that uses, without any adjustment, expressions that capture the effect of conversion and monomer levels on k_p and k_t rate coefficients. As these expressions were developed based upon independent PLP studies, this agreement validates their accuracy and functional form.

The evolution of polymer MW averages and MWDs was also studied. Reasonable levels of chain transfer to monomer and a small amount of chain transfer to polymer was introduced to the model in order to match the general experimental trends. It is not clear whether the rate coefficients for these transfer reactions should be kept at a constant ratio relative to the changing k_p values (as assumed in the model), or should remain constant with conversion. The trends in

MW averages with conversion could be reasonably represented by introducing intermolecular chain transfer to polymer; however, it was necessary to adjust the rate coefficient to a higher value for polymerizations conducted with higher NVP levels. Furthermore, the exact mechanisms responsible for the shift in MWDs with conversion observed at higher NVP levels have not been identified. The general MW trends are captured by the model for both semibatch and batch modes of operation.

References

(1) Kirsh, Y. E., *Water Soluble Poly-N-vinylamides,* John Wiley & Sons, England, **1998**.

(2) A. I. Barabanova, E. V. Bune, V. F. Gromov, Vysokomol. Soedin., Ser. A Ser. B. **2001**, *43*, 732.

(3) V. F. Gromov, N. I. Galperina, T. O. Osmanov, P. M. Khomikovskii, A. D. Abkin, *Eur. Polym. J.* **1980,** *16,* 529.

(4) Y. V. Bune, A. I. Barabanova, Y. S. Bogachev, V. F. Gromov, *Eur. Polym. J.* **1997**, *33*, 1313.

(5) V. F. Gromov, Y. S. Bogachev, Y. V. Bune, I. L. Zhuravleva, E. N. Teleshov, *Eur. Polym. J.* **1991**, *27*, 505.

(6) E. Senogles, R. Thomas, *J. Polym. Sci.: Symp.* **1975**, *49*, 203.

(7) F. D. Kuchta, A. M. Van Herk, A. L. German, *Macromolecules* **2000**, *33*, 3641.

(8) S. Beuermann, D. A. Paquet, Jr, J. H. McMinn, R. A. Hutchinson, *Macromolecules* **1997**, *30*, 194.

(9) S. Beuermann, M. Buback, P. Hesse, S. Kukučková, I. Lacík, *Macromol. Symp.* **2007**, *248*, 23.

(10) I. Lacík, L. Učňová, S. Kukučková, M. Buback, P. Hesse, S. Beuermann, *Macromolecules* **2009**, *42*, 7753.

(11) S. Beuermann, M. Buback, P. Hesse, I. Lacik, *Macromolecules* **2006,** *39,* 184.

(12) S. Beuermann, M. Buback, P. Hesse, S. Kukučková, I. Lacik, *Macromol. Symp.* **2007**, *248*, 41-49.

(13) I. Lacík, S. Beuermann, M. Buback, *Macromolecules* **2003**, *36*, 9355.

(14) I. Lacík, S. Beuermann, M. Buback, *Macromol. Chem. Phys.* **2004**, *205*, 1080.

(15) S. A. Seabrook, M. P. Tonge, R. G. Gilbert, *J. Polym. Sci. Part A: Polym. Chem.* **2005**, *43*, 1357.

(16) M. Stach, M.; I. Lacík, D. Chorvat, Jr, M. Buback, P. Hesse, R. A. Hutchinson, L. Tang, *Macromolecules* **2008**, *41*, 5174.

(17) S. Beuermann, M. Buback, P. Hesse, R. A. Hutchinson, S. Kukuckova, I. Lacík, *Macromolecules* **2008**, *41*, 3513.

(18) Schrooten, S.; Buback, M.; Hesse, P.; Hutchinson, R. A.; Lacik, I. *Macromol. Chem. Phys*. **2011**, *212*, 1400-1409.

(19) M. Buback, P. Hesse, R. A. Hutchinson, P. Kasak, I. Lacík, M. Stach, I. Utz, *Ind. Eng. Chem. Res.* **2008**, *47*, 8197.

(20) Stach, M.; Lacik, I. Difference between MALLS and other calibrations, unpublished.

(21) Wako Chemicals information brochure

(22) M. Wulkow, *Macromol. React. Eng.* **2008**, *2*, 461.

(23) Tang, L., *MSc. Thesis, Queen's University* **2007**.

(24) Jiang, S.; Sudol, E. D.; Dimonie, V. L.; El-Asser, M. S. *J. App. Polym. Sci.*, **2008**, 107, 2453-2458.

(25) Hattori, M.; Sudol, E. D.; El-Asser, M. S. *J. App. Polym. Sci.*, **1993**, 50, 2027-2034.

(26) Stach, M.; Lacik, I.; Kasák, P.; Chorvát, D., Jr.; Saunders, A. J..; Santanakrishnan, S.; Hutchinson, R. A. *Macromol. Chem. Phys*. **2010**, *211*, 580-593.

Chapter 4. Polymerization Kinetics of Water-Soluble *N*-Vinyl Monomers in Aqueous and Organic Solution

This chapter is an updated version of the manuscript published in Macromolecular Symposia, **2011**, *302*, 216-223

4.1 Abstract

Free-radical batch polymerizations (FRP) of *N*-vinyl pyrrolidone (NVP) in organic (*n*-butanol) solution and *N*-vinyl formamide (NVF) in aqueous solution have been studied. The conversion and molecular weight behaviour of these systems have been compared to that of aqueous-phase polymerization of NVP (Chapter 3). The differences found in rate of monomer conversion with monomer and solvent choice correlates well with the differences in values of the propagation rate coefficients (k_p) and their variation with monomer concentration measured in independent pulsed-laser polymerization studies, a result demonstrating that a generalized understanding of water-soluble vinyl monomers can be obtained once their k_p differences have been accounted for.

Due to the scatter in the MW data for NVP in butanol and the discrepancies between the results obtained from RI and MALLS detectors, fitting of the transfer coefficients to match the MW behaviour of this system was not undertaken, and the experimental MW data for this system was compared to the model predictions using the same transfer coefficients as in the aqueous NVP model, with the inclusion of the additional transfer to butanol. Howvere, a reasonable representation of the NVF MW data was obtained by simply accounting for k_p differences in the aqueous NVP model.

4.2 Introduction

Poly(*N*-vinyl amides) are a class of water soluble polymers finding applications in science and

medical practice.[1] Poly(vinylpyrrolidone) (PVP) is one of the most commercially-important polymer in this class. PVP and its copolymers find applications in a variety of fields such as medicine, pharmaceuticals, cosmetics, food, textiles etc.[1] Other important poly(*N*-vinyl amides) include poly(vinylformamide) (PVF) and its copolymers. Due to its low toxicity, PVF and its copolymers find applications in waste water treatment, adhesives, packaging, personal care products, dispersing agents, textiles and corrosion inhibition.[2,3] As discussed in Chapter 2, despite their importance in commercial applications, the understanding of these systems has lagged behind mainly due to the deviation of their polymerization kinetics from the expected behaviour resulting from the influence of solvent medium on the polymerization kinetics. A literature review on some of the earlier studies on solvent effects by Gu et al.,[4] Gromov et al.,[5-8] Chapiro,[9] Senogles at al.[10] can be found in Chapter 2 and will not be repeated here. Although, these studies made it clear that water-soluble monomers exhibit unusual reaction kinetics, the lack of data on the individual rate coefficients in these studies made it difficult to get an improved kinetic understanding of these systems. This situation has changed considerably after the advent and application of specialized techniques such as PLP-SEC (Pulsed Laser Polymerization-Size Exclusion Chromatography) and SP-PLP-NIR (Single Pulse-Pulsed Laser Polymerization-Near Infrared), which enable the determination of individual propagation (k_p) and termination (k_t) rate coefficients. The groups of Buback and Lacík have jointly conducted extensive PLP-SEC studies on MAA[11-14] and AA.[15,16] More recent studies include the PLP-SEC study of NVP[17] and NVF[18] and SP-PLP study of the termination kinetics of NVP.[19] A complete review of all these PLP studies can also be found in Chapter 2. We have modeled the kinetic behaviour of aqueous-phase free radical polymerization of NVP using these PLP-SEC derived k_p and k_t coefficients (Chapter 3). The goal of this chapter is to model the kinetic behaviour of

organic-phase (butanol) polymerization of NVP and aqueous-phase polymerization of NVF using PLP-SEC derived k_p coefficients as well as explain the kinetic differences arising from solvent and monomer choice using the understanding gained from the PLP-SEC k_p studies.

4.3 Organic-Phase Free Radical Polymerization of N-vinyl pyrroldione (NVP)

4.3.1 Experimental

N-vinyl pyrrolidone (>99%, Aldrich, contains 100 ppm sodium hydroxide as inhibitor), *n*-butanol (99.9%, Sigma-Aldrich) and the thermal initiator 2,2´-azobis(2-methyl butyronitrile) (Vazo-67, DuPont) were used as received. Polymerizations were carried out isothermally in a 1 L automated (MT Autochem) stirred reactor under nitrogen blanket and conversion was tracked using gravimetry. Reproducibility of results was checked by repeating the experiment at 12.5 vol% NVP and 0.11 wt% V-50 at 85 °C and the results are shown in Figure 4.1. There is a very small initial inhibition period in the repeat experiment which is responsible for the slight offset between the profiles in the initial period, but, good agreement is observed within 600 s into the experiment.

SEC Analysis. Molecular weight (MW) analysis was carried out by size-exclusion chromatography (SEC) at the Polymer Institute of the Slovak Academy of Sciences using PSS GRAM column set-up which consists of three 10 μm columns of 100, 1000 and 3000 Å pore sizes. The measurements were carried out at a temperature of 45 °C uisng an injection volume of 100 μL and a flow rate of 0.8 $mL \cdot min^{-1}$. The MW data was obtained using the RI (with respect to PS calibration) and MALLS detectors. The data from RI were shifted by a correction factor of 1.53 based upon the measure of absolute MWs by light scattering of the samples prepared in this work. A comparison of the MALLS and corrected RI data for the experiment at 12.5 vol% NVP

and 0.11 wt% V-50 at 85 °C is shown in Figure 4.2. The discrepancies observed between the RI and MALLS MW data were even more significant than was observed in the aqueous NVP study (Chapter 3). The data from MALLS showed a significant shift with conversion with some very narrow or broad distribution in some cases. Furthermore, even the corrected M_w RI values did not match the MALLS results in some cases. These discrepancies have been discussed elaborately in the results and discussion section. A more complete comparison of MALLS and RI data for all the experiments is shown in Appendix A.2.

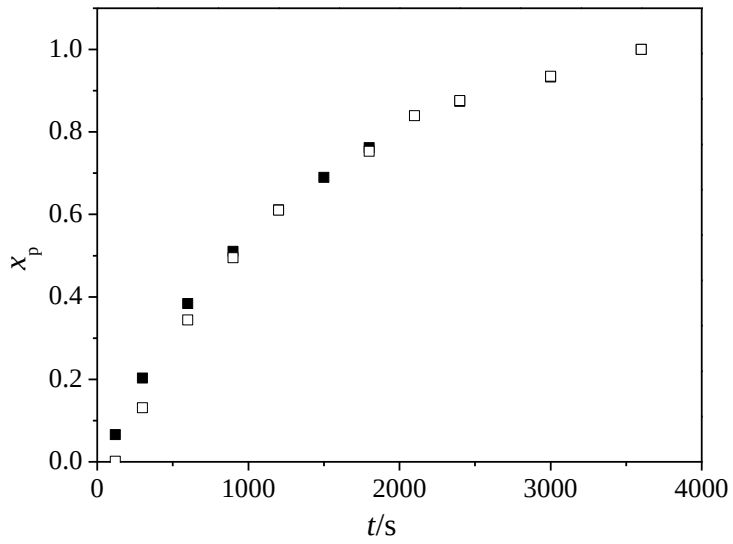

Figure 4.1. Comparison of conversion data, as measured by gravimetry, for repeat batch solution polymerizations of 12.5 vol% NVP and 0.11 wt% Vazo-67 in butanol at 85 °C.

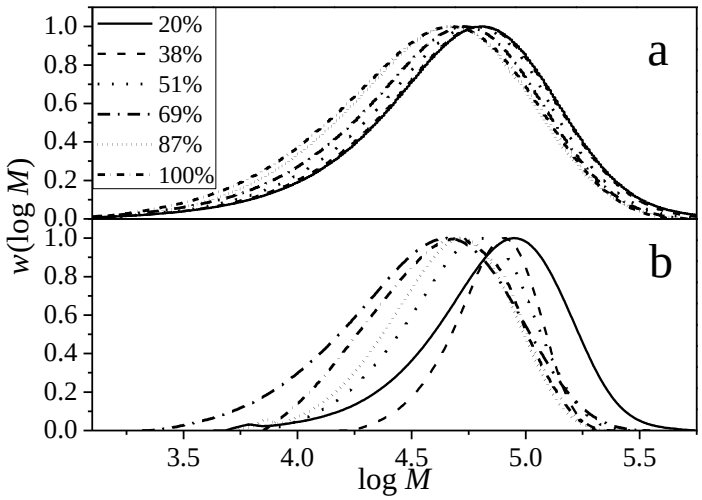

Figure 4.2. Comparison of a) corrected RI and b) MALLS data for the evolution of polymer MWDs with conversion for 12.5 vol% NVP and 0.11 wt% Vazo-67 in butanol at 85 °C. Conversion levels as indicated in the legend.

4.3.2 Model Development

As discussed in Chapter 3, the kinetic model for free-radical NVP polymerization, built using Predici©, includes the mechanisms of initiation, propagation, transfer and termination. The rate coefficients and model parameters for aqueous-phase NVP polymerization are detailed in Chapter 3, with k_p[17] and k_t[19] expressions developed from PLP studies. Both the aqueous and organic models for NVP use identical rate expressions, with the only differences arising from the k_p expressions (fit to PLP-SEC experimental data),[20] the introduction of chain transfer to *n*-butanol (for organic phase polymerization), and the initiator decomposition expressions, as two different initiators (V-50[21] in aqueous phase and Vazo-67[22] in organic phase) were used due to the insolubility of V-50 in *n*-butanol. A typical azo initiator efficiency of 0.7 was assumed for both initiators.

Table 4.1 Values and expressions for the kinetic rate coefficients and physical parameters used in the model of organic-phase free-radical polymerization of *N*-vinyl pyrrolidone

Mechanism	Rate Expression	Values @ 85 °C	Ref
Initiator decomposition	$k_{\mathrm{d}}(s^{-1}) = 1.38\times10^{15}\exp\left(\frac{-1.55\times10^{4}}{(T/\mathrm{K})}\right)$	$2.24\text{x}10^{-4}$	22
Initiator calculation*	$\left(k_d[I]_0\right)_{\text{Vazo-67}} = \left(k_d[I]_0\right)_{\text{V-50}}$		
Propagation	$\frac{k_{\mathrm{p}}}{k_{\mathrm{p,max}}} = 0.02 + 0.98\exp\left(-\frac{1.5\cdot w^{0}_{\mathrm{NVP}}\cdot\left(1-x_{\mathrm{p}}\right)}{1-w^{0}_{\mathrm{NVP}}\cdot x_{\mathrm{p}}}\right)$		
	$k_{\mathrm{p,max}}\Big/\left(\mathrm{L}\cdot\mathrm{mol}^{-1}\cdot\mathrm{s}^{-1}\right) = 1.42\times10^{7}\exp\left(-\frac{2.43\times10^{3}}{(T/\mathrm{K})}\right)$	$1.61\text{x}10^{4}$	20
Termination	$k_{\mathrm{t}}\Big/\left(\mathrm{L}\cdot\mathrm{mol}^{-1}\cdot\mathrm{s}^{-1}\right) = 1.5\times10^{8}\exp\left(-w^{0}_{\mathrm{NVP}}/0.29\right)+1.68\times10^{7}$		19
	at P = 1 bar		
Transfer to solvent	$\frac{k^{\mathrm{sol}}_{\mathrm{tr}}}{k_{\mathrm{p}}}$	$1.5\text{x}10^{-4}$	this work
Density of Butanol	$\rho_{\mathrm{Butanol}}\Big/\left(\mathrm{g}\cdot\mathrm{mL}^{-1}\right) = 0.82473 - 0.000733(T/{}^{\circ}\mathrm{C})$	0.762	20

4.3.3 Results and Discussion

Conversion data. The influence of monomer concentration on k_p is more pronounced in water than in *n*-butanol as can be seen from Figure 4.3, which summarizes an extensive PLP-SEC study of NVP in aqueous[17] and organic[20] solution. The variation of NVP k_p in *n*-butanol as a function of initial weight fraction of NVP in solution (w^0_{NVP}), temperature, and fractional conversion of monomer to polymer (x_p) is captured by Equations 4.1 and 4.2.

$$\frac{k_p}{k_{p,max}} = 0.02 + 0.98 \exp\left(-\frac{1.5 \cdot w^0_{NVP} \cdot (1 - x_p)}{1 - w^0_{NVP} \cdot x_p} \right) \tag{4.1}$$

$$k_{p,max} \Big/ \left(L \cdot mol^{-1} \cdot s^{-1} \right) = 1.42 \times 10^7 \exp\left(-\frac{2.43 \times 10^3}{(T / K)} \right) \tag{4.2}$$

The thermal initiators V-50 and Vazo-67 decompose by a first-order reaction with half-lives of 16 min[21] and 54 min[22] at 85 °C, respectively. This difference in the decomposition rates was compensated for by adjusting the moles of initiator added, in order to achieve equal initial radical generation rate in the two solvents, assuming equivalent initiator efficiencies:

$$\left(k_d [I]_0 \right)_{Vazo\text{-}67} = \left(k_d [I]_0 \right)_{V\text{-}50} \tag{4.3}$$

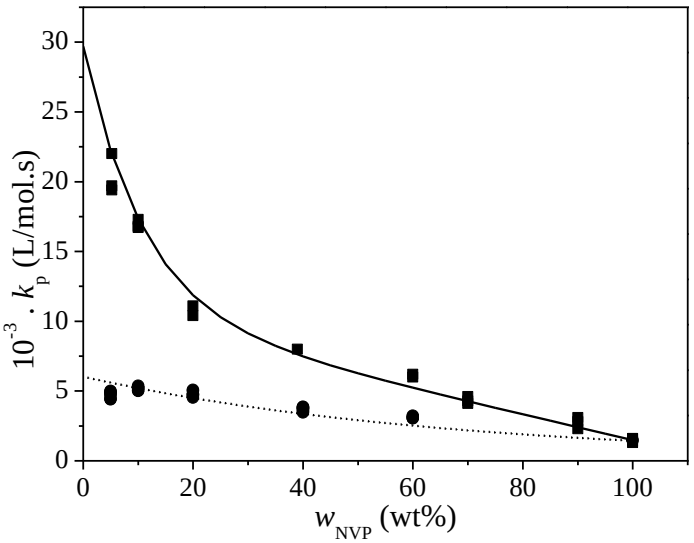

Figure 4.3. The influence of *N*-vinyl pyrrolidone concentration (w_{NVP}) on the propagation rate coefficient (k_p) for polymerization in aqueous (■)[17] and butanol (●)[20] solution, as measured by PLP-SEC experiments at 40 °C.

At the lower NVP concentrations used in batch polymerizations (w_{NVP} < 20%), it is expected that the significantly lower k_p values in *n*-butanol should result in a conversion rate significantly lower than that in aqueous solution, assuming that k_t is similar in the two systems. This difference was indeed found experimentally, as seen from the comparison of monomer conversion profiles in Figure 4.4 (a), obtained from batch polymerizations at 85 °C with 12.5 vol% NVP and the same initial radical generation rate in solution. (MW averages, shown as Figure 4.4 (b) will be discussed later.) Previous work showed that aqueous-phase NVP batch and semibatch polymerizations conducted over a range of initial monomer and initiator concentrations at 70 and 85 °C are well-represented by the FRP model parameters summarized in Chapter 3. A similar set of experiments in *n*-butanol has been completed at 85 °C. The influence of initial monomer and initiator concentrations on conversion profiles is shown in Figure 4.5 (a) and (b) respectively. As expected, the polymerization rate increases with increase in initiator concentration and this is captured very well by the model (Figure 4.5 (b)) The effect of NVP

concentration on polymerization rate (Figure 4.5 (a)) was found to be negligible in *n*-butanol, in agreement with the PLP-SEC results shown in Figure 4.3. Moreover, the model developed to describe aqueous-phase NVP polymerization also provides a good description of the conversion profiles measured in *n*-butanol over a range of monomer and initiator concentrations, once the difference in k_p behaviour is accounted for. The slight mismatch between model predictions and experimental results in Figure 4.5 may indicate a small difference in NVP k_t behaviour for the two solvents. From these results it can be concluded that the k_p expressions determined from independent pulsed laser investigations capture the differences observed for the experimental conversion profiles of NVP in aqueous and organic solution.

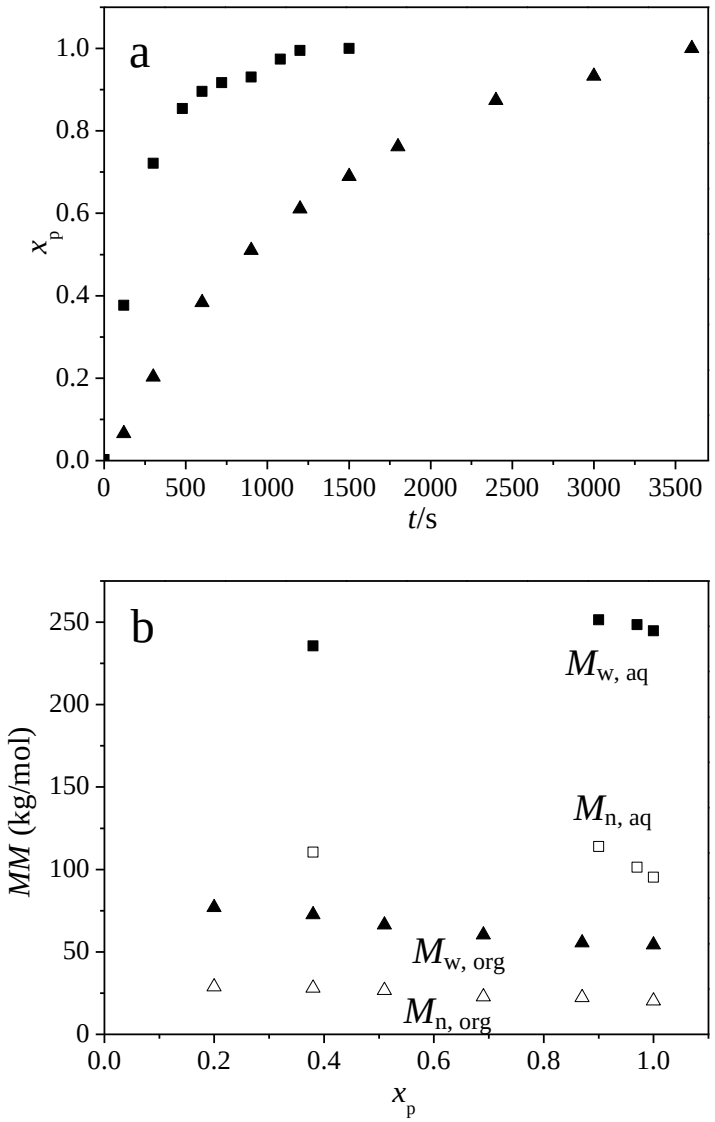

Figure 4.4. (a) Conversion profiles measured by gravimetry and (b) polymer weight and number molecular weight averages (M_w filled symbols, M_n open symbols) plotted as a function of conversion for batch polymerization of 12.5 vol% NVP at 85 °C in water (■) and butanol (▲) with the same initial radical generation rate.

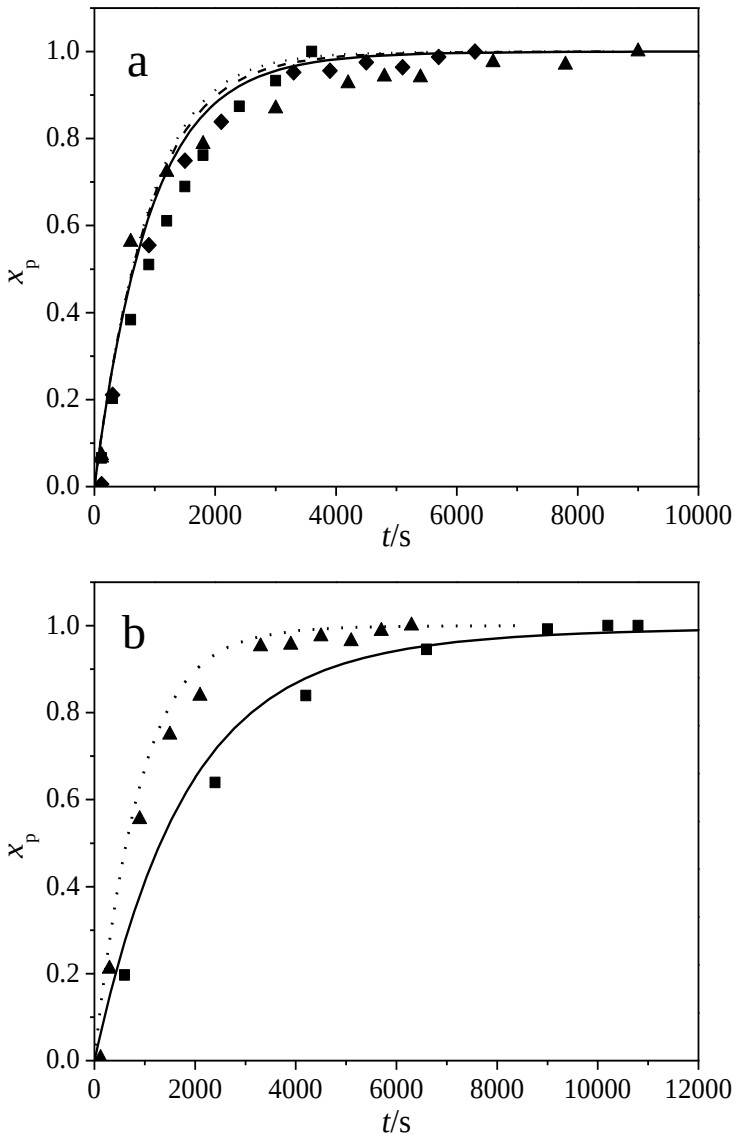

Figure 4.5. Conversion profiles, measured by gravimetry, for organic-phase batch polymerizations of NVP at 85 °C. (a) Influence of NVP concentrations of 12.5 (■, ——), 20 (◆, – – –) and 30 (▲, ·····) vol% at an initiator concentration of 0.11 wt% Vazo-67. (b) Influence of initiator concentrations of 0.027 (■,——) and 0.11 (▲,·····) wt% Vazo-67 with initial NVP level of 20 vol%. The lines represent the simulations and the symbols represent the experimental results.

Molecular weight behaviour. As discussed in Chapter 3, discrepancies between the MW data from RI and RI-MALLS detectors are not very unusual for these water-soluble systems. Although this discrepancy was observed in the PDI values of the NVP samples polymerized in aqueous solution (Chapter 3), a reasonable agreement between the MALLS and corrected RI M_w

values was obtained. However, in this study on the NVP polymerization in butanol, a significant disagreement between the MALLS and the corrected RI M_w values was observed in some cases, as shown in Figure 4.6. The significant scatter in Figure 4.6 indicates that the correction factor (1.53) may not be suitable for some experiments. This is more clearly observed from Figures 4.7-4.10 which compare the evolution of MW averages from MALLS and corrected RI with conversion, for batch experiments at varying initial monomer and initiator concentrations. These Figures show a significant disagreement between the MALLS and the corrected RI MW averages. Furthermore, the scatter in the data is high, making it difficult to understand the overall trends in some cases. Despite these uncertainties, it was attempted to model the MW behaviour of this system by comparing and contrasting their behaviour to the NVP aqueous system.

The significantly lower k_p values for polymerization in organic compared to aqueous solution also affects polymer MW, as was shown in Figure 4.4 (b); MW averages of polymer produced in *n*-butanol are significantly lower than that polymer produced in water. Most of the difference in the data can be explained by the differences in k_p values; however, a small amount of chain transfer to *n*-butanol ($k_{tr}^{sol}/k_p = 1.5\times10^{-4}$ at 85 °C) was added to the model to better match the experimental data, with the transfer to monomer and transfer to polymer ratios set to the values determined from the aqueous-phase study of NVP polymerization (Chapter 3). A comparison of the model and experimental MW averages at 12.5 vol% NVP and 0.11 wt% Vazo-67 and 20 vol% NVP and 0.027 wt% Vazo-67 is shown in Figures 4.11 (a) and (b) respectively. The MW averages show a decrease with increasing conversion in the case of the lower monomer concentration of 12.5 vol%, as is usually the case with polymerization involving chain transfer to solvent. However, at higher monomer concentration of 20 vol%, there is a dip in the averages followed by an increase. This behaviour can be explained by the chain transfer to solvent being

predominant in the initial stages which is responsible for the initial dip, but, as polymerization proceeds and the polymer concentration in the system increases, transfer to polymer may become more significant at the higher conversion levels which cause the upswing in the MW values. The shift in molecular weight with conversion is also clearly observed in the MWDs shown in Figure 4.12. It is to be noted that transfer to polymer $k_{tr}^{pol} / k_p = 6 \times 10^{-5}$ used at the low monomer concentrations in the aqueous NVP model was used at all monomer concentrations in the butanol model as increasing it to $k_{tr}^{pol} / k_p = 9 \times 10^{-5}$ did not have any significant effect in this case, as shown by the dotted line in Figure 4.11 (b). The model is observed to predict higher MW values and fails to capture the earlier time behaviour at the higher monomer concentration (Figure 4.11 (b)). However, an attempt to lower the transfer to monomer and solvent to match the initial MW values and significantly increase the k_{tr}^{pol} / k_p to match the subsequent upswing at the higher monomer concentration was unsuccessful. The transfer coefficients would need to be varied for each experiment, which is not suitable for a predictive model. Furthermore, due to the uncertainties in the correction factor and the significant scatter in the data from both MALLS and RI, fitting the transfer coefficients to match the experimental MW data in this system did not seem very promising. It was therefore decided not to pursue the MW modeling for this system further and merely compare the experimental data to the model predictions obtained by using the same monomer and polymer transfer coefficients as was used in the aqueous NVP study.

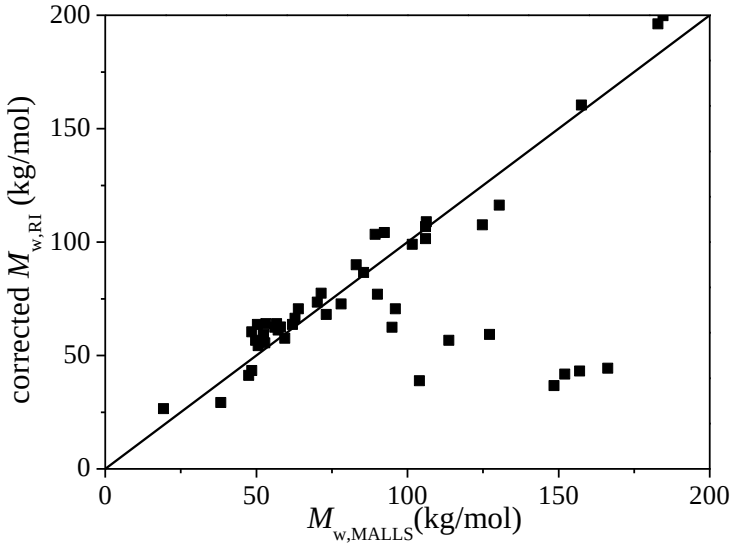

Figure 4.6. Comparison of MALLS and Corrected RI M_w values for all the NVP batch and semibatch experiments in butanol at 85 °C.

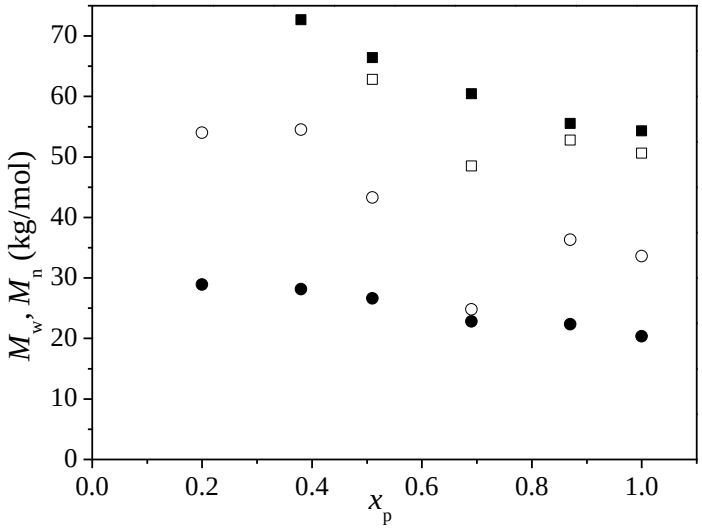

Figure 4.7. Comparison of MW averages from MALLS (open symbols) and corrected RI (filled symbols) for the batch polymerization of 12.5 vol% NVP and 0.11 wt% Vazo-67 in butanol at 85 °C. The squares and circles represent M_w and M_n values respectively.

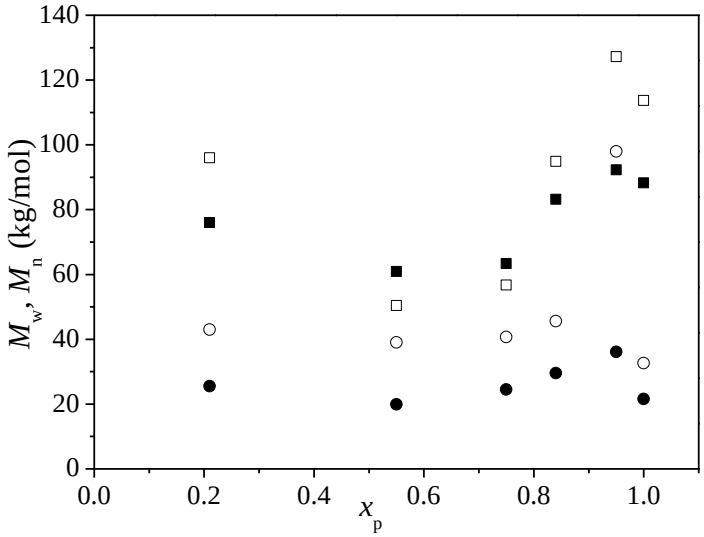

Figure 4.8. Comparison of MW averages from MALLS (open symbols) and corrected RI (filled symbols) for the batch polymerization of 20 vol% NVP and 0.11 wt% Vazo-67 in butanol at 85 °C. The squares and circles represent M_w and M_n values respectively.

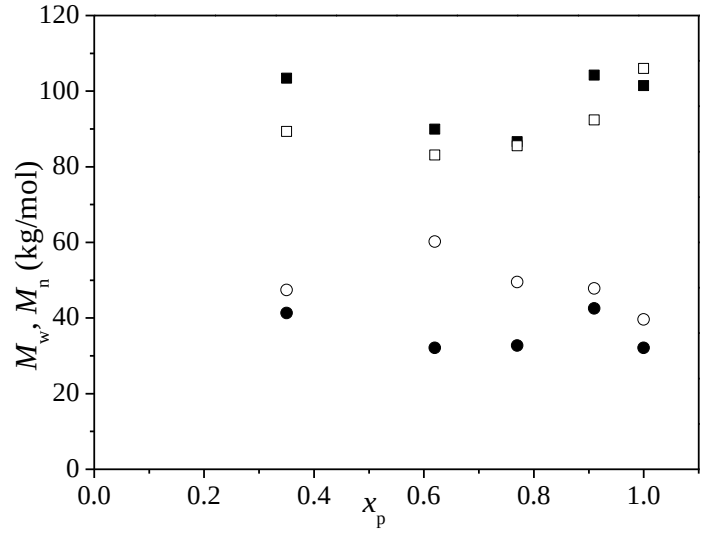

Figure 4.9. Comparison of MW averages from MALLS (open symbols) and corrected RI (filled symbols) for the batch polymerization of 30 vol% NVP and 0.11 wt% Vazo-67 in butanol at 85 °C. The squares and circles represent M_w and M_n values respectively.

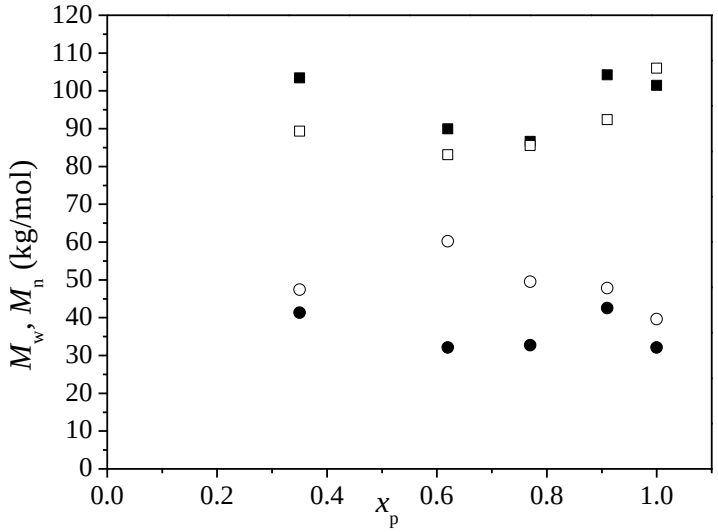

Figure 4.10. Comparison of MW averages from MALLS (open symbols) and corrected RI (filled symbols) for the batch polymerization of 20 vol% NVP and 0.027 wt% Vazo-67 in butanol at 85 °C. The squares and circles represent M_w and M_n values respectively.

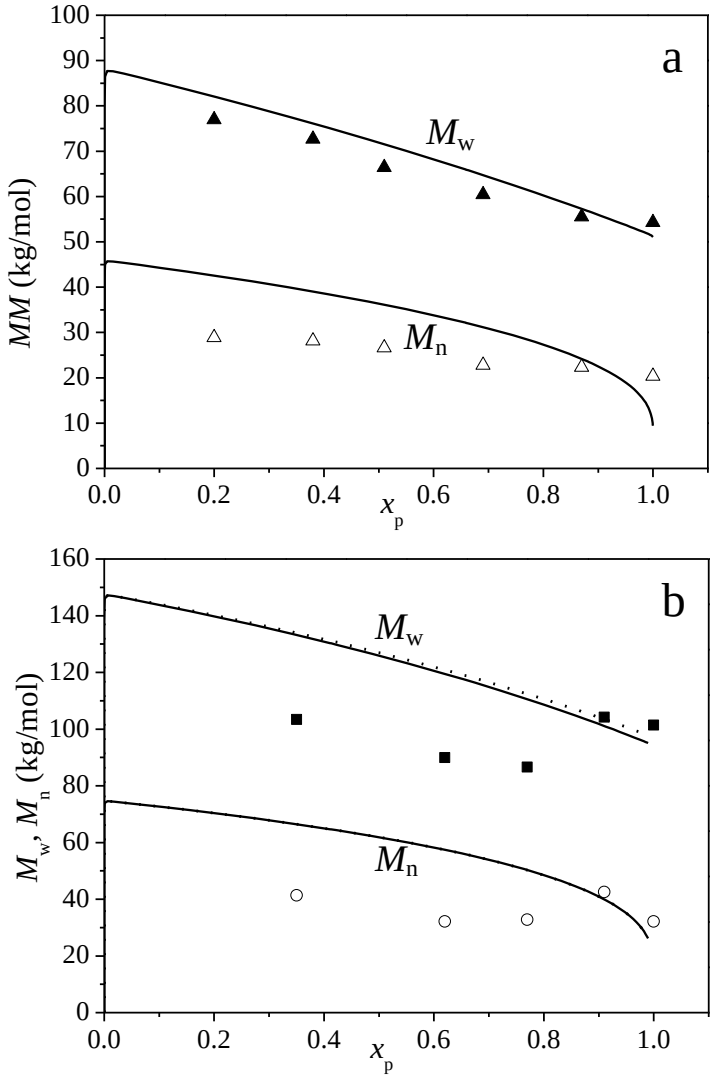

Figure 4.11. Polymer molecular-mass averages plotted as a function of conversion for batch experiments conducted in *n*-butanol at 85 °C with (a) 12.5 vol% NVP and 0.11 wt% Vazo-67 and (b) 20 vol% NVP and 0.027 wt% Vazo-67. The lines represent the simulation results and the closed and open symbols represent the experimental results for M_w and M_n, respectively. The simulations were carried out with $k_{tr}^{mon}/k_p = 6\times10^{-4}$, $k_{tr}^{pol}/k_p = 6\times10^{-5}$ (——), $k_{tr}^{pol}/k_p = 9\times10^{-5}$ (·····) and $k_{tr}^{sol}/k_p = 1.5\times10^{-4}$.

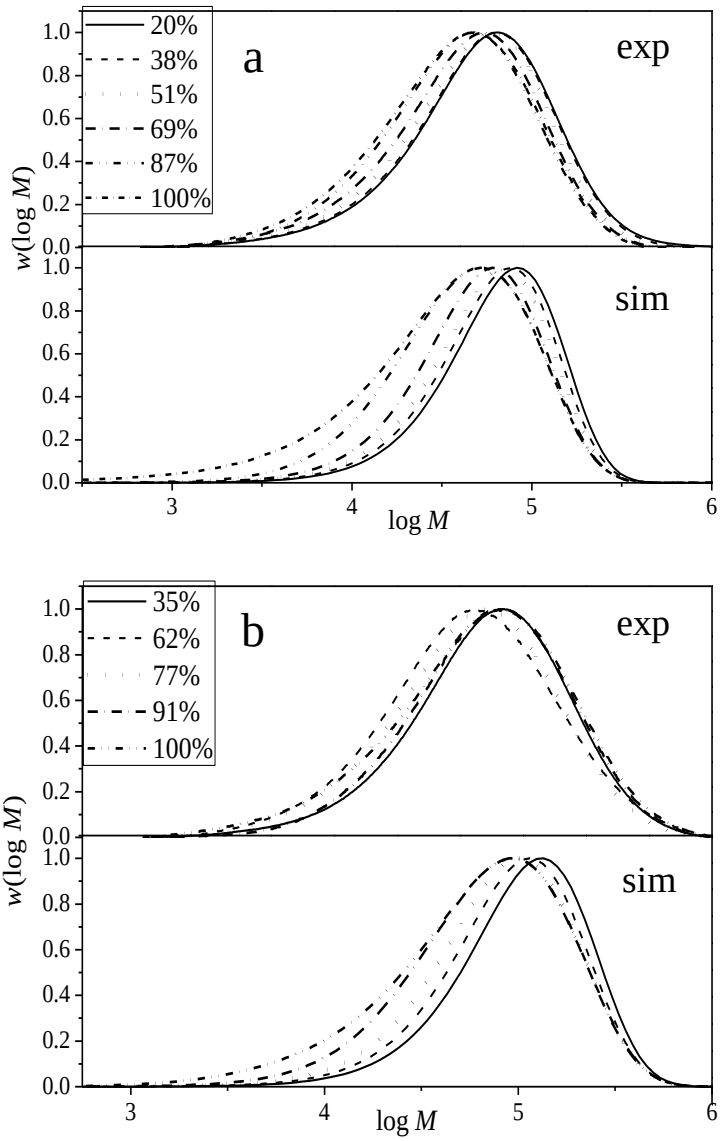

Figure 4.12. Comparison of simulation and experimental molecular-weight distributions obtained for (a) 12.5 vol% NVP and 0.11 wt% Vazo-67 and (b) 20 vol% NVP and 0.027 wt% Vazo-67 at 85 °C in *n*-butanol. Polymer conversions as indicated in the figure legends. The simulations were carried out using $k_{tr}^{mon}/k_p = 6\times10^{-4}$, $k_{tr}^{pol}/k_p = 6\times10^{-5}$ and $k_{tr}^{sol}/k_p = 1.5\times10^{-4}$.

4.3.4 Semibatch operation

Similar to the aqueous-phase studies, the predictive capabilities of the model were tested by conducting semibatch experiments of NVP in butanol. Semibatch experiments were carried out at two different monomer concentrations of 20 and 30 vol% NVP fed over a period of 30 minutes and 0.11 wt% Vazo-67 at 85 °C. A comparison of the experimental and model

conversion data for the two experiments is shown in Figure 4.13. Due to the very similar monomer levels at any instant and the relatively small monomer dependence of k_p, the conversion profiles for both the experiments were very similar, as expected. As for the batch experiments, a good agreement between the experimental and model data was obtained; the small offset with the model predicting slightly higher values, also found in batch, may indicate small k_t differences in the two solvents. A comparison of the experimental (MALLS and corrected RI) and model MW averages for the semibatch experiments at 20 and 30 vol% NVP in butanol is shown in Figure 4.14. As was discussed earlier for the batch experiments, due to the discrepancy between the MALLS and the corrected RI data coupled with the scatter in the data, the transfer coefficients were not adjusted to improve the fit and were just set to the same values used in the aqueous NVP study. Although the fit to the M_w values is not very good, the model fits the M_n values reasonably well.

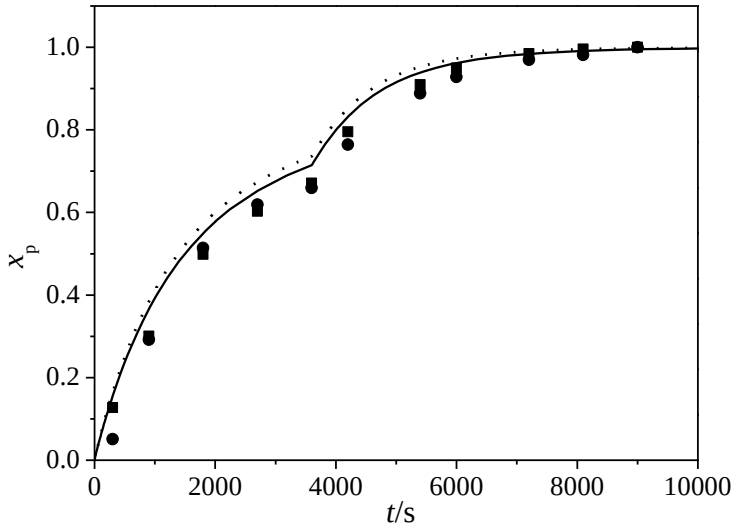

Figure 4.13. Comparison of experimental and model conversion data for the semibatch polymerization of 20 (■, ——) and 30 (●, ·····) vol% NVP fed over a period of 30 minutes in butanol at 0.11wt% Vazo-67 at 85 °C. The lines represent the model predictions and the symbols represent the experimental results measured by gravimetry.

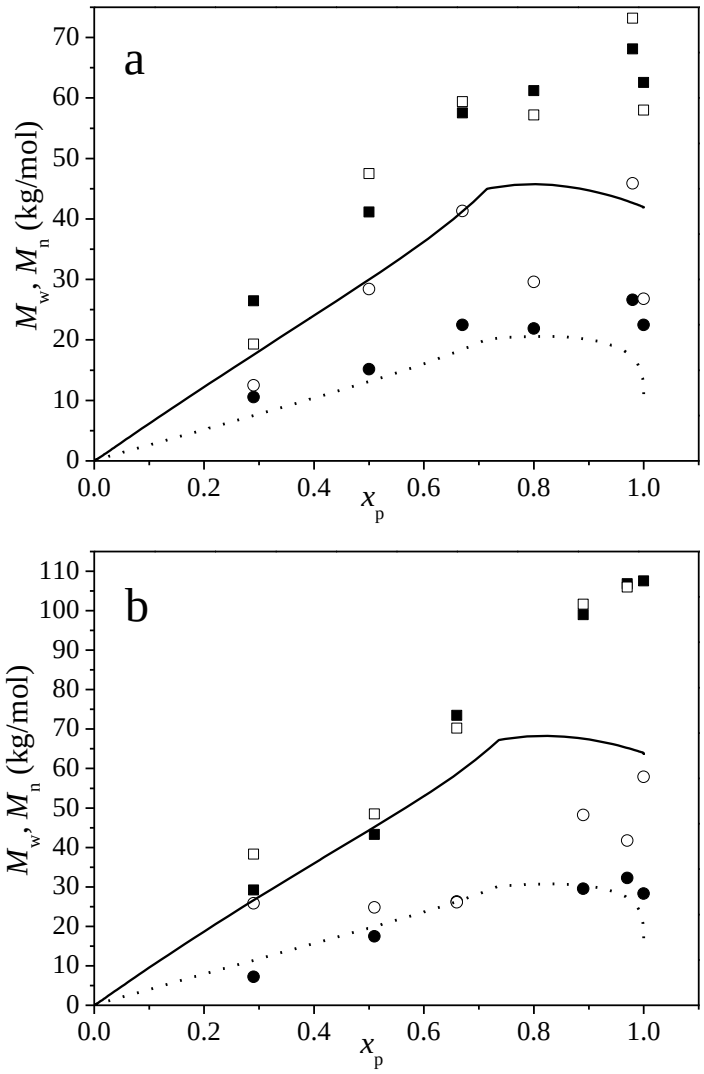

Figure 4.14. Comparison of MALLS (open), corrected RI (filled) and model MW averages for the semibatch polymerization of a) 20 and b) 30 vol% NVP fed over a period of 30 minutes in butanol at 0.11wt% Vazo-67 at 85 °C. The lines and symbols represent the model and experimental results, with the squares and circles representing M_w and M_n values respectively.

4.4 Aqueous Phase Polymerization of *N*-vinylformamide (NVF)

4.4.1 Experimental

N-vinylformamide (98%, Aldrich, contains ~0.0025-0.0055% 4-hydroxy-2,2,6,6-tertramethylpiperidinoxyl as inhibitor) and the thermal initiator 2,2'-azobis (2-methylpropionamidine) dihydrochloride (V-50, Fluka, $\geq 98\%$) were used as received. The experiments were carried out in a similar fashion as the NVP experiments and conversion levels were tracked using online IR and offline gravimetry and NMR analysis.

ReactIR. A React-IR 4000 (MT Autochem) was used to track the extent of monomer conversion online by integrating the area under the peak representing the vinyl double bond, appearing in the range of ~951 - 1012 cm^{-1}, and converting to monomer concentration using a calibration established via off-line studies. This online measurement yields an estimate of conversion every 2 min.

NMR Analysis. The NMR spectrums of NVF and PVF are shown in Figure 4.16, with peak assignments labeled according to Figure 4.15. NVF exists as cis (~30%) and trans (~70%) isomers,[1] which are indicated by the letters c and t in the spectrum. The isomer conformations have been indicated with reference to the position of the H attached to the carbonyl group in relation to the vinyl group, in accordance with the literature reference.[1] As peaks 1 and 3 integrate for one hydrogen each, the peaks 1c and 1t should match that of 3c and 3t respectively. From the spectra, it can be noted that the peak 3' encompasses the monomer peak 3t as well as the peak representing the H attached to the carbonyl group in the polymer, Conversion is therefore given by $x_p = \frac{(\text{peak3'-peak1t})}{(\text{peak3'+peak1c})}$

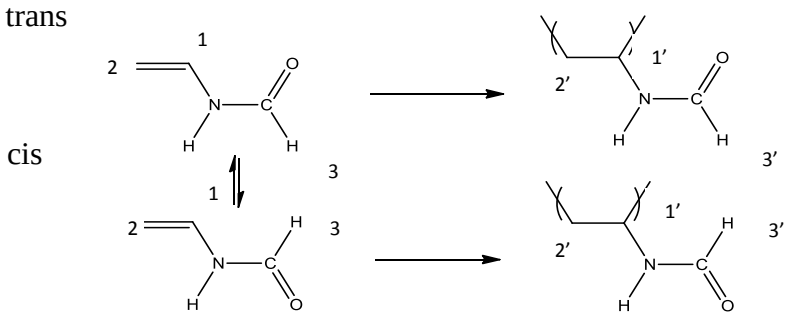

Figure 4.15. Conversion of *N*-vinyl formamide (NVF) to poly(*N*-vinyl formamide) (PVF).

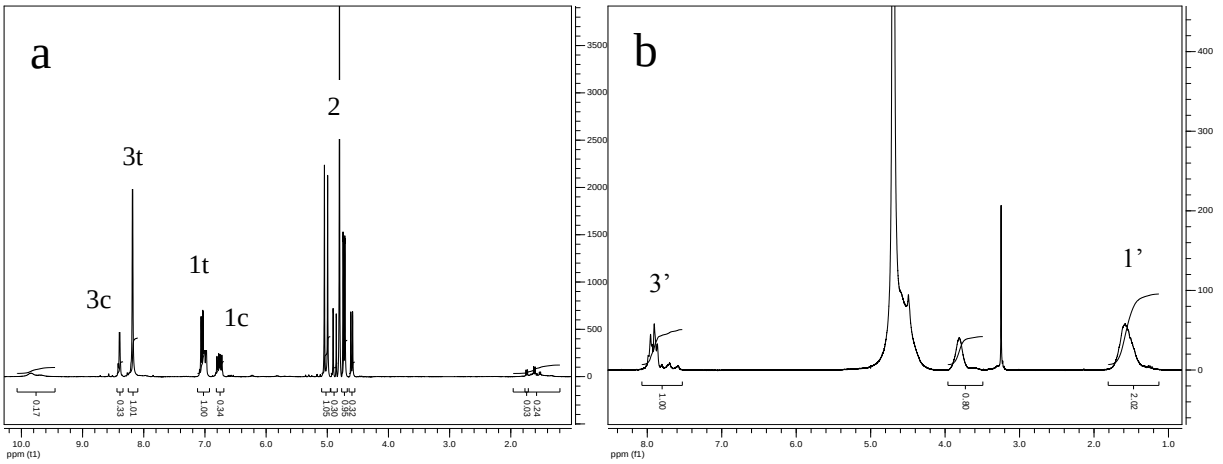

Figure 4.16. NMR spectrums of (a) NVF and (b) PVF.

SEC Analysis. Molecular weight analysis was carried out by size-exclusion chromatography (SEC) at the Polymer Institute of the Slovak Academy of Sciences, Bratislava using TosoH Biosep column setup which consists of 6 mm x 40 mm guard column and three 7.8 mm x 300 mm column of pore sizes 200, 1000 and >1000 Å in a column heater . The measurements were carried out at 25 °C. The eluent used was a mixture of water/acetonitrile (80:20) with 0.15 M NaCl and 0.03 M NaH_2PO_4. The MW values were obtained using RI (effective calibration towards poly(ethylenle oxide) (PEO)/poly(ethylene glycol) (PEG)) and MALLS detectors. The data from RI were shifted by a correction factor of 0.41, based on the absolute MWs obtained by

light scattering technique. A comparison of the corrected RI and MALLS data for the experiment at 12.5 vol% NVF and 0.02 wt% V-50 in water at 85 °C is shown in Figure 4.17. As was observed for the NVP experiments, there was a discrepancy between the data from the RI and MALLS detectors, with the data from MALLS showing a much higher shift with conversion. As done for the other systems, the corrected RI data will be used for the rest of the discussion. A complete comparison of the RI and MALLS data for the different NVF experiments is shown in Appendix A.3

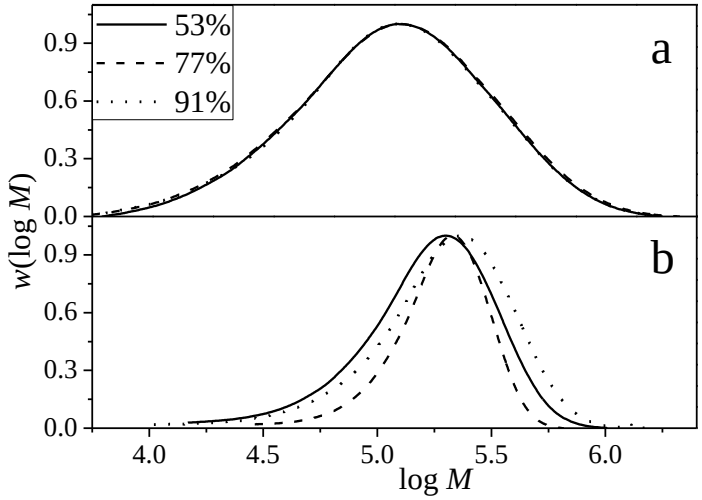

Figure 4.17. Comparison of a) corrected RI and b) MALLS data for the evolution of MWDs with conversion for 12.5 vol% NVF and 0.02 wt% V-50 in water at 85 °C. Conversion levels as indicated in the legend.

4.4.2 Model Development

NVF was modeled using the same kinetic model developed for aqueous-phase polymerization of NVP, with the only differences arising from the propagation behaviour of the two monomers, as shown in Figure 4.18 from the extensive PLP studies on the two monomers. The PLP-SEC derived k_p expression for NVF in water is described in eqn. 4.4 and 4.5.[18] The model makes use

of the same k_t[19] and transfer coefficients as was used in the aqueous-phase NVP model (Chapter 3).

$$\frac{k_p}{k_{p,max}} = 0.47 + 0.53\exp\left(-\frac{5.7\cdot w_{NVF}^0\cdot(1-x_p)}{1-w_{NVF}^0\cdot x_p}\right) - \frac{0.30\cdot w_{NVF}^0\cdot(1-x_p)}{1-w_{NVF}^0\cdot x_p} \quad (4.4)$$

$$k_{p,max}\Big/\left(\mathrm{L\cdot mol^{-1}\cdot s^{-1}}\right) = 11.9\times10^6\exp\left(-\frac{2.345\times10^3}{(T/\mathrm{K})}\right) \quad (4.5)$$

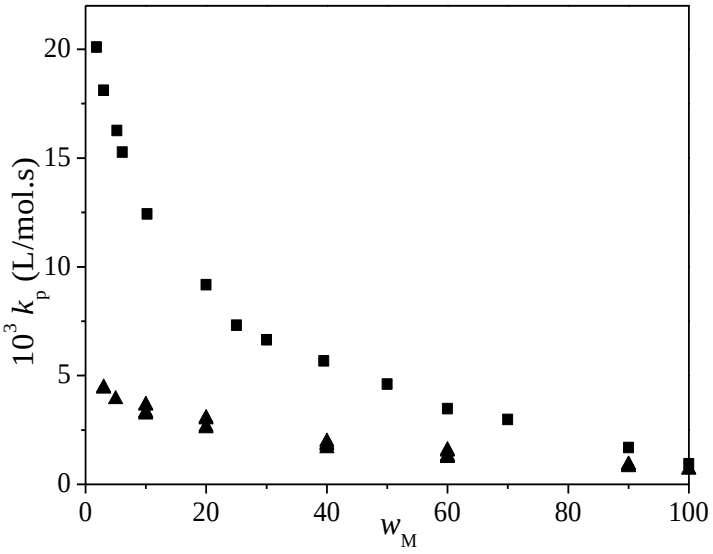

Figure 4.18. The influence of NVP[17] (■) and NVF[18] (▲) concentration (w_{NVP}) on their propagation rate coefficient (k_p). in aqueous solution at 25 °C.

4.4.3 Results and Discussion

Conversion data. The previous section illustrates that the large differences observed in NVP polymerization rate and polymer MW in organic and aqueous solution are not at all surprising, as long as a-priori knowledge of k_p behaviour is known. A second example illustrating this point is provided by comparing aqueous-phase batch polymerization of NVP and NVF. A PLP-SEC study of NVF in aqueous solution indicates that, while the same general behaviour is observed,

the absolute value of NVF k_p is lower than that of NVP under identical conditions and the increase with decreasing monomer concentration is not as large.[18] This difference in the magnitude of variation of k_p with monomer concentration for NVP and NVF was explained by differences in their structures and their relative ability to interact with themselves and with water.[18] Although no PLP studies of NVF k_t have been conducted, preliminary batch polymerization experiments in this lab indicated that observed differences in the initial rates of monomer conversion correlated well to the measured differences in k_p values.[18] We have completed a larger number of NVF batch experiments, and have applied the aqueous-phase NVP polymerization model to represent the results, only changing the monomer density and k_p expressions[18] and assuming that termination and chain-transfer rate coefficients are identical for the two monomers. A comparison of NVP and NVF conversion profiles at 12.5 vol% initial monomer and 0.02 wt% initiator concentration is shown in Figure 4.19 (a). The incomplete conversion in NVF is due to the depletion of V-50 initiator, which has a half-lif of 16 min. at 85 °C,[21] as shown in Figure 4.19 (b). This is not a problem in the case of NVP due to the much faster rate of NVP. The initial rates of reactions at identical conditions for NVP and NVF are summarized in Table 4.2. The experimental differences compare very well to their respective differences in k_p ($k_{p,NVP} = 3*k_{pNVF}$) measured by PLP-SEC,[18] suggesting that k_t values for the two monomers must be similar in magnitude. The influence of initial NVF and initiator concentration on conversion is shown in Figure 4.20. The initial rate increases with increasing initiator concentration as expected. The influence of monomer concentration on initial rate is negligible, as the small difference between k_p values for 12.5 and 20 vol% NVF is counteracted by the corresponding changes in k_t. The polymerization model developed for NVP (but utilizing the known k_p behaviour of NVF) provides a reasonable representation of the conversion profiles as

shown in Figure 4.21.

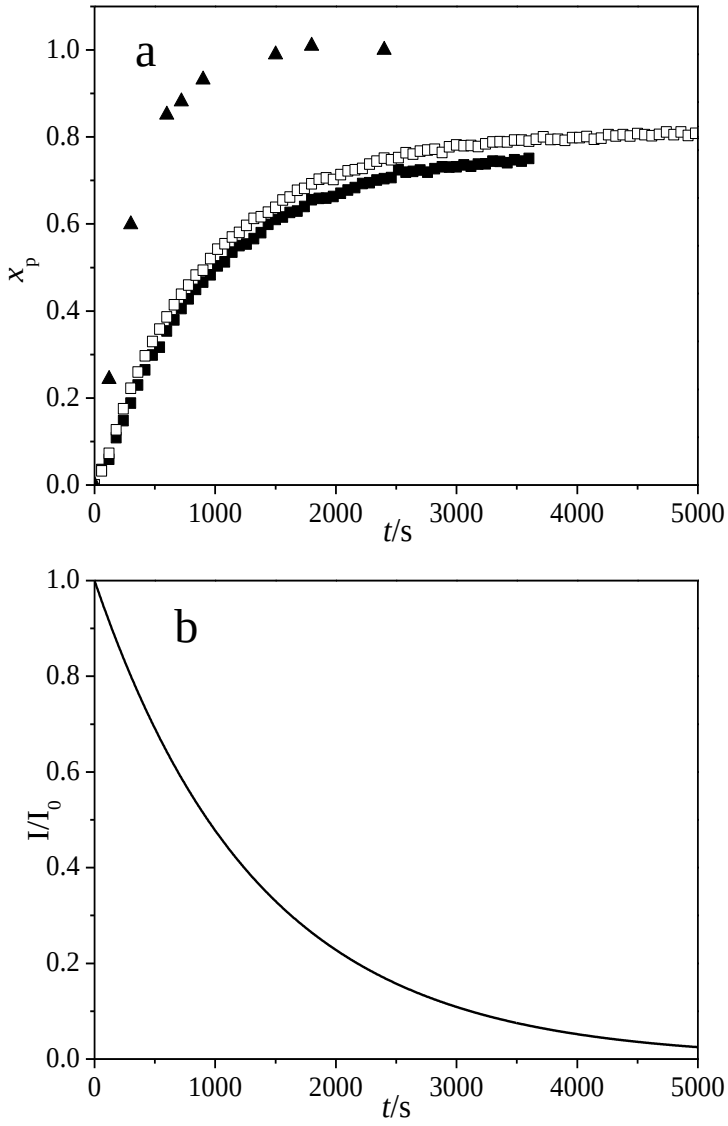

Figure 4.19. (a) Comparison of conversion profiles for batch polymerizations of 12.5 vol% NVF (■) and NVP (▲) at an initiator concentration of 0.02 wt% V-50 at 85 °C. The open symbols represent repeat results. (b) Depletion of initiator (V-50) with time, calculated using literature half-life of 16 min.[21] The NVF conversion data was measured by online IR while that of NVP was measured by gravimetry.

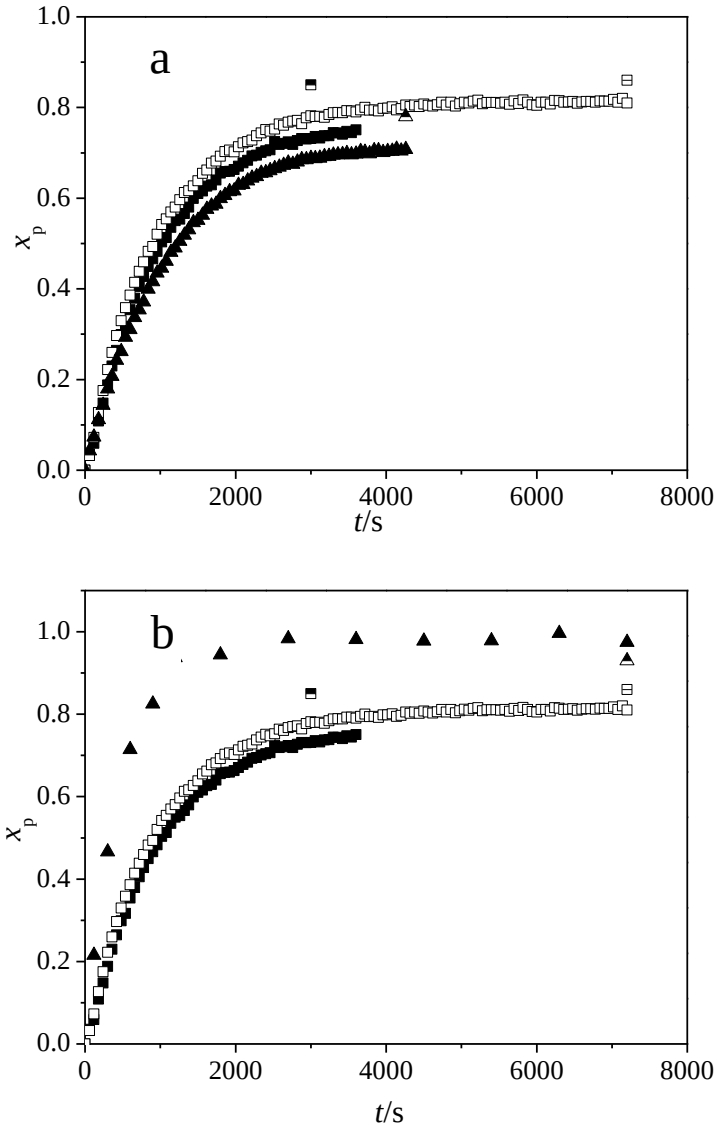

Figure 4.20. Conversion profiles for batch polymerizations of NVF at 85 °C. (a) Influence of NVF concentrations of 12.5 (■), and 20 (▲) vol% at an initiator concentration of 0.02 wt% V-50. (b) Influence of initiator concentrations of 0.02 (■) and 0.04 (▲) wt% V-50 with initial NVF level of 12.5 vol%. All the data with the exception of the data represented by triangles in b) (measured by gravimetry) and the partly-filled symbols (measured by NMR) were measured by online IR. The open symbols represent repeat results.

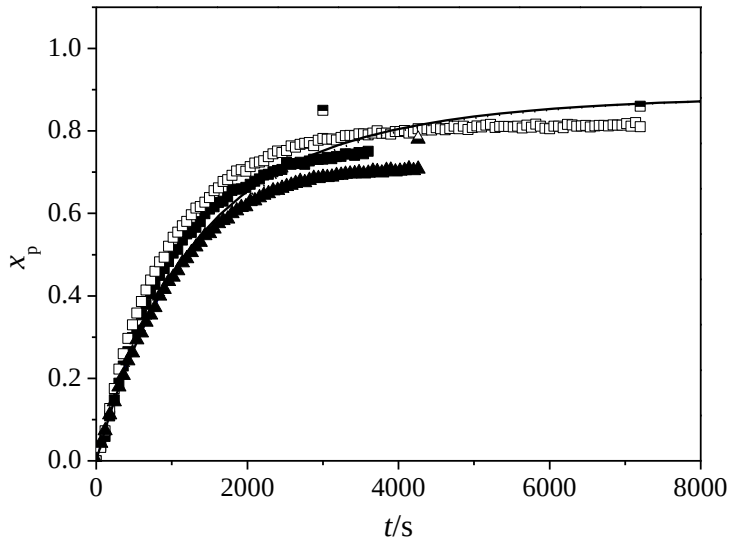

Figure 4.21. Conversion profiles for batch polymerization of NVF at 85 °C for initial NVF concentrations of 12.5 (■,——) and 20 (▲,·····) vol% at an initiator concentration of 0.02 wt% V-50. The lines represent the simulations and the symbols represent the experimental results; the partly filled symbols represent conversion determined by NMR, while the remaining data was measured by online IR. The open symbols represent repeat results.

Table 4.2. Comparison of initial rates of monomer conversion for aqueous-phase batch polymerizations of NVP and NVF at 85 °C with 0.02 wt% V-50 initiator.

Monomer level, vol%	**Initial conversion rate (dx_p/dt)**		**NVP/NVF ratio**	
	NVP	**NVF**	**Average**	
20	0.00176 0.00175	0.00060	2.94 2.92	2.93
12.5	0.0020	0.00060 0.00070	3.32 2.83	3.07

Molecular Weight behaviour. Polymer MW averages and MWDs obtained in the NVP and NVF polymerizations are compared in Figures 4.22 and 4.23 respectively for two different levels of initial monomer concentration. Clearly, poly(NVF) MWs are much lower compared to poly(NVP). The absence of data at higher conversion levels for NVF makes it difficult to

comment on the importance of chain-transfer to polymer in the system. However, the small increase in poly(NVF) weight-average MW values observed with increasing conversion for the experiment with 20 vol% NVF (Figure 4.22 (b)) is consistent with the upswing seen for NVP at high (>80%) conversion levels. Moreover, 2-D NMR on poly(NVF) showed evidence for transfer to the polymer backbone.[18] So, the same levels of transfer rate coefficients as used in the NVP aqueous model were used to model the NVF molecular weight behaviour as well and reasonable model predictions were obtained as can be seen from Figure 4.22.

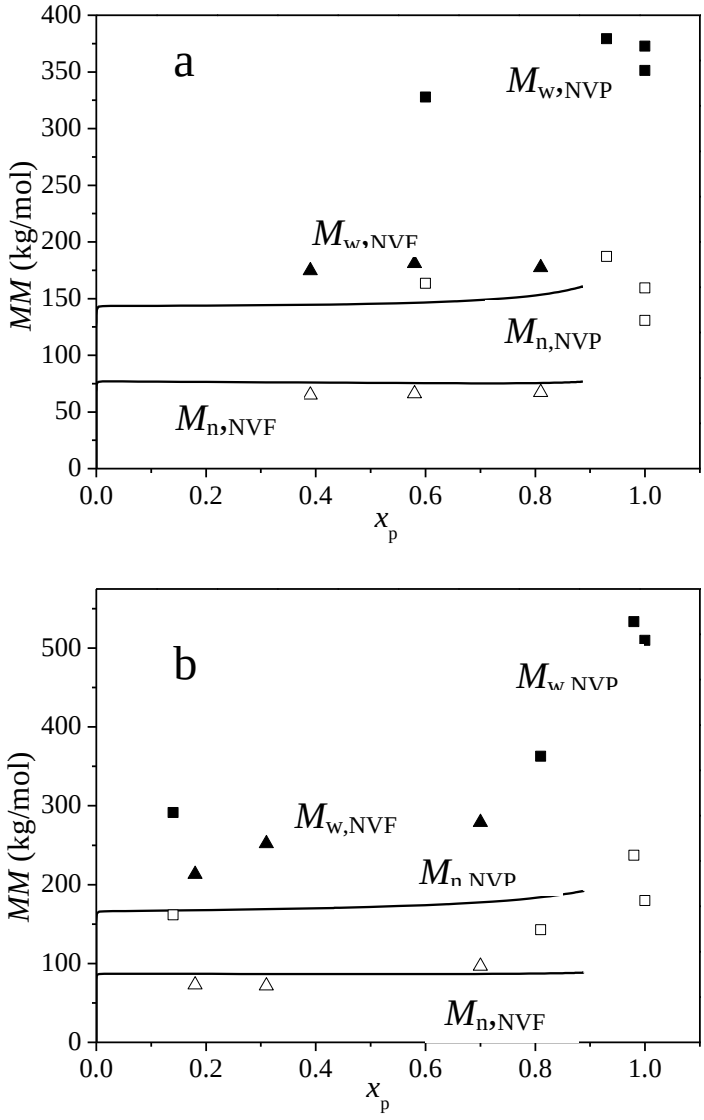

Figure 4.22. Comparison of the evolution of number and weight molecular weight averages (M_w, M_n) with monomer conversion for NVP (■) and NVF (▲) batch experiments conducted with monomer concentrations of (a) 12.5 vol% and (b) 20 vol% with an initiator concentration of 0.02 wt% at 85 °C. The closed and open symbols represent the experimental results for M_w and M_n respectively, and the lines represent simulation results for the NVF system (see text).

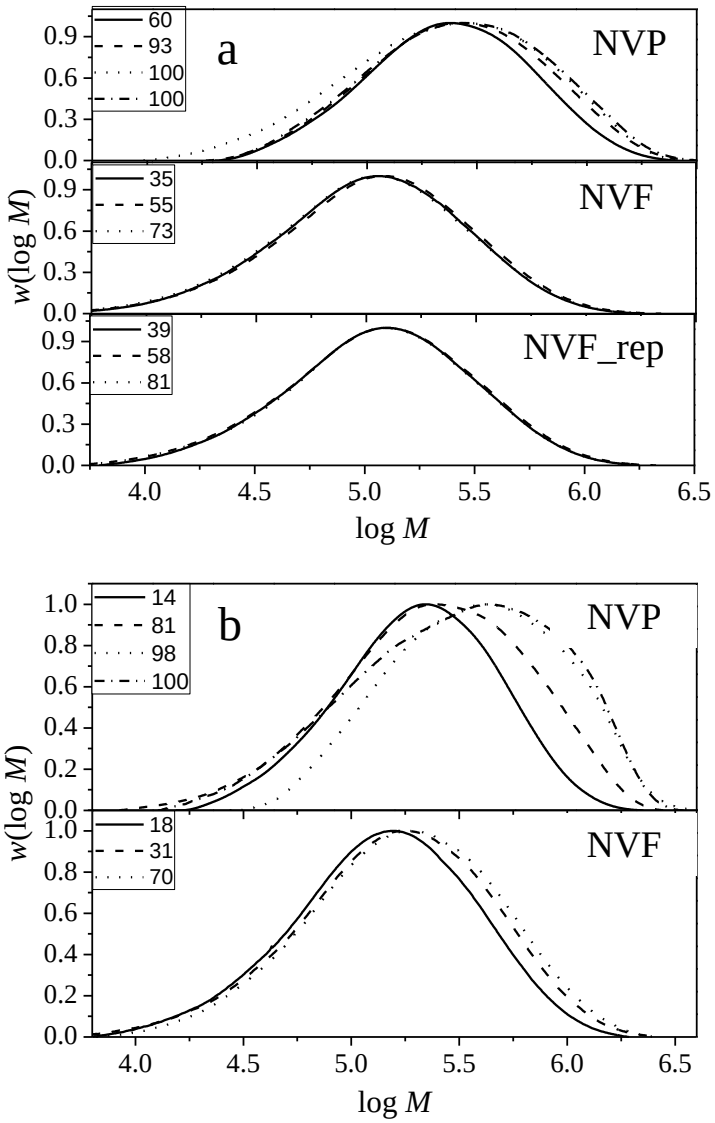

Figure 4.23. Comparison of the evolution in molecular weight distributions with monomer conversion for NVP and NVF batch experiments conducted with monomer concentrations of (a) 12.5 vol% and (b) 20 vol% with an initiator concentration of 0.02 wt% at 85 °C.

4.5 Conclusions

The free-radical polymerization of NVP in organic (*n*-butanol) solution and NVF in aqueous solution has been studied and their behaviour compared to that of aqueous-phase polymerization of NVP (Chapter 3). A significant decrease in both rates of monomer conversion and polymer MW averages is found for NVP polymerization in *n*-butanol compared to aqueous-phase

polymerization at the moderate monomer contents under investigation. Similarly, it is found that NVF aqueous-phase polymerization is slower and produced lower-MW polymer compared to NVP polymerization under identical conditions. The differences in polymerization rates correlate very well with the effect of monomer and solvent choice on k_p measured in independent PLP-SEC experiments. Although, the MW data for NVP polymerized in butanol could not be captured well, mainly due to experimental uncertainties in the results, the polymer MW data for the aqueous NVF system was represented reasonably well by using the same transfer coefficients as was used in the aqueous NVP study. Indeed, a single model can represent, at the very least, conversion behaviour of all three systems reasonably well, by only accounting for changes in the k_p behaviour. These results suggest that a generalized understanding of the kinetic behaviour of water-soluble *N*-vinyl amide monomers can be obtained once their k_p differences have been accounted for.

References

1. Kirsh, Y. E., *Water Soluble Poly-N-vinylamides,* John Wiley & Sons, England, **1998**
2. BASF Technical Bulletin on Lupamin® 9095
3. BASF Technical data sheet on Lupamin® 9030
4. Gu, L.; Zhu, S.; Hrymak, A. N.; Pelton, R. H. *Polymer* **2001**, *42*, 3077-3086.
5. Barabanova, A. I.; Bune, E. V.; Gromov, V. F. *Vysokomol. Soedin., Ser. A Ser. B*. **2001**, *43*, 732-736.
6. Gromov, V. F.; Galperina, N. I.; Osmanov, T. O.; Khomikovskii, P. M.; Abkin, A. D. *Eur. Polym. J.* **1980,** *16,* 529-535.
7. Bune, Y. V.; Barabanova, A. I.; Bogachev, Y. S.; Gromov, V. F. *Eur. Polym. J.* **1997***, 33*, 1313-1323.
8. Gromov, V. F.; Bogachev, Y. S.; Bune, Y. V.; Zhuravleva, I. L.; Teleshov, E. N. *Eur. Polym. J.* **1991***, 27*, 505-508.

9. Chapiro, A. *Eur. Polym. J.* **1973,** *9*, 417-427.

10. Senogles, E.; Thomas, R. *J. Polym. Sci.: Symp.* **1975**, *49*, 203-210

11. Beuermann, S.; Buback, M.; Hesse, P.; Kukuckova, S.; Lacik, I. *Macromol. Symp.* **2007**, *248*, 23-32.

12. Lacík, I.; Učňová, L.; Kukučková, S.; Buback, M.; Hesse, P.; Beuermann, S. *Macromolecules* **2009**, *42*, 7753-7761.

13. Beuermann, S.; Buback, M.; Hesse, P.; Lacik, I. *Macromolecules* **2006,** *39*, 184-193.

14. Beuermann, S.; Buback, M.; Hesse, P.; Kukuckova, S.; Lacik, I. *Macromol. Symp.* **2007,** *248*, 41-49.

15. Lacik, I.; Beuermann, S.; Buback, M. *Macromolecules* **2003**, *36*, 9355-9363.

16. Lacik, I.; Beuermann, S.; Buback, M. *Macromol. Chem. Phys*. **2004**, *205*, 1080-1087.

17. Stach, M.; Lacik, I.; Chorvat, D., Jr.; Buback, M.; Hesse, P.; Hutchinson, R. A.; Tang, L. *Macromolecules* **2008**, *41*, 5174-5185.

18. Stach, M.; Lacik, I.; Kasák, P.; Chorvát, D., Jr.; Saunders, A. J..; Santanakrishnan, S.; Hutchinson, R. A. *Macromol. Chem. Phys*. **2010**, *211*, 580-593.

19. Schrooten, S.; Buback, M.; Hesse, P.; Hutchinson, R. A.; Lacik, I. *Macromol. Chem. Phys*. **2011**, *212*, 1400-1409.

20. L. Učňová, M. Stach, I. Lacík, *Polymer Institute of the Slovak Academy of Sciences, Bratislava*, unpublished data.

21. Wako Chemicals information brochure.

22. Akzo Nobel Chemicals information brochure.

Chapter 5. Aqueous-Phase Free-Radical Polymerization of *N*-vinylimidazole (NVI) and Quaternized vinylimidazole (QVI)

5.1 Abstract

Aqueous-phase free radical batch polymerization of QVI and NVI were conducted at varying initial monomer concentrations, initiator concentrations and temperatures. Both QVI and NVI exhibited lower rates in comparison to NVP and NVF, with NVI rates being especially low. This was attributed to the occurrence of degradative addition to monomer in NVI free radical polymerization (FRP) as proposed by Bamford. The rates were improved by decreasing the pH to 4 and 1 by the addition of HCl, with the rates matching that of QVI at pH 1, as expected. The improved rates achieved by lowering the pH values can be explained by the degradative addition to monomer being partially (at pH 4) and completely (at pH 1) hindered by the protection of the 2-position of the monomer at these lower pH levels. The influence of initial monomer concentration on initial rate of monomer conversion was especially significant at 12.5 wt% and below for both the monomers, a result consistent with the PLP-SEC studies on NVP and NVF showing the variation of k_p with monomer concentration to be especially significant at the lower concentrations. The initial rates for both NVI and QVI were observed to be independent of temperature, in agreement with preliminary PLP studies on QVI conducted by our co-workers in the PISAS. The polymer molecular weight data for both monomers showed an increase with increasing monomer and decreasing initiator concentrations, as well as with decreasing pH levels in case of NVI, in agreement with the rate behaviour. However, the molecular weight values of both poly(NVI) and poly(QVI) were higher than both poly(NVP) and poly(NVF) produced at comparable monomer concentrations, in contradiction to the expected behaviour. However, as

SEC analysis of cationic polymers is complicated by a number of non-size exclusion effects, a quantitative comparison of the MW data of these cationic polymers with that of the non-ionic poly(NVP) and poly(NVF) is difficult. The same kinetic model built using Predici© could reasonably represent both QVI and NVI at the different pH levels, by turning on/off the degradative addition mechanism accordingly. The transfer to polymer was kept at the same levels as that of NVP. Although the predicted molecular weight data was lower than that of the experimental data, the shapes and shift with monomer, initiator and pH levels, of the predicted and experimental molecular weight distributions were in good agreement.

5.2 Introduction

In order to get a generalized understanding of water soluble monomers, our study on *N*-vinyl amides, such as *N*-vinylformamide (NVF) and *N*-vinylpyrrolidone (NVP) has been extended to *N*-vinylimidazole (NVI) and its quaternized form (3-methyl-1-vinylimidazolium methyl sulphate, QVI). NVI finds application as reactive diluent for UV coatings, UV inks, UV adhesives and general coatings.[1] It is also used as a monomer for water soluble specialty polymers and copolymers. Poly(vinylimidazole) (PVI) is a weak base which can protonate depending on the pH in aqueous solutions yielding a polycation.[2] Due to the remarkable ability of the imidazole group to complex with both organic substrates as well as metal ions,[3] their homopolymers and copolymers find applications in printing application, adhesive compositions, as dye transfer inhibitors etc.[4] *N*-vinylimidazole can be quaternized in the 3-position to yield a variety of quaternized monomers, which find application in the production of copolymers used in detergent compositions.[4]

Despite the importance of vinylimidazole homopolymers, copolymers and derivatives, very few studies exist in the literature on these monomers. As discussed in Chapter 2, the two important aspects in the free-radical polymerization of NVI include the degradative addition to monomer proposed by Bamford[3] and a possible chain transfer to polymer proposed by Chapiro.[5] The few other studies in literature on NVI by Joshi et al.,[6] Dambatta et al.[7] and Arioso et al.[8] have used one of these two proposed mechanisms to explain some of their observations. Although, these monomers have been studied in copolymerization, no one has looked at a full analysis of their homopolymerization behaviour. Furthermore, the non-availability of PLP-SEC data on the k_p behaviour of these monomers, due to problems associated with the pulsed laser polymerization of these cationic systems and the MWD analysis, makes it all the more difficult to model them. Thus, the goal of this work is to investigate the influence of initial monomer and initiator concentrations on the polymerization rate and molecular weight behaviour of both NVI and QVI in comparison to that of the better understood NVP and NVF systems. Additionally, a simple model built using Predici© will be used to represent the behaviour of these systems based on our understanding and existing knowledge in the literature.

5.3 Aqueous-Phase Free-Radical Polymerization of Quaternized vinylimidazole (QVI)

5.3.1 Experimental

Quaternized vinyl imidazole (QVI) was used as received (3-methyl-1-vinylimidazolium methyl sulphate salt dissolved in water at ~50% by weight) from BASF. The concentration was verified using thermogravimetric analysis. Thermal initiator 2,2'-azobis (2-methylpropionamidine) dihydrochloride (V-50, Fluka, ≥ 98%) was added as a solution dissolved in de-ionized water. Batch polymerizations were carried out isothermally using deionized water

as solvent in a 1 L automated (MT Autochem) stirred reactor under nitrogen blanket. Conversion was tracked by online IR and verified by offline NMR analysis.

5.3.2 Characterization

NMR analysis. Proton NMR analysis was performed using deuterated water as solvent. The ^{1}H-NMR spectra for the monomer, with peak positions as indicated in the structure (Figure 5.1) and reaction sample containing a mixture of monomer (*M*) and polymer (*P*) are shown as Figures 5.2 (a) and (b) respectively. Conversion is given by $x_{\mathrm{p}} = \dfrac{P}{(M+P)}$.

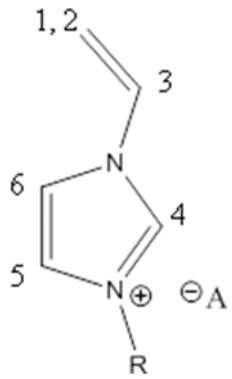

Figure 5.1. Structure of QVI (A- methyl sulphate and R – methyl)

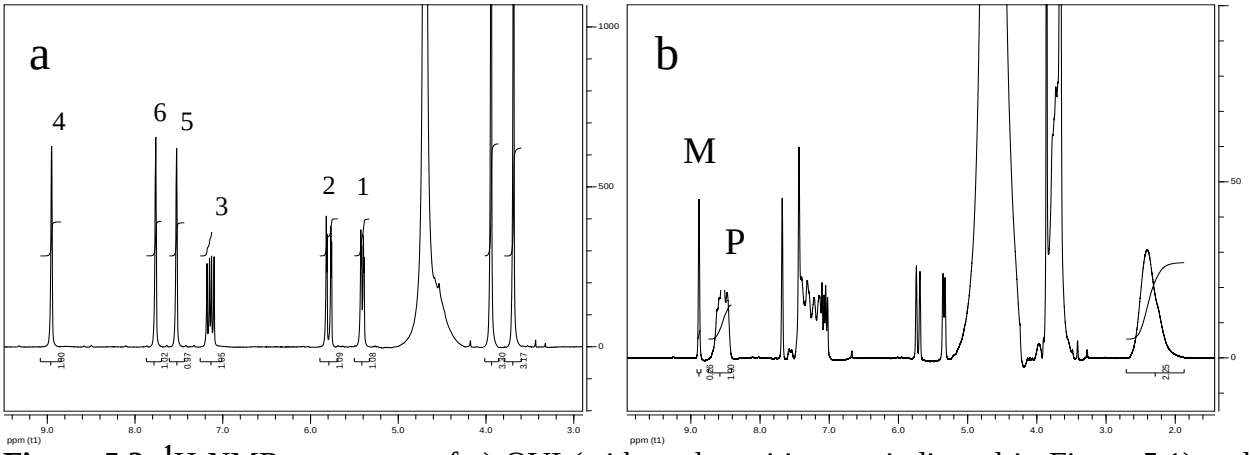

Figure 5.2. ^{1}H-NMR spectrums of a) QVI (with peak positions as indicated in Figure 5.1) and b) reaction sample from the batch polymerization of 25 wt% QVI and 0.04 wt% V-50 at 85 °C and a monomer conversion of 79%. The monomer and polymer peaks used in conversion determination are labeled M and P respectively.

ReactIR. A React-IR 4000 (MT Autochem) was used to track the extent of monomer conversion online. The monomer content in the system was tracked by the area under the peak appearing in the range of ~ 946 - 969 cm^{-1}. A calibration curve was established by obtaining the peak area (A) at various monomer levels and is shown in Figure 5.3. The monomer weight fraction in the system was calculated using eqn. 5.1, obtained by fitting the calibration data in excel.

$$[QVI], wt\% = -58.25 * A^2 + 111.73 * A + 2.9914 \quad (5.1)$$

where, A is the area under the peak appearing in the range of ~ 946 - 969 cm^{-1}.

A comparison of conversion data from IR and NMR analysis for the experiment at 25 wt% QVI and 0.02 wt% V-50 at 85 °C is shown in Figure 5.4. Reproducibility was checked by repeating the experiment at 12.5 wt% QVI and 0.02 wt% V-50 at 85 °C. However, IR data was not available for the repeat experiment and the NMR comparison of the repeat experiment is shown in Figure 5.5, where a good agreement is observed between the two sets of data.

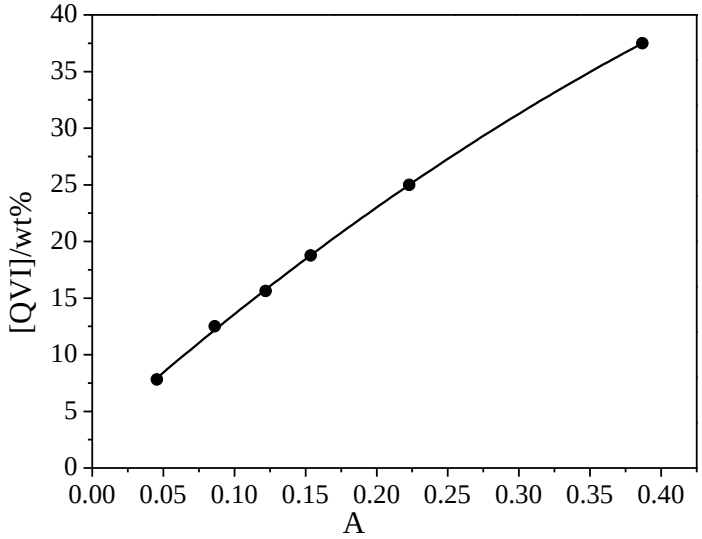

Figure 5.3. QVI IR calibration curve at 85 °C.

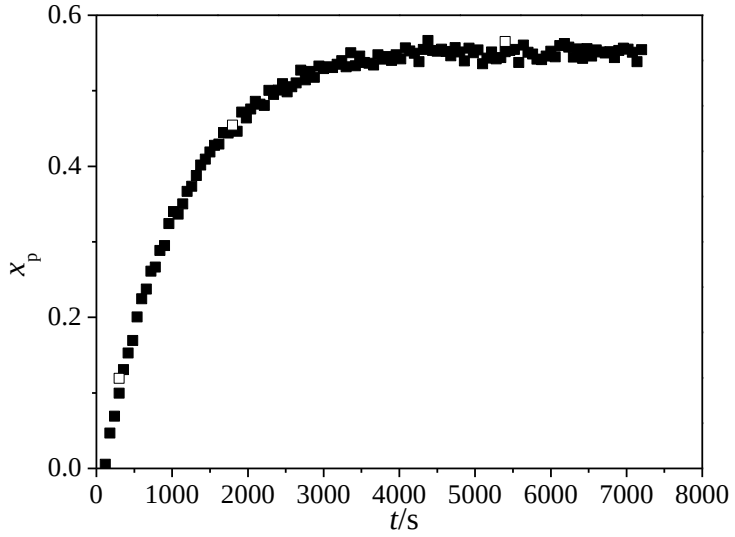

Figure 5.4. Comparison of IR (■) and NMR (□) data for the polymerization of 25 wt% QVI and 0.02 wt% V-50 at 85 °C.

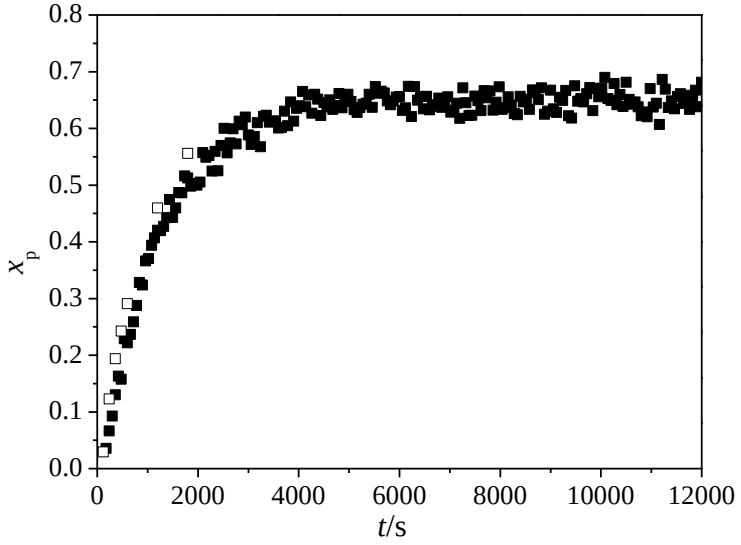

Figure 5.5. Comparison of conversion data for repeat batch solution polymerizations of 12.5 wt% QVI and 0.02 wt% V-50 in water at 85 °C. The open symbols represent the repeat experiment, measured by NMR, while the filled sybols represent online IR data.

SEC analysis. The molecular weight analysis for poly(QVI) was carried out at BASF and at the Polymer Institute of the Slovak Academy of Sciences (PISAS), Bratislava. The analysis at BASF was carried out using an RI detector calibrated with pullulan standards, suprema-gel (HEMA) columns, and 0.02 mol.L^{-1} formic acid+0.2 mol.L^{-1} potassium chloride (KCl) in water as the

eluent. The analysis at PISAS was carried out in a Polymer Standards Services (PSS) Suprema-Max column set-up which consists of a 8 x 50 mm PSS GRAM 10 μm guard column and three 8 x 300 mm PSS GRAM 10 μm columns with pore sizes of 100, 1000 and 3000 Å, placed in heater set to a temperature of 30 °C. The set-up makes use of multi-angle laser light scattering (MALLS) and RI (using pullulan standards) detectors. Ethylene glycol was used as the flow marker to control the flow rate at 1 $mL.min^{-1}$ and the injection volume was set to 100 μL. The dn/dc value of poly(Quaternized vinylimidazole) (poly(QVI)) in 0.3 M formic acid (eleunt) was determined to be 0.126 $mL.g^{-1}$. The samples were dialyzed in water at pH 7 and subsequently lyophilized and then dissolved in the eluent at a concentration of ~ 2$mg.mL^{-1}$. Data from the different sources are compared in the results and discussion section.

5.3.3 Results & Discussion

Conversion data. The influence of monomer concentrations of 6.25, 12.5, 25 and 37.5 wt% (Figure 5.6 (a)), initiator concentrations of 0.02 and 0.04 wt% (Figure 5.6 (b)) and temperatures (Figure 5.7 (a)) of 70 and 85 °C on QVI reaction rate was investigated. In all the cases, a limiting conversion was reached due to the depletion of initiator, as shown in Figure 5.7 (b), and was also observed in the case of NVF (Chapter 4). The polymerization rate was observed to increase with increasing initiator concentration, but, no significant dependence of initial rate on monomer concentration was observed in the region of 20 to 37.5 wt% QVI. However, an increase in rate was observed as the monomer concentration was decreased to 12.5 and 6.25 wt%, as more clearly observed from a comparison of the initial rate of conversion in Figure 5.6 (b) and the higher limiting conversion achieved at the lower monomer concentration levels (Figure 5.6 (a)). As for the influence of temperature on polymerization rate, the experiments using 6.25 wt% QVI were conducted keeping the initial radical generation rate the same at both 70 and 85 °C by

increasing the initiator loading at the lower temperature . The initial rate was observed to be independent of the polymerization temperature, as can be seen from Figure 5.7 (a), with the limiting conversions at the two temperatures showing good agreement with the initiator depletion profiles, shown in Figure 5.7 (b). This independence of initial rate on temperature, while surprising, is in good agreement with the observations from preliminary PLP-SEC experiments on QVI conducted by our co-workers in Bratislava.

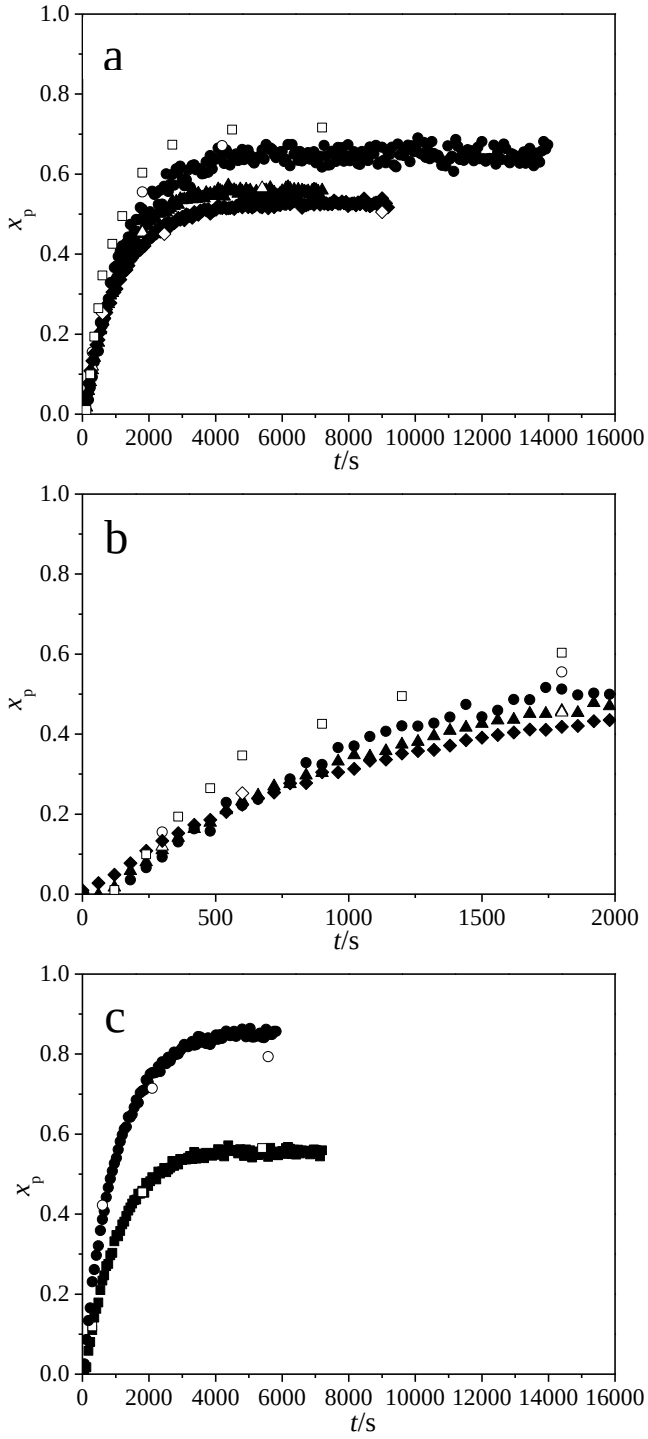

Figure 5.6. Conversion profiles for the batch polymerization of QVI at 85 °C. a) Full conversion profiles and b) initial rate of conversion for the influence of monomer concentrations of 6.25 (■), 12.5 (●), 25 (▲) and 37.5 (♦) wt% at an initiator concentration of 0.02 wt%. c) Influence of initiator concentrations of 0.02 (■) and 0.04 (●) wt% at a monomer concentration of 25 wt%. Open and closed symbols represent NMR and IR data respectively.

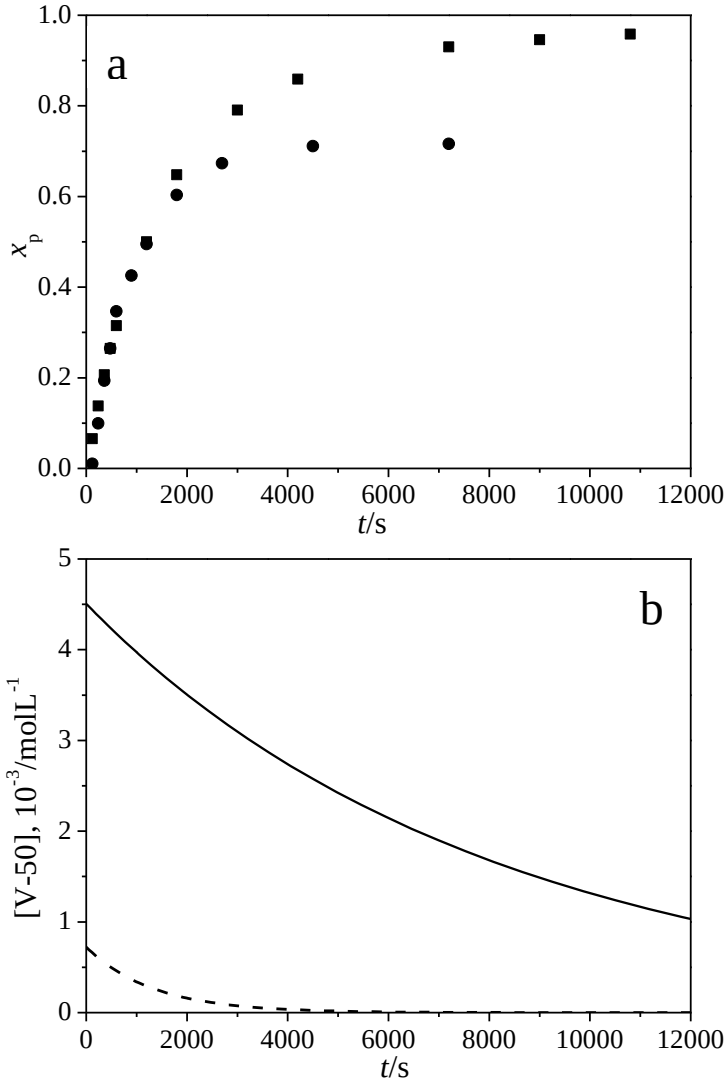

Figure 5.7. Comparison of the a) conversion, measured by NMR and b) initiator depletion profiles at 70 °C (■,——) and 85 °C (●, -----) at the same initial radical generation rate for the batch polymerization of 6.25 wt% QVI in water.

Molecular weight behaviour. The molecular weight analysis for QVI was carried out at BASF using RI detector (using pullulan standard) and at PISAS, Bratislava using multi-angle laser light scattering (MALLS) and RI (using pullulan standard) detectors, as discussed in the experimental section. A comparison of the three sets of molecular weight averages (M_w and M_n) is shown in Table 5.1. As the RI data was obtained using pullulan standards, it should be corrected with reference to absolute (MALLS) data. However, a ratio of the M_w values from RI and MALLS

shown in Table 5.1 indicates that the correction factor for the samples (marked with an asterisk) at higher monomer concentrations of 20 and 30 wt% almost doubles, with very strange mono-disperse PDI from MALLS. These data were therefore not considered in the calculation of correction factor for RI data, estimated to be 0.38±0.04 from the other samples. A comparison of the BASF-RI, PISAS-corrected RI and PISAS-MALLS data at varying conversion levels (as indicated in the Figure legends) are shown in Figures 5.8-5.12. The influence of monomer and initiator concentrations on molecular weight distributions is shown in Figures 5.13 and 5.14 respectively. Some of the molecular weight distributions (Figures 5.8 and 5.9) from BASF RI data have an unexpected shoulder not seen in the analyses from PISAS, suggesting that the shoulder may just be a GPC artifact. The RI data from the PISAS was observed to be a little higher than that from BASF in some cases. Furthermore, as was observed for NVP and NVF, the PDI from MALLS data was unreasonably low in some cases. As the two SEC RI analyses (BASF and PISAS) use the same pullulan calibration strategy, the discrepancy in the MW data from the two sources must result from the different solvents, column types and sample preparation protocols used. Solvent choice is especially important with polyelectrolytes, as their size in solution is controlled to by the ionic strength of the solvent which in turn influences the electrostatic interactions between the macromolecules.[9] Furthermore, the SEC of polycations is complicated by several non-size exclusion effects as discussed in Chapter 2, such as adsorption of these cationic samples to the packing material, which in turn affects the recovery rate and reproducibility of results.[10] Although no significant shift in MW is observed with change in initiator concentration, a shift towards higher MW with increasing monomer concentration is clearly observed from Figure 5.9 (b). The corrected RI data will be used for comparison with model predictions in the subsequent section.

Table 5.1. QVI molecular weight averages at varying monomer and initiator concentrations at 85 °C

Experiment	x_p	BASF, RI			PISAS, MALLS			PISAS, RI			PISAS M_wMALLS/M_wRI
		M_n kg.mol^{-1}	M_w kg.mol^{-1}	PDI	M_n kg.mol^{-1}	M_w kg.mol^{-1}	PDI	M_n kg.mol^{-1}	M_w kg.mol^{-1}	PDI	
[M]=10 wt% [I]=0.04 wt%	0.27	91	194	2.13	187	276	1.48	565	756	1.34	0.37
	0.76	87	184	2.13	140	232	1.66	523	700	1.34	0.33
	0.88	91	185	2.03	123	222	1.80	519	705	1.36	0.31
M]=10 wt% [I]=0.02 wt%	0.16	97	229	2.37	285	348	1.22	555	783	1.41	0.44
	0.56	118	249	2.11	232	307	1.33	598	789	1.32	0.39
	0.67	116	256	2.21	233	317	1.36	598	801	1.34	0.40
[M]=10 wt% [I]=0.01 wt%	0.08	112	246	2.20	277	344	1.24	630	845	1.34	0.41
	0.25	114	264	2.32	218	315	1.45	626	828	1.32	0.38
	0.30	110	250	2.27	196	301	1.54	598	815	1.36	0.37
[M]=20 wt% [I]=0.02 wt%	0.12	133	398	2.99	509	544	1.07	651	908	1.40	0.60
	0.45	226	487	2.15	571	595	1.04	750	979	1.31	0.61
	0.56	173	478	2.76	680	680	1.00	911	1 081	1.19	0.63
[M]=30 wt% [I]=0.02 wt%	0.25	244	620	2.54	692	717	1.04	727	1 022	1.41	0.70
	0.45	196	679	3.46	758	771	1.02	784	1 088	1.39	0.71
	0.51	236	710	3.01	747	776	1.04	739	1 117	1.51	0.69

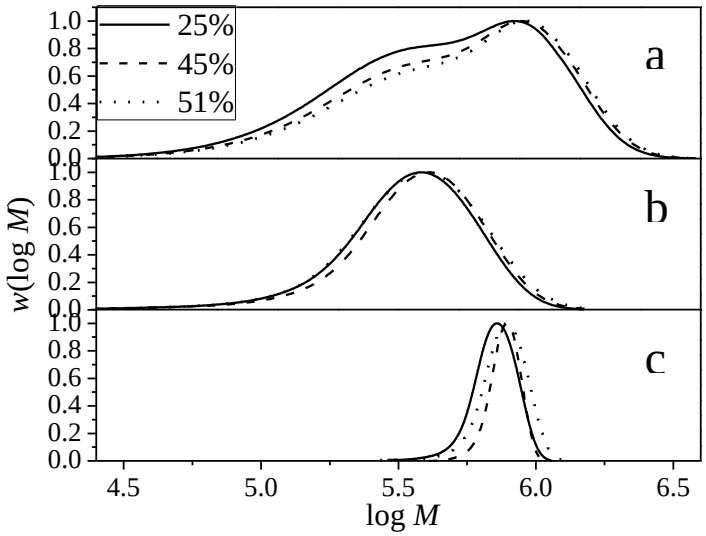

Figure 5.8. Comparison of molecular weight distributions from a) BASF-RI, b) PISAS.-RI corrected and c) PISAS-MALLS for the batch polymerization of 37.5 wt% QVI and 0.02 wt% V-50 at 85 °C at various conversion levels as indicated in the Figure legend.

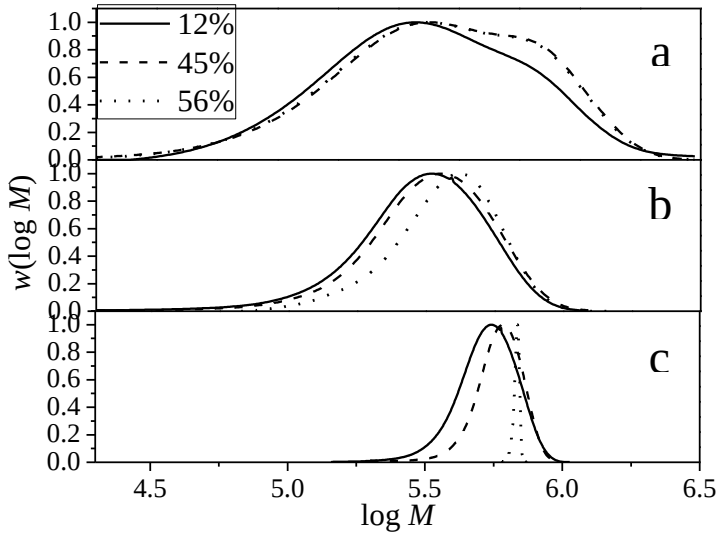

Figure 5.9. Comparison of molecular weight distributions from a) BASF-RI, b) PISAS-RI corrected and c) PISAS-MALLS for the batch polymerization of 25 wt% QVI and 0.02 wt% V-50 at 85 °C at various conversion levels as indicated in the Figure legend.

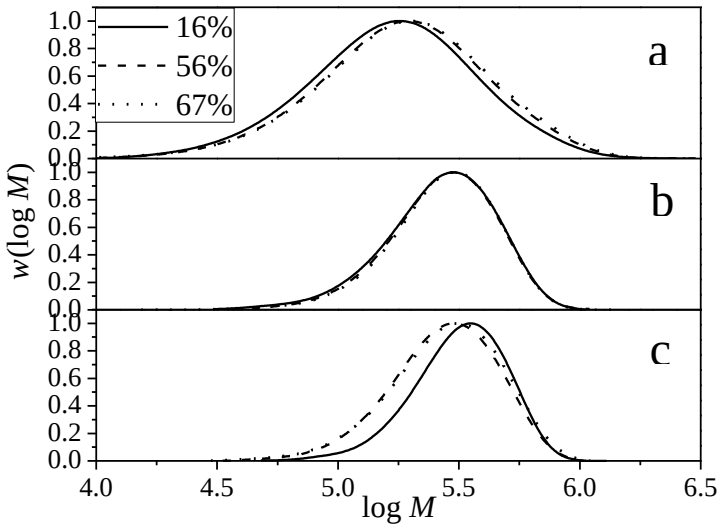

Figure 5.10. Comparison of molecular weight distributions from a) BASF-RI, b) PISAS-RI corrected and c) PISAS-MALLS for the batch polymerization of 12.5 wt% QVI and 0.02 wt% V-50 at 85 °C at various conversion levels as indicated in the Figure legend.

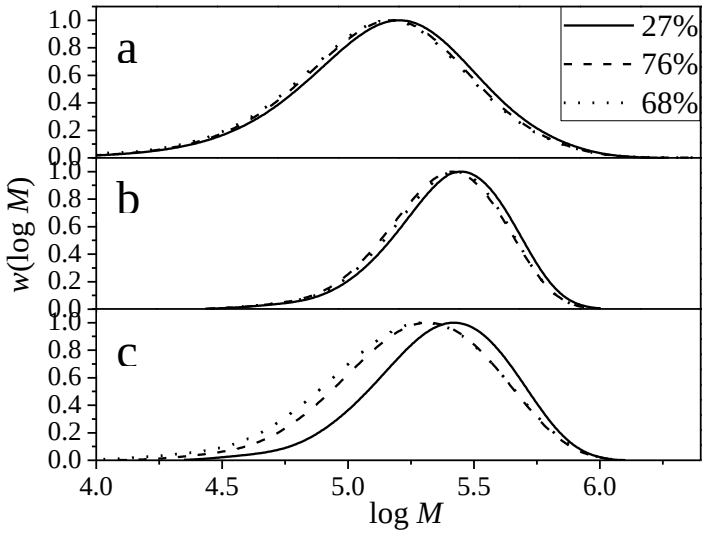

Figure 5.11. Comparison of molecular weight distributions from a) BASF-RI, b) PISAS-RI corrected and c) PISAS-MALLS for the batch polymerization of 12.5 wt% QVI and 0.01 wt% V-50 at 85 °C at various conversion levels as indicated in the Figure legend.

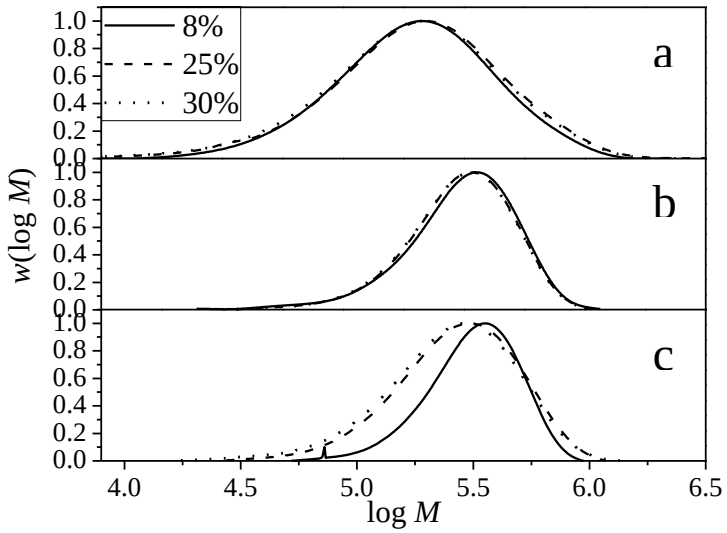

Figure 5.12. Comparison of molecular weight distributions from a) BASF-RI, b)PISAS-RI corrected and c) PISAS-MALLS for the batch polymerization of 12.5 wt% QVI and 0.04 wt% V-50 at 85 °C at various conversion levels as indicated in the Figure legend.

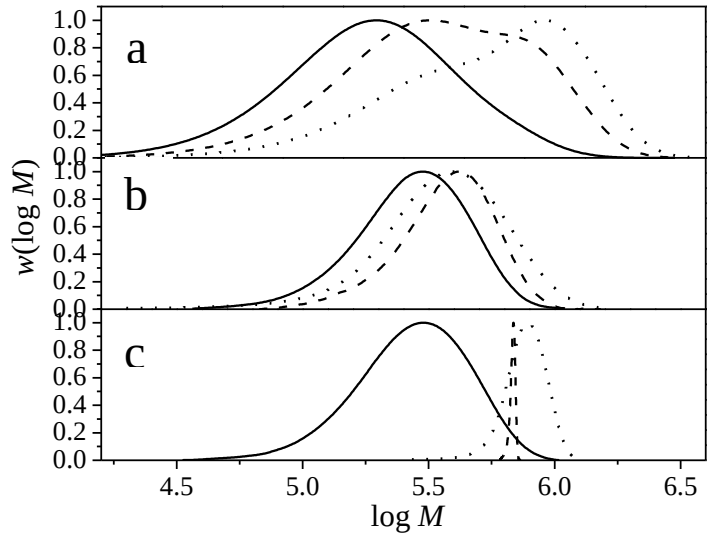

Figure 5.13. Comparison of molecular weight distributions from a) BASF-RI, b) PISAS-RI corrected and c) PISAS-MALLS for the batch polymerization of QVI at 0.02 wt% V-50 and 85 °C at varying monomer concentrations of 12.5 (——), 25 (-----) and 37.5 (·····) wt%.

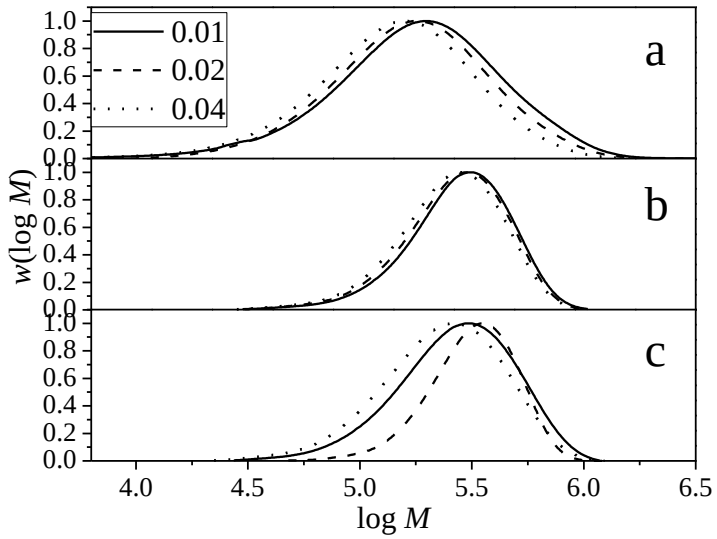

Figure 5.14. Comparison of molecular weight distributions from a) BASF-RI, b) PISAS-RI corrected and c) PISAS-MALLS for the batch polymerization of 12.5 wt% QVI at 85 °C at varying initiator concentrations of 0.01 (——), 0.02 (-----) and 0.04 (·····) wt%.

5.3.4 Model Development

The same kinetic model used to describe NVP polymerization was adapted for QVI by making changes to the monomer properties (MW and densities) and setting the k_p to vary as a ratio to $k_t^{0.5}$. The value of $k_p/k_t^{0.5}$ was estimated by fitting to the QVI and NVI rate data at pH 1, as k_p has not yet been measured for this system. The transfer coefficients and PLP derived k_t expression used for NVP were retained, following the same strategy as used for NVF in the previous chapter and in ref.[11] The mechanistic scheme describing the free radical polymerization of QVI is shown in Table 5.2 and the expressions and values of the kinetic rate coefficients used in the model are shown in Table 5.3.

A comparison of the experimental and model predictions for the influence of monomer concentration, initiator concentration and temperature on conversion data is shown in Figures 5.15 (a), (b) and (c) respectively. Although the model captures reasonably well the influence of initiator concentration and temperature, it fails to capture the differences with initial monomer

level observed at lower monomer concentrations (see Figure 5.6 (b)). This model mismatch is most likely attributable to the absence of a monomer concentration dependent k_p expression. Once PLP-SEC studies of this system are completed, the batch polymerization data can be re-evaluated using an expression that captures the change in k_p with monomer concentration.

As a next step, the molecular weight data for this system was modeled. A comparison of the experimental and model data for the experiment at 12.5 wt% QVI and 0.02 wt% initiator concentration at 85 °C is shown in Figure 5.16. It is observed that the shapes of the profiles predicted by the model and the experimental data are very similar but the model data is slightly lower compared to the experimental data. The influence of monomer and initiator concentrations on molecular weight data are shown in Figures 5.17 and 5.18 respectively. As expected, the model predicts a shift towards higher molecular weight with increasing monomer and decreasing initiator concentrations. The shapes of the profiles are also in good agreement with the experimental data.

Table 5.2. Mechanistic scheme for the free radical polymerization of QVI

Initiator Decomposition	$I \xrightarrow{k_d} 2 f I^{\bullet}$
Chain Initiation	$I^{\bullet} + M \xrightarrow{k_p} P_1^{\bullet}$
Chain Propagation	$P_n^{\bullet} + M \xrightarrow{k_p} P_{n+1}^{\bullet}$
Chain Termination	
By Combination	$P_n^{\bullet} + P_m^{\bullet} \xrightarrow{k_{tc}} D_{n+m}$
By Disproportionation	$P_n^{\bullet} + P_m^{\bullet} \xrightarrow{k_{td}} D_n + D_m$

Table 5.3. Values and expressions for the kinetic rate coefficients and physical parameters used in the kinetic modeling of free radical polymerization of QVI at 85 °C

Mechanism	Rate Expression	Values	Ref
Initiator decomposition	$k_d(s^{-1}) = 9.17\times10^{14}\exp\left(\frac{-1.49\times10^4}{(T/\mathrm{K})}\right)$	$7.5209\text{x}10^{-4}$	12
Lumped rate constant	$k_p/k_t^{0.5}$	0.674	this work
Termination	$k_t\Big/\left(\mathrm{L\cdot mol^{-1}\cdot s^{-1}}\right) = 1.5\times10^8\exp\left(-w_{QVI}^0/0.29\right)+1.68\times10^7$ at P = 1 bar		13
Density of Water	$\rho_{H2O}\Big/\left(\mathrm{g\cdot mL^{-1}}\right) = 0.9999 + 2.3109\cdot10^{-5}(T/^{\circ}\mathrm{C}) - 5.44807\cdot10^{-6}(T/^{\circ}\mathrm{C})^2$	0.959	14
Density of QVI		1.3256	this work

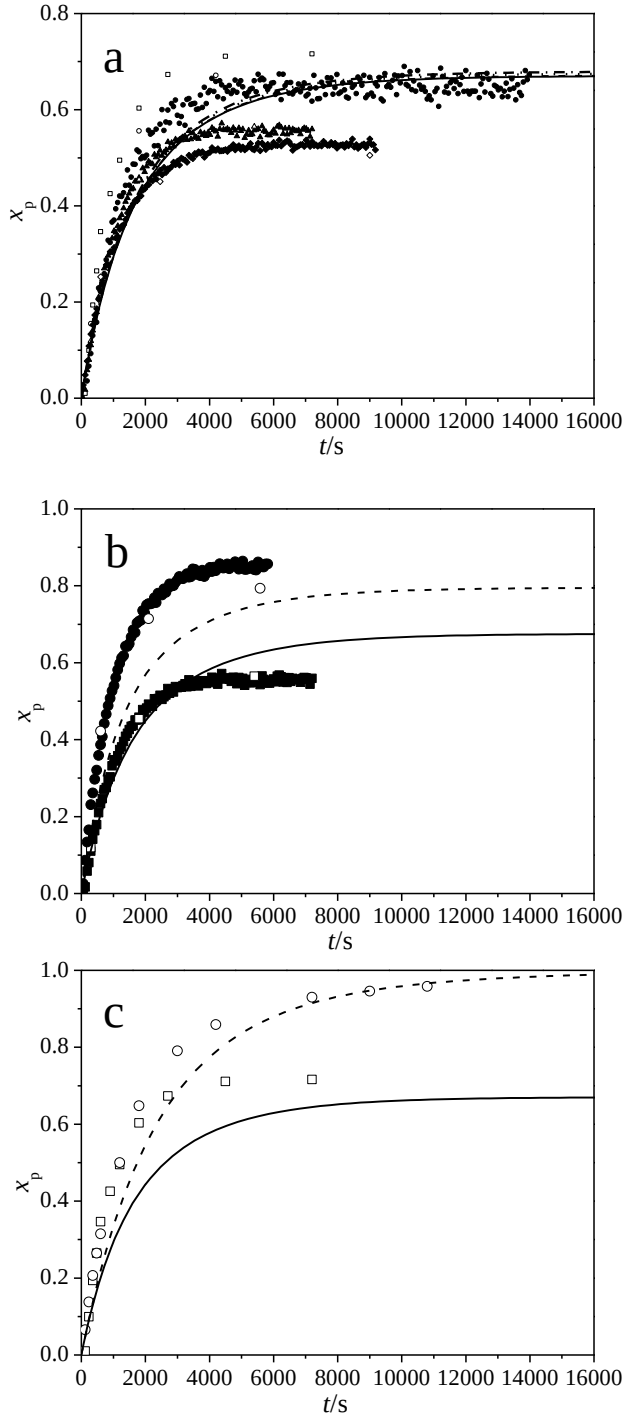

Figure 5.15. Conversion profiles for the batch polymerization of QVI at 85 °C. a) Influence of monomer concentrations of 6.25 (——, □), 12.5 (-----, ●), 25 (·····, ▲) and 37.5 (— · —, ♦) wt% b) Influence of initiator concentrations of 0.02 (——, ■) and 0.04 (-----, ●) wt% at 12.5 wt% QVI and c) Influence of temperatures of 70 (——, □) and 85 (-----, ○) °C. Symbols and lines represent experimental and model results respectively; the open and filled symbols represent NMR and IR data respectively.

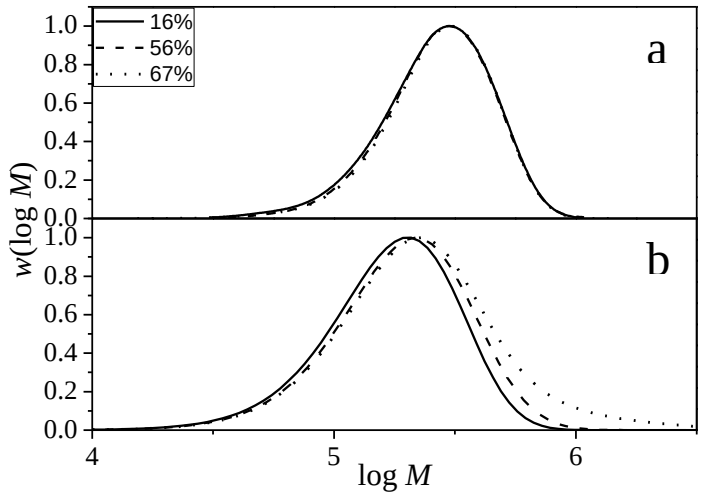

Figure 5.16. Comparison of a) corrected RI and b) simulated molecular weight distributions for the batch polymerization of 12.5 wt% QVI and 0.02 wt% V-50 at 85 °C at varying conversion levels as indicated in the Figure legend.

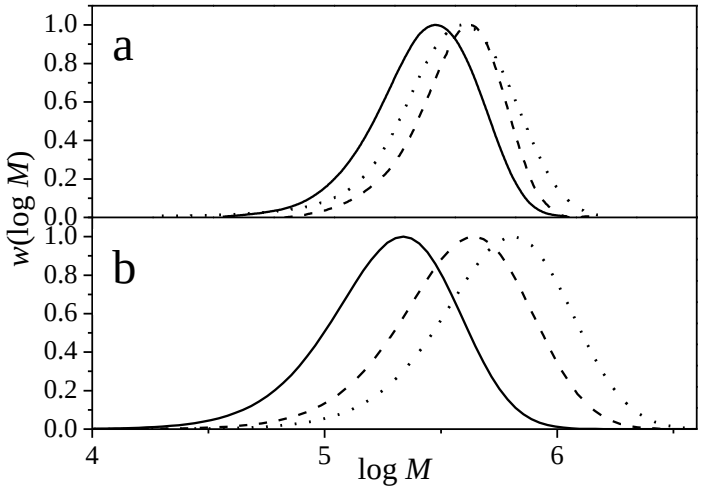

Figure 5.17. Comparison of a) corrected RI and b) simulated molecular weight distributions for the batch polymerization of QVI at 0.02 wt% V-50 at 85 °C at varying monomer concentrations of 12.5 (——), 25 (-----) and 37.5 (·····) wt%.

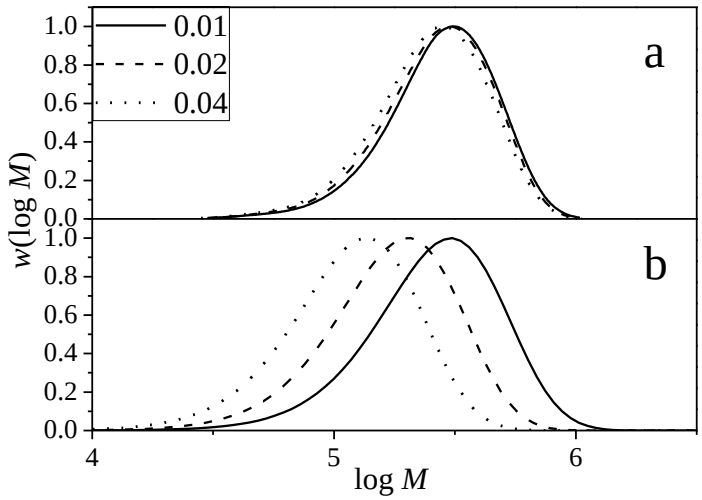

Figure 5.18. Comparison of a) corrected RI and b) simulated molecular weight distributions for the batch polymerization of 12.5 wt% QVI at 85 °C at varying initiator concentrations of 0.01 (——), 0.02 (-----) and 0.04 (·····) wt%.

5.4 Aqueous-Phase Free Radical Polymerization of *N*-vinylimidazole (NVI)

5.4.1 Experimental

N-vinylimidazole (99.5%, BASF) was used as received. Thermal initiator 2,2'-azobis (2-methylpropionamidine) dihydrochloride (V-50, Fluka, ≥ 98%) was added as a solution dissolved in de-ionized water. Similar to the QVI experiments, batch polymerizations were carried out isothermally using deionized water as solvent in a 1 L automated (MT Autochem) stirred reactor under nitrogen blanket. Conversion was tracked using gravimetry (exception of pH adjusted experiments) and ^{1}H-NMR analysis. For gravimetry, the samples were dried in an air stream followed by oven drying for ~48-72 h at a temperature of 85 °C. Experiments were conducted at varying monomer concentrations, initiator concentrations and pH levels (adjusted using hydrochloric acid (HCl, Fisher Scientific)).

5.4.2 Characterization

NMR analysis. Proton NMR analysis was performed using deuterated water as solvent. The structure of NVI is shown in Figure 5.19. The respective ^{1}H-NMR spectra for the monomer, with peak positions as indicated in Figure 5.19 and a reaction sample containing a mixture of monomer and polymer are shown Figures 5.20 (a) and (b) respectively. Conversion is given by $x_p = \frac{P/2}{[M + (P/2)]}$. The agreement between NMR and gravimetry data is shown in Figure 5.21.

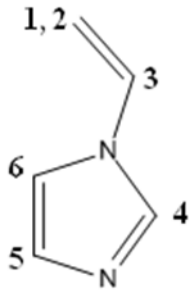

Figure 5.19. Structure of *N*-vinylimidazole.

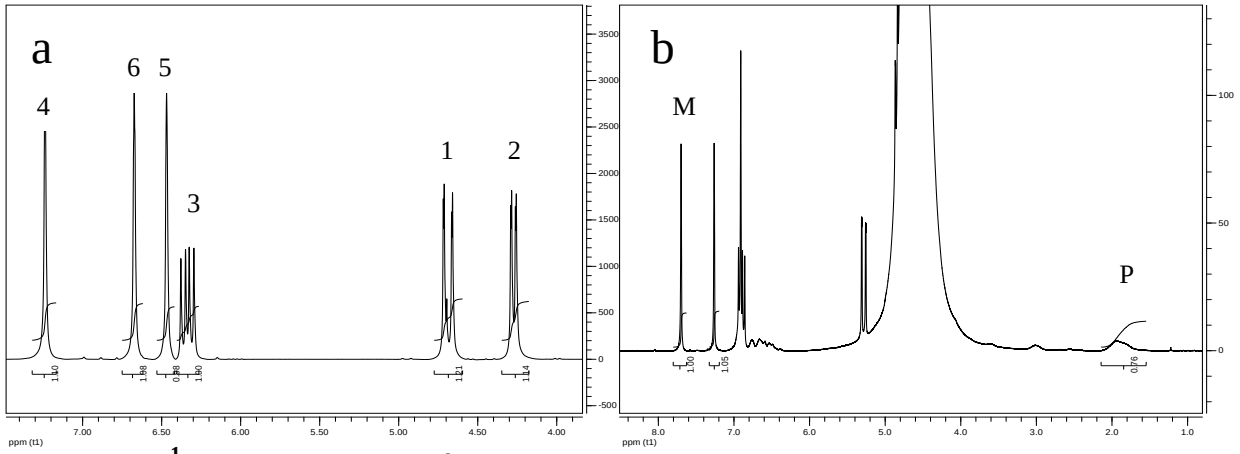

Figure 5.20. ^{1}H-NMR spectrum of a) NVI (with peak positions as indicated in Figure 5.19) and b) reaction sample from the batch polymerization of 6.25 vol% NVI and 0.02 wt% V-50 at 85 °C and monomer conversion of 28%. The monomer and polymer peaks used for conversion determination have been labeled M and P respectively.

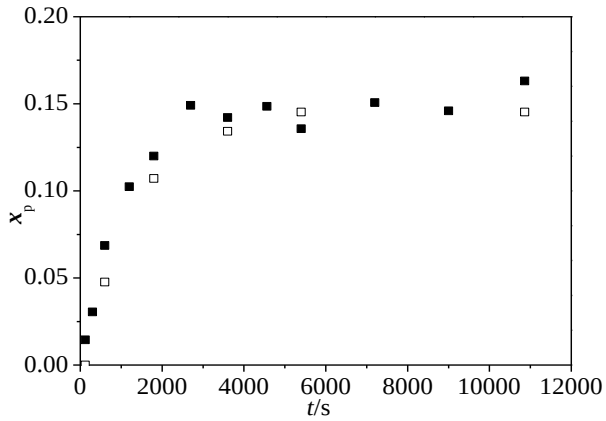

Figure 5.21. Comparison of gravimetry (■) and NMR (□) data for 12.5 vol% NVI and 0.02 wt% V-50 at 85 °C and natural pH of 9.

SEC analysis. Molecular weight analysis was carried out in PISAS, Bratislava using a PSS Suprema-Max column set-up, described earlier in the QVI section. Here again, multi-angle laser light scattering (MALLS) and RI (using pullulan standards) detectors were used. Toluene was used as a flow marker to control a flow rate of 0.8 mL.min^{-1} and the injection volume was set to 100 μL. Dimethylacetamide (DMAc) with 0.1 wt% lithium bromide (LiBr) was used as the eluent and the dn/dc value of poly(*N*-vinylimidazole) (PNVI) in this eluent was determined to be 0.098 mL.g^{-1}. The samples from the adjusted pH experiments were first dialysed against water at pH 10 through regenerated cellulose Spectra/Por® dialysis membrane (Spectrum Laboratories, Inc.) with a molecular cut off < 3500 g.mol^{-1}, followed by lyophilisation and then dissolved in the eluent at a concentration of ~ 3mg.mL^{-1}. The RI data was evaluated against polystyrene standards and was therefore corrected by a correction factor of 0.43±0.08, calculated from a comparison of the MALLS and RI M_w values shown in Table 5.4. The samples indicated by an asterisk in Table 5.4 were not included in the calculation of the correction factor due to poor MALLS signal. A comparison of the corrected RI and MALLS data for the different experiments are shown in Figures 5.22-5.25. As was observed for NVP, NVF and QVI, the MWDs from MALLS are generally narrower than that from RI, with some unusually narrow distributions

occasionally reported (Figure 5.23). Moreover, some of the samples from the pH adjusted experiments (Figures 5.24 and 5.25) clogged the filters, which may have affected the results.

Table 5.4. Comparison of RI and MALLS data for polymer produced from aqueous-phase batch polymerization of NVI at 85 °C.

Initial conditions	x_p	**RI (pullulan calibration)**			**MALLS**			$M_{w,MALLS}/M_{w,RI}$
		M_w [kg.mol^{-1}]	M_n [kg.mol^{-1}]	PDI	M_w [kg.mol^{-1}]	M_n [kg.mol^{-1}]	PDI	
[M] = 12.5 vol%; [I]=0.02 wt%; pH=9	0.11	535	247	2.17	256	181	1.41	0.48
	0.15	538	280	1.93	257	184	1.40	0.48
[M] = 12.5 vol%; [I]=0.02 wt%; pH=9	0.11*	193	161	1.67	123	116	1.06	0.64
	0.82	510	208	2.45	303	153	1.98	0.59
[M] = 12.5 vol%; [I]=0.02 wt%; pH=9	0.04	1162	550	2.11	495	260	1.91	0.43
	0.15	792	505	1.57	299	210	1.42	0.38
	0.36*	596	87	6.84	487	207	2.35	0.82
	0.49*	776	216	3.59	564	374	1.51	0.73
	0.62*	784	246	3.19	568	345	1.65	0.72
[M] = 12.5 vol%; [I]=0.02 wt%; pH=9	0.03	752	313	2.40	303	151	2.01	0.40
	0.08	462	303	1.52	165	125	1.32	0.36
	0.32	602	354	1.70	215	138	1.55	0.36
	0.35	517	304	1.70	192	127	1.51	0.37
Average $M_{w,MALLS}/M_{w,RI}$								0.43 ± 0.08

*These samples have not been included in the calculation of the correction factor due to poor MALLS signal

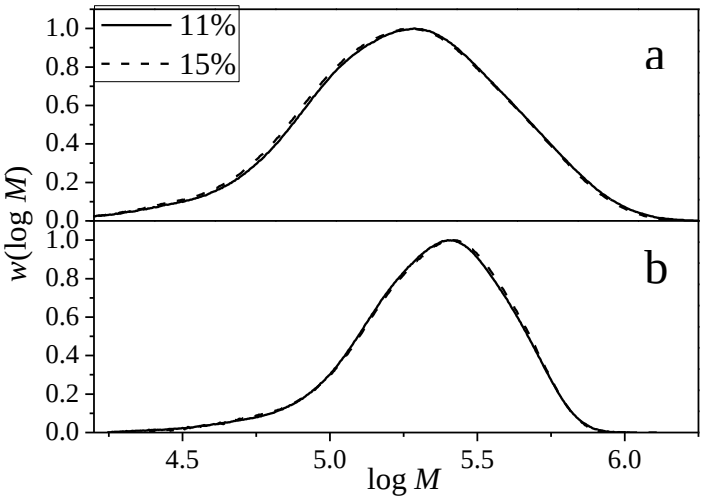

Figure 5.22. Comparison of a) RI (corrected) and b) MALLS molecular weight data for polymer produced with 12.5 vol% NVI and 0.02 wt% V-50 at pH 9 and temperature of 85 °C at varying conversion levels as indicated.

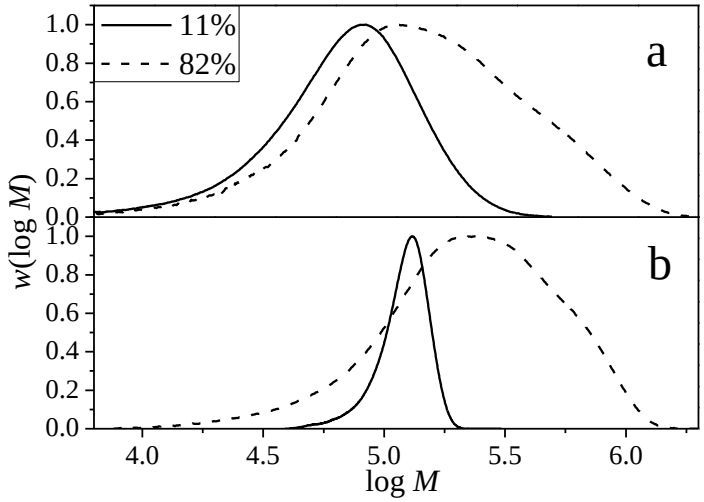

Figure 5.23. Comparison of a) RI (corrected) and b) MALLS molecular weight data for polymer produced with 12.5 vol% NVI and 0.2 wt% V-50 at pH 9 at 85 °C and varying conversion levels as indicated.

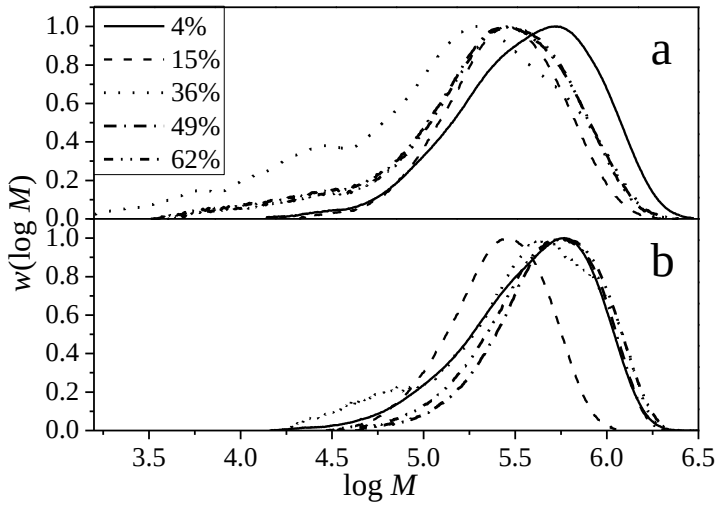

Figure 5.24. Comparison of a) RI (corrected) and b) MALLS molecular weight data for 12.5 vol% NVI and 0.02 wt% V-50 at pH 1 and temperature of 85 °C at varying conversion levels as indicated.

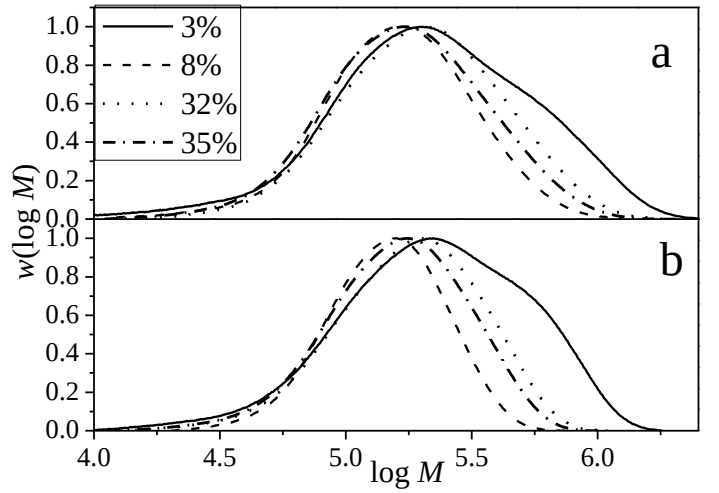

Figure 5.25. Comparison of a) RI (corrected) and b) MALLS molecular weight data for 12.5 vol% NVI and 0.02 wt% V-50 at pH 4 and temperature of 85 °C at varying conversion levels as indicated.

5.4.3 Results & Discussion

Conversion. Similar to the study on QVI, the influence of initial monomer concentrations, initiator concentrations and temperatures on polymerization rate of NVI was investigated. NVI batch polymerization experiments exhibited very low initial rates, lower by a factor of approximately 26, 11 and 7 in comparison with NVP, NVF and QVI respectively, at a monomer

concentration of 12.5 vol% and V-50 concentration of 0.02 wt% at 85 °C. A comparison of the conversion profiles for the different monomers is shown in Figure 5.26. This very low initial rate of NVI was attributed to the degradative addition to monomer, wherein the propagating radical adds to the monomer resulting in the formation of a resonance stabilized radical (X),[3] as shown in Scheme 2.1 in Chapter 2. This degradative addition reaction, however, can be overcome by reducing the pH to levels below 3, wherein the monomer is quaternized and is therefore protected from the degradative addition reaction.[3] This was verified by conducting experiments at an adjusted pH of 4 and 1 using hydrochloric acid. As expected, the rate increased with decreasing pH values as can be seen from Figure 5.27, which shows a comparison of the data at the three pH levels of 1, 4 and 9 (natural pH). At the natural pH, all of the monomer units are susceptible to degradative addition, at the intermediate pH of 4 some of the monomer units are protected and the degradative addition is therefore only partially prevented, and at pH 1 all the monomer is protected and the degradative addition is completely prevented. As decreasing the pH of NVI to 1 quaternizes the monomer, the behaviour of this system is expected to be similar to that of QVI. This was verified by the excellent agreement between the NVI (at pH 1) and QVI conversion data at comparable monomer concentrations at both 70 °C (Figure 5.28 (a)) and 85 °C (Figure 5.28 (b)).

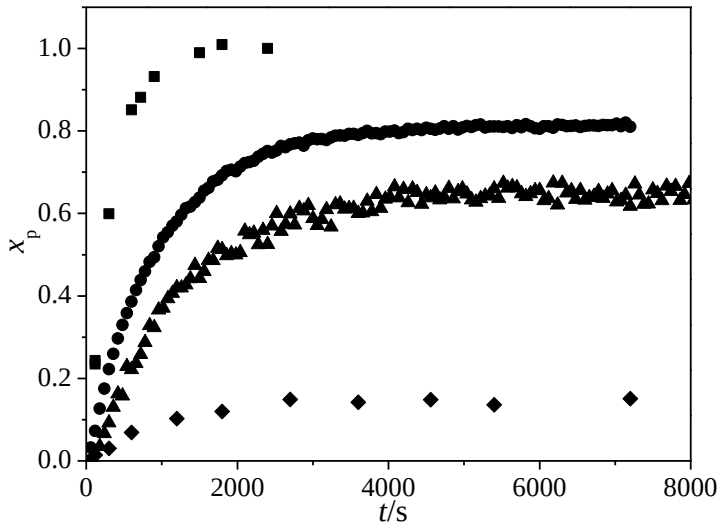

Figure 5.26. Comparison of conversion profiles from the batch polymerization of 12.5 vol% monomer in aqueous solution and 0.02 wt% V-50 at 85 °C for NVP (■) (measured by gravimetry), NVF (●) (measured by online IR), QVI (▲) (measured by online IR) and NVI (♦) (measured by NMR).

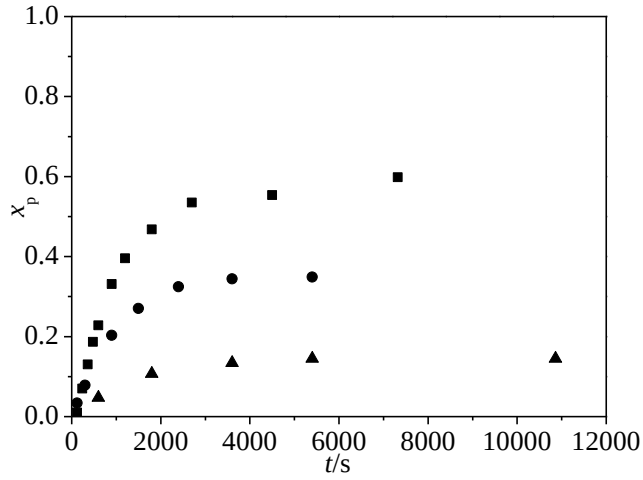

Figure 5.27. Conversion profiles, measured by NMR, for the batch polymerization of 12.5 vol% NVI and 0.02 wt% V-50 at 85 °C at pH values of a) 1 (■), 4 (●) and 9 (▲).

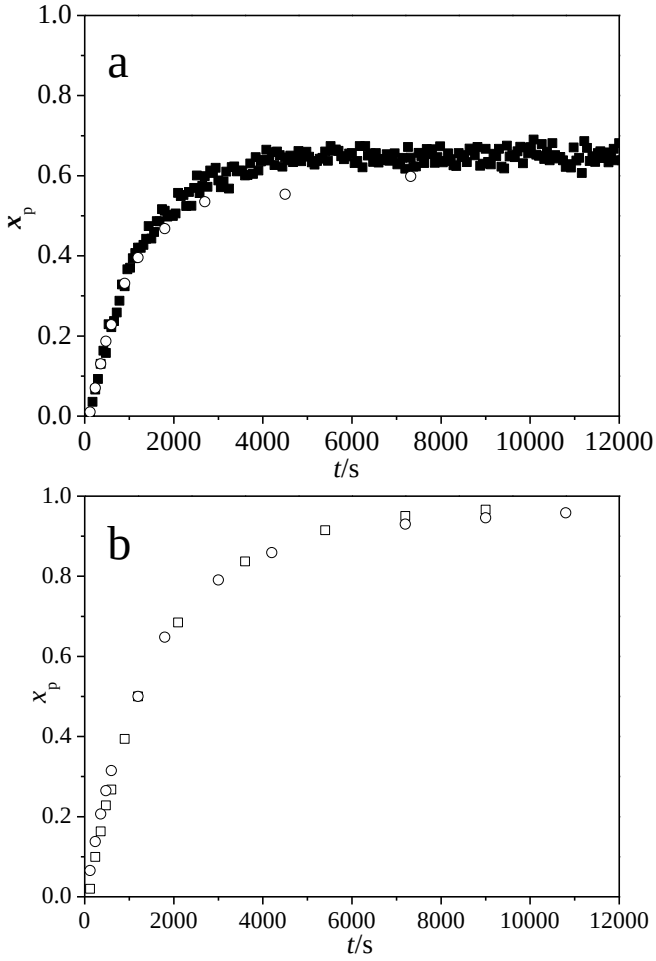

Figure 5.28. Comparison of conversion profiles for the batch polymerization QVI (squares) and NVI (at pH1) (circles) using 0.02 wt% V-50 at a monomer concentration of a) 12.5 wt% at 85 °C and b) 6.25 wt% at 70 °C. The open and filled symbols represent data measured by NMR and IR data respectively.

In order to check for monomer concentration dependence of k_p, as is common with water-soluble monomers in aqueous solution,[14-16] experiments were conducted at varying monomer concentrations at an initiator concentration of 0.02 wt% at both the natural pH of 9 (Figure 5.29 (a)) as well as at an adjusted pH of 1 (Figure 5.30). The monomer dependence of the initial rate at pH 1 was very similar to that of the QVI system, as expected. The monomer dependence of the initial rate at pH 9 was quite small at concentrations above 12.5 vol%, but, the initial rate of conversion was observed to almost double as the concentration was decreased from 12.5 to 6.25 vol%, at pH 9 (Figure 5.29(a)). This increased variation of the initial rate with monomer

concentration at the lower monomer concentration of 12.5 vol% and below is in good agreement with the observation for QVI as well as with the PLP-SEC measured k_p variation of NVP and NVF.

Polymerization rate showed a significant increase with increasing initiator concentration from 0.02 to 0.2 wt% V-50, as shown in Figure 5.29 (b). The influence of temperature on polymerization rate was investigated by conducting the experiment of 6.25 vol% NVI (adjusted pH of 1) and 0.02 wt% V-50 at 70 °C, keeping the initial radical generation rate same as that used at 85 °C to eliminate any differences in rate arising as a result of differences in initiator decomposition rates at the two temperatures. The initial rate was observed to be independent of the temperature as shown in Figure 5.31, a finding in good agreement with observations from preliminary PLP data on QVI from our co-workers in the PISAS, as well as with our investigation on temperature dependence of QVI conversion rate. The limiting conversions at the two temperatures are also in good agreement with the initiator depletion profiles at the two temperatures, as was shown for QVI.

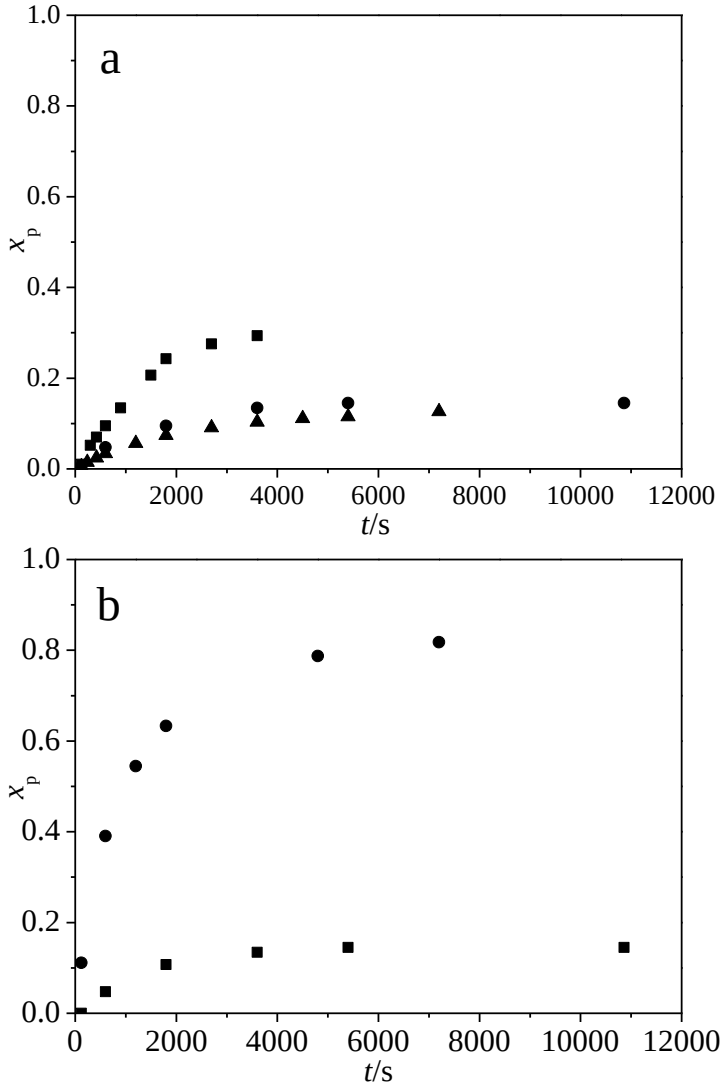

Figure 5.29. Conversion profiles, measured by NMR, for the batch polymerization of NVI (natural pH of 9) at 85 °C. a) Influence of monomer concentrations of 6.25 (■), 12.5 (●) and 20 (▲) vol% at an initiator concentration of 0.02 wt%. b) Influence of initiator concentration of 0.02 (■) and 0.2 (●) wt% at a monomer concentration of 12.5 vol%. Symbols and lines represent experimental and model results respectively.

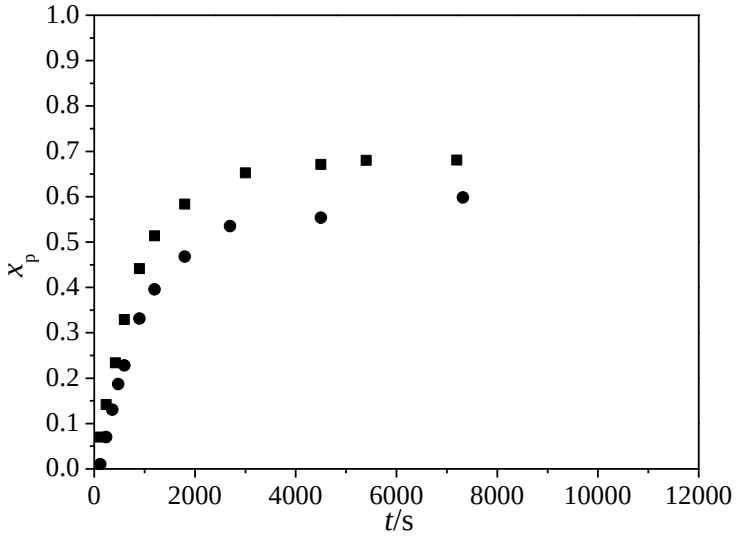

Figure 5.30. Influence of monomer concentrations of 6.25 (■) and 12.5 (●) vol% on the conversion profiles for the batch polymerization of NVI at an adjusted pH of 1 at 85 °C.

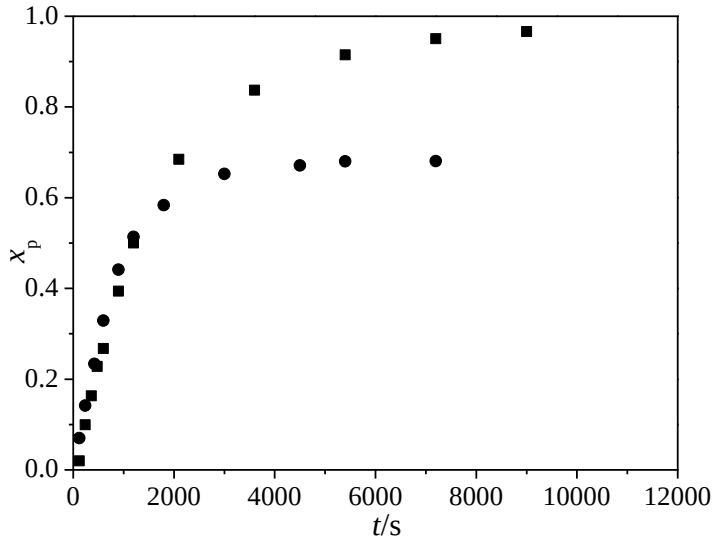

Figure 5.31. Comparison of the conversion profiles, measured by NMR, at 70 °C (■) and 85 °C (●) at the same initial radical generation rate for the batch polymerization of 6.25 vol% NVI.

Molecular weight behaviour. As a next step, it was of interest to investigate how these differences in rate with pH and initiator influence the polymer molecular weight. The influence of initiator concentrations of 0.02 and 0.2 wt% on poly(NVI) molecular weight distributions (MWDs) is shown in Figure 5.32. As expected, there is a shift towards higher molecular weight

with decreasing initiator concentration. Similarly, as the pH is decreased from 9 to 4 to 1, there is a shift towards higher molecular weight (Figure 5.33). This result is in agreement with the increasing rate observed with decreasing pH. However, no specific trend in molecular weight is observed with conversion. Some of the samples from the experiments at adjusted pH levels of 4 (3%) and 1 (all with the exception of 15%), indicated by an asterisk in the figure legends, clogged the filters and may have affected the results accordingly. A similar problem was reported in a recent study on the copolymerization of NVP and NVI,[8] where it was proposed that the clogging was a result of gelled polymer due to the possible cross-linking in the NVI system arising as a result of the chain transfer to polymer.[8] The tailing in the low molecular weight region in the samples from the experiment at pH 1 may be due to possible adsorption of the polycation to the packing material in the SEC columns, which can delay the elution time and recovery rate, a common problem for polycations.[10]

A comparison of the MWDs for the four *N*-vinyl monomers (NVP, NVF, QVI and NVI (at pH 1)) investigated at 12.5 vol% monomer concentration and 0.02 wt% V-50 concentration at 85 °C and monomer conversion of ~60% is shown in Figure 5.34. Similar to conversion data, the molecular weight behaviour of poly(QVI) and poly(NVI) (at pH 1) is expected to be similar. Although the peak MW values for the two polymers are similar, the MWD for poly(NVI) is much broader than that of poly(QVI), a result which might be an indication of long chain branching in NVI, as has also been reported in some studies.[5,8] However, the peak MW values of both poly(NVI) and poly(QVI) are significantly higher than poly(NVF) and similar to poly(NVP) produced under identical conditions. This behaviour, more clearly observed in the evolution of M_w with conversion in Figure 5.35, is quite unexpected considering the significantly lower rates of polymerization for NVI and QVI compared to NVF and NVP.

The rate of polymerization and the instantaneous degree of polymerization are given by eqns. 5.2 and 5.3 respectively, as derived under the quasi-steady state approximation for a batch reactor:

$$R_p = k_p M \left(\frac{2 f k_d I}{k_t} \right)^{0.5} \tag{5.2}$$

$$DP_n^{inst} = \frac{k_p[M]}{(k_{td} + 0.5k_{tc})[P_{tot}] + k_{tr}^{mon}[M] + k_{tr}^{sol}[S]} \tag{5.3}$$

Eqn. 5.3 can be re-written in terms of R_p as shown in eqn. 5.4

$$\frac{1}{DP_n^{inst}} = \frac{(k_{td} + 0.5k_{tc})R_p}{k_p^2[M]^2} + \frac{k_{tr}^{mon}}{k_p} + \frac{k_{tr}^{sol}[S]}{k_p[M]} \tag{5.4}$$

It is clear from eqns. 5.2 and 5.4 that both R_p and DP_n^{inst} are proportional to $\frac{k_p^2}{k_t}$, making it evident that it is impossible to come up with a combination of k_p and k_t that increases and decreases the rate and molecular weight, respectively. Moreover, as the molecular weight differences between the systems investigated in the earlier studies (Chapter 4) could be explained well by k_p differences, these contradictory results might indicate the occurrence of some additional mechanisms. However, as discussed in Chapter 2 and earlier in this chapter, non-size exclusion effects such as ion inclusion, adsorption of the polymer onto the packing material in the SEC columns and electrostatic interactions can significantly influence the apparent MW results of polycations. Although electrostatic effects can be counteracted by the addition of low molecular weight salts, the type and concentration of salt is specific to each system, which makes it difficult to comment on whether or not the concentration of LiBr added in this case was sufficient to completely screen all the electrostatic interactions. Moreover, the significantly high MW values of poly(NVI) and poly(QVI) are best explained by the electrostatic interactions resulting in expanded polymer conformation and thereby the higher MW values.

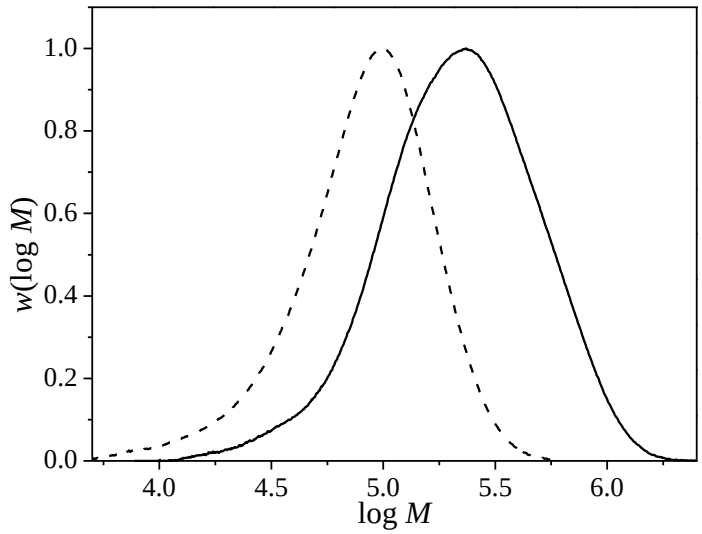

Figure 5.32. Comparison of the MWDs for the batch polymerization of 12.5 vol% NVI at a natural pH of 9 and a temperature of 85 °C at varying V-50 concentrations of 0.02 (——) and 0.2 (-----) wt%.

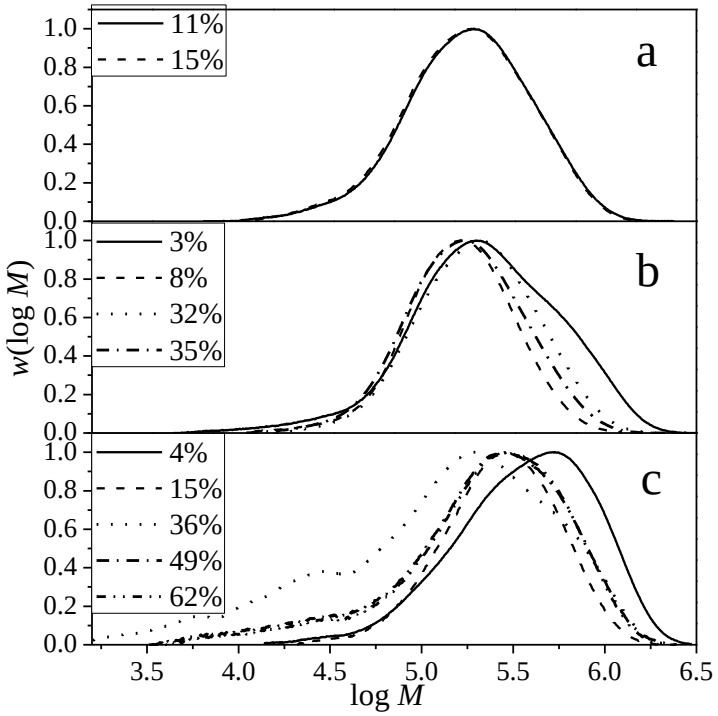

Figure 5.33. Evolution of molecular weight distributions with conversion for the batch polymerization of 12.5 vol% NVI and 0.02 wt% V-50 concentration at 85 °C at varying pH levels of 9 (a), 4 (b) and 1 (c). Conversion levels as indicated in the Figure legends. The asterisk indicates the samples that clogged the filters.

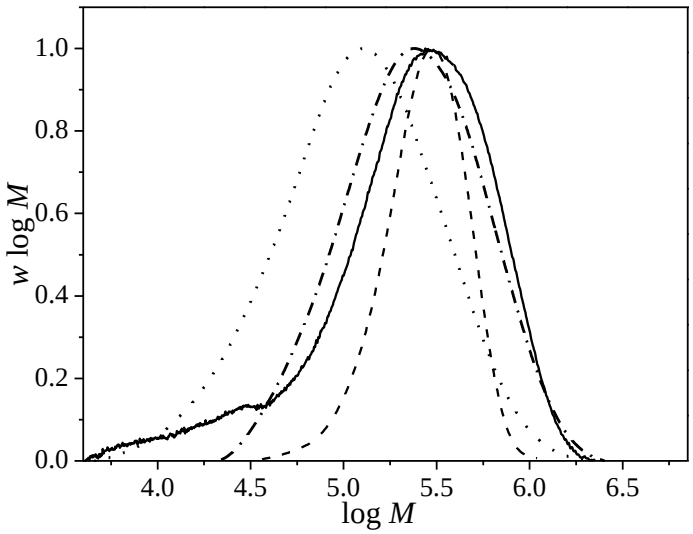

Figure 5.34. Comparison of the MWD for the polymer obtained from the batch polymerizations of 12.5 vol% NVI(at pH 1) (——), QVI (-----), NVF (·····) and NVP (– · – · –) and 0.02 wt% V-50 at 85 °C and monomer conversion of ~60%.

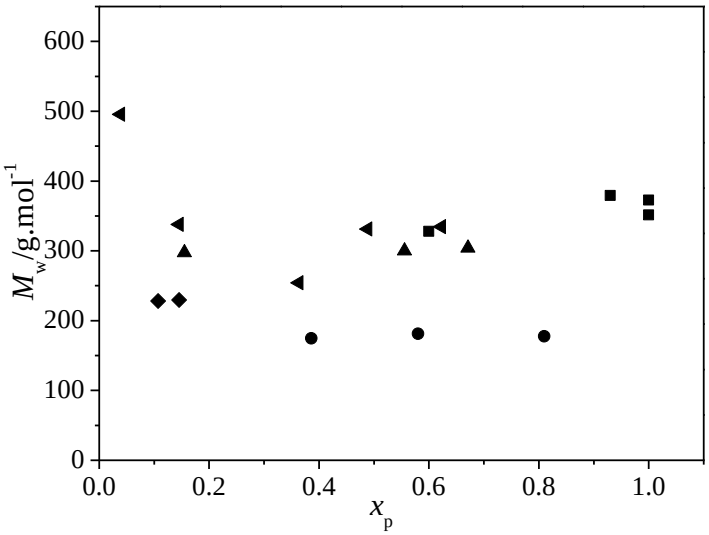

Figure 5.35. Evolution of weight average molecular weight (M_w) with conversion for the polymer obtained from 12.5 vol% NVP (■), NVF (●), QVI (▲), NVI at pH 9 (♦) and NVI at pH 1(◀) and 0.02 wt% V-50 at 85 °C.

5.4.4 Model Development

The QVI model was adapted for NVI by changing the monomer physical properties and adding mechanisms to describe the degradative addition to monomer and subsequent termination of the stable radicals (X) with the regular propagating radicals (P). Due to the greatly reduced reactivity

of the stable radicals, their participation in propagation and termination amongst themselves have been ignored, as suggested by Bamford.[3] The mechanistic scheme describing the free radical polymerization of NVI is shown in Table 5.5 and the expressions and values of the kinetic rate coefficients used in the model are shown in Table 5.6. The value of $k_p / k_t^{0.5}$ was estimated to be 0.674, by fitting it to the QVI and NVI data at pH 1, which gives a k_p value of ~7.2x10^3 L. mol^{-1}.s^{-1}, which is in accordance with the rate differences between QVI, NVP (k_p =3.58x10^4 L.mol^{-1}.s^{-1}) and NVF (k_p = 1.26x10^4 L.mol^{-1}.s^{-1}). It is assumed that the rate decreases at the higher pH levels in NVI are due to the competitive degradative addition to monomer (k_{tr}^{deg}). Thus, the value of k_{tr}^{deg} / k_p at the different pH levels were estimated by fitting it to the rate data at the respective pH levels. As was done for QVI, the transfer to polymer and PLP derived k_t expression for NVP was retained assuming similar termination behaviour of these water-soluble monomers. A k_t^{deg} value lower than k_t by a factor of 4500 was estimated for termination between X and P by fitting to the experimental data at pH 9, where the sensitivity to this parameter was highest due to the high concentration of X. Mechanisms describing the degradative addition to monomer and subsequent termination of the formed stable radicals are ignored for the NVI system at pH 1.

Table 5.5. Mechanistic scheme for the free radical polymerization of *N*-vinylimidazole.

Initiator Decomposition	$I \xrightarrow{k_d} 2 f I^{\bullet}$
Chain Initiation	$I^{\bullet} + M \xrightarrow{k_p} P_1^{\bullet}$
Chain Propagation	$P_n^{\bullet} + M \xrightarrow{k_p} P_{n+1}^{\bullet}$
Chain Termination	
By Combination	$P_n^{\bullet} + P_m^{\bullet} \xrightarrow{k_{tc}} D_{n+m}$
By Disproportionation	$P_n^{\bullet} + P_m^{\bullet} \xrightarrow{k_{td}} D_n + D_m$
Degradative addition to monomer	$P_n^{\cdot} + M \xrightarrow{k_{tr}^{deg}} X_n^{\cdot}$
Termination of stable radicals	$P_n^{\cdot} + X_m^{\cdot} \xrightarrow{k_t^{deg}} D_{n+m}$

Table 5.6. Values and expressions for the kinetic rate coefficients and physical parameters used in the kinetic modeling of free radical polymerization of *N*-vinylimidazole at 85 °C.

Mechanism	Rate Expression	pH 9	pH 4	pH 1	Ref
Initiator decomposition	$k_d(s^{-1}) = 9.17\times10^{14}\exp\left(\frac{-1.49\times10^4}{(T/\mathrm{K})}\right)$		$7.5209\text{x}10^{-4}$		12
Lumped rate constant	$k_p / k_t^{0.5}$		0.674		this work
Degradative addition	k_{tr}^{deg} / k_p	$3.5\text{ x}10^{-3}$	$8.6\text{x}10^{-4}$	0	this work
Termination of regular radicals	$k_t \Big/ \left(\mathrm{L\cdot mol^{-1}\cdot s^{-1}}\right) = 1.5\times10^8\exp\left(-w_{NVI}^0 / 0.29\right) + 1.68\times10^7$ at P = 1 bar				13
Termination of stable radicals	$k_t^{deg} = k_t / 4500$				this work
Density of Water	$\rho_{H2O} \Big/ \left(\mathrm{g\cdot mL^{-1}}\right) = 0.9999 + 2.3109\cdot10^{-5}(T/^\circ\mathrm{C}) - 5.44807\cdot10^{-6}(T/^\circ\mathrm{C})^2$		0.959		14
Density of NVI			1.039		17

A comparison of the experimental and simulated conversion results is shown in Figures 5.36-5.39. As discussed earlier, the variation of initial rate with initial monomer concentration is more significant at pH 9 than at pH 1. It is observed that the model captures the influence of pH (Figure 5.36) and the influence of monomer (Figure 5.37(a)) and initiator (Figure 5.37(b)) concentrations at pH 9 quite well. The simulated differences in rate with monomer concentration results from the variation in the concentration of degradative radicals estimated at varying monomer concentrations at pH 9. However, there is an offset between the experimental and model predictions, with the model predicting slightly lower reaction rates, perhaps indicating the need for a monomer-dependent k_p function. Although the model predicts slightly lower rates, the independence of the initial rate on temperature assumed in the model by using a temperature independent k_p matches the experimental results reasonably well, as shown in Figure 5.39. The agreement between the experimental and model results can be improved by the use of a PLP-SEC derived monomer dependent k_p expression, for which experiments are currently underway by our co-workers.

A comparison of the experimental and simulated molecular weight distributions with ($k_{tr}^{pol}/k_p = 6\times10^{-5}$) and without transfer to polymer is shown in Figures 5.40 (effect of initiator concentration) and 5.41 (effect of pH). The addition of chain transfer to polymer at the same level as used for NVP modeling has little effect on the simulated MWDs, as high conversions are not reached. In all the cases, the model predictions are lower than the experimental data. As discussed earlier, the MW values for NVI are higher than that expected based on its rate comparison to the other *N*-vinyl monomers investigated. This might be an indication of the occurrence of some additional mechanisms in this system such as gelling due to significant cross-linking, not captured by the model or may be an analysis artifact caused by non-size

exclusion effects. Despite this offset in the model predictions, the shift in molecular weight towards higher values with decreasing initiator concentration and pH levels is captured well.

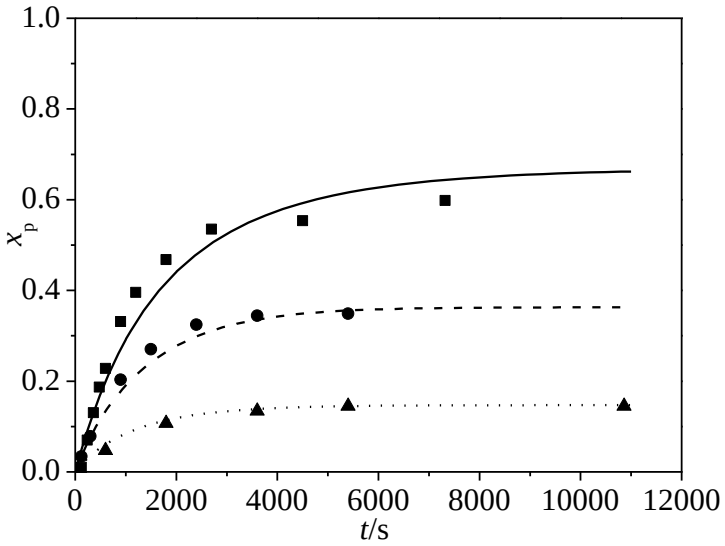

Figure 5.36. Conversion profiles for the batch polymerization of 12.5 vol% NVI and 0.02 wt% V-50 at 85 °C at pH values of a) 1 (——, ■), 4 (-----, ●) and 9 (·····, ▲). Symbols and lines represent experimental (measured by NMR) and model results respectively.

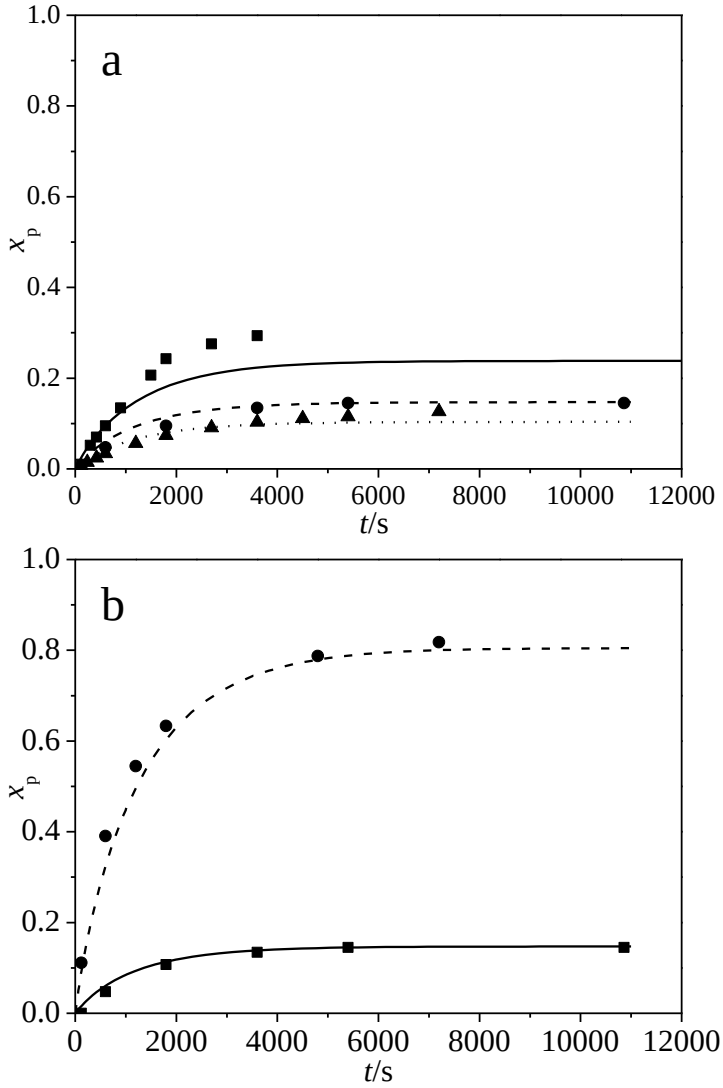

Figure 5.37. Conversion profiles for the batch polymerization of NVI at 85 °C and natural pH of 9. a) Influence of monomer concentrations of 6.25 (——, ■), 12.5 (-----, ●) and 20 (·····, ▲) vol% at an initiator concentration of 0.02 wt%. b) Influence of initiator concentration of 0.02 (——, ■) and 0.2 (-----, ●) wt% at a monomer concentration of 12.5 vol%. Symbols and lines represent experimental (measured by NMR) and model results respectively.

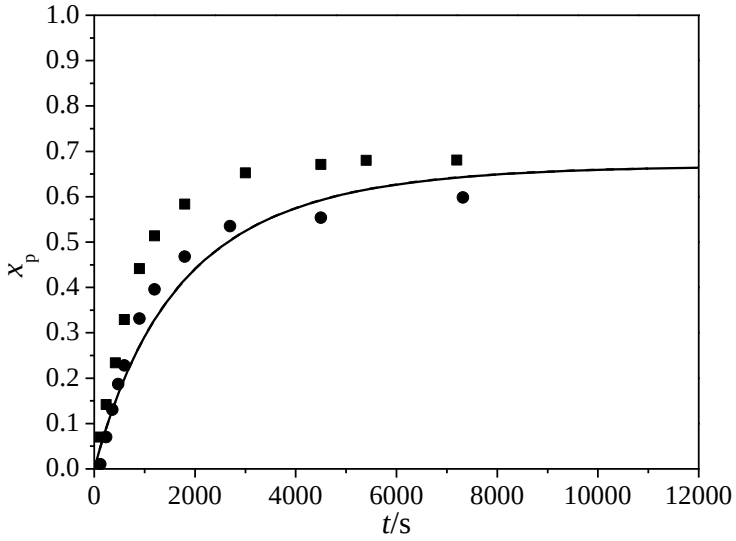

Figure 5.38. Influence of monomer concentrations of 6.25 (——, ■) and 12.5 (-----, ●) vol% on the conversion profiles for the batch polymerization of NVI at an adjusted pH of 1 at 85 °C. Symbols and lines represent experimental (measured by NMR) and model results respectively.

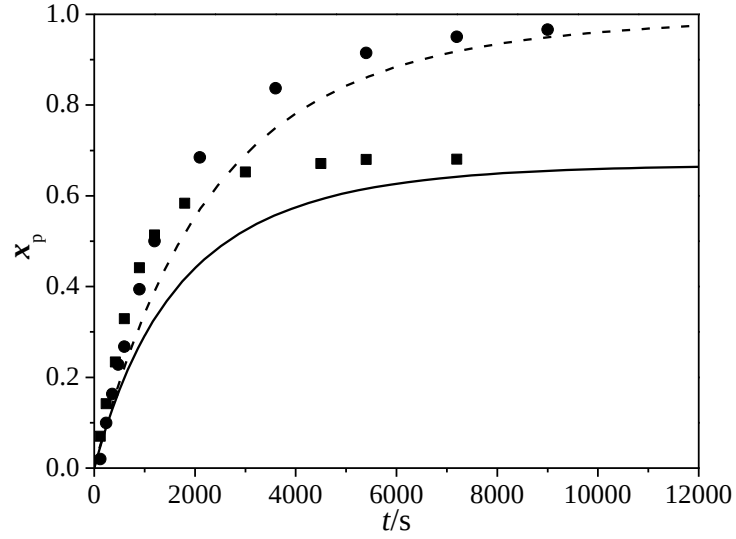

Figure 5.39. Comparison of experimental (symbols), measured by NMR, and simulated (lines) conversion profiles at 70 °C (■) and 85 °C (●) at the same initial radical generation rate for the batch polymerization of 6.25 vol% NVI at pH 1.

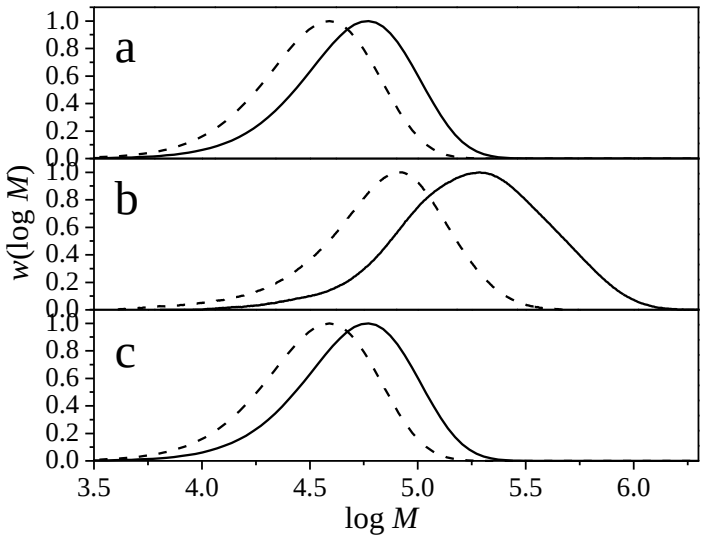

Figure 5.40. Comparison of experimental (b) and simulated molecular weight distributions with $k_{tr}^{pol}/k_p = 6\times10^{-5}$ (a) and without (c) transfer to polymer for the batch polymerization of 12.5 vol% NVI at a monomer conversion of 11% and a temperature of 85 °C at varying initiator concentrations of 0.02 (——) and 0.2 (-----) at natural pH of 9.

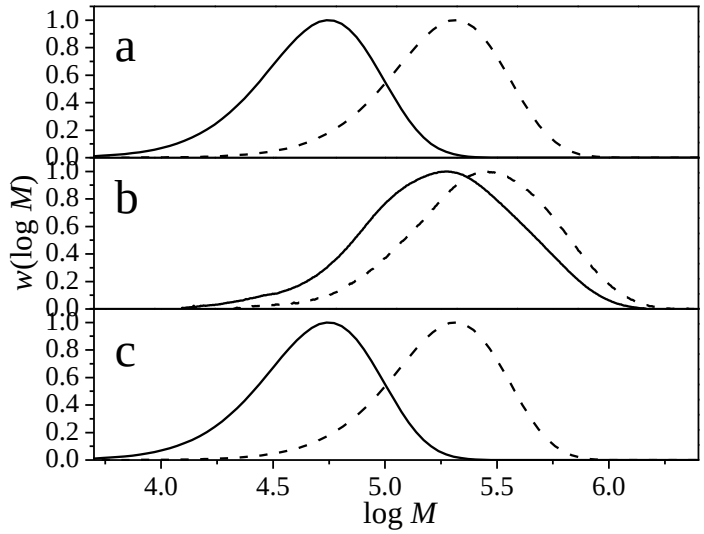

Figure 5.41. Comparison of experimental (b) and simulated molecular weight distributions with $k_{tr}^{pol}/k_p = 6\times10^{-5}$ (a) and without (c) transfer to polymer for the batch polymerization of 12.5 vol% NVI and 0.02 wt% V-50 at a monomer conversion of 15% and temperature of 85 °C at varying pH levels of 1 (——) and 9 (-----)**.**

5.5 Conclusions

Aqueous-phase free-radical batch polymerizations of NVI and QVI have been studied at varying initial monomer concentrations, initiator concentrations and temperatures. The influence of pH was also investigated for the NVI system. Due to the lack of PLP-SEC k_p data for these monomers, the batch conversion and MW experimental data were used to examine kinetic behaviour in comparison to the better understood NVP and NVF systems. The polymerization rates of both NVI and QVI were lower than those of NVP and NVF, with the very low rates found for NVI explained by Bamford's degradative addition mechanism.[3] Adjusting the pH of the NVI system to lower values by HCl addition increased the reaction rates by partially (at pH 4) and completely (at pH 1) hindering the degradative addition by protecting the 2-position of the monomer, with the rates matching that of QVI at pH 1. The initial rates of both monomers showed a small monomer dependence at monomer concentrations above 20 vol%, with the rates increasing considerably at concentration below 12.5 vol%. The polymerization rates of both NVI and QVI showed no temperature dependence, in good agreement with the observations from the preliminary PLP-SEC experiments on QVI conducted by our co-workers.

Although the NVI MWDs were broader than that of QVI (possibly due to long chain branching in NVI), the peak molecular weight values of the NVI system at pH 1 and the QVI system were in good agreement. A comparison to NVP and NVF showed the MW values of poly(QVI) and poly(NVI) to be unexpectedly higher than those for poly(NVP) and poly(NVF) produced at identical experimental conditions. However, the discrepancies in the SEC results measured using different detectors and at different sites and the experimental difficulties of obtaining reliable SEC data for these polycations due to the prevalence of non-size exclusion effects, made it difficult to make any quantitative comparison with the other systems.

The same kinetic model built for NVP was modified to describe both QVI and NVI by retaining the k_t expression and the transfer to polymer used for NVP and ratioing k_p value to $k_t^{0.5}$ (lumped rate constant). Additionally, Bamford's degradative addition mechanism[3] was incorporated for the NVI system at the higher pH levels. The same model was used for both NVI and QVI only by adjusting the rate coefficient for degradative addition (set to zero for NVI at pH 1). The model was capable of capturing the conversion profiles for both the monomers reasonably well, with the slight offset between the model and experimental results expected to be improved by independent measure of the k_p behaviour for both monomers. The model predictions of the molecular weight data were lower than that of the experimental data for both the monomers. It is difficult to conclude whether this difference was due to some additional mechanisms such as gelling, as has been reported in some of the other studies,[5,8] not captured by the model or just the influence of non-size exclusion effects on polymer molecular weight.

Although these monomers have been widely used in a number of copolymerization studies, a complete kinetic study on their homopolymerization behaviour was not available until now. This work greatly improves the kinetic understanding of these systems and provides a simple model which can reasonably describe the conversion behaviour of these systems. Further advances are possible with the PLP measure of k_p, and with refinements in the SEC techniques used to characterize the polymer MW of these polycations.

References

1) BASF datasheet,http://www.basf.com/group/corporate/en/brand/1_VINYLIMIDAZOLE.
2) Masaki, M.; Ogawa, K.; Kokufuta, E. *Colloid Polym. Sci*., **2009**, *287*, 1405-1415.
3) Bamford, C. H.; Schofield, E. *Polymer*, **1981**, *22*, 1227-1235.

4) Fink, J. K.; Ch. 8 in *Handbook of Engineering and Speciality Polymer: Volume 2: Water Soluble Polymers,* Scrivener, USA, **2011**.

5) Chapiro, A. *Radiat. Phys. Chem*. **1992**, *40*, 89-93.

6) Joshi, M.; Rodriguez, F. *J. Polym. Sci.***1984**, *29*, 1354-1354.

7) Dambatta, B. B.; Ebdon, J. R. Eur. Polym. J. **1986**, *22*, 783-786.

8) Arosio, P.; Mosconi, M.; Storti, G.; Banaszak, B.; Hungenberg, K. D.; Morbidelli, M. *Macromol. React. Eng.*, **2011**, *5*, 501-517.

9) Striegel, A. M.; Yau, W. W.; Kirkland, J. J.; Bly, D. D. Ch. 12 in *Modern Size Exclusion Liquid Chromatography: Practice of Gel Permeation and Gel Filtration Chromatography,* John Wiley and Sons, New Jersey, **2009**.

10) Tosoh Bioscience, Separation report No. 106, Aqueous SEC columns for analysis of cationic polymers.

11) Santanakrishnan, S.; Hutchinson, R. A.; Učňová, L.; Stach, M.; Lacik, I.; Buback, M. *Macromol. Symp*, **2011**, *302*, 216-223.

12) Wako Chemicals information brochure

13) Schrooten, S.; Buback, M.; Hesse, P.; Hutchinson, R. A.; Lacik, I. *Macromol. Chem. Phys*. **2011**, *212*, 1400-1409.

14) Stach, M.; Lacik, I.; Chorvat, D., Jr.; Buback, M.; Hesse, P.; Hutchinson, R. A.; Tang, L. *Macromolecules* **2008**, *41*, 5174-5185.

15) I. Lacík, L. Učňová, S. Kukučková, M. Buback, P. Hesse, S. Beuermann, *Macromolecules*, **2009**, *42*, 7753..

16) Stach, M.; Lacik, I.; Kasák, P.; Chorvát, D., Jr.; Saunders, A. J..; Santanakrishnan, S.; Hutchinson, R. A. *Macromol. Chem. Phys*. **2010**, *211*, 580-593.

17) Sigma Aldrich material data sheet

Chapter 6. Aqueous-Phase Free Radical Copolymerization of *N*-vinylpyrrolidone (NVP) and *N*- vinylformamide (NVF)

6.1 Abstract

Aqueous-phase batch copolymerization of NVP and NVF was conducted at temperatures of 60 and 85 °C with varying initial monomer mixture compositions and monomer to water ratio. The rate of copolymerization was observed to increase with increasing NVP mole fraction (f_{NVP}) in the monomer mixture as well as with decreasing total monomer concentration, in accordance with the expected behaviour based on the homopolymerization kinetics of the individual monomers. The copolymer composition (F_{NVP}) was found to be the same as that of the monomer mixture composition (f_{NVP}), indicating monomer reactivity ratios to be unity. Both the rate and composition behaviour of this copolymerization system could be explained well by the terminal model using the known behaviour of the propagation rate coefficient (k_p) of the individual monomers.

6.2 Introduction

Poly(*N*-vinylamides) are a class of water soluble polymers finding applications in science and medical practice.[1] Poly(vinylpyrrolidone) (PVP) is one of the most commercially-important polymer in this class. PVP and its copolymers find applications in a variety of fields such as medicine, pharmaceuticals, cosmetics, food, textiles etc.[1] Other important poly(*N*-vinylamides) include poly(vinylformamide) (PVF) and its copolymers. Due to its low toxicity, PVF and its copolymers find applications in waste water treatment, adhesives, packaging, personal care products, dispersing agents, textiles and corrosion inhibition.[2] The presence of a primary amino group in this polymer allows it to hydrogen bond with the surface cellulose molecules in fibers, improving inter-fiber bonding and thus enhancing a variety of paper properties. Despite the

important commercial applications of poly(*N*-vinyl amides) and their copolymers, it is only fair to say that the understanding of these systems is quite far from complete. Recent PLP studies on the homopolymerization of some of the water soluble *N*-vinyl amides have shown the propagation rate coefficient (k_p) of these monomers to exhibit a strong dependence on the monomer concentration in water, as discussed in Chapter 2. Despite the improved understanding of the homopolymerization kinetics of these monomers, few studies have explored the copolymerization behaviour of these systems.

Some of the earlier studies include those by Chapiro et al.[3] on the gamma irradiated copolymerization of NVP with AA in bulk, ethanol, toluene and DMF and with methacrylic acid (MAA) in methylene chloride. Although both MAA and AA formed complexes with NVP, the molecular associations were observed to have negligible influence on the copolymer composition. In all cases, the reactivity of NVP was observed to be lower than either of AA and MAA. Both temperature (20 to -63 °C) and solvent choice had negligible influence on these systems with the exception of NVP-AA in DMF, where the complexation of AA with DMF resulted in a slightly higher incorporation of AA in the copolymer compared to the other solvents. However, as the composition differences were very small, the solvent influence was concluded to be negligible. The influence of pH on the copolymerization of NVP and acrylic acid (AA) over a range of pH values ranging from 4-9 was studied by Ponratnam et al.[4] The AA reactivity ratio (r_1) exhibited a significant dependence on pH, decreasing from 5.2 to 1.3 as the pH was varied from 4 to 5 followed by an increase to 8.1 at pH 7 and a subsequent fluctuation between 6 to 7 at pH values of 7 to 9. These fluctuations in r_1 were explained by electrostatic repulsion which is responsible for the initial dip at pH 5 followed by the subsequent counter-ion shielding at the higher pH values. Although the reactivity ratio of NVP (r_2) was observed to be

very close to zero at all pH values studied, a relatively high value of 0.31 was observed at a pH of 5. This was also attributed to the lower local concentration of AA around the polymer at this pH which facilitates the addition of NVP over AA. These variations in reactivity ratios may also be influenced by the effect of pH on AA k_p, as measured by the PLP/SEC technique.[5] Similar studies on NVP and MAA[6] over a pH range of 2-10 showed a behaviour quite similar to the AA-NVP system. The reactivity ratio of MAA (r_1) was observed to drop from ~6-8 to 2.9 as the pH was increased from 2-3 to 4 followed by an increase to 4.9-4 at pH values of 5-7 and it reaches its minimum of 0.81 at a pH of 8. The two minima in r_1 reached at pH values of 4 and 8 were attributed to the closeness in the pH values to the pKa values of the acid and the polyacid respectively. A further increase in pH to 10 resulted in an increase in r_1 to 3.6. This behaviour in the reactivity ratio of MAA was also explained by the initial electrostatic repulsion and the subsequent shielding by counter-ions as the pH was increased. Similar to the AA-NVP system, the reactivity ratio of NVP (r_2) was very close to zero with relatively high values of 0.28 and 0.67 reached at pH values of 7 and 8, a result explained by the almost fully ionized state of the polymeric macroradicals at this pH which facilitates the incorporation of NVP over MAA (methacrylate ions). More recent study on the copolymerization of AA and acrylamide (AM) by Rintoul et al. have shown the electrostatic effects arising as a result of the variation of the ionization of AA with pH to be primarily responsible for the variation of the reactivity ratios of AA and AM with pH.[7] As these systems are complicated by the effect of pH on MAA/AA k_p, this study will focus on copolymerization among the *N*-vinyl amide family.

Studies on the copolymerization of NVP and *N*-vinylimidazole (NVI) by Martinez-Piña et al.[8] showed the formation of random copolymers with monomer reactivity ratios of 1 and 0.07 for NVP and NVI respectively. The formed copolymer was soluble in water, methanol and ethanol

at all compositions while the solubility in chloroform, *n*-butanol and *n*-propanol depended on the copolymer composition. Bulk copolymerization of NVP and 2-hydroxyethyl methacrylate (HEMA)[9] showed HEMA to be much more reactive than NVP. Copolymerization of NVP and 2- and 4- vinylpyridine, studied by Gatica et al.[10] showed NVP to have a lower reactivity than either of 2-and 4-vinylpyridine with the reactivity ratio of NVP ranging at ~0.3-0.5 and that of 2- and 4- vinylpyridine ranging at 5.4-6.3 and 3.1-3.6 respectively. Kathmann et al. have studied the copolymerization of *N*-vinylformamide (NVF) with acrylamide (AM) and sodium acrylate (NA) in aqueous solution and with butyl acrylate (BA) in THF.[11] A strong alternating tendency was observed in all three cases. The alternating behaviour was explained in terms of formation of a mild electron donor-accepting pair in the NVF-AM system. While, the alternating tendency in the NVF-NA pair was explained by the higher electrostatic repulsion between the sodium acrylate units which favors the addition of an NVF unit after an NA pendant group and the higher stability of the NA group which favors the addition of an NA group after an NVF pendant group. NVF was also observed to form an alternating copolymer with maleic anhydride.[12] The precipitative copolymerization of NVF with MAA and AA in isopropanol[13] showed MAA to have a higher reactivity than NVF, while an alternating tendency was observed for the NVF-AA system. A study on the precipitative copolymerization of NVP and NVF in isopropanol by Kirsh et al.[1] showed both these monomers to have a reactivity of unity in isopropanol, attributing this behaviour to the hydrogen-bonding and dipole-dipole interactions arising as a result of their respective structural conformations.[1]

With literature studies existing on precipitative polymerization in organic (isopropanol) solvent, it was of interest to study the influence of water on the copolymerization behaviour of this co-monomer pair. Moreover, with recent advances in the understanding of NVP[14,15] and NVF[16]

achieved by PLP-SEC studies made it all the more interesting to understand how knowledge on their homopolymerization kinetics can be extended to understand the copolymerization behaviour.

6.3 Experimental

N-vinyl pyrrolidone (>99%, Aldrich), *N*-vinyl formamide (98%, Aldrich), and the thermal initiator 2,2'-azobis (2-methylpropionamidine) dihydrochloride (V-50, Fluka, ≥ 98%) were used as received. Preliminary low conversion experiments were carried out in sealed 30 mL glass vials under nitrogen purge and continuously stirred using magnetic pellets. The monomer-water mixtures was pre-mixed and heated to reaction temperature of 60 °C before the addition of initiator solution (V-50 in distilled water). Each vial was treated as an individual sample and the reactions were stopped by the addition of inhibitor and removing the vial to an ice bath. The stop times were decided by a trial and error method. The first few experiments were carried out to ~2-10 minutes, taking care to keep the conversion levels below 10%. However, due to the very low NVP content in the precipitated copolymer produced from these samples, the subsequent experiments were conducted for relatively longer periods. As discussed later, the significant scatter in the NMR data from these low conversion experiments led to a change in procedure, with copolymerization batch experiments with frequent sampling conducted to get a better kinetic understanding of this system. The batch experiments were carried out in 1 L automated labmax reactor under nitrogen blanket. The experiments at higher monomer concentration of 50 wt% were terminated at shorter times due to high system viscosities. The formed copolymer remained dissolved in the mixture and was precipitated using acetone, and dried at a temperature of ~100 °C under vacuum for composition analysis by NMR. Trace amounts of monomer and acetone were detected in the isolated copolymer sample, which have been quantified and

accounted for accordingly in the calculation of copolymer composition as detailed in Appendix B.2. All conversion data in this section was measured by offline gravimetry, wherein samples were dried in an air stream followed by hot air oven for ~72 h to remove the residual monomer and water from the polymer sample.

6.4 Characterization

NMR Analysis. Deuterated water was used as the solvent for NMR analysis. The ^{1}H-NMR spectrums of the respective homopolymers (PVP and PVF) and monomers (NVP and NVF) can be found in Chapters 3 and 4. The ^{1}H-NMR spectrum of a precipitated copolymer sample from the experiment at 10 wt% monomer concentration at f_{NVP}=0.5, 0.1 wt% initiator concentration, at 60 °C and monomer conversion of ~42%, is shown in Figure 6.1. The peaks representing the CH in the formamide group of NVF and CH_2 in the pyrrolidone ring of NVP, appearing at ~7.4-8.05 and ~1.8-2 ppm respectively, as indicated in Figure 6.1, were used in determining the copolymer composition. As some of the monomer peaks appear at the same peak positions as the polymer peaks used for the composition analysis, any trace levels of monomer present in the precipitated polymer may influence the copolymer composition. Therefore, any trace levels of monomer detected in the samples were quantified and accounted for in the calculation of copolymer composition as explained in Appendix B.2.

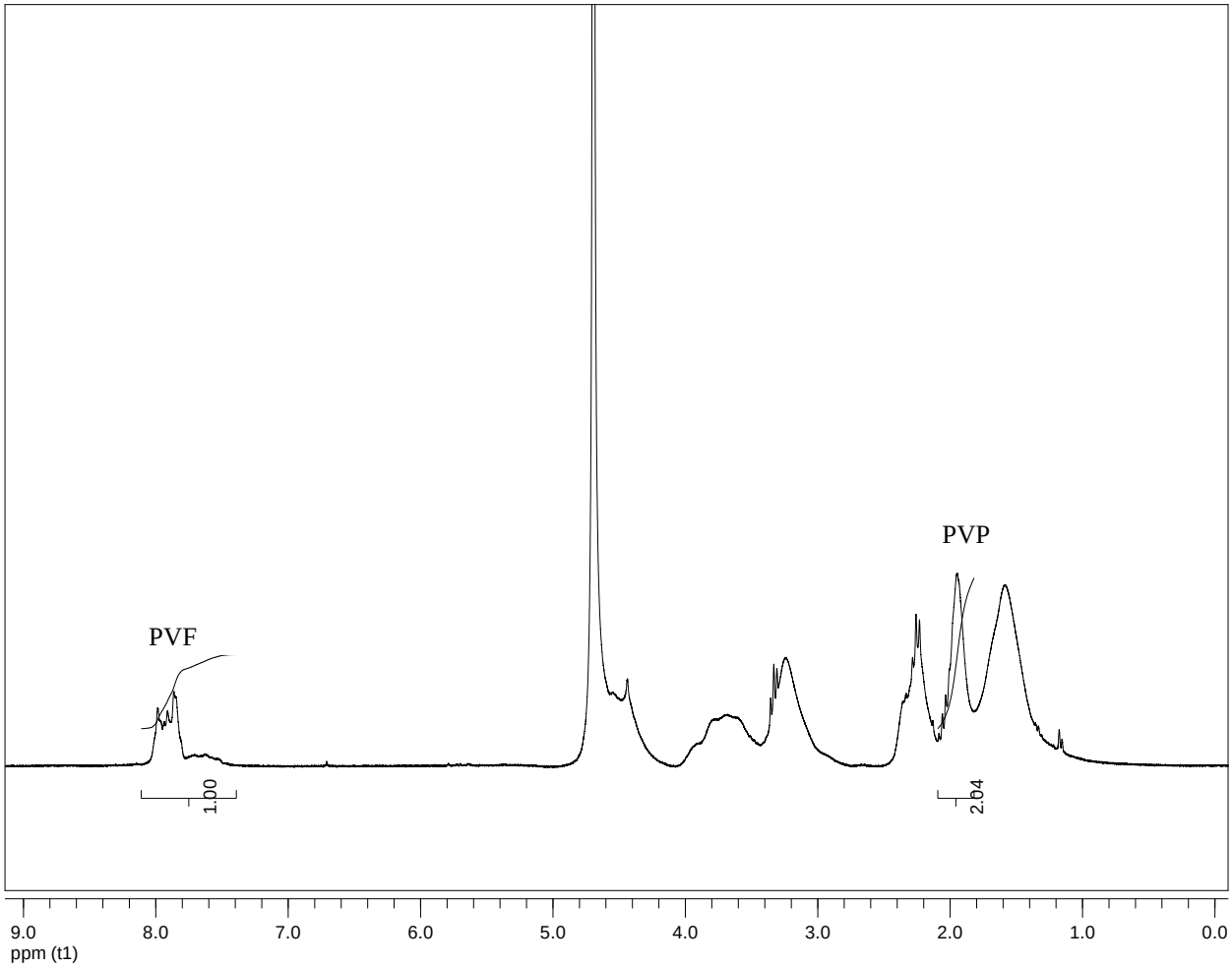

Figure 6.1. NMR spectrum of copolymer produced from 10 wt% monomer at f_{NVP} of 0.5, 0.1 wt% V-50 at ~42% monomer conversion and temperature of 60 °C in water. The CH_2 in the pyrrolidone ring of NVP (at ~1.8-2 ppm) and CH (at ~7.4-8.05 ppm) in the formamide group of NVF have been labeled PVP and PVF respectively.

SEC Analysis. Molecular weight analysis was carried out by size-exclusion chromatography (SEC) at the Polymer Institute of the Slovak Academy of Sciences, Bratislava using the Polymer Standards Services (PSS, Mainz, Germany) column setup which consists of an 8 x 50mm PSS GRAM 10µm guard column and three 8 x 300mm PSS GRAM 10µm columns with pore sizes 100, 1000 and 3000 Å placed in a column heater set to a temperature of 60 °C. The samples were dissolved in the eluent (mixture of water/acetonitrile (80:20) with 0.15 M NaCl and 0.03 M NaH_2PO_4) at a concentration of ~2-3 $mg.mL^{-1}$. The MW values were obtained using multi angle

laser light scattering (MALLS) and RI (effective calibration towards pullulan standard). Ethylene glycol was used as the flow marker to control the flow rate at 1 mL.min^{-1} and the injection volume was set to 100 μL. The dn/dc values of polyvinylpyrrolidone (PVP) and polyvinylformamide (PVF) in the eluent were determined to be 0.135 and 0.143 respectively and the dn/dc values for the various copolymer compositions were calculated by the weighted composition average of the dn/dc values of the individual homopolymers, as has been reported in other studies.[17] Likewise the correction factors for the RI data also varied with copolymer compositions, as shown in Table 6.1, containing a comparison of the RI and MALLS MW data. A comparison of the M_w values from MALLS and corrected RI is shown in Figure 6.2. With the exception of a few values, all other values are aligned along the diagonal indicating a good agreement between the MALLS and the corrected RI M_w values. A complete summary of all the MALLS and RI data for the different copolymer samples is contained in Appendix A.5.

Table 6.1. Comparison of RI and MALLS data for copolymer produced from aqueous-phase batch polymerization of NVP and NVF.

Initial conditions	F_{NVP}	x_p	RI (pullulan calibration)			MALLS			$M_{w,MALLS}/M_{w,RI}$
			M_n kg.mol^{-1}	M_w kg.mol^{-1}	PDI	M_n kg.mol^{-1}	M_w kg.mol^{-1}	PDI	
[M]=10 wt% [V-50]=0.02 wt% T=85 °C	0.1	0.21	123	335	2.7	107	166	1.5	0.49
		0.83	143	351	2.4	115	177	1.5	0.51
	0.5	0.18	134	327	2.4	86	121	1.4	0.37
		1	101	341	3.3	108	214	1.9	0.63
	0.9	0.21	79	275	3.5	144	257	1.7	0.93
		1	52	390	7.4	115	608	5.2	1.56
[M]=10 wt% [V-50]=0.1 wt% T=60 °C	0	0.11	171	428	2.5	178	230	1.2	0.54
	0.1	0.09	169	392	2.3	151	212	1.4	0.54
	0.25	0.11	180	411	2.2	180	268	1.4	0.65
	0.5	0.11	124	387	3.1	159	249	1.5	0.64
	0.5	0.12	136	381	2.8	172	265	1.5	0.70
	0.5	0.11	139	355	2.5	171	295	1.7	0.83
	0.9	0.14	130	511	3.9	184	297	1.6	0.58
		0.75	102	327	3.2	236	391	1.6	1.2
	1	0.12	106	307	2.8	208	318	1.5	1.04
		0.7	151	430	2.8	285	425	1.4	0.99
[M]=25 wt% [V-50]=0.1 wt% T=60 °C	0	0.11	209	589	2.8	184	283	1.5	0.48
		0.71	267	845	3.1	258	448	1.7	0.53
	0.1	0.09	143	606	4.2	179	310	1.7	0.51
		0.86	296	913	3.0	264	466	1.7	0.51
	0.5	0.13	140	483	3.4	190	306	1.6	0.63
		0.86	196	720	3.6	215	499	2.3	0.69
	0.9	0.12	131	410	3.1	205	342	1.6	0.84
		0.97	110	637	5.7	212	605	2.8	0.95
	1	0.15	82	251	3.0	190	287	1.5	1.14
		1	55	450	8.1	155	524	3.3	1.16
[M]=50 wt% [V-50]=0.2 wt%	1	0.14	103	319	3.1	222	327	1.4	1.03
	0.1	0.11	132	515	3.8	144	335	2.3	0.65
	0.5	0.11	249	562	2.2	247	318	1.2	0.57
	0.9	0.13	119	325	2.7	209	329	1.5	1.01
	0	0.13	293	808	2.7	305	439	1.4	0.54
								Avg. $M_{w,MALLS}/M_{w,RI}$ at F_{NVP} =	**0** 0.52
									0.1 0.54
									0.25 0.65
									0.5 0.67
									0.9 1.01
									1 1.07

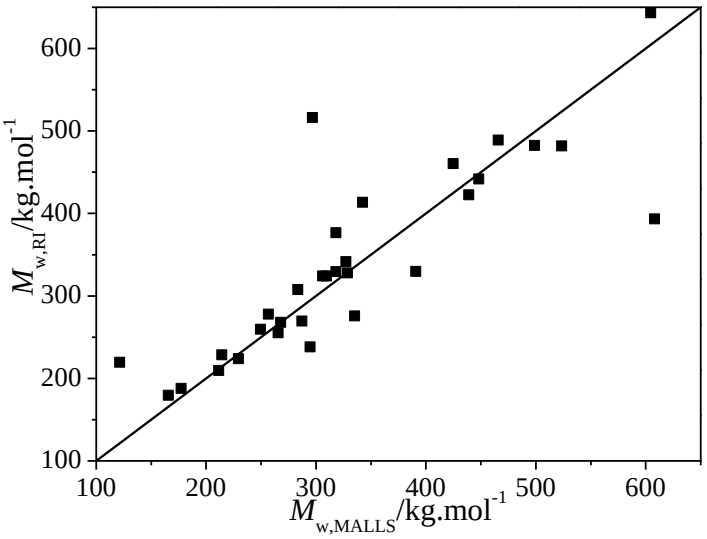

Figure 6.2. Comparsion of MALLS and corrected RI M_w values for the copolymers produced from aqueous-phase batch polymerization of NVP and NVF.

6.5 Results & Discussion

A comparison of the monomer concentration dependent k_p trends for NVP[14] and NVF[16] in water, determined via the PLP-SEC technique, are shown in Figure 6.3. It is observed that the k_p of NVP is both higher as well as exhibits a higher sensitivity towards monomer concentration, in comparison to NVF. It is of interest to see how this knowledge on the homopolymerization kinetics of NVP and NVF can be extended to study their behaviour in a copolymerization system.

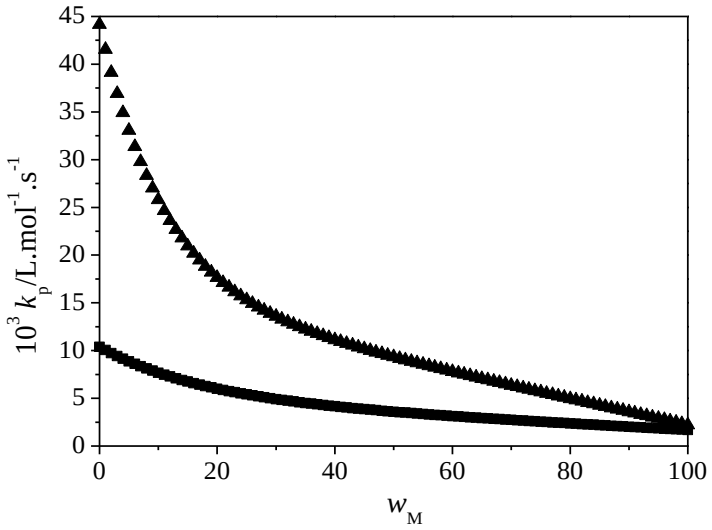

Figure 6.3. The influence of NVF (■) and NVP (▲) concentration (w_{NVP}) on their propagation rate coefficient (k_p). in aqueous solution at 60 °C.[14, 16]

Low conversion copolymerization experiments were carried out at initial monomer concentrations of 10, 25 and 50 wt% and initiator concentration of 0.02 wt% in water at a temperature of 60 °C over a range of f_{NVP} levels from 0 to 1. It is to be noted that as the f_{NVP} levels increased the isolation of polymer using acetone became increasingly difficult and especially at f_{NVP} >0.7, the reaction times were increased in order to allow for the formation of sufficient polymer levels to facilitate easy isolation, while still maintain the conversion levels below 10 %. The copolymer compositions from these experiments are shown in Figures 6.4 (a), (b) and (c) for the experiments with 10, 25 and 50 wt% monomer concentrations, respectively. This data suggested that there was a preferential incorporation of NVF over NVP especially at lower f_{NVP} levels, as can be seen from Figure 6.4. However, the significant scatter in the data made it difficult to draw any firm conclusions. In order to get a better understanding of this system, copolymerization batch experiments with frequent sampling were carried out at 25 wt% monomer and 0.02 wt% initiator concentrations at f_{NVP} levels of 0.1, 0.5 and 0.9 at a temperature of 60 °C in the 1L reactor system. The conversion from these experiments, shown in Figure 6.5

(a), indicated that there was an inhibition period upto ~2000s, which was also observed for the homopolymerization of NVP at 70 °C.[19] The small conversion levels observed at t=0 in Figure 6.5 is due to problems associated with the complete removal of NVF to isolate the copolymer sample, due to the high boiling point of NVF (210 °C). This was dealt with by increasing the drying time for the subsequent samples. The composition data from the batch experiments at 60 °C, shown in Figure 6.5 (b), exhibited an unusual drift at the initial stages showing a preferential incorporation of NVF over NVP, but, the PVP levels in the copolymer (F_{NVP}) gradually increased with conversion to eventually reach f_{NVP}. This unusual drift in the initial copolymer composition was correlated to the initial inhibition period. Although it is difficult to understand how the incorporation of NVP is retarded, the copolymer composition during this inhibition period is not representative of that formed later. Also, at t=0, x_p>0 is observed from Figure, which was due to difficulties in isolating the polymer by heating it in the oven, due to the very high boiling point of 210 °C for NVF.

The problems with this inhibition period were prevented by conducting batch experiments at a higher temperature of 85 °C. However, in order to avoid any exotherm, as is usually common at higher temperatures, a lower monomer concentration of 10 wt% and 0.02 wt% initiator concentration was used. The time-conversion and the conversion-composition profiles for the experiments at 85 °C are shown in Figures 6.6 (a) and (b) respectively. The initial rate was observed to increase with increasing NVP mole fraction in the initial monomer mixture, in accordance with the higher k_p of NVP. The composition data showed that the levels of NVP in the copolymer (F_{NVP}) were the same as the levels of NVP in the initial monomer mixture (f_{NVP}), indicating that the reactivity ratios of both monomers were very close to unity.

It was also of interest to investigate the influence of monomer concentration on rate behaviour, as both NVP[14] and NVF[16] exhibit monomer-concentration dependent k_p expressions. However, due to temperature control issues arising as a result of the exotherm formed at higher monomer concentrations at 85 °C, the influence of monomer concentration was investigated at the lower temperature of 60 °C. The temperature could be controlled within a deviation of ±2 °C at all monomer concentrations, as shown in Appendix B.3. The problem with the inhibition at this temperature was dealt with by using higher initiator concentrations of 0.1 wt% for the experiments at 10 and 25 wt% monomer concentrations and to 0.2 wt% for the experiments at 50 wt% monomer concentration. Batch experiments were conducted over a range of f_{NVP} levels at the three different monomer concentrations. The time-conversion and conversion-composition profiles from these experiments are shown in Figures 6.7 and 6.8 respectively. Despite the increased initiator concentration, a small inhibition period was still observed in the experiments at 60 °C. However, the initial rates after the inhibition period was found to increase with increasing f_{NVP} and the NVP mole fraction in the copolymer (F_{NVP}) was found to be, for the most part, constant at f_{NVP}, similar to the behaviour observed at 85 °C. Despite the experimental difficulties, the complete body of data indicate that both reactivity ratios are very close to unity.

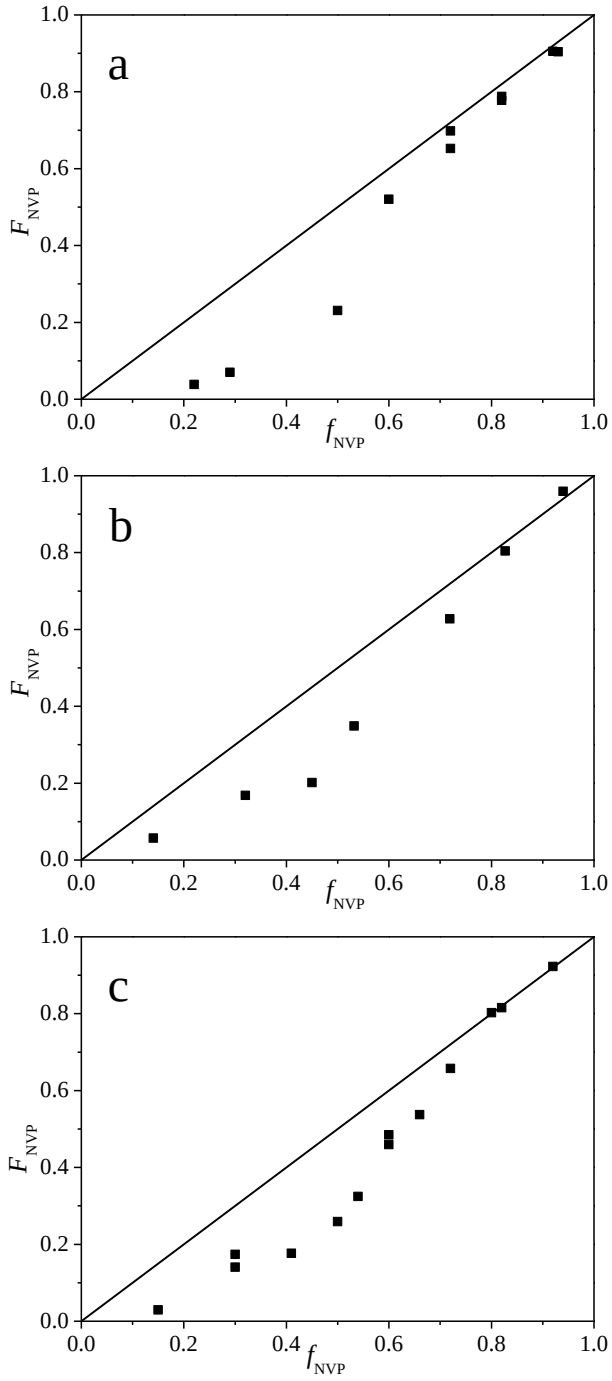

Figure 6.4. Plot of NVP mole fraction in the initial monomer mixture (f_{NVP}) vs copolymer composition (F_{NVP}) for NVP-NVF copolymerization at varying total monomer concentrations of a) 10 wt% b) 25 wt% and c) 50 wt% in water at 60 °C, with the diagonal representing the azeotropic compositions (F=f).

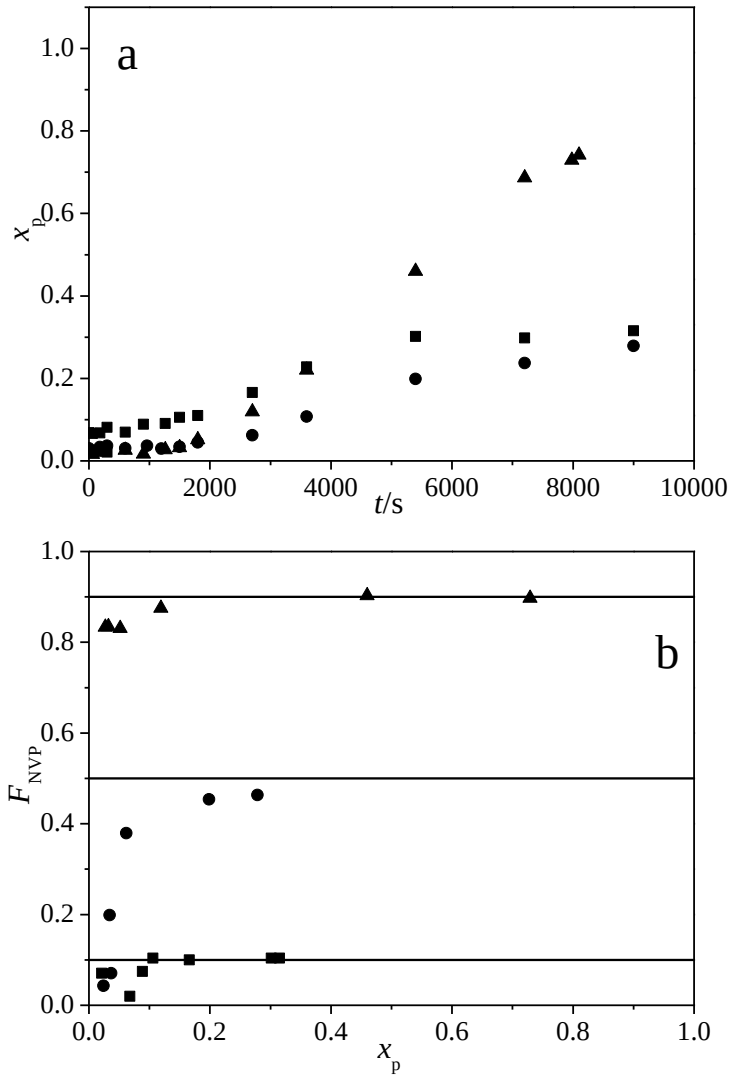

Figure 6.5. a) Time-conversion and b) conversion-composition profiles for the polymerization of 25 wt% monomer and 0.02 wt% V-50 concentrations at 60 °C at varying f_{NVP} levels of 0.1 (■), 0.5 (●) and 0.9 (▲).

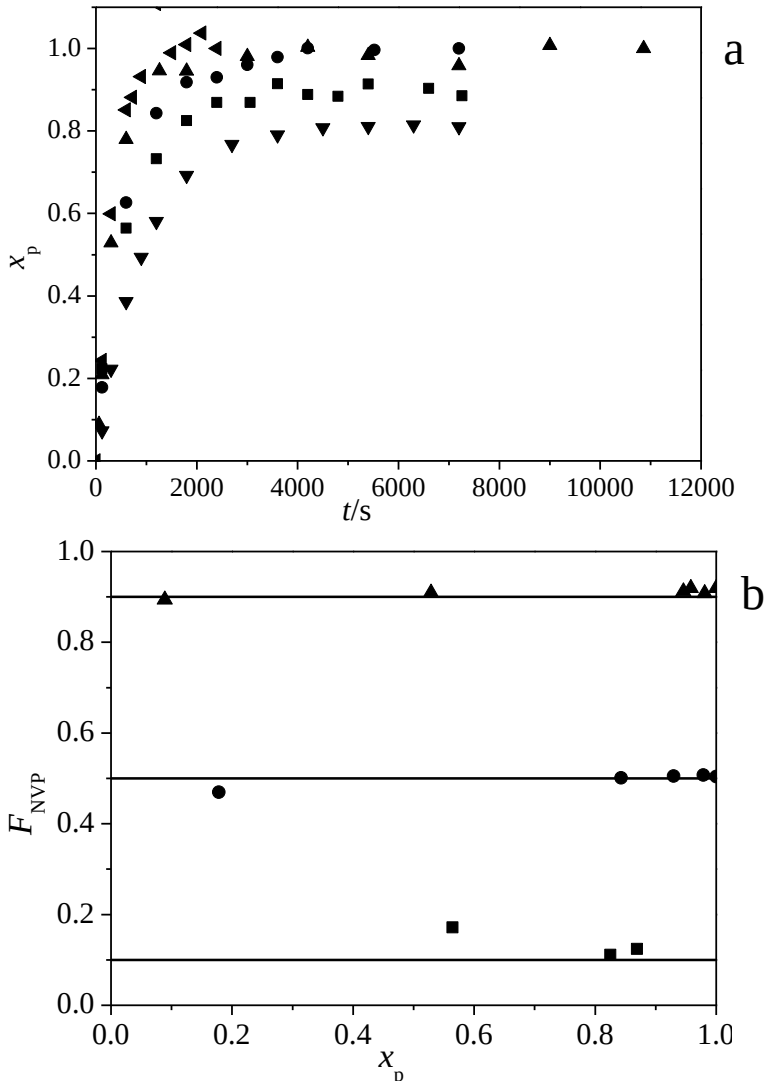

Figure 6.6. a) Time-conversion and b) conversion-composition profiles for the polymerization of 10 wt% monomer 0.02 wt% V-50 concentrations at 85 °C, at varying f_{NVP} levels of 0 (▼), 0.1 (■), 0.5 (●), 0.9 (▲) and 1 (◄).

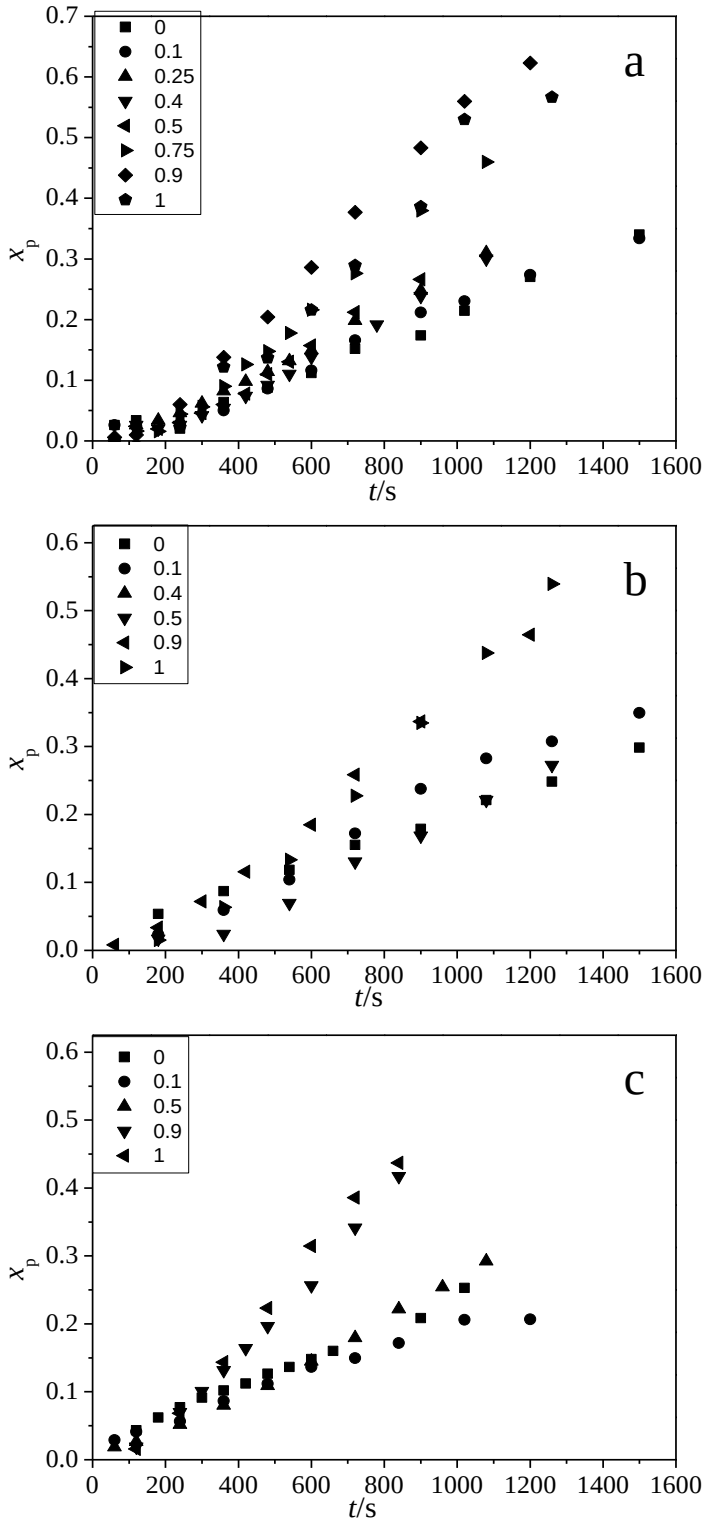

Figure 6.7. Time-conversion profiles for the batch NVP/NVF copolymerization in aqueous solution at 60 °C with a) 10 wt% monomer and 0.1 wt% V-50 b) 25 wt% monomer and 0.1 wt% V-50 and c) 50 wt% monomer and 0.2 wt% V-50. Varying f_{NVP} levels are as indicated in the Figure legends.

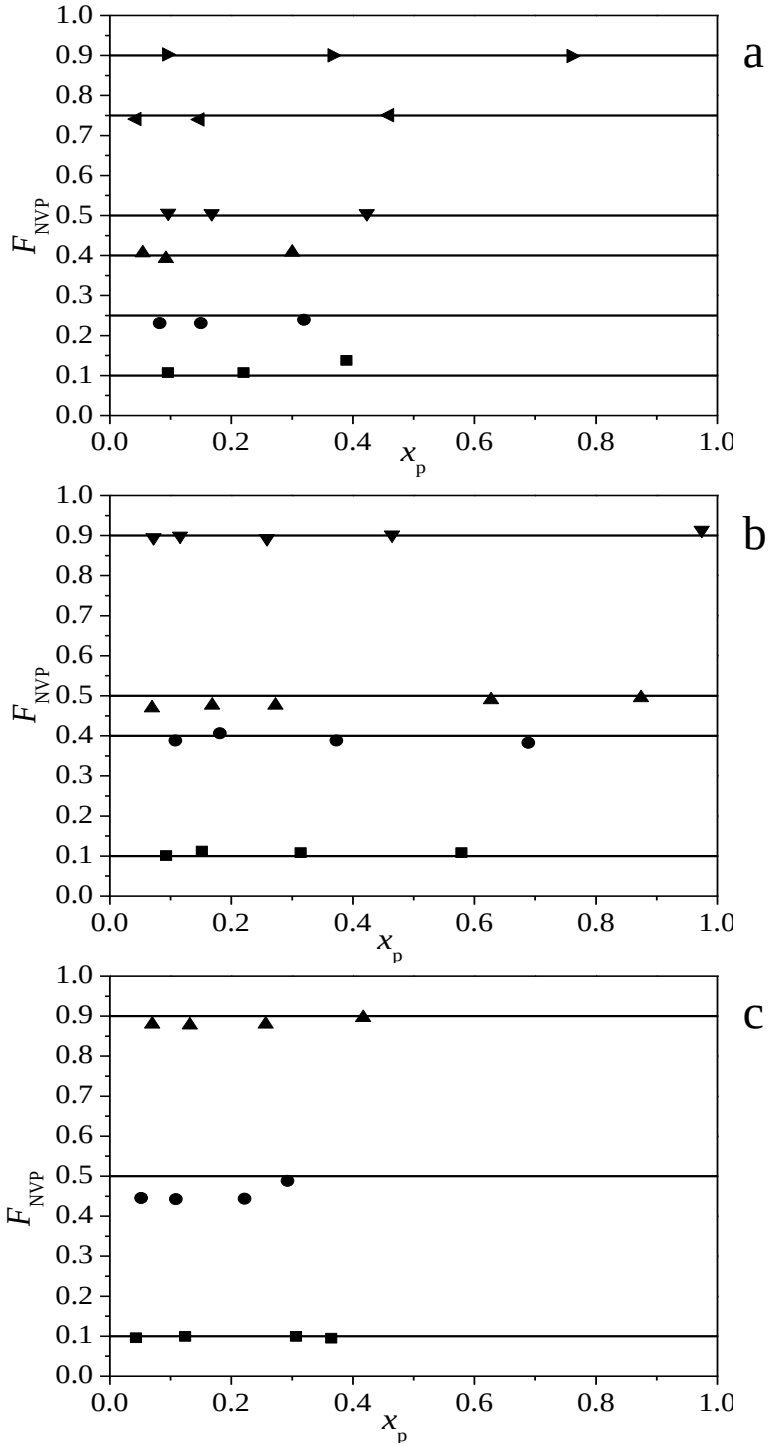

Figure 6.8. Evolution of copolymer composition (F_{NVP}) with conversion for the NVP/NVF copolymerization experiments at 60 °C with a) 10 wt% monomer and 0.1 wt% V-50 b) 25 wt% monomer and 0.1 wt% V-50 and c) 50 wt% monomer and 0.2 wt% V-50. Initial f_{NVP} levels indicate by the horizontal lines, with experimental copolymer composition data indicated by the data points.

Molecular weight data. A comparison of the MALLS and RI MW data along with the correction factors was shown in the experimental section in Table 6.1. The variation of the correction factors with copolymer composition (F_{NVP}) is expected, and increase between the PVF and PVP homopolymer correction factors. The polymer MWDs obtained at varying initial monomer concentrations and temperatures is shown in Figures 6.9-6.12. with varying f_{NVP} levels as indicated in the figure legends. A shift towards higher molecular weight with increasing NVP fraction in the copolymer, in accordance with the rate behaviour, is clearly observed in most cases.

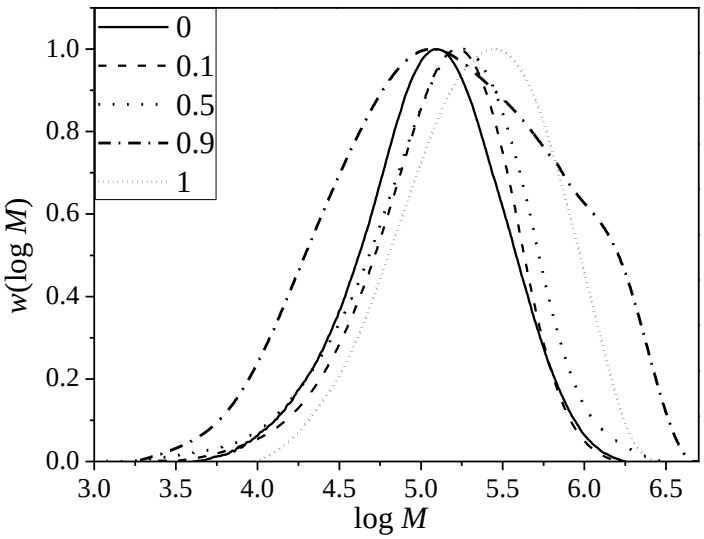

Figure 6.9. Molecular weight distributions of NVF/NVP copolymer produced from 10 wt% monomer concentration, 0.02 wt% V-50 concentration at 85 °C and varying f_{NVP} levels as indicated.

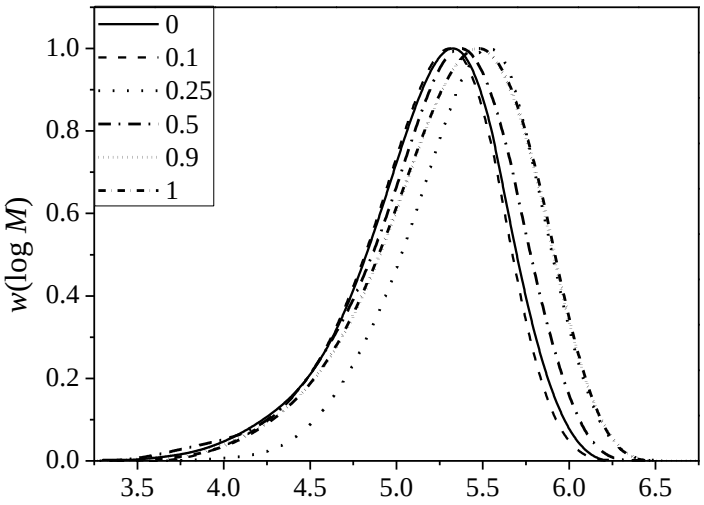

Figure 6.10. Molecular weight distributions of NVF/NVP copolymer produced from 10 wt% monomer concentration, 0.1 wt% V-50 concentration at 60 °C and varying f_{NVP} levels as indicated.

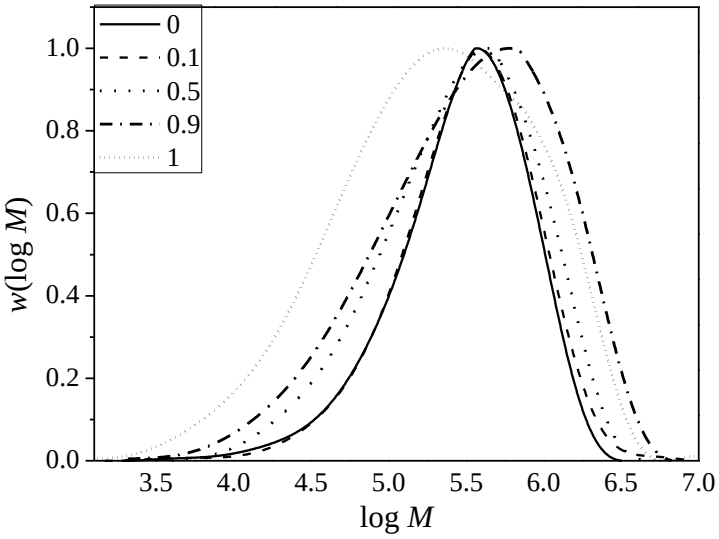

Figure 6.11. Molecular weight distributions of NVF/NVP copolymer produced from 25 wt% monomer concentration, 0.1 wt% V-50 concentration at 60 °C and varying f_{NVP} levels as indicated.

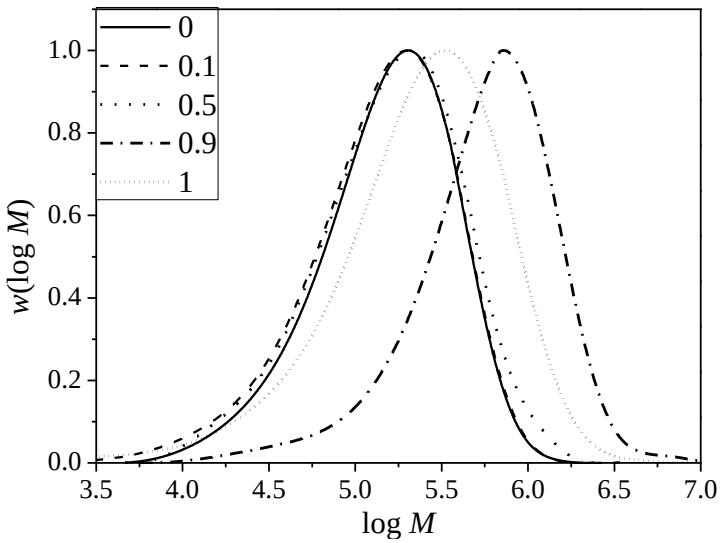

Figure 6.12. Molecular weight distributions of NVF/NVP copolymer produced from 50 wt% monomer concentration, 0.2 wt% V-50 concentration at 60 °C and varying f_{NVP} levels as indicated.

6.6 Model Development

The terminal model of copolymerization has been widely used and has proven to explain the copolymerization rate and copolymer composition behaviour of monomers with similar reactivity ratios quite well, and was therefore adapted to model this copolymerization system. A simple kinetic model, which takes into consideration initiation, propagation, termination and transfer events was built using Predici©. The PLP-SEC derived propagation expressions of NVP and NVF were used to describe both propagation and cross-propagation of the radicals ending with the respective terminal unit, as both monomers have a reactivity ratio of unity. The same initiator decomposition rate expression, initiator efficiency, termination and transfer coefficients as were used in the NVP model were used, as the kinetic behaviour of NVF has been shown to be represented reasonably well using the same expressions (Chapter 4). The values and expressions for the rate coefficients used in the model are shown in Table 6.2.

Table 6.2. Values and expressions for the kinetic rate coefficients and physical parameters used in the model of aqueous-phase free-radical copolymerization of NVP and NVF

Mechanism	Rate Expression	60 °C	85 °C	Ref
Initiator decomposition	$k_{\mathrm{d}}(s^{-1}) = 9.17\times10^{14}\exp\left(\frac{-1.49\times10^{4}}{(T/\mathrm{K})}\right)$	$1.22\text{x}10^{-4}$	$7.52\text{x}10^{-4}$	18
Propagation				
$kp_{11} = kp_{12} = kp_{\mathrm{NVP}}$	$\frac{k_{\mathrm{p}}}{k_{\mathrm{p,max}}} = 0.36 + 0.64\exp\left(-\frac{9.2\cdot w_{\mathrm{mon}}^{0}\cdot(1-x_{\mathrm{p}})}{1-w_{\mathrm{mon}}^{0}\cdot x_{\mathrm{p}}}\right) - \frac{0.31\cdot w_{\mathrm{mon}}^{0}\cdot(1-x_{\mathrm{p}})}{1-w_{\mathrm{mon}}^{0}\cdot x_{\mathrm{p}}}$			14
	$k_{\mathrm{p,max}}/\left(\mathrm{L}\cdot\mathrm{mol}^{-1}\cdot\mathrm{s}^{-1}\right) = 2.57\times10^{7}\exp\left(-\frac{2.12\times10^{3}}{(T/\mathrm{K})}\right)$	$5.38\text{x}10^{4}$	$6.97\text{x}10^{4}$	14
$kp_{22} = kp_{21} = kp_{\mathrm{NVF}}$	$\frac{k_{\mathrm{p}}}{k_{\mathrm{p,max}}} = 0.47 + 0.53\exp\left(-\frac{5.7\cdot w_{\mathrm{mon}}^{0}\cdot(1-x_{\mathrm{p}})}{1-w_{\mathrm{mon}}^{0}\cdot x_{\mathrm{p}}}\right) - \frac{0.30\cdot w_{\mathrm{mon}}^{0}\cdot(1-x_{\mathrm{p}})}{1-w_{\mathrm{mon}}^{0}\cdot x_{\mathrm{p}}}$			16
	$k_{\mathrm{p,max}}/\left(\mathrm{L}\cdot\mathrm{mol}^{-1}\cdot\mathrm{s}^{-1}\right) = 11.9\times10^{6}\exp\left(-\frac{2.345\times10^{3}}{(T/\mathrm{K})}\right)$	$1.28\text{x}10^{4}$	$1.7\text{x}10^{4}$	16
Termination	$k_{\mathrm{t,NVP}}/\left(\mathrm{L}\cdot\mathrm{mol}^{-1}\cdot\mathrm{s}^{-1}\right) = 1.5\times10^{8}\exp\left(-w_{\mathrm{mon}}^{0}/0.29\right) + 1.68\times10^{7}$			15
$kt_{22} = kt_{22} = kt_{12} = kt_{\mathrm{NVP}}$	at P = 1 bar			
Transfer to monomer	$\frac{k_{\mathrm{tr}}^{\mathrm{mon}}}{k_{\mathrm{p}}}$	$4.8\text{x}10^{-4}$	$6\text{x}10^{-4}$	19
Transfer to polymer	$\frac{k_{\mathrm{tr}}^{\mathrm{poly}}}{k_{p}}$	$6\text{x}10^{-5}$	$6\text{x}10^{-5}$	19
Density of NVP	$\rho_{\mathrm{NVP}}/\left(\mathrm{g}\cdot\mathrm{mL}^{-1}\right) = 1.0592 - 7.7772\cdot10^{-4}(T/{}^{\circ}\mathrm{C}) - 4.6649\cdot10^{-7}(T/{}^{\circ}\mathrm{C})^{2}$	1.002	0.989	14
Density of NVF	$\rho_{\mathrm{NVF}}/\left(\mathrm{g}\cdot\mathrm{mL}^{-1}\right) = 1.0257 - 7.3597\cdot10^{-4}(T/{}^{\circ}\mathrm{C}) - 9.5848\cdot10^{-8}(T/{}^{\circ}\mathrm{C})^{2}$	1.002	0.989	16
Density of Water	$\rho_{\mathrm{H2O}}/\left(\mathrm{g}\cdot\mathrm{mL}^{-1}\right) = 0.9999 + 2.3109\cdot10^{-5}(T/{}^{\circ}\mathrm{C}) - 5.44807\cdot10^{-6}(T/{}^{\circ}\mathrm{C})^{2}$	0.972	0.959	14

The terminal model describes the composition-averaged propagation rate of copolymerization (k_p^{cop}) and the rate of conversion in a copolymerization by eqns. 6.1. and 6.2

$$k_p^{cop} = \frac{r_1 f_1^2 + 2 f_1 f_2 + r_2 f_2^2}{(r_1 f_1 / kp_{11}) + (r_2 f_2 / kp_{22})} \tag{6.1}$$

$$\frac{dx_p}{dt} = k_p^{cop} \left(\frac{f k_d [I]}{k_t} \right)^{0.5} \left(1 - x_p\right) \tag{6.2}$$

As k_p of NVP is higher than that of NVF, as shown in Figure 6.3, and the reactivity ratios of both monomers are unity, the k_p^{cop} and thereby the rate of conversion will increase with increasing NVP mole fraction (f_{NVP}) in the monomer mixture. Moreover, as both NVP and NVF have monomer-dependent propagation expressions, it is most likely that their copolymerization also varies with monomer concentration. A plot of the evolution of the initial experimental rate of conversion (dx_p / dt) with f_{NVP} for the experiments at 60 °C is shown in Figure 6.13. The initial rates were estimated from conversion data in the range of ~240 - 600 s for the experiments at 10 wt% monomer and 0.1 wt% initiator and 50 wt% monomer and 0.2 wt% initiator concentration and from ~500 – 900s for the experiments at 25 wt% monomer and 0.1 wt% initiator concentration in accordance with the inhibition periods, as described in Appendix B.1 The calculation of the 95% confidence intervals has also been detailed in Appendix B.1. The large error bars observed in some of the cases is due to the smaller sample size (n) used in the estimation of slope. In case of the experiments at 50 wt% monomer concentration where the initiator concentration was doubled to 0.2 wt%, the rates were normalized by a factor of 1.414 to allow for a quantitative comparison with the experiments at 10 and 25 wt% monomer concentrations. As can be seen from Figure 6.13, the initial rate increases with increasing f_{NVP} at all the monomer concentrations studied. Further, the rates also increase with decreasing

monomer concentration, in good agreement with the expected behaviour based on the homopolymerization kinetics of the individual monomers. A plot of the evolution of the composition-averaged propagation rate coefficient for copolymerization (k_p^{cop}) and lumped rate constant ($k_p^{cop}/k_t^{0.5}$) determined by the terminal model, with f_{NVP} is shown in Figure 6.14 and 6.15 respectively. As can be seen, the shape of the profiles and the increase in k_p^{cop} with increasing f_{NVP}, predicted by the model and the experimental initial rates are in very good agreement.

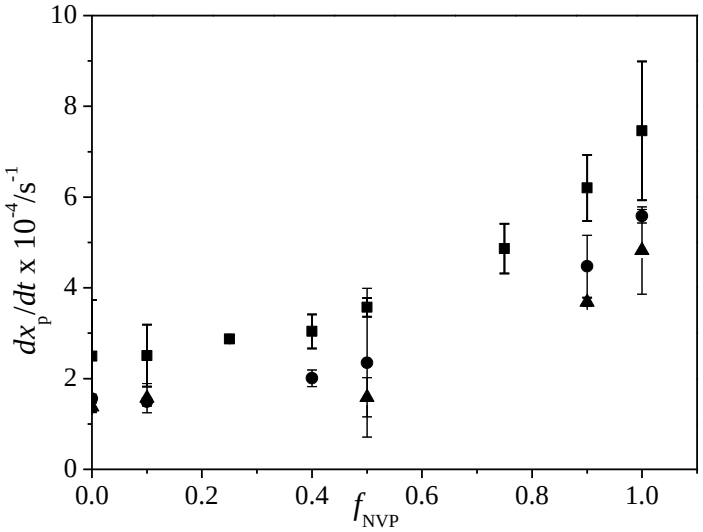

Figure 6.13. Evolution of initial rate (dx_p/dt)with f_{NVP} for the experiments at 10 wt% monomer and 0.1 wt% V-50 (■), 25 wt% monomer and 0.1 wt% V-50 (●) and 50 wt% monomer and 0.2 wt% V-50 (▲) concentrations at 60 °C. The data at 50 wt% monomer concentration has been corrected to account for differences in initiator concentration. The error bars represent the 95% confidence intervals.

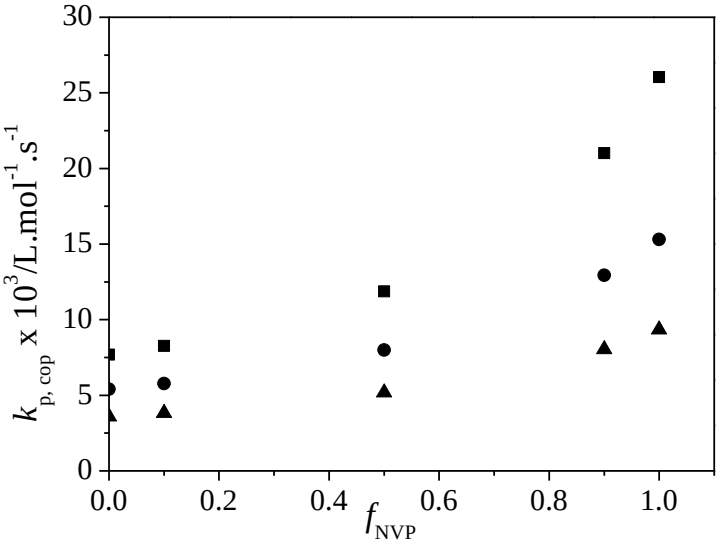

Figure 6.14. Evolution of k_p^{cop} with f_{NVP} for the experiments at 10 wt% (■), 25 wt% (●) and 50 wt% (▲) monomer concentrations, as predicted by the terminal model, using reactivity ratios of r_1=r_2=1.

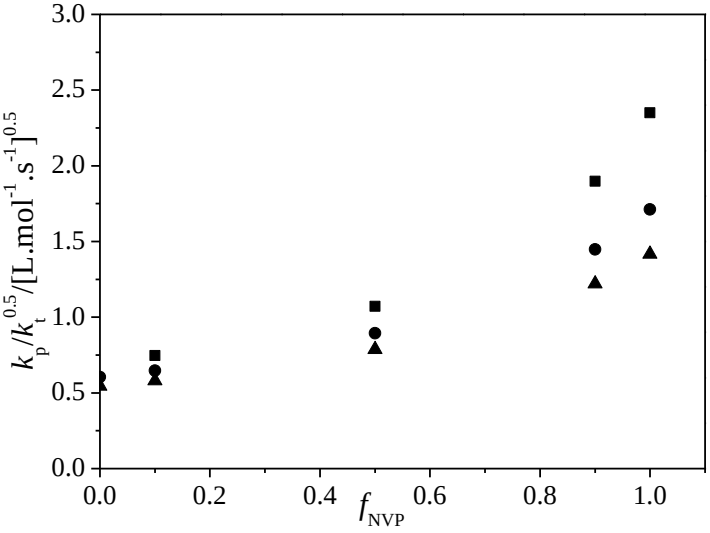

Figure 6.15. Evolution of $k_p^{cop}/k_t^{0.5}$ with f_{NVP} for the experiments at 10 wt%, (■), 25 wt% and 50 wt% (▲) monomer concentrations, as predicted by the terminal model, using reactivity ratios of r_1=r_2=1.

A comparison of the experimental and simulated conversion profiles at varying initial monomer concentrations and temperatures is shown in Figure 6.16-6.19. The model captures the increase in rate with increasing f_{NVP} as well as with decreasing monomer concentration (Figure 6.20)

reasonably well. The data at 50 wt% monomer and 0.2 wt% initiator concentration at 60 °C in Figure 6.2 has been corrected for initiator differences in order to allow for a quantitative comparison with the data at 10 and 25 wt% monomer and 0.1 wt% initiator concentration. It is to be noted that instead of including a small inhibition period in the model, the experimental data has been shifted by ~ 120 s along the time (x-axis) in order to correct for the small initial inhibition. The slight offset observed between the experimental and model data may be due to small differences in the k_t behaviour of the two monomers not captured by the model as is uses the same NVP k_t expression for both monomers as well as cross termination.

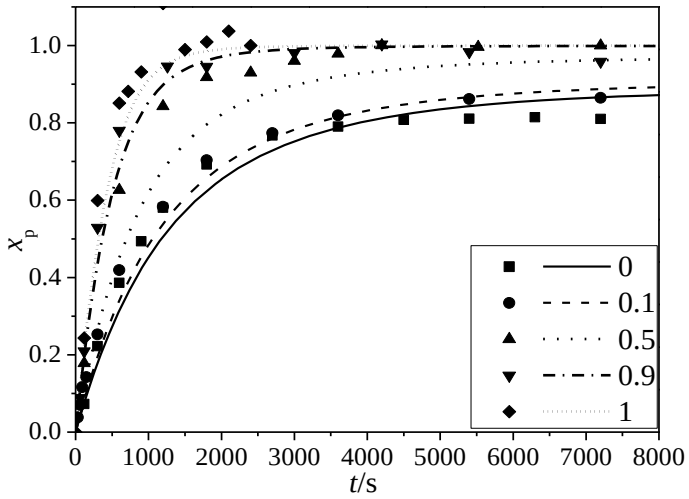

Figure 6.16. Comparison of experimental (symbols) and model (lines) conversion profiles for the batch NVP/NVF copolymerization of 10 wt% monomer concentration, 0.02 wt% V-50 concentration at 85 °C and varying f_{NVP} levels as indicated.

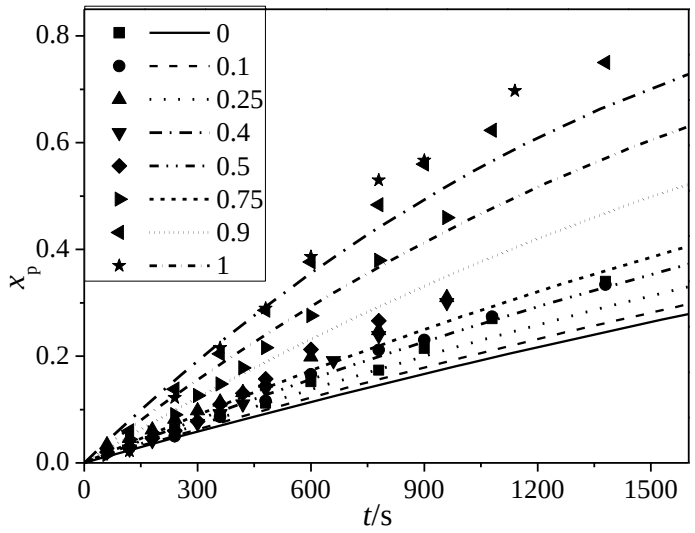

Figure 6.17. Comparison of experimental and model conversion profiles for the batch NVP/NVF copolymerization of 10 wt% monomer concentration, 0.1 wt% V-50 concentration at 60 °C and varying f_{NVP} levels as indicated.

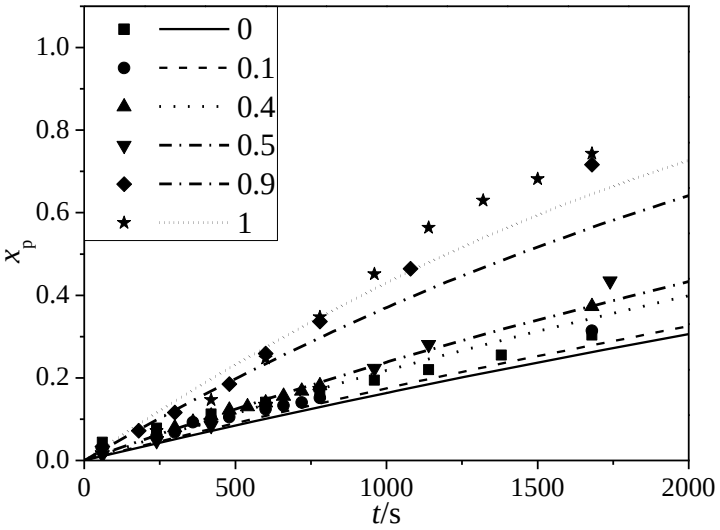

Figure 6.18. Comparison of experimental (symbols) and model (lines) conversion profiles for the batch NVP/NVF copolymerization of 25 wt% monomer concentration, 0.1 wt% V-50 concentration at 60 °C and varying f_{NVP} levels as indicated.

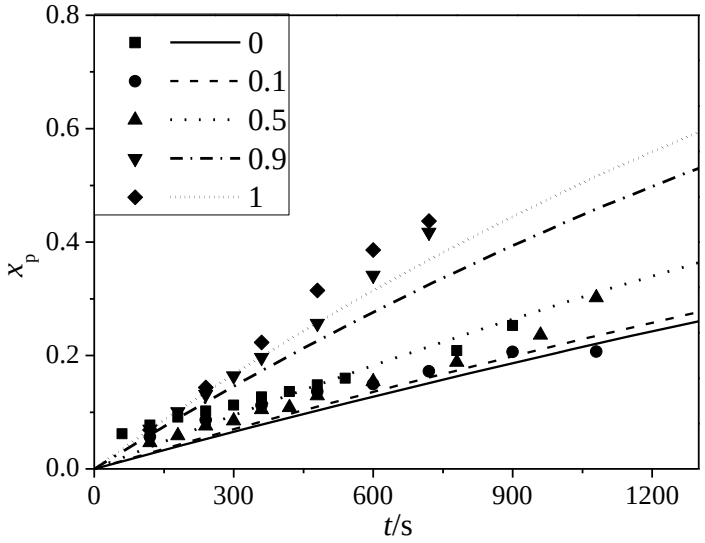

Figure 6.19. Comparison of experimental (symbols) and model (lines) conversion profiles for the batch NVP/NVF copolymerization of 50 wt% monomer concentration, 0.2 wt% V-50 concentration at 60 °C and varying f_{NVP} levels as indicated.

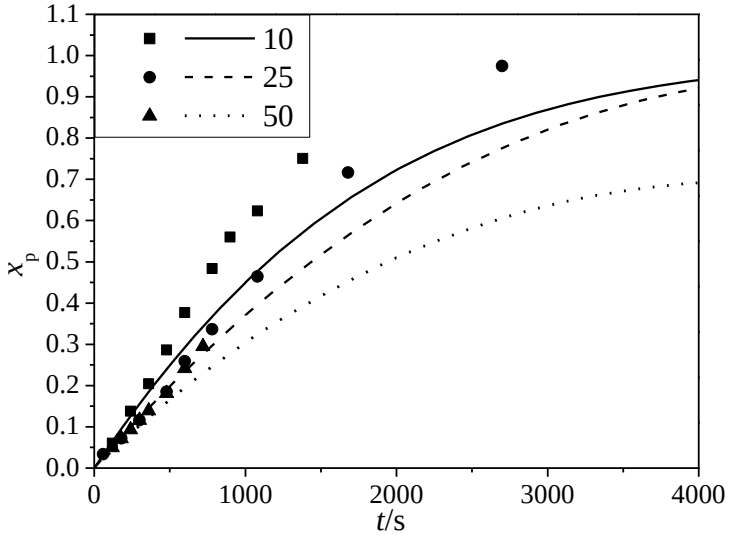

Figure 6.20. Comparison of experimental (symbols) and model (lines) conversion profiles for the influence of monomer concentrations (as indicated) on the conversion profiles for the batch copolymerization of NVP and NVF at f_{NVP}=0.9 and temperature of 60 °C. The conversion profile at 50 wt% monomer concentration has been normalized to account for initiator differences (see text).

The next step of interest is to model the molecular weight behaviour of this copolymerization system using the same transfer coefficients that captured the MW behaviour of NVP and NVF homopolymers. A comparison of the experimental (corrected RI) and model MWDs for the

copolymer produced from 10 wt% monomer concentration and 0.1 wt% initiator concentration at 60 °C and varying F_{NVP} levels is shown in Figure 6.21. Similar to the rate behaviour, the MW shifts towards higher values with increasing levels of f_{NVP} (=F_{NVP}). Although narrower than the experimental profiles, the overall shift with F_{NVP} as well the peak MW values predicted by the model are in good agreement with the experimental data. The experimental and predicted influence of monomer concentration on MW is shown in Figure 6.22. Here again, the expected shift towards higher values with increasing monomer concentration has been captured very well by the model.

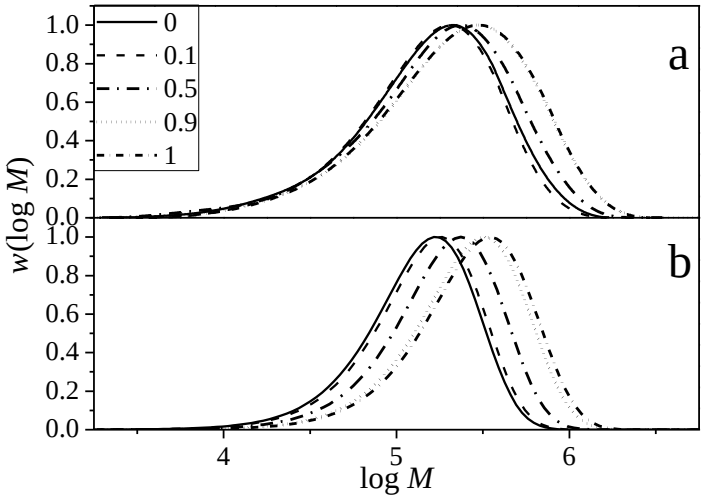

Figure 6.21. Comparison of a) experimental and b) model molecular weight distributions of NVP/NVF copolymer produced from 10 wt% monomer concentration, 0.1 wt% V-50 concentration at 60 °C and varying f_{NVP} levels as indicated.

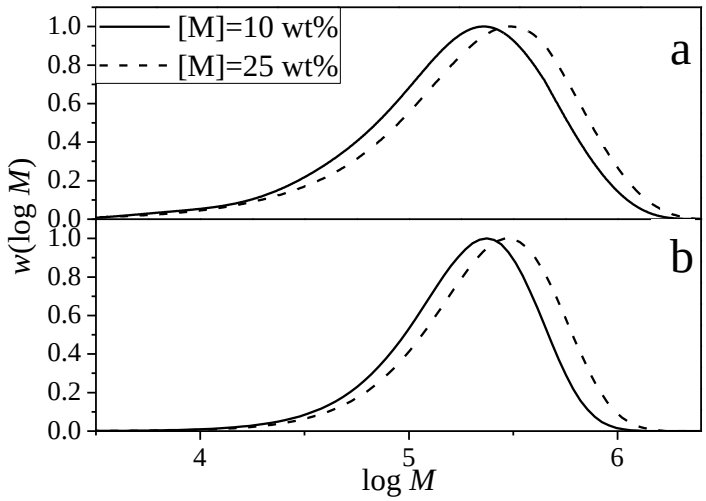

Figure 6.22. Comparison of a) experimental and b) model molecular weight distributions of NVP/NVF copolymer produced from 10 wt% monomer concentration at f_{NVP}=0.5, 0.1 wt% V-50 concentration at 60 °C and varying monomer concentrations as indicated.

6.7 Conclusions

Aqueous-phase free radical copolymerization of NVP and NVF was studied at temperatures of 60 and 85 °C. The influence of initial monomer concentration and NVP mole fraction in the initial monomer mixture on both rate and molecular weight behaviour was investigated by conducting low conversion as well as batch experiments. The low conversion and preliminary batch experimental data at 60 °C and 0.02 wt% V-50 concentration was later discarded due to the significant initial inhibition period at this temperature and initiator concentration, hindering NVP incorporation in the copolymer. The subsequent batch experiments conducted at higher initiator concentrations showed the copolymer composition to be constant throughout the course of the experiment and equaled the initial monomer mixture composition at all f_{NVP} levels, indicating both reactivity ratios to be unity. The initial rate was observed to increase with both increasing f_{NVP} as well as with decreasing monomer concentrations, in accordance with the expected behaviour based on the higher k_p values of NVP and the monomer dependent propagation rate

coefficients of both NVP and NVF. As expected, the molecular weight data showed a shift towards higher values with increasing F_{NVP} levels as well as increasing monomer concentration.

A simple kinetic terminal model was built using Predici© to capture the kinetic and molecular weight behaviour of this system. The same propagation, termination and transfer coefficients used in the homopolymerization studies of NVP and NVF were adopted for copolymerization, with reactivity ratios set to unity. The variation of the initial rate of copolymerization with f_{NVP} was in good agreement with the variation of k_p^{cop} with f_{NVP} and the model gave a reasonable representation of the conversion profiles at varying initial conditions. Although slightly narrower than the experimental profiles, the model predicted shift in MW towards higher values with increasing F_{NVP} as well as monomer concentrations and the peak values of the distributions were in very good agreement with the experimental data. Thus, it can be concluded that both rate and molecular weight behaviour of aqueous-phase copolymerization of NVP and NVF has been represented quite well by a terminal model built using PLP-SEC derived kinetic rate coefficients used to describe the homopolymerization behaviour of the respective monomers.

References

1) Kirsh, Y. E., *Water Soluble Poly-N-vinylamides*, John Wiley & Sons, England, **1998**.

2) BASF Technical Bulletin

3) Chapiro, A.; Trung, L.D. *Eur. Polym. J.* **1974**, *10*, 1103-1106.

4) Ponratnam, S.; Kapur, S. L. *J. Polym. Sci*. **1976**, *14*, 1987-1992.

5) Lacik, I.; Beuermann, S.; Buback, M. *Macromol. Chem. Phys*. **2004**, *205*, 1080-1087.

6) Ponratnam, S.; Rao, S. P.; Joshi, S. G.; Kapur, S. L. *J. Macrol. Sci., Part A* **1976**, *6*, 1055-1062.

7) Rintoul, I.; Wandrey, C. *Polymer*, **2005**, *46*, 4525-4532.

8) Martinez-Pină, F.; Gargallo, L.; Radić, D. *Polym. Int*. **1998**, *47*, 340-344.

9) Faragalla, M. M.; Hill, D. J. T.; Whittaker, A. K. *Polym. Bull*. **2002**, *47*, 421-427.

10) Gatica, N.; Gargallo, L.; Radić, D. *Polym. Int*. **1998**, *45*, 285-290.

11) Kathmann, E. E. L.; McCormick, C. L. *Macromolecules*, **1998**, *26*, 5249-5242.

12) Chang, Y.; McCormick, C. L. *Macromolecules*, **1998**, *26*, 4814-4817.

13) Nesteriva, N. A.; Gavrilova, I. I.; Panarin, E. F. *Russ. J. Appl. Chem*. **2009**, *82*, 618-621.

14) Stach, M.; I. Lacík, D. Chorvat, Jr, M. Buback, P. Hesse, R. A. Hutchinson, L. Tang, *Macromolecules* **2008**, *41*, 5174.

15) Schrooten, S.; Buback, M.; Hesse, P.; Hutchinson, R. A.; Lacik, I. *Macromol. Chem. Phys*. **2011**, *212*, 1400-1409.

16) Stach, M.; Lacik, I.; Kasák, P.; Chorvát, D., Jr.; Saunders, A. J..; Santanakrishnan, S.; Hutchinson, R. A. *Macromol. Chem. Phys*. **2010**, *211*, 580-593.

17) Fu, Y.; Cunningham, M. F. Hutchinson, R. A. *Macromol. Symp*. **2007**, 259, 151-163.

18) Wako Chemicals Information Brochure.

19) Santanakrishnan, S.; Tang, L.; Hutchinson, R. A.; Stach, M.; Lacik, I.; Schrooten, S.; Hesse, P.; Buback, M. *Macromol. React. Eng*. **2010**, *4*, 499-509.

Chapter 7. Conclusions & Recommendations

7.1 Conclusions

Free radical homopolymerization and copolymerization of water-soluble *N*-vinyl monomers have been studied at varying initial conditions. The influence of initial monomer, initiator (for homopolymerization), initial monomer mixture composition (for copolymerization) and temperature on both rate and molecular weight behaviour have been investigated through extensive experimental work and represented by kinetic models built using Predici©. The kinetic models make use of k_p and k_t expressions derived through independent PLP-SEC studies, thereby demonstrating the generality of these expression as well as validating their functional form.

7.1.1 Homopolymerization

The homopolymerization of NVP in water and butanol, NVF in water and NVI and QVI in water have been investigated through continuously initiated batch and semibatch experiments.

- The NVP study in water, combined with the PLP-SEC and SP-PLP-NIR studies by the research groups of Dr. Buback and Dr. Lacik, has made it possible to develop a complete kinetic model to represent the rate of polymerization as well as polymer molecular weight. This fundamental model, verified by batch and semibatch studies, was extended to similar water-soluble *N*-vinyl monomers by making according changes to their k_p behaviour.

- The experimental data collected for homopolymerization of NVP in butanol and for NVF in water are well-represented by the base NVP model, with the differences in polymerization rate and polymer MWs simply accounted for by the differences in k_p for

the different systems. This result demonstrates that a generalised understanding of water-soluble *N*-vinyl monomers can be obtained by accounting for their k_p differences, and that the k_t behaviour of these systems must be quite similar.

- The homopolymerization study of NVI and QVI has advanced our understanding of the aqueous-phase polymerization behaviour of these monomers without a priori PLP-SEC measurement of k_p. The experimental study demonstrates the importance of the degradative addition to monomer predominant in the NVI kinetics and its dependence on the pH of the reaction medium, with NVI behaviour identical to QVI at pH=1. The model developed to represent the rate and molecular weight behaviour of these systems was again based upon the original NVP model. While providing an adequate representation of the observed trends, the model can be improved once PLP-SEC studies of k_p are completed.

These homopolymerization studies have advanced our knowledge of some of the industrially-important water-soluble *N*-vinyl monomers, to aid in process and product development as well as providing a basis for the copolymerization studies of these monomers.

7.1.2 Copolymerization

The study on the aqueous-phase copolymerization of NVP and NVF resulted in a model which can represent both the rate and complete molecular weight behaviour as a function of comonomer composition and initial monomer content. Reactivity ratios were determined to be very close to unity for the system; this information was combined with the same k_p and k_t expressions used in the NVP and NVF homopolymerization studies with no other additional parameters required. This result demonstrates that the improved homopolymerization knowledge

of these water-soluble monomers can be easily extended to understand their behaviour in copolymerization.

7.2 Recommendations for Future Work

While this research has significantly advanced our understanding of the polymerization behaviour of industrially-important water-soluble monomers, it also lays ths groundwork for some interesting follow-up studies.

- The generality of the model developed in the aqueous-phase NVP study can be tested by the application of the model to similar water-soluble *N*-vinyl monomers in addition to those investigated in this study. The model developed to represent the NVI and QVI FRP in water can be improved by PLP-SEC studies on their propagation behaviour. This additional information will also help to validate the k_p and k_t values currently used in the model, and allow better estimation of the rate coefficients associated with degradative addition. These PLP-SEC experiments are currently underway by our co-workers in the PISAS, Bratislava.

- Refinements in the SEC analysis of poly(cations) will help address some of the uncertainties related to the relatively high molecular weights of poly(QVI) and poly(NVI). The presence of non-size exclusion effects in these analyses can be checked by varying the ionic strength (salt concentration) of the eluent and monitoring any changes in the molecular weight. Alternately, the poly(NVI) from the pH adjusted experiments can be treated as poly(QVI) and analyzed using poly(QVI) SEC conditions to check for MW differences with varying SEC protocols.

- A copolymerization study of the NVP/NVI system at varying pH levels would make an interesting follow-up copolymerization study, especially with the advanced understanding of the homopolymerization behaviour of these systems. The pH influence will be manifested by the varying NVI rate behaviour, thereby influencing the apparent reactivity ratios of both monomers accordingly. Modeling of this system can be greatly benefited by the improved understanding of NVI behaviour at the different pH levels.

- The copolymerization of the NVP/NVI system can also be investigated for solvent effects by conducting the study in the aqueous and organic solvents, which was not possible for the NVP/NVF system due to solubility issues.

Appendix A

The molecular weight analyses of the all the different systems investigated in this thesis have been conducted using MALLS and RI detectors in the Polymer Institute of the Slovakian Academy of Sciences. The SEC conditions have been described in respective Chapters for the different systems. As described in Chapter 2, differences in the MW data determined from MALLS and RI detectors are not surprising and the differences are usually dealt with by correcting the RI data by a suitable correction factor developed from a ratio of $M_{w,MALLS}/M_{w,RI}$, as M_w values from MALLS are expected to be accurate for reasons described in Chapter 3. In this appendix, a comparison of all the MWDs from MALLS and RI (corrected) detectors for the different systems (exception: QVI data is presented in Chapter 5; MALLS data for copolymerization is not available) is presented.

A.1 Comparison of RI and MALLS MWDs for Aqueous-Phase Polymerization of NVP (Chapter 3)

The correction factor for this set of data was ascertained to be 1.17.

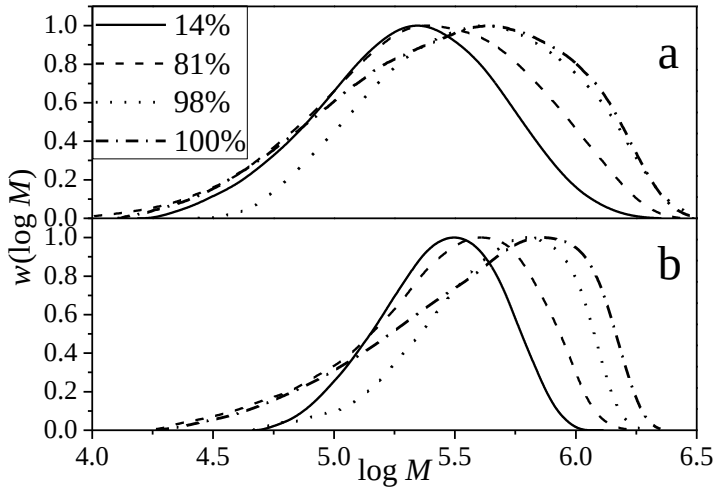

Figure A.1.1. Comparison of a) RI (corrected) and b) MALLS MWDs for the polymer produced from batch polymerization of 20 vol% NVP and 0.02 wt% V-50 in water at 85 °C and varying conversion levels as indicated.

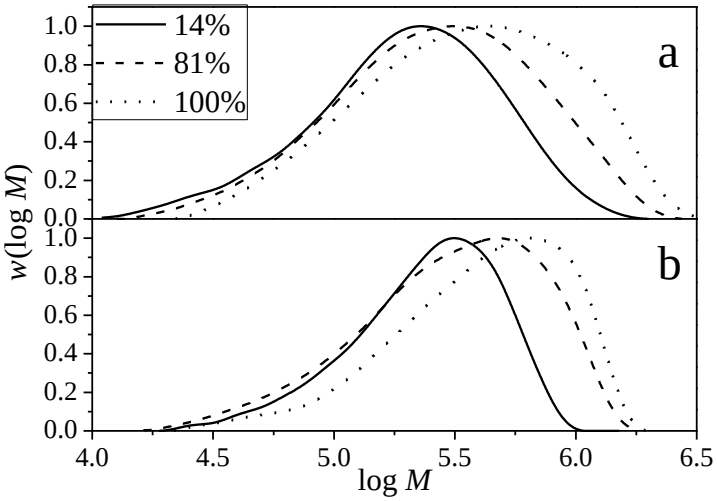

Figure A.1.2. Comparison of a) RI (corrected) and b) MALLS MWDs for the polymer produced from batch polymerization of 20 vol% NVP and 0.02 wt% V-50 in water at 85 °C and varying conversion levels as indicated.

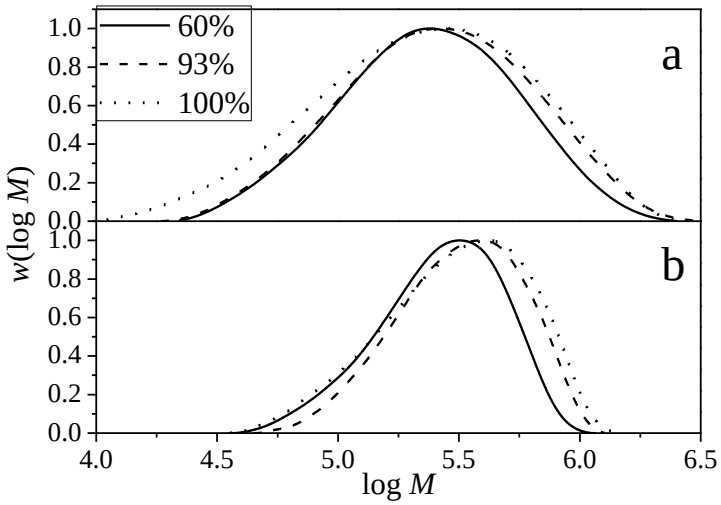

Figure A.1.3. Comparison of a) RI (corrected) and b) MALLS MWDs for the polymer produced from batch polymerization of 12.5 vol% NVP and 0.02 wt% V-50 in water at 85 °C and varying conversion levels as indicated.

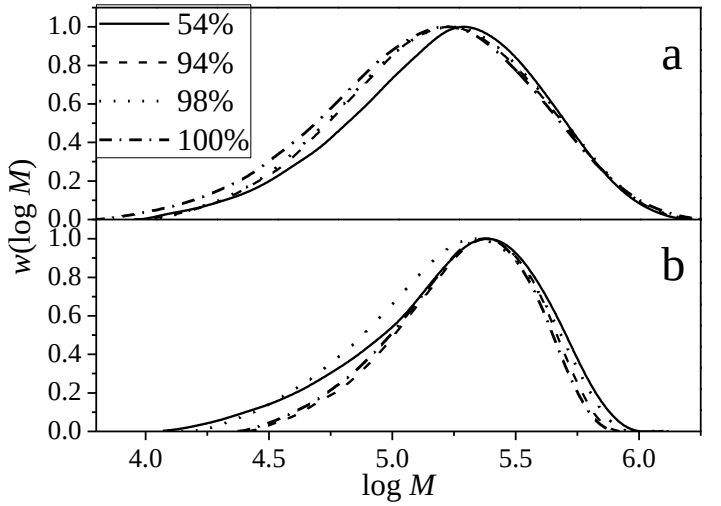

Figure A.1.4. Comparison of a) RI (corrected) and b) MALLS MWDs for the polymer produced from batch polymerization of 6.25 vol% NVP and 0.02 wt% V-50 in water at 85 °C and varying conversion levels as indicated.

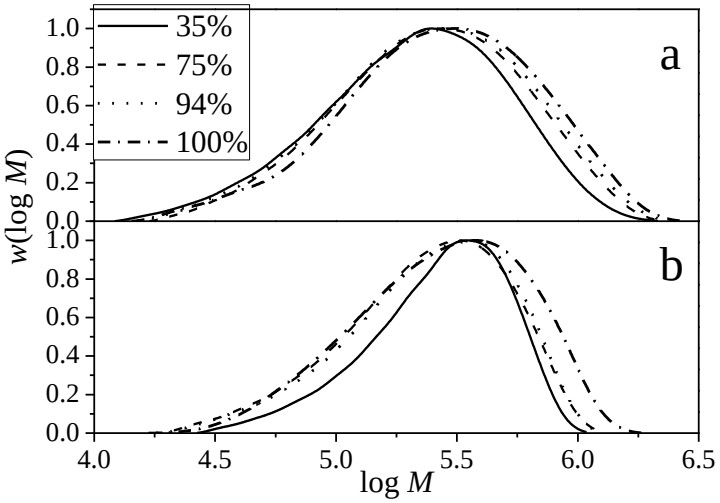

Figure A.1.5. Comparison of a) RI (corrected) and b) MALLS MWDs for the polymer produced from batch polymerization of 12.5 vol% NVP and 0.01 wt% V-50 in water at 85 °C and varying conversion levels as indicated.

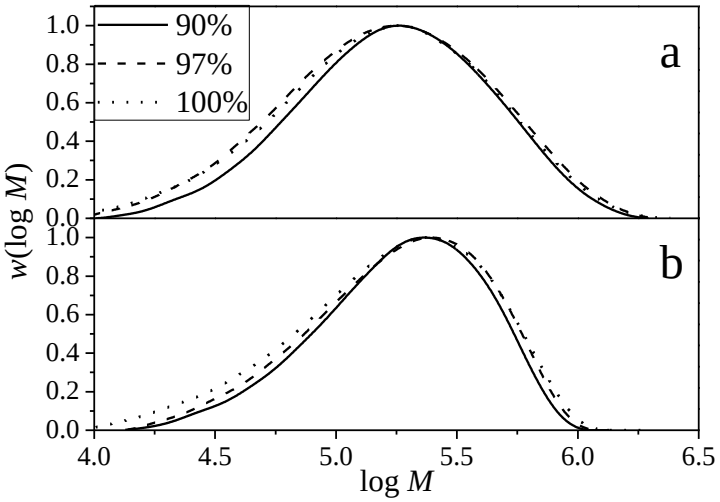

Figure A.1.6. Comparison of a) RI (corrected) and b) MALLS MWDs for the polymer produced from batch polymerization of 12.5 vol% NVP and 0.04 wt% V-50 in water at 85 °C and varying conversion levels as indicated.

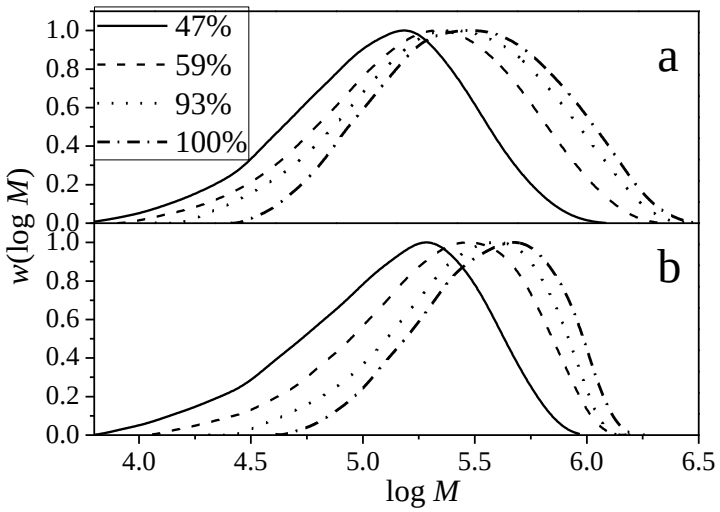

Figure A.1.7. Comparison of a) RI (corrected) and b) MALLS MWDs for the polymer produced from semibatch polymerization of 20 vol% NVP dosed over a period of 30 minutes and 0.02 wt% V-50 in water at 85 °C and varying conversion levels as indicated.

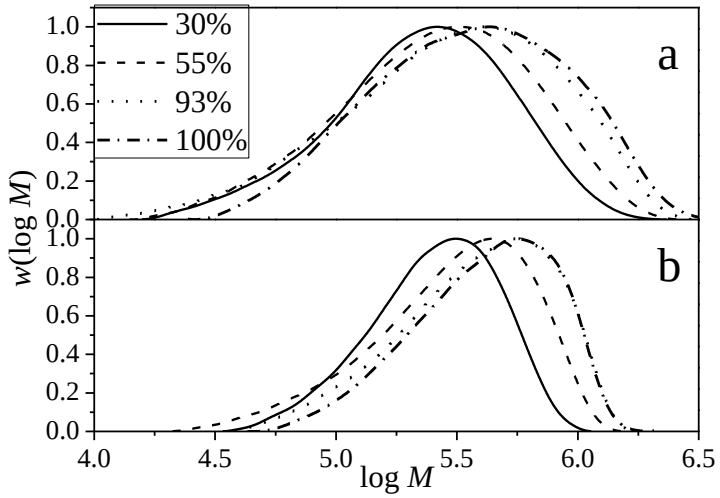

Figure A.1.8. Comparison of a) RI (corrected) and b) MALLS MWDs for the polymer produced from semibatch polymerization of 20 vol% NVP and 0.02 wt% V-50, mixed and dosed over a period of 30 minutes in water at 85 °C and varying conversion levels as indicated.

A.2 Comparison of RI and MALLS MWDs for Organic-Phase (Butanol) Polymerization of NVP (Chapter 4)

The correction factor for this set of data was ascertained to be 1.53.

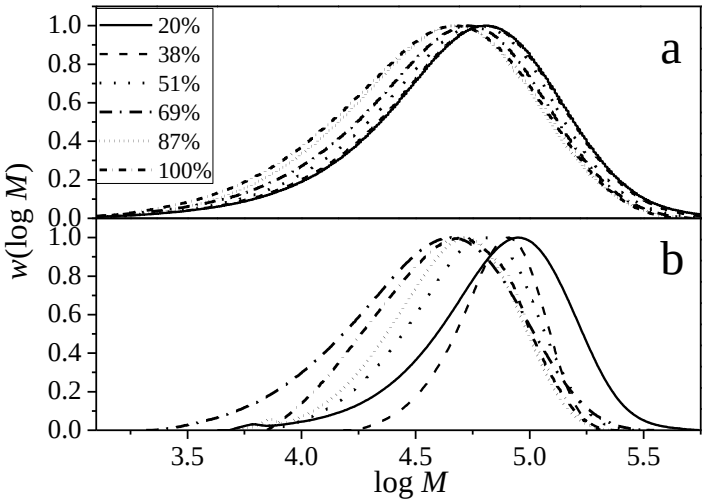

Figure A.2.1. Comparison of a) RI (corrected) and b) MALLS MWDs for the polymer produced from batch polymerization of 12.5 vol% NVP and 0.11 wt% Vazo-67 in butanol at 85 °C and varying conversion levels as indicated.

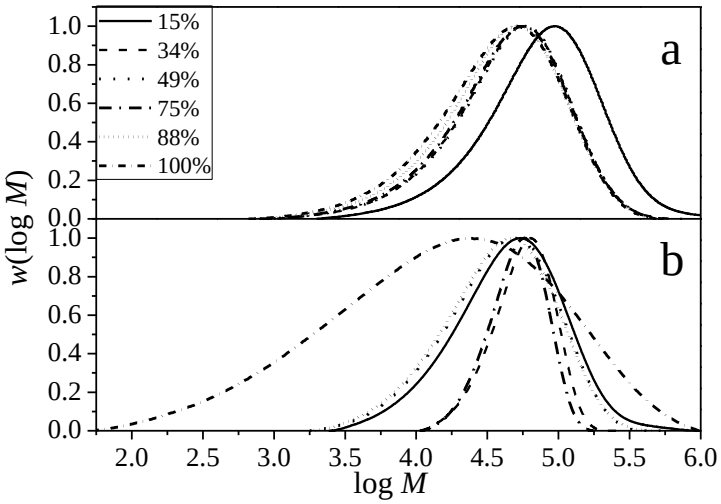

Figure A.2.2. Comparison of a) RI (corrected) and b) MALLS MWDs for the polymer produced from batch polymerization of 12.5 vol% NVP and 0.11 wt% Vazo-67 in butanol at 85 °C and varying conversion levels as indicated.

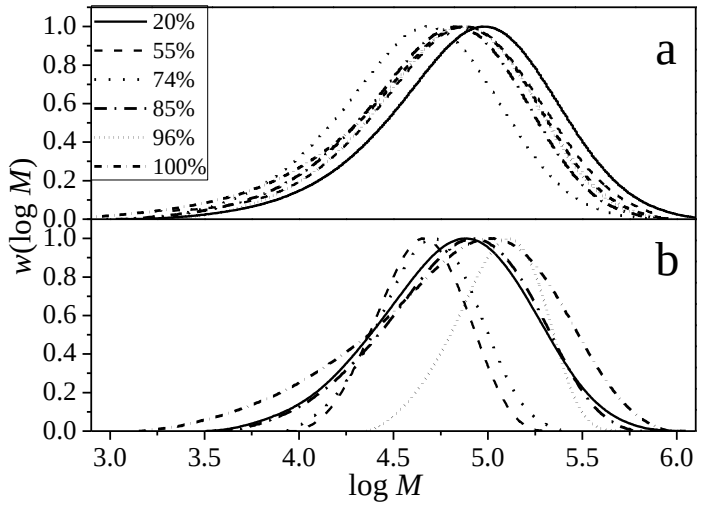

Figure A.2.3. Comparison of a) RI (corrected) and b) MALLS MWDs for the polymer produced from batch polymerization of 20 vol% NVP and 0.11 wt% Vazo-67 in butanol at 85 °C and varying conversion levels as indicated.

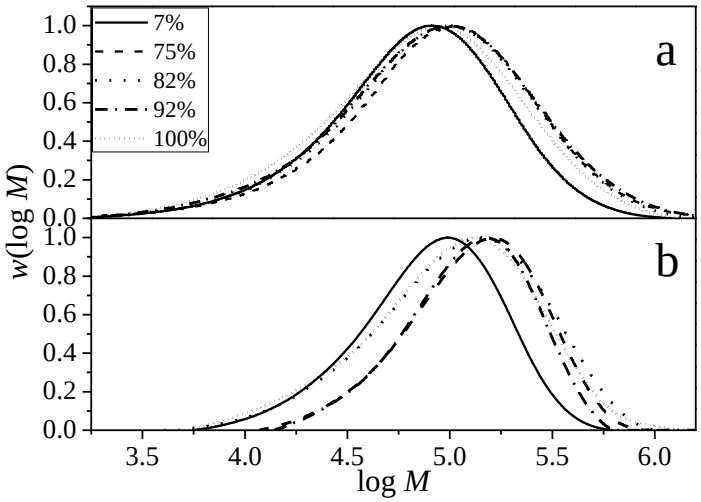

Figure A.2.4. Comparison of a) RI (corrected) and b) MALLS MWDs for the polymer produced from batch polymerization of 30 vol% NVP and 0.11 wt% Vazo-67 in butanol at 85 °C and varying conversion levels as indicated.

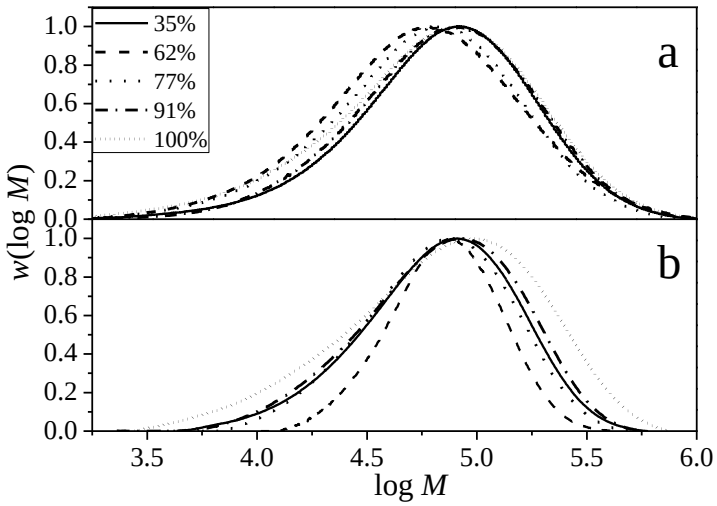

Figure A.2.5. Comparison of a) RI (corrected) and b) MALLS MWDs for the polymer produced from batch polymerization of 20 vol% NVP and 0.027 wt% Vazo-67 in butanol at 85 °C and varying conversion levels as indicated.

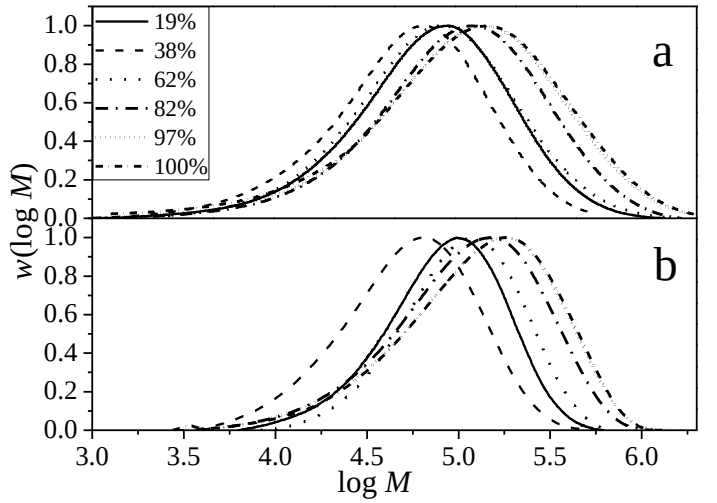

Figure A.2.6. Comparison of a) RI (corrected) and b) MALLS MWDs for the polymer produced from batch polymerization of 30 vol% NVP and 0.027 wt% Vazo-67 in butanol at 85 °C and varying conversion levels as indicated.

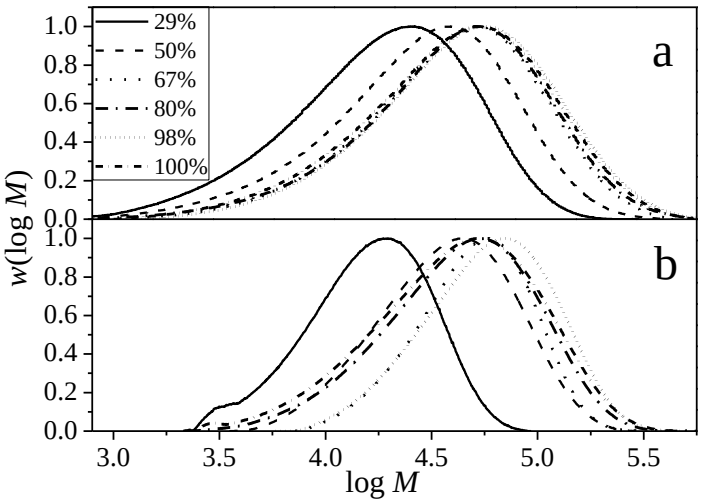

Figure A.2.7. Comparison of a) RI (corrected) and b) MALLS MWDs for the polymer produced from semibatch polymerization of 20 vol% NVP dosed over a period of 30 minutes and 0.11 wt% Vazo-67 in butanol at 85 °C and varying conversion levels as indicated.

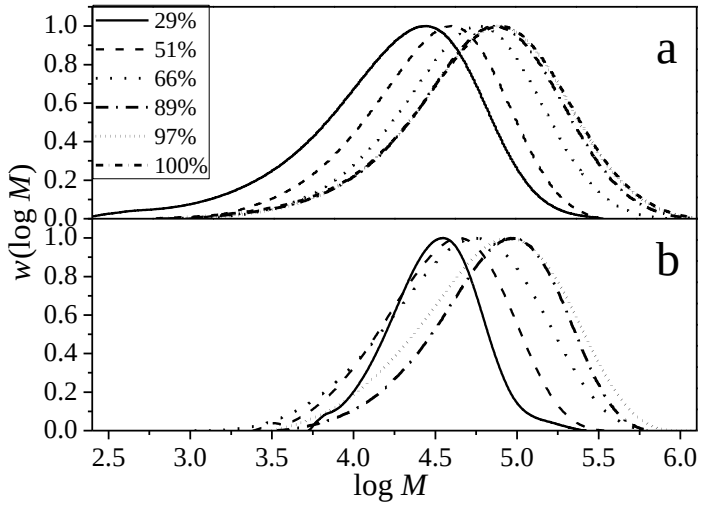

Figure A.2.8. Comparison of a) RI (corrected) and b) MALLS MWDs for the polymer produced from semibatch polymerization of 30 vol% NVP dosed over a period of 30 minutes and 0.11 wt% Vazo-67 in butanol at 85 °C and varying conversion levels as indicated.

A.3 Comparison of RI and MALLS MWDs for Aqueous-Phase Polymerization of NVF (Chapter 4)

The correction factor for this set of data was ascertained to be 0.41.

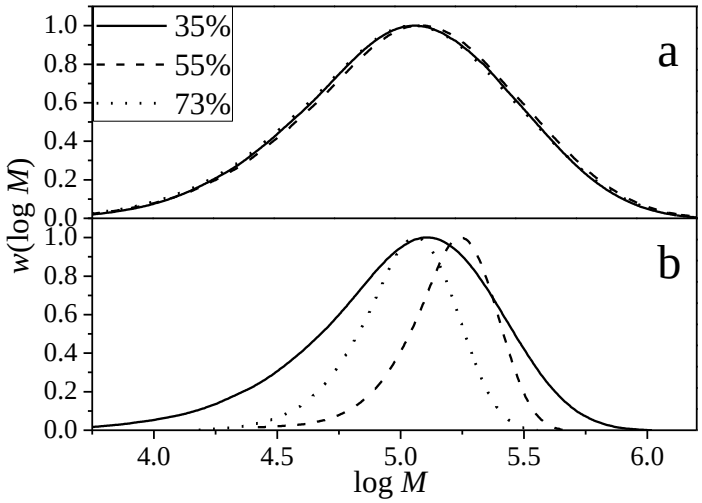

Figure A.3.1. Comparison of a) RI (corrected) and b) MALLS MWDs for the polymer produced from batch polymerization of 12.5 vol% NVF and 0.02 wt% V-50 in water at 85 °C and varying conversion levels as indicated.

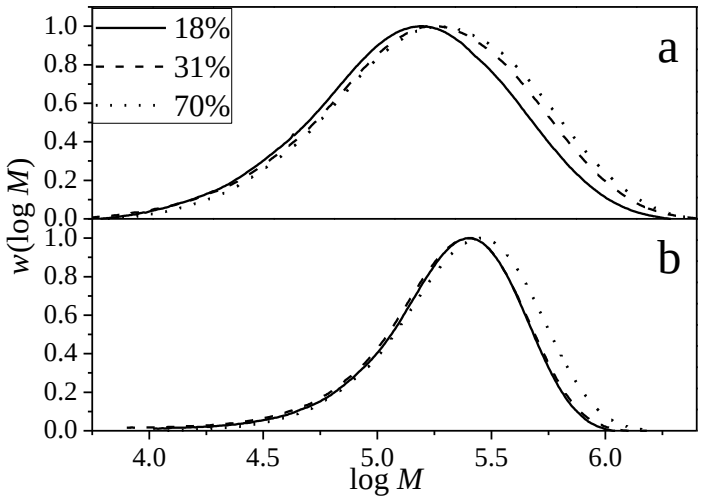

Figure A.3.2. Comparison of a) RI (corrected) and b) MALLS MWDs for the polymer produced from batch polymerization of 20 vol% NVF and 0.02 wt% V-50 in water at 85 °C and varying conversion levels as indicated.

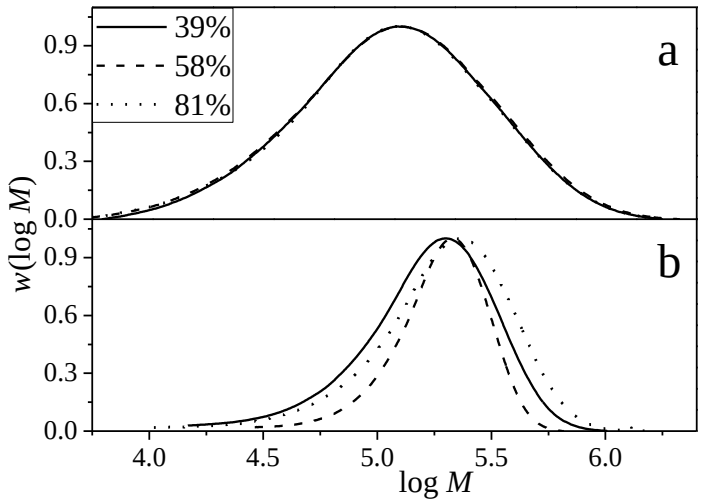

Figure A.3.3. Comparison of a) RI (corrected) and b) MALLS MWDs for the polymer produced from batch polymerization of 12.5 vol% NVF and 0.02 wt% V-50 in water at 85 °C and varying conversion levels as indicated.

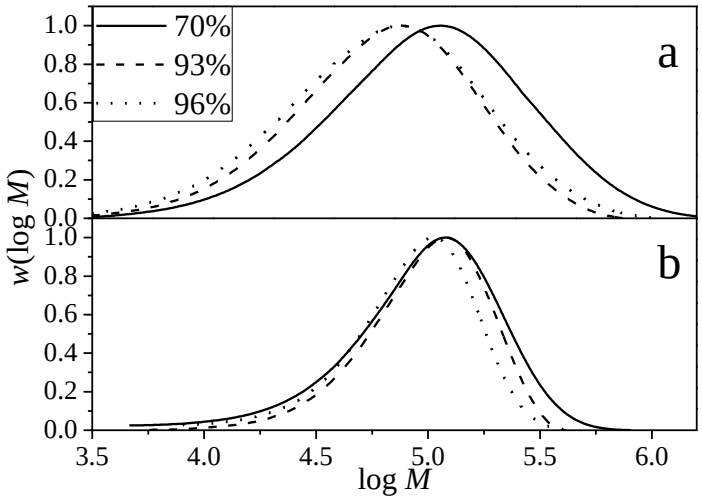

Figure A.3.4. Comparison of a) RI (corrected) and b) MALLS MWDs for the polymer produced from batch polymerization of 12.5 vol% NVF and 0.04 wt% V-50 in water at 85 °C and varying conversion levels as indicated.

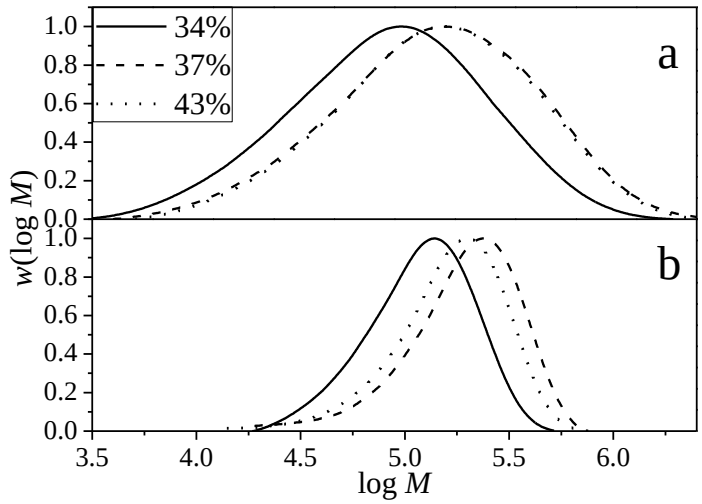

Figure A.3.5. Comparison of a) RI (corrected) and b) MALLS MWDs for the polymer produced from batch polymerization of 20 vol% NVF dosed over a period of 30 minutes and 0.02 wt% V-50 in water at 85 °C and varying conversion levels as indicated.

A.4 Comparison of RI and MALLS MWDs for Aqueous-Phase Polymerization of NVI (Chapter 5)

The correction factor for this set of data was ascertained to be 0.52.

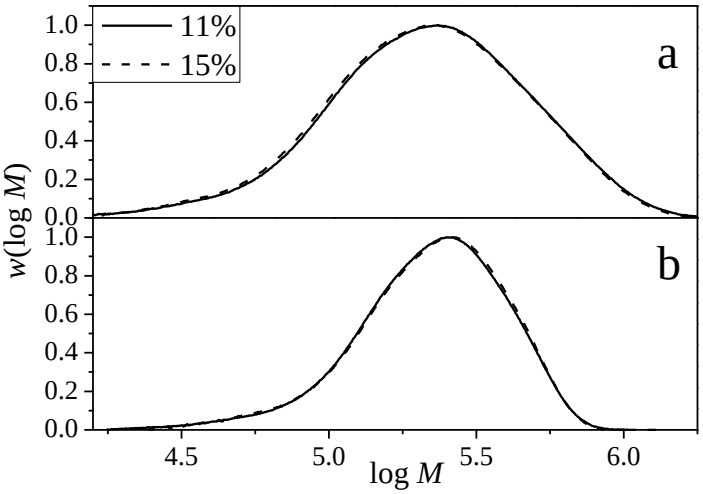

Figure A.4.1. Comparison of a) RI (corrected) and b) MALLS MWDs for the polymer produced from batch polymerization of 12.5 vol% NVI and 0.02 wt% V-50 in water at 85 °C and varying conversion levels as indicated.

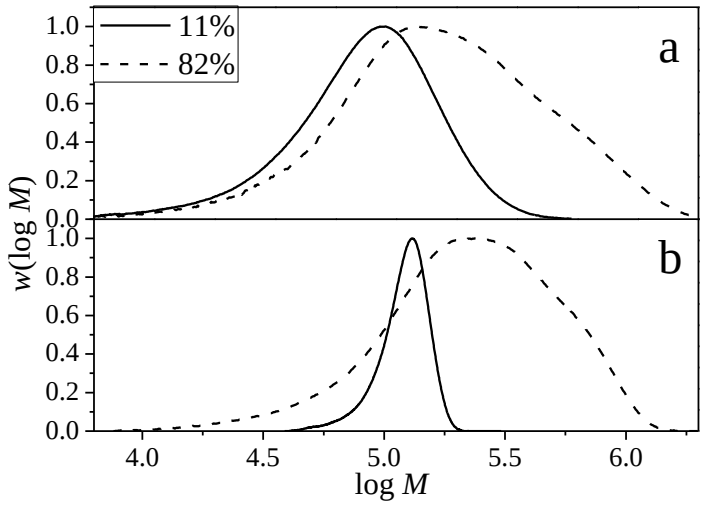

Figure A.4.2. Comparison of a) RI (corrected) and b) MALLS MWDs for the polymer produced from batch polymerization of 12.5 vol% NVI and 0.2 wt% V-50 in water at 85 °C and varying conversion levels as indicated.

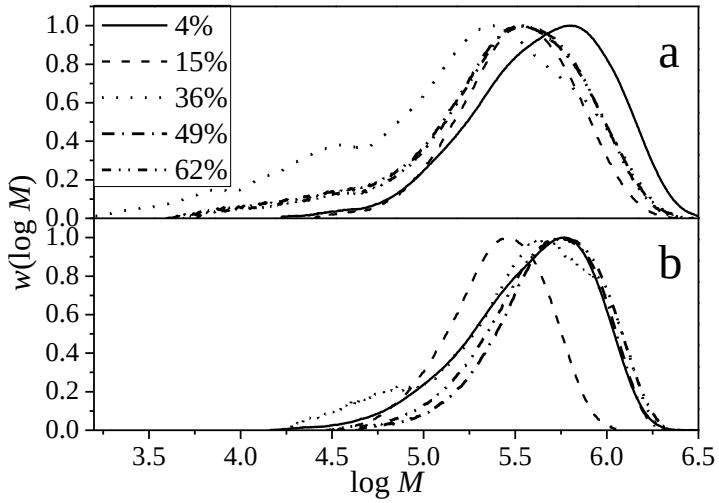

Figure A.4.3. Comparison of a) RI (corrected) and b) MALLS MWDs for the polymer produced from batch polymerization of 12.5 vol% NVI and 0.02 wt% V-50 in water at an adjusted pH of 1 and temperature of 85 °C, at varying conversion levels as indicated.

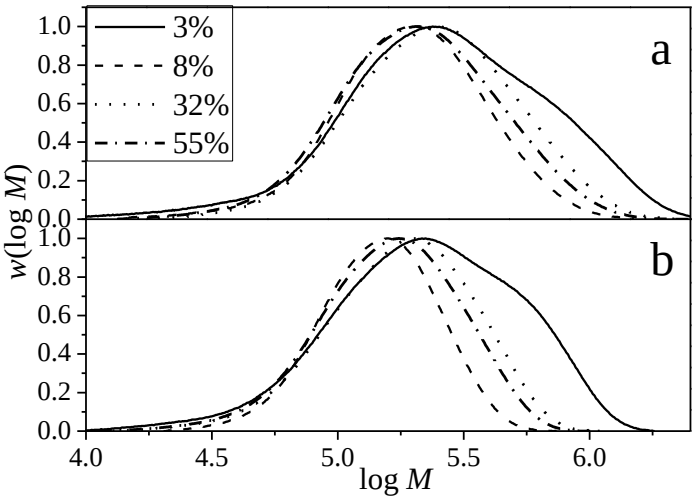

Figure A.4.4. Comparison of a) RI (corrected) and b) MALLS MWDs for the polymer produced from batch polymerization of 12.5 vol% NVI and 0.02 wt% V-50 in water at an adjusted pH of 4 and temperature of 85 °C, at varying conversion levels as indicated.

A.5 Comparison of RI and MALLS MWDs for Aqueous-Phase Copolymerization of NVP & NVF (Chapter 6)

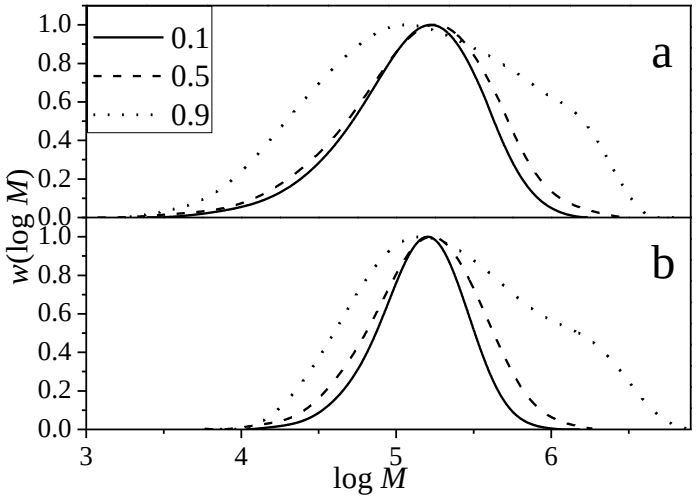

Figure A.5.1. Comparison of a) RI (corrected) and b) MALLS MWDs for the polymer produced at high conversion levels (>80%) from batch copolymerization of 10 wt% monomer and 0.02 wt% V-50 in water at 85 °C, at varying f_{NVP} levels as indicated.

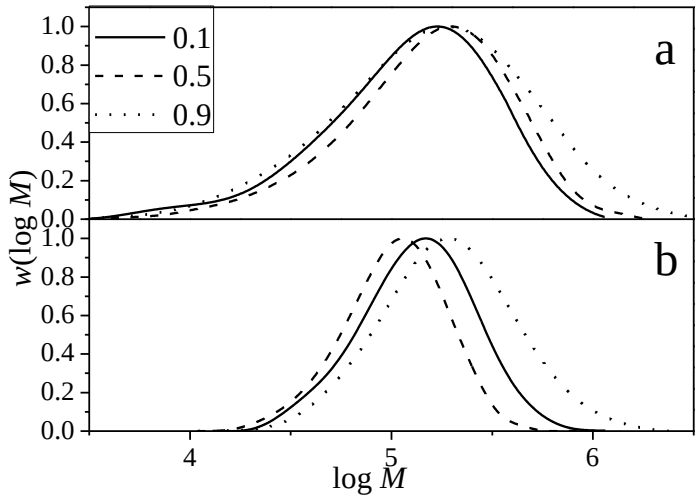

Figure A.5.2. Comparison of a) RI (corrected) and b) MALLS MWDs for the polymer produced at low conversion levels (~20%) from batch copolymerization of 10 wt% monomer and 0.02 wt% V-50 in water at 85 °C, at varying f_{NVP} levels as indicated.

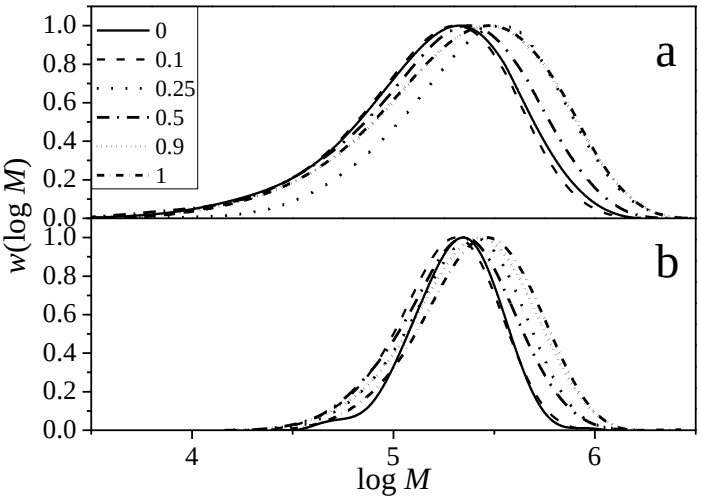

Figure A.5.3. Comparison of a) RI (corrected) and b) MALLS MWDs for the polymer produced at low conversion levels (~10%) from batch copolymerization of 10 wt% monomer and 0.1 wt% V-50 in water at 60 °C, at varying f_{NVP} levels as indicated.

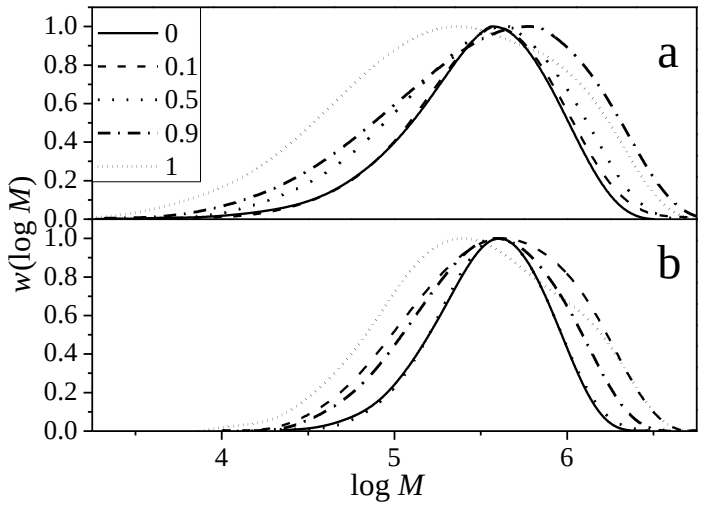

Figure A.5.4. Comparison of a) RI (corrected) and b) MALLS MWDs for the polymer produced at high conversion levels (>80%) from batch copolymerization of 25 wt% monomer and 0.1 wt% V-50 in water at 60 °C, at varying f_{NVP} levels as indicated.

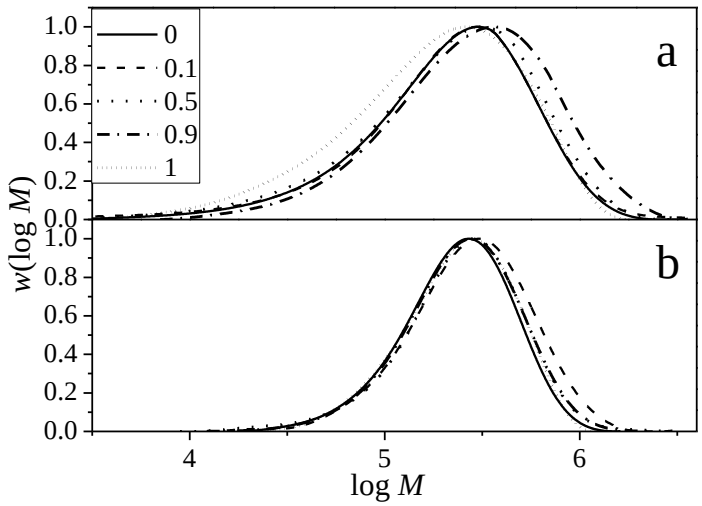

Figure A.5.5. Comparison of a) RI (corrected) and b) MALLS MWDs for the polymer produced at low conversion levels (~10 %) from batch copolymerization of 25 wt% monomer and 0.1 wt% V-50 in water at 60 °C, at varying f_{NVP} levels as indicated.

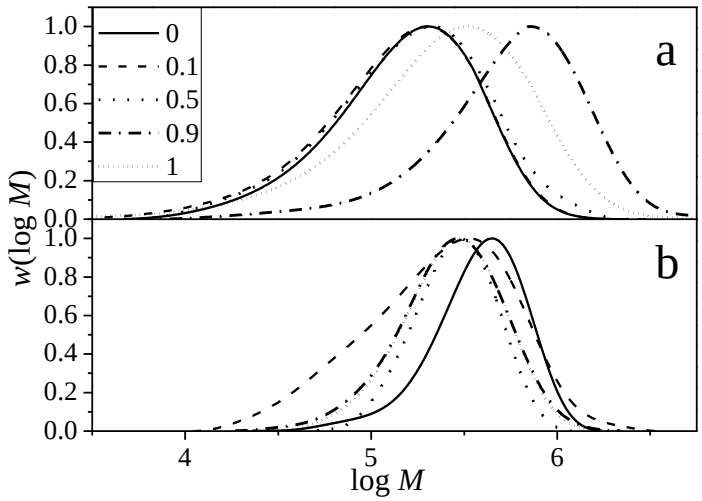

Figure A.5.6. Comparison of a) RI (corrected) and b) MALLS MWDs for the polymer produced at low conversion levels (~10 %) from batch copolymerization of 50 wt% monomer and 0.2 wt% V-50 in water at 60 °C, at varying f_{NVP} levels as indicated.

Appendix B

B.1 Estimation of initial rates for the copolymerization batch experiments (Chapter 6)

The initial rate and 95% confidence intervals for the copolymerization batch experiments were obtained by performing a regression analysis using Excel® on the time-conversion data. The data points for the initial rate determination were chosen from ~240 s to ~ 600 s for experiments at 10 and 50 wt% monomer with 0.1 and 0.2 wt% initiator concentrations respectively and from ~500 to 900 s for the experiments conducted at 25 wt% monomer and 0.1 wt% initiator concentration, due to the longer inhibition period in the latter. An example of the regression analysis result for a copolymerization experiment (50 wt% monomer concentration and 0.2 wt% initiator concentration and f_{NVP} of 0.5 at 60 °C, shown in Figure B.1.1) is presented below. The standard deviation and the 95% confidence intervals were calculated using stdev and confidence commands in excel. The regression statistics and the parameters for the 95% confidence intervals are shown in Tables B.1.1 and B.1.2 respectively. The high R^2 and the reasonable adjusted R^2 values indicate a good fit to the data. This can also be seen from the good agreement between the estimated slope and the initial rate data presented in Figure B.1.2 and the random scatter in the residual plot, shown in Figure B.1.3.

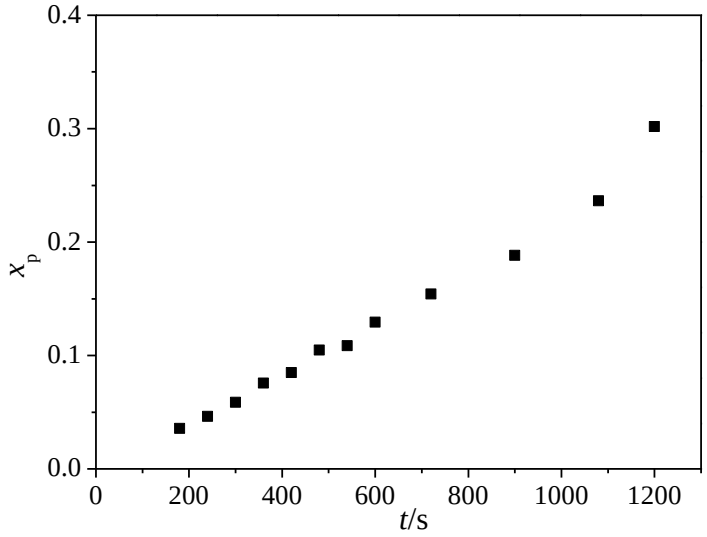

Figure B.1.1. Conversion profile for the batch polymerization of 50 wt% monomer concentration at f_{NVP} of 0.5 and 0.2 wt% initiator concentration at a temperature of 60 °C.

Table B.1.1. Regression statistics parameters and values for the excel fit of the initial slope for the batch polymerization of 50 wt% monomer concentration at f_{NVP} of 0.5 and 0.2 wt% initiator concentration at a temperature of 60 °C.

Multiple R	0.990511
R Square	0.981112
Adjusted R Square	0.97639
Standard Error	0.003907
Observations	6

Table B.1.2. 95% confidence interval parameters for excel estimated initial slope for the batch polymerization of 50 wt% monomer concentration at f_{NVP} of 0.5 and 0.2 wt% initiator concentration at a temperature of 60 °C, shown in Figure B.1

	Coefficients	**Standard Error**	**t Stat**	**P-value**	**Lower 95%**	**Upper 95%**
Intercept	-0.00736	0.007184	-1.02401	0.363715	-0.0273025	0.012589469
X Variable 1	0.000224	1.56E-05	14.41451	0.000135	0.000181158	0.000267594

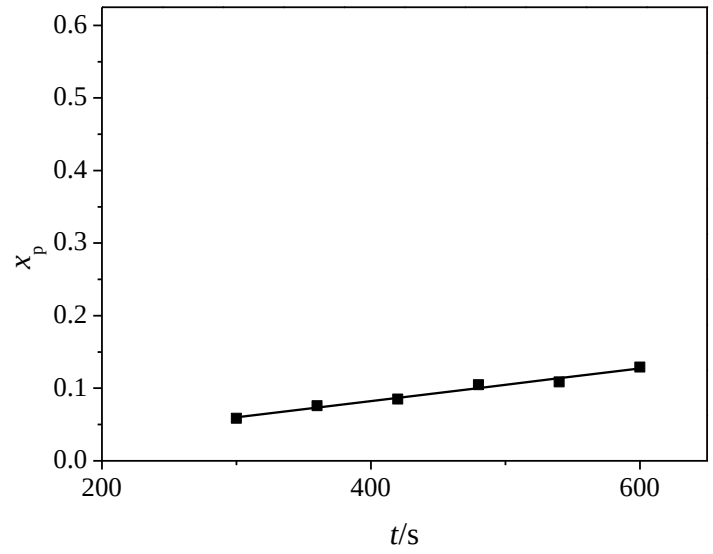

Figure B.1.2. Excel fit of the initial rate of conversion for the batch polymerization of 50 wt% monomer concentration at f_{NVP} of 0.5 and 0.2 wt% initiator concentration at a temperature of 60 °C in water.

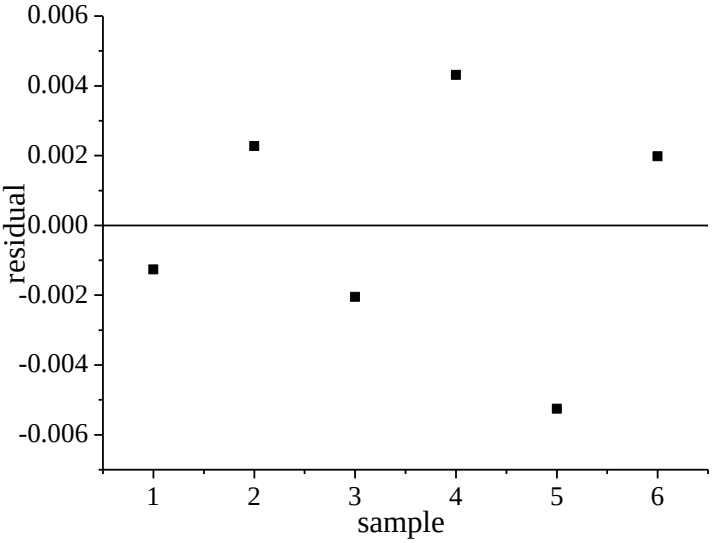

Figure B.1.3. Residual plot for the initial slope fit shown in Figure B.1.2.

Alternately, the error in the rate was estimated by conducting repeat experiments at the same initial conditions. The experiment at 10 wt% monomer concentration at f_{NVP}=0.5 and 0.1 wt% initiator concentration at 60 °C was repeated four times, with conversion profiles shown in Figure B.1.4. The initial slope from each set of data was determined by fitting the initial data from ~240 to 600 seconds using excel, as explained above. The initial rates for each of the repeat experiments (obtained by performing a regression analysis on each data set) and the 95% confidence intervals, obtained using Excel®, are tabulated in Table B.1.3. The mean value and 95% confidence interval for this set of results was determined to be $3.57 \times 10^{-4} \pm 2.077 \times 10^{-5}$.

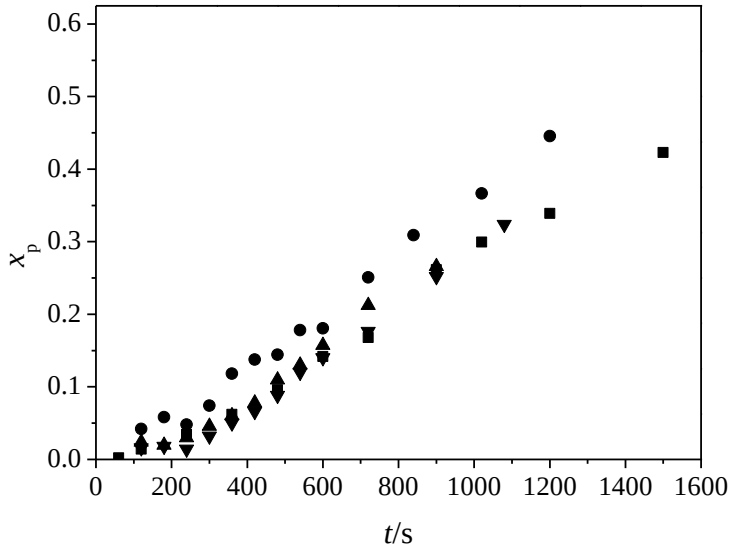

Figure B.1.4. Conversion profiles for repeat batch polymerization of 10 wt% monomer concentration at f_{NVP}=0.5 and 0.1 wt% initiator concentration at a temperature of 60 °C.

Table B.1.3. Estimates of rates and 95% confidence intervals for the excel estimated slopes for the repeat batch experiments shown in Figure B.2. 1

Experiment #	**Rate x 10^{-4}**	**95% confidence intervals**
1	3.27	3.47E-05
2	3.76	9.81517E-05
3	3.57	5.19509E-05
4	3.67	5.65E-05

B.2. Quantification of trace levels of monomer in the copolymer sample for composition analysis

The copolymer samples were precipitated from the reaction mixture using acetone and dried in an air stream followed by vacuum drying for ~48 to 72 hours. The samples were then analyzed by ^{1}H-NMR in order to determine the copolymer compositions. From the NMR spectra, trace levels of monomer were detected for some of the samples. As some of the monomer peaks interfere with the polymer peak used in the estimation of composition analysis, the monomer levels were quantified and accounted for accordingly.

The NMR spectrums for NVP, NVF and a precipitated copolymer sample produced from the batch polymerization of 50 wt% monomer concentration at f_{NVP}=0.5, 0.2 wt% initiator concentration at 60 °C in water are shown in Figures B.2.2, B.2.3 and B.2.4 respectively. The peak positions in the monomer spectrums are labeled in accordance with their structures as shown in Figures B.2.1 (a) and (b) for NVP and NVF respectively. NVF monomer exists in cis (c) and trans (t) forms, as shown in Figure B.2.1 (b), in approximately 1:3 ratio, in agreement with literature. The poly (vinylpyrrolidone) (PVP) and poly(vinylformamide) (PVF) peaks used in the estimation of the copolymer composition have been labeled in Figure B.2.4. As can be seen from the spectrums, the 3t peak (at ~8-8.3 ppm) representing the CH in the NVF trans isomer and peak 2 (at ~ 2-2.2 ppm) representing the CH_2 in the ring of NVP interfere with the PVF and PVP peaks used is the copolymer composition estimation respectively. However, the levels of NVP and NVF in the copolymer sample can be estimated by using the vinyl peaks of the monomers that appear between 6.8 – 7 ppm (peak 4; CH in vinyl group of NVP) and between 6.7 - 6.85 ppm (peak 1t; CH in vinyl group of trans NVF) and 6.59 - 6.72 ppm (peak 1c; CH in the vinyl group of cis NVF). The level of NVP in the PVP peak is estimated by multiplying the

integral value of peak 4 by 2 (in order to account for the two protons in the CH_2 group in the pyrrolidone ring) and the level of NVF in the PVF peak can be obtained from peak 1t or by multiplying the value of peak 1c by 3. The copolymer composition can therefore be estimated using the following expression

$$F_{\mathrm{NVP}} = \frac{\left[(\text{peak PVP} - 2*\text{peak 4})/2\right]}{(\text{peak PVF})\text{-}(\text{peak 1t})+\left[(\text{peak PVP} - 2*\text{peak 4})/2\right]}$$

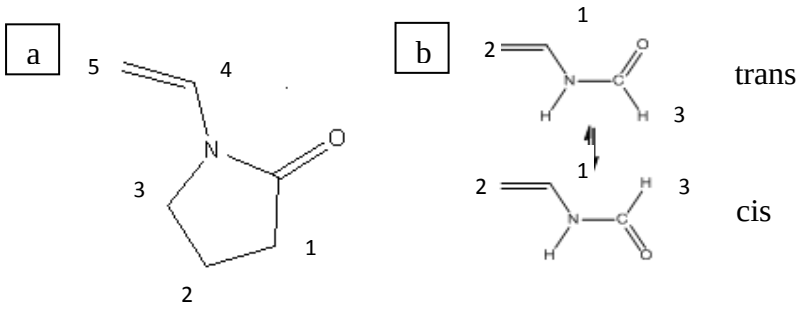

Figure B.2.1. Structure of a) *N*-vinyl pyrrolidone and b) *N*-vinyl formamide

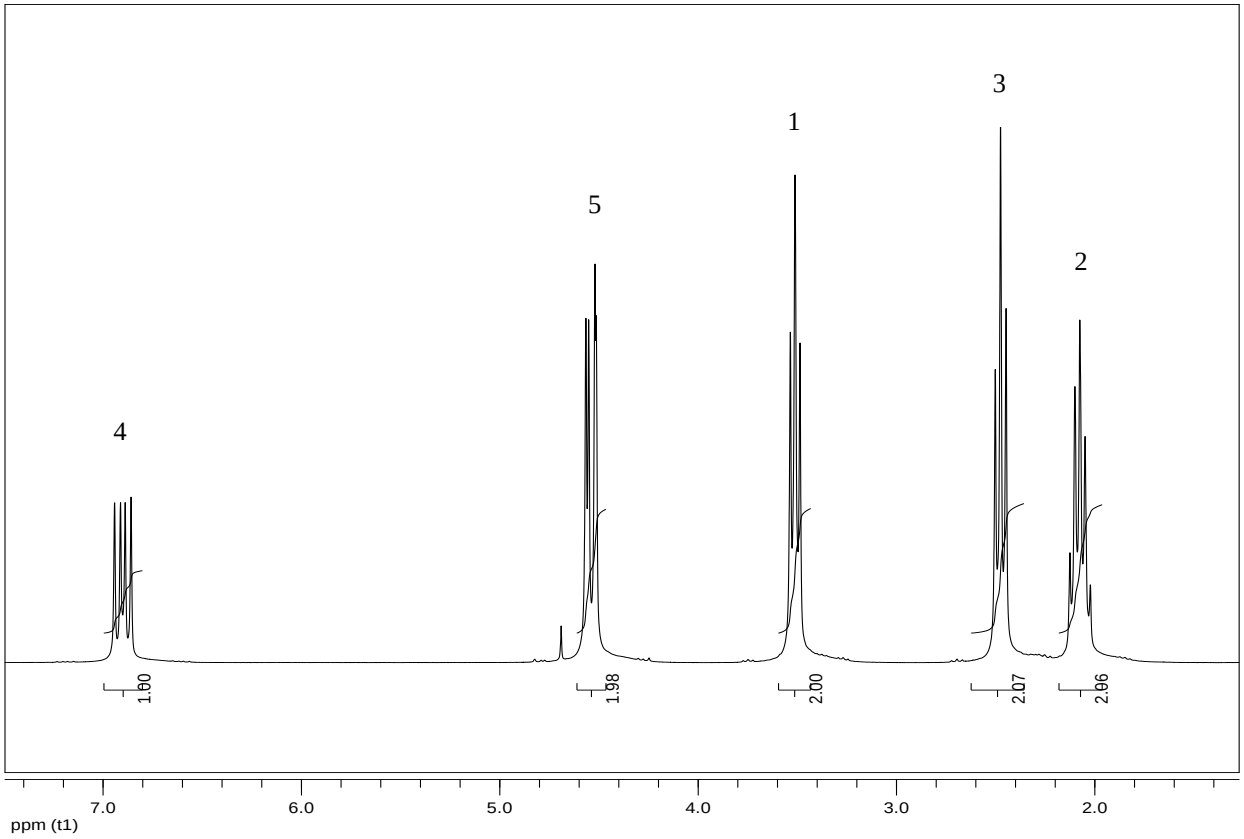

Figure B.2.2. NMR spectrum of *N*-vinyl pyrrolidone (NVP)

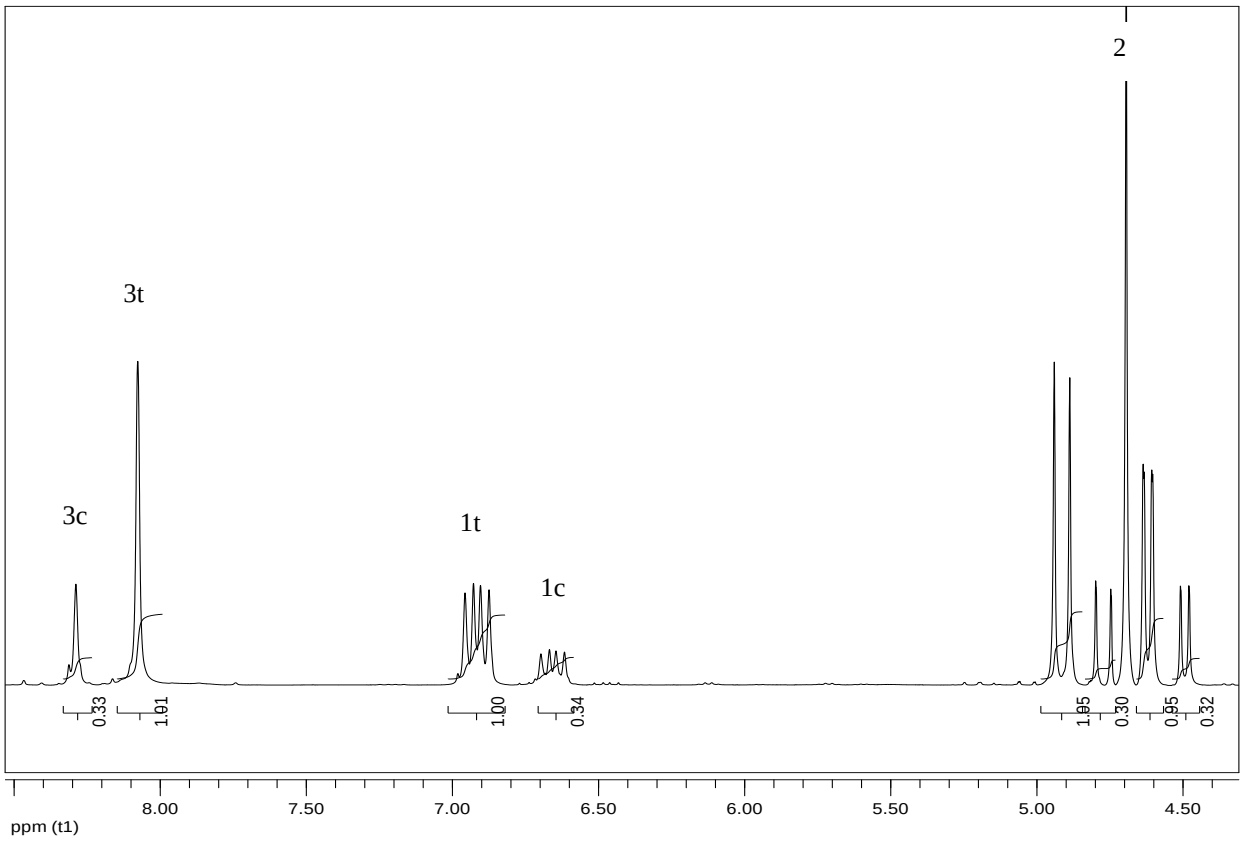

Figure B.2.3. NMR spectrum of *N*-vinyl formamide (NVF)

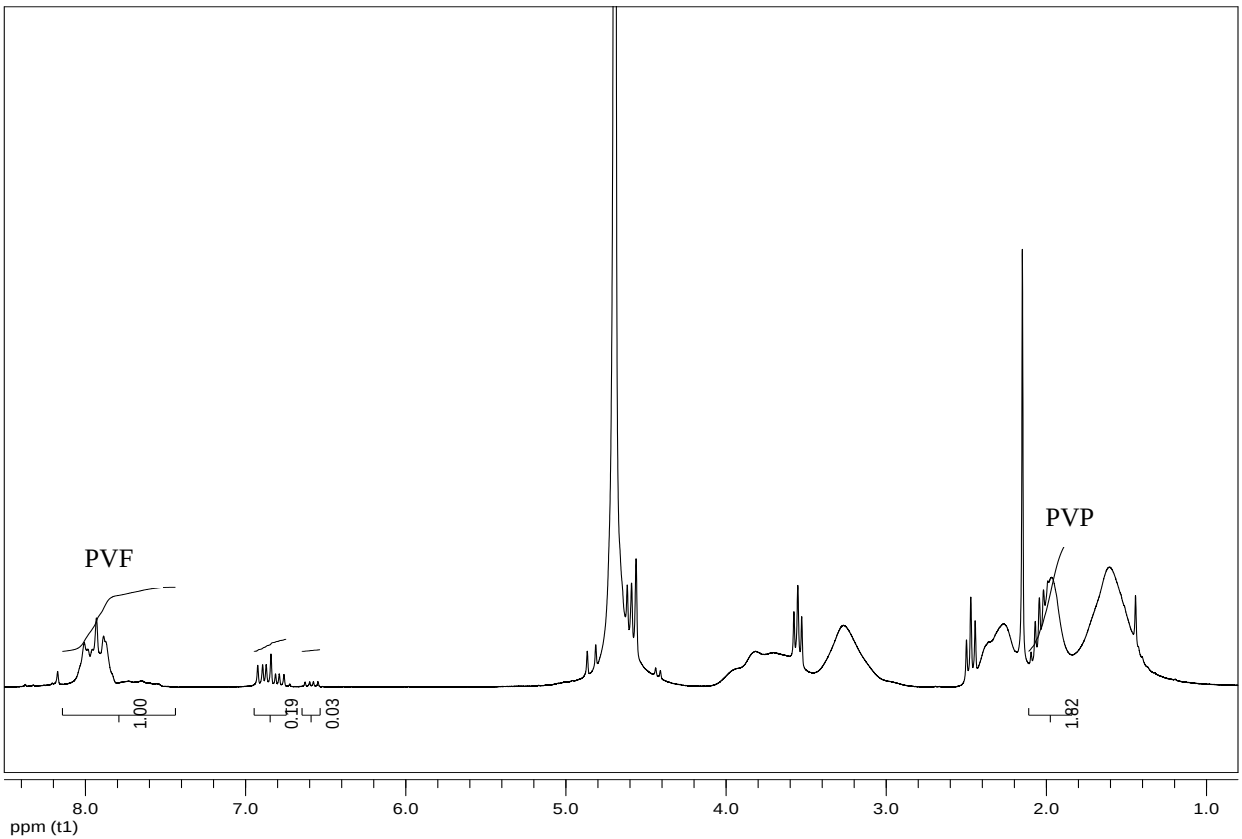

Figure B.2.4. NMR spectrum of a poly(NVP-co-NVF) sample produced from the batch polymerization of 50 wt% monomer concentration at f_{NVP}=0.5, 0.2 wt% initiator concentration at 60 °C in water.

B.3. Temperature control in the copolymerization batch experiments

The copolymerization batch experiments were carefully planned in order to avoid any exotherm issues and to ensure precise temperature control. As initial exotherm becomes an issue at high monomer concentrations, the batch experiments with 25 and 50 wt% monomer concentrations were conducted at a temperature of 60 °C. In all cases, the temperature was controlled within a deviation of ±2 °C. The temperature profiles at the monomer concentrations of 10, 25 and 50 wt% are shown in Figures B.3.1, B.3.2 and B.3.3 respectively.

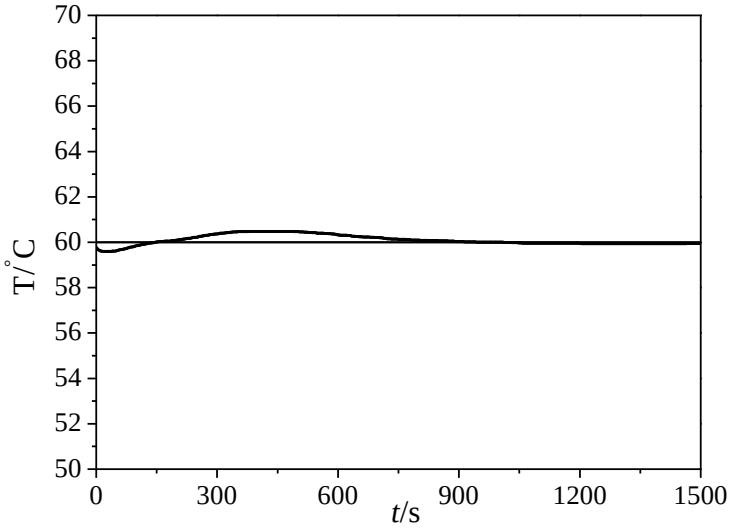

Figure B.3.1. Temperature profile for the copolymerization batch experiment at f_{NVP}=0.5 with 10 wt% monomer and 0.1 wt% initiator at 60 °C.

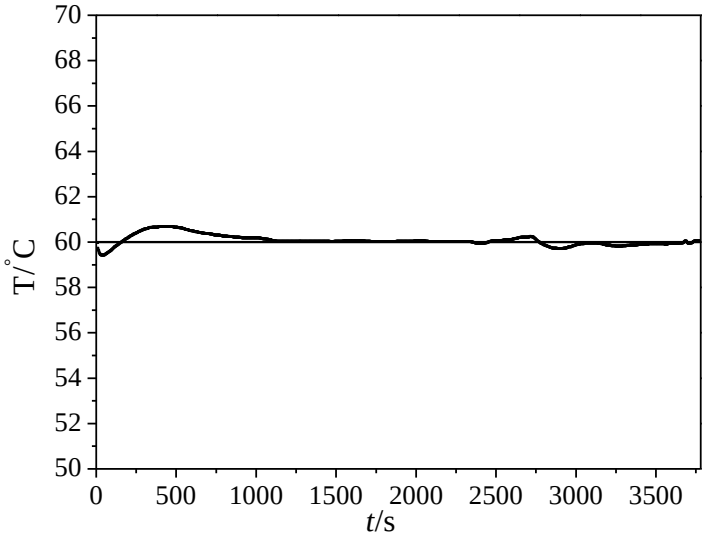

Figure B.3.2. Temperature profile for the copolymerization batch experiment at f_{NVP}=0.5 with 25 wt% monomer and 0.1 wt% initiator at 60 °C.

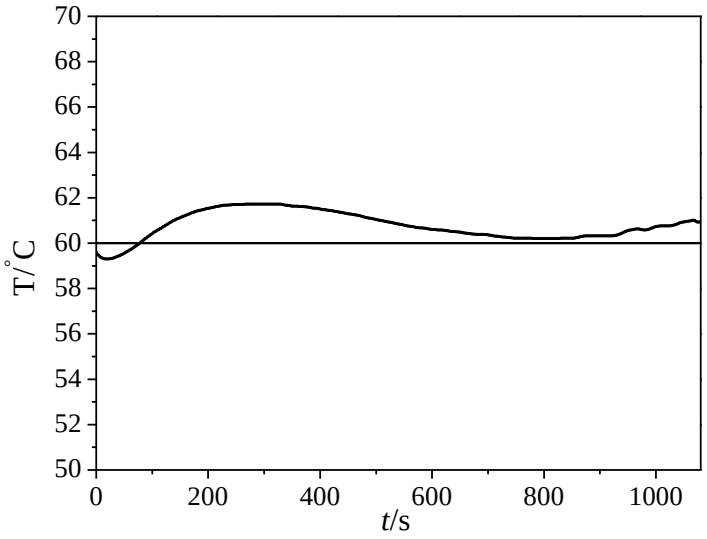

Figure B.3.3. Temperature profile for the copolymerization batch experiment at f_{NVP}=0.5 with 50 wt% monomer and 0.2 wt% initiator at 60 °C.